POLITECNICO
MILANO 1863

DIPARTIMENTO DI MECCANICA

Marco Boniardi e Andrea Casaroli

Steel metallurgy

Volume I

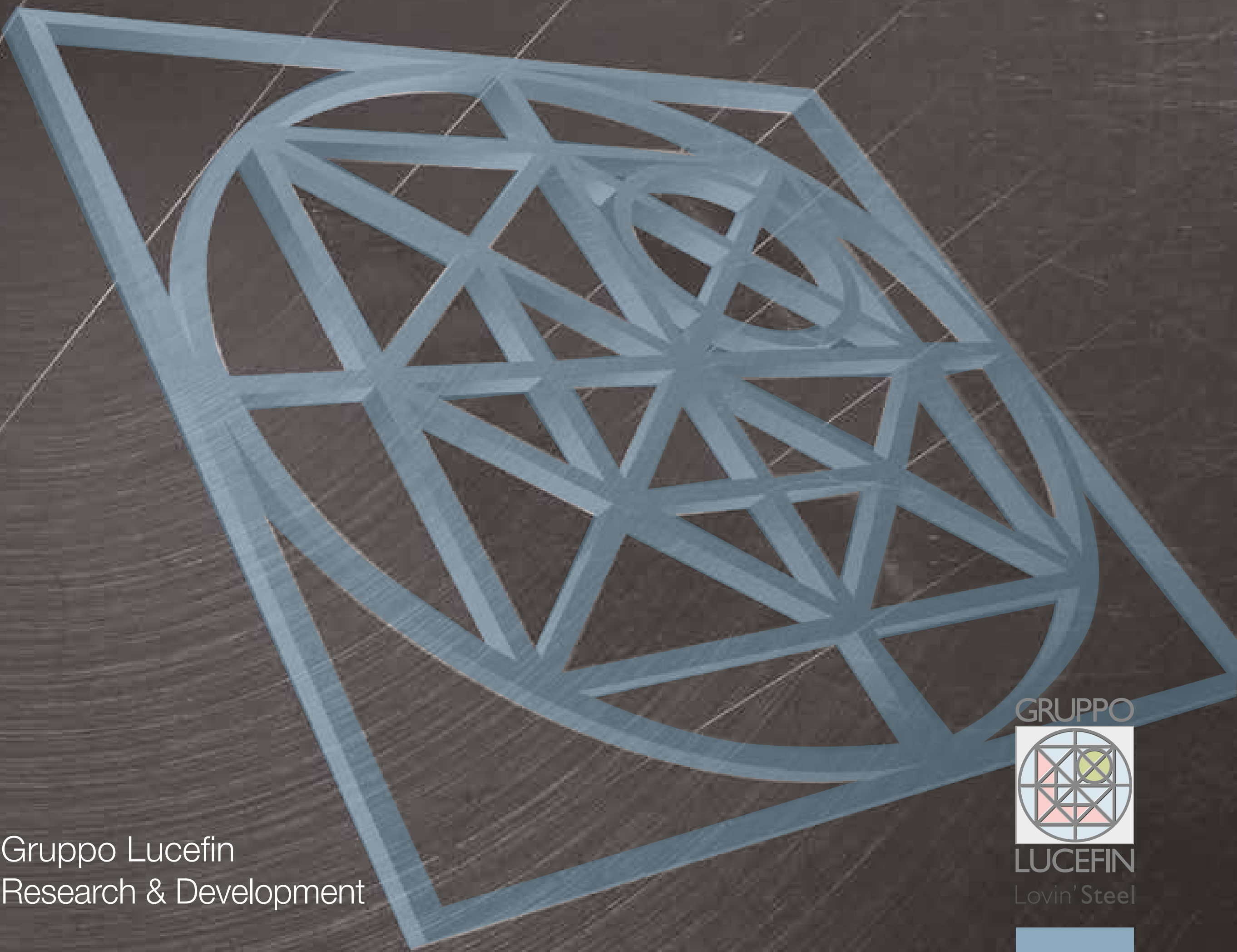

Gruppo Lucefin
Research & Development

GRUPPO
LUCEFIN
Lovin'Steel

This book is dedicated to Davide and Pietro:
before them lays a future that awaits them.

You do not teach what you wish to.
I would even dare to say that you do not teach what you know or what you think you know.
You teach, and you can only teach, what you are.

Jean Jaurès, Speech to the Chamber, 1910

TABLE OF CONTENTS

PREFACE

"Steel Metallurgy": procedure towards continuing to recount our materials and our history... since we have always believed in this!
We believe in what we do, with professionalism, commitment, and dedication.
We believe in culture. In the culture of the industry and in the culture of knowledge, turning towards those who live this profession with intensity and passion, or to those who are just simply at the beginning.
We believe that our work, to which we dedicate a lifetime, should not just be an everyday experience, but the desire for continuity.
We believe in the collaboration among people and the value of projects that arise from collaborations. In the end, we believe that the future of our industry depends only on us.

I thank the authors. Great professionals but, above all, great people, and I thank all those who made this initiative possible.

Giorgio Buzzi, Esine (Brescia), April 15th, 2017

I think I will not wrong anyone in saying that the preface of a book is usually written last, even if the term indicates precisely the opposite. Usually, in a preface, authors explain why they have decided to write that certain book, why it is useful, and for which readers it was thought for and created.

I, who work as a teacher (it would be nice to say "a master"... but that is not a profession), I always write and teach with a mental tare in my head: Will I be able to make them understand what I'm trying to say or not?

With this idea, my intention was to print the volume you are holding. I wanted to write a simple - but not simplistic - book that explained the basics of steel metallurgy with a language that was comprehensible to everyone. Often, when I read technical-scientific texts in this discipline (but also in others), I have the unpleasant feeling that the author is only talking to those who are in the field, the so-called "initiates", whom are already familiar with metallurgy. That is exactly what I did not want to do.

I thought of a "bottom-up" approach towards the problems. Something that could be useful to my students and all those who already work in the metallurgic industry. For the first, my desire was to whet their interest in a topic not yet known to them. For the latter, I wanted to complete some theoretical gaps that will explain the relevant daily practice.

If you want to write well, you must have an altruistic approach. Writing a book is an act of love for the reader. A good writer, like a good teacher, is not one who sums up all possible knowledge regarding a given topic or one who is capable of effectively transferring a great deal of information. Instead, a good writer is one who seduces, suggests, stimulates. One who, in order to convey true knowledge, generates in those who read a kind of void that, from that moment forward, must be filled. Or else, as Massimo Recalcati observed, "True teachers are not those who have filled our heads with already established knowledge, therefore already dead knowledge, but those who have created gaps, in order to animate a new desire towards "knowing". They are those who have raised questions without offering pre-established answers.[1]

I wonder if I have succeeded in all this? Only the readers will be able to say.

Marco V. Boniardi, Cusano Milanino (Milano), March 4th, 2017

---

[1] *Massimo Recalcati, L'ora di lezione - per un'erotica dell'insegnamento, Giulio Einaudi Editore, Torino, 2014.*

This book represents the continuation of a work begun back in 2014, along with the Lucefin group: the first result was the publication of the volume, "Stainless steels".

Over the last three years, a recurring question has continued to spin in my head: why write another book on metallurgy? Certainly not for money or academic "honor": there are better ways to achieve these goals. The real motivation is found in the individual. "Writing a Book" has to do with the will to create a useful tool for the reader (... not just for the writer).

We live in a time that precedes the race. Perhaps it would be best to learn to walk before running. One must be efficient; even better if effective.

The book you have in your hands holds the presumption to serve this purpose: to learn how to walk one step at a time, to solve problems, and to be effective.

In the pages that follow, you will find yourself walking through the paths - sometimes winding - that have led metallurgy to what it is today. Roads that are often neglected and forgotten, without which it is not possible to fully appreciate the "why" and "how" of a very important discipline that, unfortunately, is taken for granted by now.

My hope is that this work has not been created in vain. That the time I have devoted to it passes from me to you and that it will allow you to run or take new roads in the future.

Andrea Casaroli, Sarmato (Piacenza), February 27th, 2017

ACKNOWLEDGMENTS

Writing a book is like contracting a debt with many. Not wanting to recognize it is not only wrong but presumptuous. In the case of this book, the list of people and institutions to be thanked has been necessarily very large. We apologize in advance for anything or anyone forgotten.

First of all, a heartfelt thank you to our teachers.

The love and passion for Metallurgy - as for any other thing - always arises from an encounter with a person. In this case, with Prof. Giuseppe Silva and with his way of teaching, working, and being. We certainly learned a lot more than what the professor himself thought to have left us.

We also owe a great deal to Professor Mario Balbi and Professor Walter Nicodemi, to what they have constructed, to the work they achieved, and to what they have transmitted to us.

An acknowledgment of equal importance goes to all of our students in mechanical engineering at the Politecnico di Milano (Bovisa, Leonardo, Lecco, and Piacenza branches), and Università di Pavia. During the years, they have urged and forced us to question ourselves, induced us to better understand things, and to improve our way of recounting them. Many of them have also made a significant contribution to revising the final drafts of this book.

We cannot forget the colleagues from our department - professors and researchers - with whom we discuss all the issues of this very interesting discipline on a daily basis. Therefore, we also thank all the Professors. Maurizio Vedani, Carlo Mapelli, Elisabetta Gariboldi, Barbara Rivolta, Nora Lecis, Fabrizio D'Errico, Riccardo Gerosa, Silvia Barella, Andrea Gruttadauria, Riccardo Casati, and Davide Mombelli.

Another duly deserved acknowledgment goes to Mr. Piero Pellin, Mr. Maurizio Pardi, Engineer Ludovica Rovatti, and Engineer Luca Signorelli, some of the most valued technicians in the Laboratories of the Department of Mechanical Engineering of Politecnico di Milano: their scientific competence - this term is not used at random - has always been of great support and help. We cannot forget our secretary, Mrs. Cinzia Farina: she is the best in understanding people and always knows how to "deal with them".

The things you will find written in this book are also the result of collaborations developed over time with many university colleagues that are not from the Politecnico di Milano: Professor Benedetto Bozzini of the Università di Lecce, and Professors Roberto Roberti and Marina La Vecchia from the Università di Brescia, Professor Francesco Iacoviello from the Università di Cassino, Professor Donato Firrao from the Politecnico di Torino, and Professor Giovanni Straffelini from the Università di Trento. We also owe a great deal to Engineers Gianmatteo Martinelli, Mattia Bellogini, Marco Feraboli, Gianmarco Vimercati, Silvia Cincera, and Alessia Sironi who have by now transferred their sphere of interest outside the academic world.

It is not possible to speak of metallurgy without also looking at the industrial world. Studying steel is not a theoretical experiment, but a continuous practical application.Therefore, a thank you to Mr. Emilio Rocchi at Acciai Vender, to Engineer Mario Cusolito, and Engineer Enrico Mariani at Rodacciai, to Mr. Antonio Vienna, to Mr. Gabriele Rampinini, and to Engineer Chiara Tagliabue at Forgiatura Vienna, to Engineer Valentina Vicario at Fomas, and to Engineer Guido Perricone at Brembo. A special thought goes to all the technicians and friends at Tenaris Dalmine, Engineers Renato Spelgatti, Barbara Scarabelli, Stefano Farè, Gianluca Bassanini, Maurizio Bellingardi, Emanule Paravicini Bagliani, and Tiziana Nani and Carolina Lussana, Phds.

We also must not forget the support received from industrial laboratories that work in the field of steel metallurgy. Confronting oneself with intelligent individuals helps to increase your wealth of knowledge: thank you Engineer Luca Bonvini and Engineer Andrea Tombretta at Hammer, to Ms. Patrizia Maio and Engineer Matteo Borgonovo at Kaizenlab, to Engineer Alessandra Marelli, to Engineer Marco Casaril and Engineer HC Clemente Marelli at Omeco, Mr. Giovanni Rivolta at RTM Breda, Mrs. Elena Bresciani, and Dr. Mauro Ostacoli at Exova.

Last but not least, immense thank you to Luigi and Giorgio Buzzi, Massimo Sperto, Vittorio Boneschi, and Domenico Surpi at the Lucefin steel group, who have believed in us and who have offered us this editorial opportunity.

Our final thought goes to those who are always close to us and who support us every day: Dolores, Piero and Marcella, Pinuccia, Francesco and Elena.

For all the micrographs in the text, we received support from the following organizations:
Laboratori del Dipartimento di Meccanica del Politecnico di Milano, I-20156 Milan, Via La Masa, 1;
Laboratorio Hammer Srl, I-20017 Rho (MI), Via Risorgimento, 69/22;
Laboratorio Omeco Srl, I-20900 Monza (MB), Via Monviso, 56;
Laboratorio Exova Srl, I-26013 Crema (CR), Via della Pierina snc

Although it is true that the work involved in preparing and observing the samples was performed by people - and our thanks goes to them - without the required laboratory tools, not much could have been done.

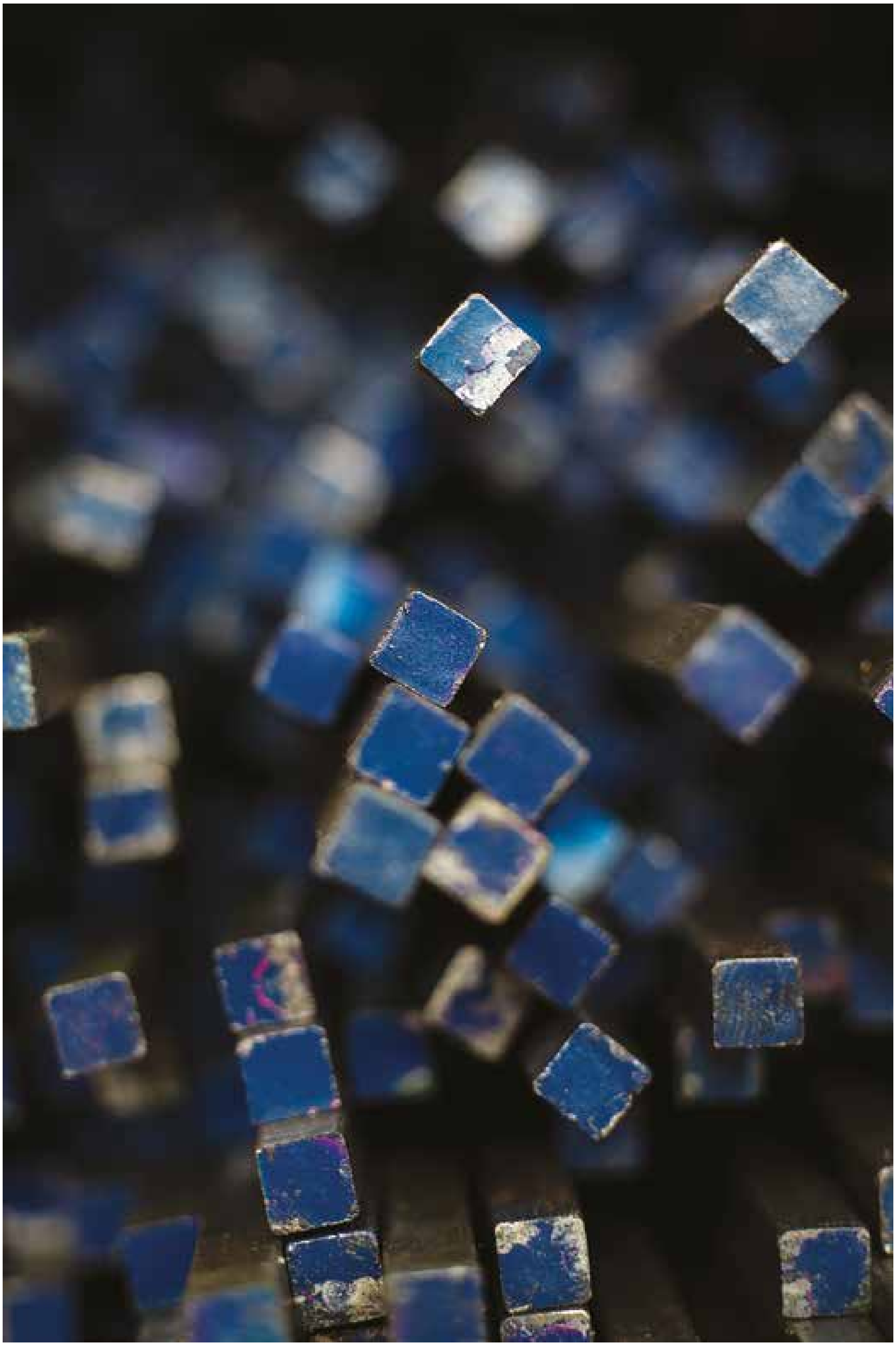

Each book - and this is not a flaw - is "alive",
and wishes to continue to live.

For this to occur, your help is needed.
Any suggestions or advice you would like to give us,
and any images or micrographs you would like to send us,
will be well accepted and very appreciated.
You will help us improve the quality of the next edition.

We urge you to write to the following addresses:
marco.boniardi@polimi.it and andrea.casaroli@polimi.it

Thank you everyone in advance... for everything!

1. IRON AND ITS CRYSTAL STRUCTURE

1.1 What is iron?

Iron (symbol: *Fe*) is a metal chemical element belonging to the eighth group of the periodic system (transition metals), with atomic number 26, an atomic mass of 55.847 amu1[1], and an atomic radius at room temperature of 0.124 nm.

Iron is one of the chemical species most commonly found on the Earth's crust, second only to aluminum. It has a melting temperature of 1,538°C and a density of about 7,870 kg/m^3. It is a ferromagnetic metal and its magnetic behavior decreases as temperature increases, until it cancels itself out at 770°C (Curie temperature). The thermal conductivity of iron at room temperature is in the order of 80 W/mK, while its electrical conductivity is approximately $10 \cdot 10^6$ $(\Omega m)^{-1}$.

Iron, like most pure metals, has no significant mechanical properties. The ultimate tensile strength ranges between 250 and 270 MPa, while hardness is between 70 and 80 HB.

The main physical and mechanical properties of pure iron are shown in Table 1.1.

Physical and mechanical properties of pure iron[1]	
Atomic number	26
Atomic mass [amu]	55.85
Number of protons/electrons	26
Number of neutrons	30
Symbol	*Fe*
Color	silvery gray
Density ρ [kg/m^3]	7,860 -7,875
Electro-negativity [Pauling scale]	1.83
Melting temperature [°C]	1,538
Boiling temperature [°C]	2,750-2,870
Specific heat [J/kg·K]	440-450

Physical and mechanical properties of pure iron[1]	
Electrical conductivity $[\Omega \cdot m]^{-1}$	$9.90 \cdot 10^6$-$10.4 \cdot 10^6$
Thermal conductivity [W/m·K]	79.5-80.4
Linear thermal expansion [μm/m·K]	11.7-1.8
Speed of sound [m/s]	4,910-5,120
Mohs Hardness [Mohs scale]	4
Longitudinal elastic module E [GPa]	196-205
Transverse Elastic Module G [GPa]	79-82
Ultimate tensile strength [MPa]	250-270
Yield stress [MPa]	80-120
Elongation at fracture [%]	40-60
Brinell Hardness [HB]	70-80

[1] Unless specified otherwise, they are measured at 20°C and at atmospheric pressure.

Table 1.1 - Physical and mechanical properties of pure iron.

---

[1] *L'amu (atomic mass unit) is the unit of measure used to express the mass of atoms or of their molecules.The amu is defined as the twelfth part of the mass of a carbon-12 atom and corresponds to $1.660538921 \cdot 10^{-27}$ kg. This unit of measure is convenient because, in general, each atom has a mass equal to the sum of its protons and neutrons. Therefore, with carbon having 6 protons, 6 neutrons, and 6 electrons, it has an atomic mass of about 12 amu (electrons have a negligible mass), while hydrogen, with only one proton, has an atomic mass equal to 1 amu.*

The chemical bond that allows iron atoms to join together is referred to as a metal bond: it has peculiar characteristics that are very different from those of the ion bond or the covalent bond, typical of non-metal solids (ceramic materials and polymeric materials).

Let us see in detail what a metal bond is.

Iron, like most of the so-called "metal elements" of the periodic table, has a limited number of electrons in its outer orbit (valence electrons).This leads to the element having a low electronegativity and a reduced ionization energy and, therefore, it can easily lose its valence electrons (in the case of iron, these are generally two electrons).

The metal bond develops when valence electrons reach energy levels above a given threshold, called the Fermi level. The electrons are separated from the original atoms and generate a cloud with a negative charge that surrounds all the iron cations (that is, all the iron atoms that have lost their valence electrons and, consequently, gained a positive charge).

Iron cations occupy positions of equilibrium in space and are surrounded by an electronic cloud formed by all the valence electrons. The cloud of delocalized electrons (or electronic gas) is the adhesive that holds the iron cation system together. The binding energy derives from the electromagnetic interaction between the negative charges of the valence electrons and the positive charges of the iron cations. An exemplification of the crystal obtained in relation to the model described is shown in Figure 1.1.

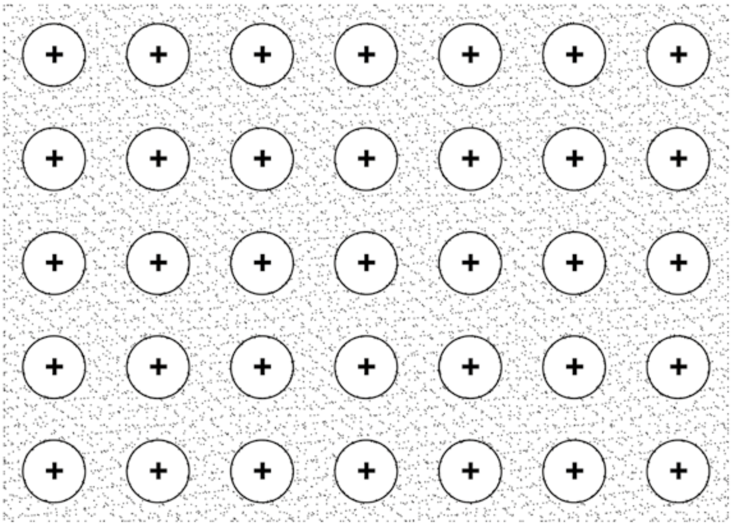

Figura 1.1 – Schematic representation of the metal bond of an iron crystal.

The metal bond model allows to explain many physical and mechanical properties of iron and of metallic materials. For example, thermal conductivity and electrical conductivity are closely related to the presence of the cloud of valence electrons. Not being directly involved in the bond between one atom and another, delocalized electrons can move freely in space, and their mobility explains the phenomenon of the transfer of thermal and electrical energy in metals and alloys[2].

This also makes sense in relation to the fact that iron, and all metal materials, has the ability to reflect light: this is due to the interaction of the photons from light radiation with the electronic cloud that surrounds the iron cations.

The mobility of the valence electrons always justifies, at least partially, the characteristics of ductility and malleability of iron and of metal materials, in general[3]. Since there are no localized links between the various iron atoms that would stiffen the structure, if we apply a shear stress to the lattice, the cations slide with respect to each other within the cloud of electric charges that, like a gelatinous adhesive, holds together the system. On the contrary, in ceramic materials, the same deformation mode is prevented and the fragile fracture is observe, due to the repulsion between electric charges that are the same (Figure 1.2).

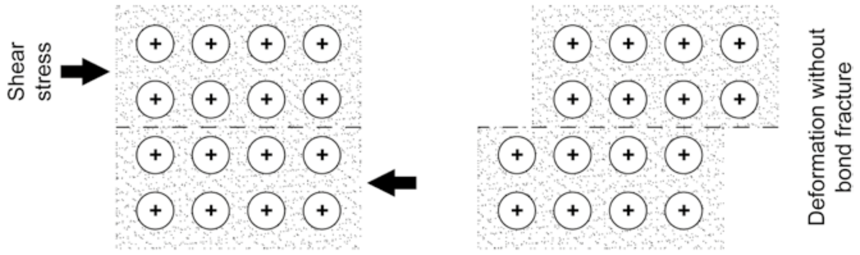

Solid with metallic bond

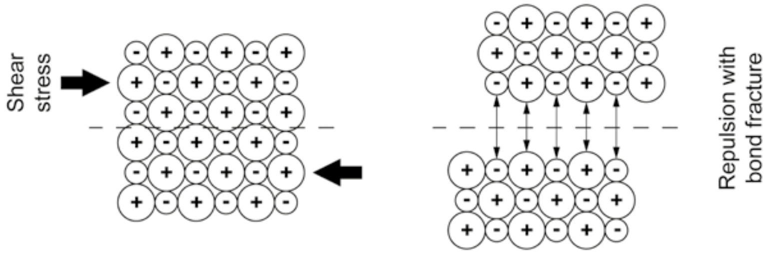

Solid with ionic bond

Figure 1.2 - Schematic representation of the plastic deformation mechanism of a solid with a metal bond (above) and of the fragile fracture of a solid with an ion bond (below).

---

[2] *Polymeric materials and ceramic materials generally have poor electrical and thermal conductivity, due to the covalent or ion bond that keeps the electrons of the outer orbits engaged in the bond.*

[3] *Ductility is defined as the capacity of a metal (or metal alloy) to be reduced to wires. Malleability, on the other hand, describes the aptitude to be reduced to plates. Both properties are closely related to the deformability of the metal mass.*

1.2 Crystal lattices of iron

The position of iron atoms[4] in space is not random but follows a well-defined order. In particular, a basic arrangement of a certain number of atoms is always detectable and is repeated indefinitely in the three dimensions.

The base unit of this regular repetition is called elementary unit cell. By multiplying the unit cell in space, the crystal (or crystallite) of the metal material is obtained. The elementary unit cell is, therefore, the smallest set of atoms that, repeated in the three dimensions, generates the entire crystal structure (Figure 1.3).

This repetitive structure is typical of metal materials, and it is the characteristic feature of all crystal solids[5].

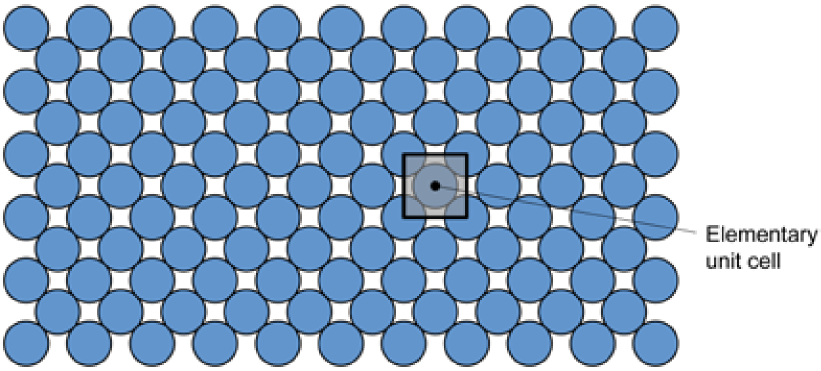

Figure 1.3 - Schematic representation of a metal lattice. Atoms are represented by the rigid sphere model.

By placing many identical unit cells next to each other, an actual crystallographic building can be created, called a crystallite. This is somewhat like piling many identical bricks onto each other, therefore, constructing the wall of a building (Figure 1.4).

The unit cell of iron does not always have the same characteristics. Iron is, in fact, a polymorphic metal. Its lattice takes on various shapes, called allotropic forms, as temperature varies.

Continuing with the analogy of the construction industry, it can be said that the elementary unit cells of iron are not all the same, yet, just like the bricks that form the walls of a building, they may have very different characteristics among themselves.

---

[4] *In the continuation of the discussion, the term "iron atoms" will always be used, as is customary in the metallurgic field. However, in fact, we are speaking of iron cations, that is, of iron atoms that have surrendered valence electrons to the electronic gas that surrounds them.*

[5] *The term, crystalline solids, is used because the spatial regularity of the crystal is a common element, not only to metal materials, but also in many ceramic materials and some polymeric materials. Glass, on the contrary, is an amorphous solid, that is, non-crystalline. Its atoms are randomly arranged in space without a well-defined regularity, not even at short-range.*

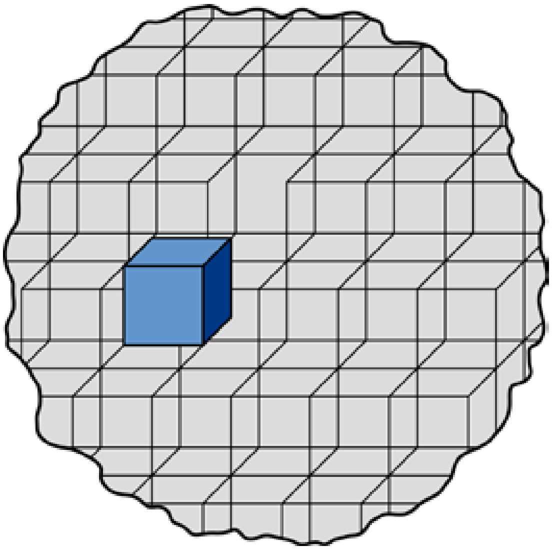

Figure 1.4 - Schematic representation of the elementary unit cell (brick) and the crystallite (wall).

The material used for making bricks - the iron atoms - is the same, but the bricks - the unit cells - can be of different types: full bricks, semi-full bricks, perforated bricks, etc. Therefore, the walls, meaning the supporting structure of the metal mass, can be constructed using bricks that are full, semi-full, perforated, and so on.

At atmospheric pressure, there are two allotropic forms of iron: two different unit cells where the iron atoms are arranged in space[6]. This is the elementary unit cell with a body-centered cubic lattice and the elementary unit cell with a face-centered cubic lattice. Usually, we speak of B.C.C. and F.C.C. cells or lattices, also called α-iron (or δ-iron)[7] and γ-iron. In both cases, however, these are cubic cells in which the side, indicated by the letter " a ", is called the lattice parameter.

The graphic representation of the two iron lattices, using the rigid sphere atomic model[8], is shown in Figure 1.5.

---

[6] *If, in addition to temperature, the variable pressure is also considered, a third allotropic form can be observed for iron, called ε-iron, with a compact hexagonal lattice, existing at room temperature for pressures greater than 100,000 bar.*

[7] *One of the two allotropic forms of iron, exists in two different temperature ranges. This is the body-centered cubic lattice (B.C.C.), called α-iron, between 20°C and 912°C or δ-iron, between 1,394°C and 1,538°C. The name changes (α-iron or δ-iron), but the characteristics of the lattice are the same. By contrast, γ-iron, with a face-centered cubic lattice (F.C.C.), only exists between 912°C and 1,394°C.*

[8] *This is a simple representation method where the atoms are assimilated to rigid spheres having a radius equal to the atomic radius of the chemical element.*

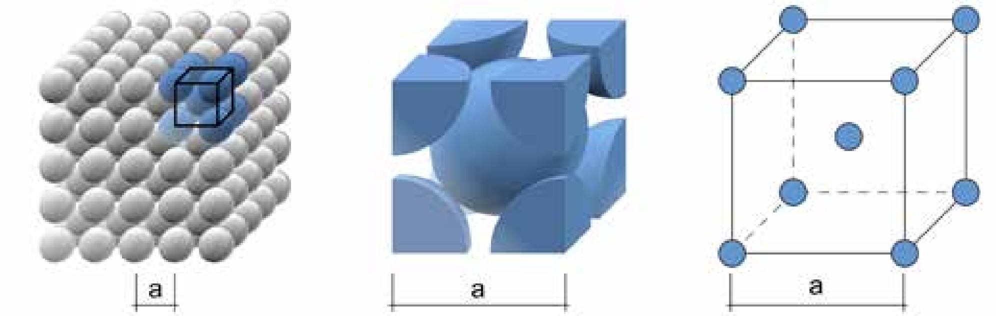

Body-centered cubic lattice (B.C.C.)

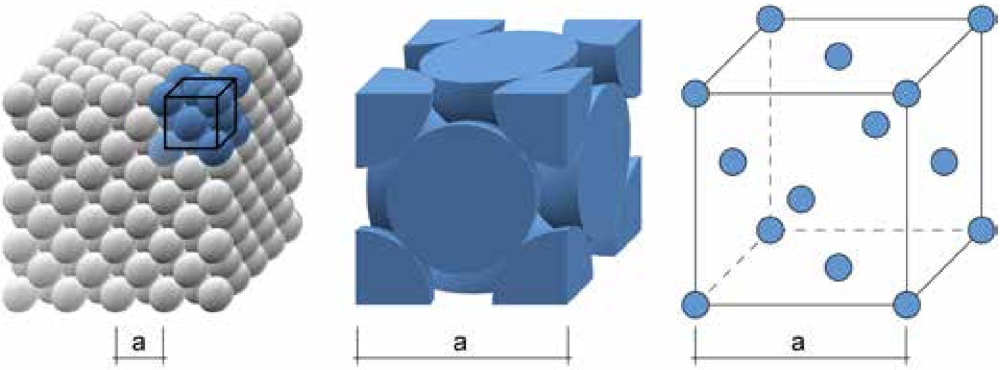

Face-centered cubic lattice (F.C.C.)

Figure 1.5 - Elementary unit cell of the body-centered cubic lattice (above) and elementary unit cell of the face-centered cubic lattice (below) [from Callister 2007].

1.3 Characteristics of iron lattices

The B.C.C. unit cell has an iron atom at the center of the cube. Around it there are eight iron atoms (four above and four below) located at each of the eight vertices of the cell. In the body-centered cubic system, the rigid spheres, representing the iron atoms, are tangent among each other at the diagonal of the cube[9]. On the contrary, in the F.C.C. unit cell, an iron atom is centered on each of the six sides of the cube. Also, in this second case, there are eight iron atoms at each of the eight vertices of the cube. However, in the face-centered cubic system, the contact between the iron atoms takes place along the diagonals of the sides of the cube.

---

[9] *Being a the side of the unit cell (or lattice parameter), the diagonal of each of the side of the cube equals* $a\sqrt{2}$ *while the diagonal of the cube equals* $a\sqrt{3}$.

Taking into account the ray R of the atom and the diagonals along which the atoms touch, through simple geometric calculations, the value of length a of the side of the cell can be obtained. The cell side is $a \cong 2{,}309\ R$ for the B.C.C. lattice and $a \cong 2{,}828\ R$ for the F.C.C. lattice.

Consequently, at the same atomic radius R, volume a^3 of the body-centered cubic cell is much less than the volume of the face-centered cubic cell ($V_{B.C.C.} \cong 12.32\ R^3$ and $V_{F.C.C.} \cong 22.63\ R^3$).

However, the F.C.C. cell contains its own double number of atoms as compared to the B.C.C. cell: four atoms for the face-centered cubic cell, two for the body-centered cubic cell[10].

As a result the so-called, Atomic Packing Factor (A.P.F.) of the cell[11], or the volume of the cell that is actually occupied by its atoms, is greater in the case of the F.C.C. cell (~74%) than that of the B.C.C. cell (~68%). Therefore, the face-centered cubic cell is slightly denser (i.e. more constrained by its atoms) as compared to the body-centered cubic cell, although the latter occupies a much smaller volume in space.

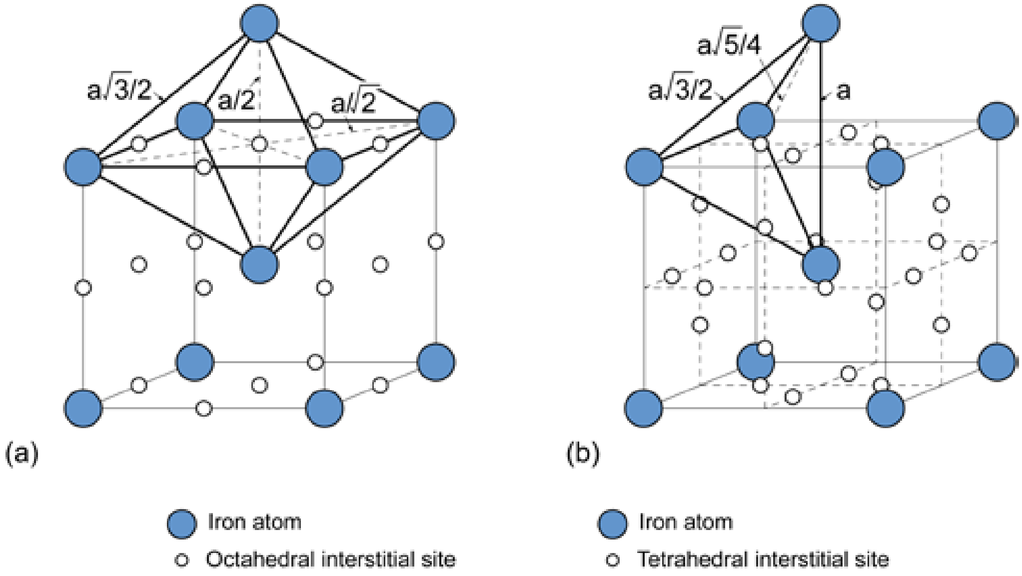

Figure 1.6 - (a) octahedral interstitial site and (b) tetrahedral interstitial site of the body-centered cubic lattice [from Krauss 2005].

---

[10] *In the B.C.C. system, there is an atom at the center of the cell (1) and eight atoms at the eight vertices of the cell shared with other eight adjacent cells (8 ·1/8 = 1): total of two atoms (1 + 1). In the F.C.C. system, however, there are six atoms on the six sides of the cell, is shared with the adjacent cells (6 ·1/2 = 3) and eight atoms at the eight vertices of the cell shared with another eight adjacent cells (8 ·1/8 = 1): total of four atoms (3 + 1).*

[11] *The "Atomic Packing Factor" is the level of atomic compaction of the cell.*

Another important aspect to consider is the free space within the lattice: these portions of cell volume not occupied by atoms are called interstitial sites. Octahedral and tetrahedral interstitial sites of the body-centered cubic cell and the face-centered cubic cell are shown in Figures 1.6 and 1.7. The white balls identify the center of the various interstitial sites, while the blue balls represent the iron atoms of the lattice[12].

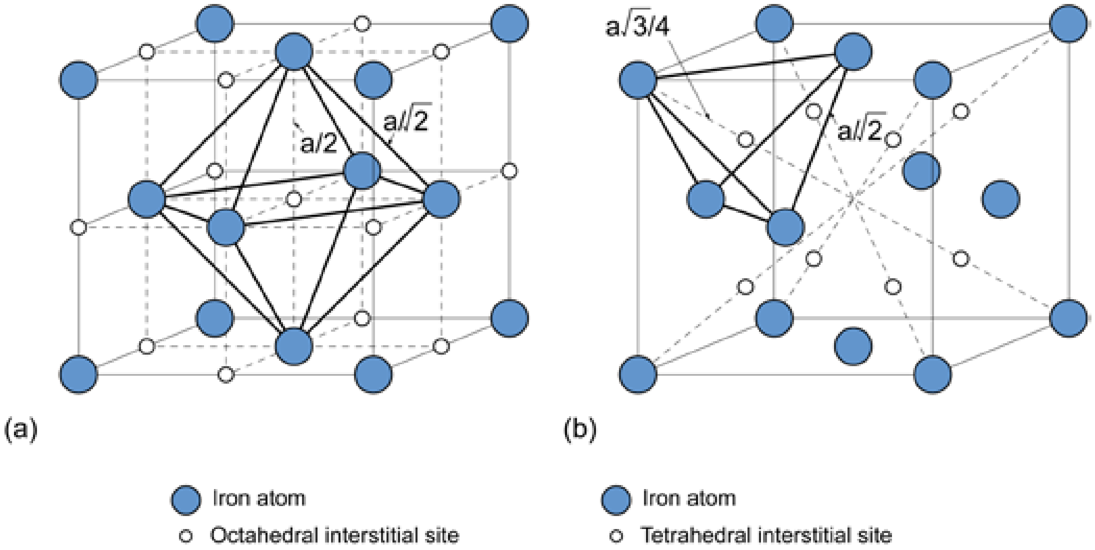

Figure 1.7 - (a) octahedral interstitial sites and (b) tetrahedral interstitial sites of the face-centered cubic lattice [from Krauss 2005].

If on one hand the face-centered cubic lattice has a interstitial site with the greatest absolute volume (the octahedral interstitial site at the center of the cell), on the other hand, the body-centered cubic lattice has the largest total number of interstitial sites (B.C.C.: 6 octahedral interstitial sites + 12 tetrahedral interstitial sites; F.C.C.: 4 octahedral interstitial sites + 8 tetrahedral interstitial sites).

The set of characteristics of the two iron lattices are found in Table 1.2.

---

[12] *The interstitial sites in crystal lattices are called octahedral or tetrahedral in relation to the geometric characteristics of the solid that delimits the portion of space not occupied by the atoms of the lattice. The vertices of this solid are the iron atoms around the interstitial site.*

Characteristic parameters of the iron crystal lattice

	α-Iron (20°C - 912°C)	γ-Iron (912°C - 1,394°C)	δ-Iron (1,394°C - 1,538°C)
Atomic Radius R [Nm]	0.124 - 0.126	0.126 - 0.127	0.127
Type of lattice	B.C.C.	F.C.C.	B.C.C.
Theoric lattice constant a [nm] as a function of R	$(4/\sqrt{3})\ R \cong 0.286 - 0.290$	$(4/\sqrt{2})R \cong 0.356 - 0.359$	$(4/\sqrt{3})R \cong 0.293$
Experimental lattice constant a [nm]	~0.287 at 20°C ~0.291 at 912°C	~0.369 at 912°C ~0.373 at 1394°C	~0.293 at 1394°C ~0.294 at 1538°C
Number of atoms (N_A) per cell	$1 + 8 \cdot \frac{1}{8} = 2$	$6 \cdot \frac{1}{2} + 8 \cdot \frac{1}{8} = 4$	$1 + 8 \cdot \frac{1}{8} = 2$
Atom volume (V_A) as a function of R	$\frac{4}{3}\ \pi R^3$	$\frac{4}{3}\ \pi R^3$	$\frac{4}{3}\ \pi R^3$
Cell volume (V_C) as a function of R	$\frac{64\sqrt{3}}{9}\ R^3$	$16\sqrt{2}R^3$	$\frac{64\sqrt{3}}{9}\ R^3$
Atomic Packing Factor ($N_A V_A/V_C$)	~0.68	~0.74	~0.68
Number of octahedral interstitial sites per cell	6	4	6
Number of tetrahedral interstitial sites per cell	12	8	12
Radius of the octahedral interstitial site [nm] as a function of R	$0{,}155R \cong 0{,}0194$	$0{,}414R \cong 0{,}0524$	$0{,}155R \cong 0{,}0197$
Radius of the tetrahedral interstitial site [nm] as a function of R	$0{,}291R \cong 0{,}0364$	$0{,}225R \cong 0{,}0285$	$0{,}291R \cong 0{,}0370$

Table 1.2 - Parameters of the body-centered cubic lattice (B.C.C.) and of the face-centered cubic lattice (F.C.C.) of pure iron.

1.4 Allotropic transformations of iron

The aggregation of iron atoms, according to the B.C.C. lattice or F.C.C. lattice is not random, but it is a function of temperature.

To understand what is really occurring, we put an iron bar to heat slowly from room temperature, until it melts. We, then, cool it down very slowly[13]. Figure 1.8 shows the iron bar temperature over time.

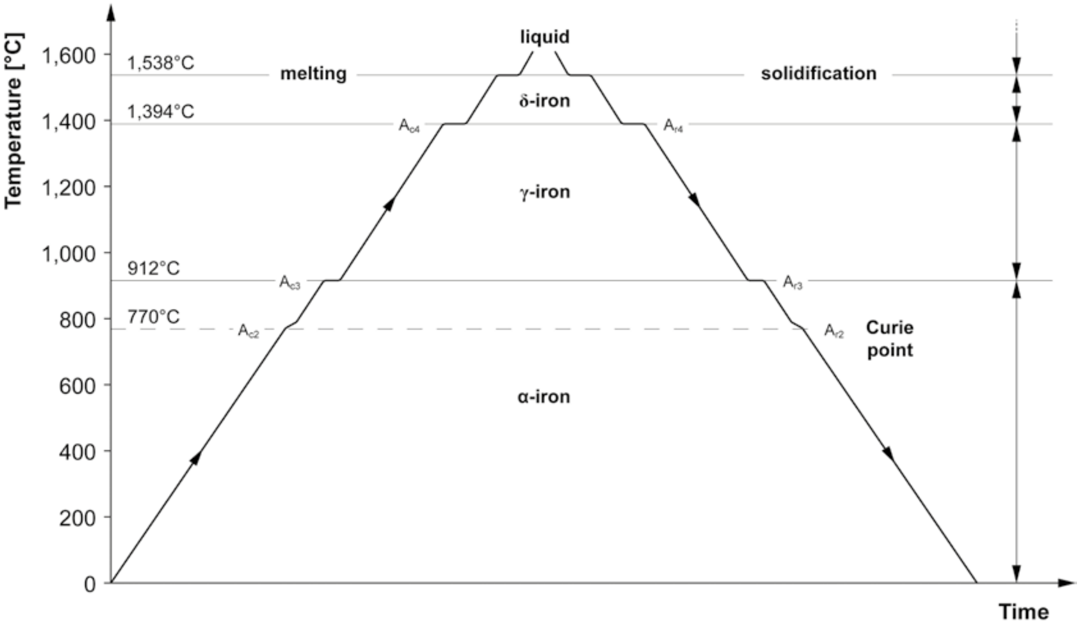

Figure 1.8 - Heating and cooling of an iron bar with indication of the critical points [from Thelning 1975].

Both in heating and cooling, the curve shows three points (912°C, 1,394°C, 1,538°C), where the temperature remains constant over a short interval of time. These temperatures, called critical points, indicate the allotropic transformations temperature of iron, that is, the transformations temperatures of the iron lattice (critical point A_3 = 912°C; critical point A_4 = 1,394°C; melting temperature T_f = 1,538°C).

---

[13] *If heating and cooling are very slowly, we can speak of equilibrium transformations. In these cases, the change in temperature* T*, in time* t*, tends towards zero: resulting in* $dT/dt \rightarrow 0$*. During equilibrium transformations, heat is supplied or subtracted from the system very slowly, giving the system time to return to the states of equilibrium, that is, in a state where pressure and temperature are equal at all the points in space, and the homogeneous portions of matter (phases) have the same chemical composition.*

Starting from room temperature until the liquid state is reached, pure iron has[14]:

- a body-centered cubic lattice cell (B.C.C.) from 20°C up to 912°C (called: α-iron);
- a face-centered cubic lattice cell (F.C.C.) from 912°C to 1,394°C (called: γ-iron);
- a body-centered cubic lattice cell (B.C.C.) from 1,394°C to 1,538°C, (called: δ-iron);
- liquid state above 1,538°C.

Further observations are required, in order to explain some of the peculiarity of the curve in Figure 1.8.

First of all, the allotropic transformations of iron always involve the absorption of heat from the surrounding environment if they occur during heating, or heat transfer to the surrounding environment if they occur during cooling. Consequently, thermostatation (temperature stop) are always observed at critical points, both for heating and cooling. In summary, allotropic transformations of iron occur at a constant temperature, analogous to what occurs with the changes of the aggregation state of pure substances[15].

In addition to the three critical points already mentioned, a further discontinuity at 770°C can be observed: this temperature, called the Curie point, does not represent an allotropic transformation, but the change in behavior of iron from iron magnetic ($T < 770$°C) to paramagnetic ($T > 770$°C)[16].

All critical points are indicated by the letter A (from the French*, arrêter* = to interrupt, suspend) and by a progressive number (1, 2, 3, and 4). There is also the letter c if the measurement of the critical point occurred when heating (*chauffer* = to heat), or the letter r when cooling (*refroidir* = to cool).

Lastly, let us consider that the distinction between δ-iron and α-iron is only formal having, in both cases, the same B.C.C. crystal lattice. In this respect, Figure 1.9 shows the trend of lattice parameter a for the three allotropic forms of iron (α, γ, and δ) when temperature changes.

---

[14] *Referring to the critical points of iron and of iron-carbon alloys, numerous references are available in literature, often slightly different from each other. In this discussion, the decision was made to follow what was proposed in [Chipman 1972]. The data indicated therein are also taken up in [Abbaschian et al.2009] and in [Krauss 2005].The indications proposed, on the other hand, are those commonly used in Italy in university textbooks, as in [Nicodemi 2007].*

[15] *During allotropic transformations ($\alpha \leftrightarrow \gamma$; $\gamma \leftrightarrow \delta$; $\delta \leftrightarrow$ liquid) the bar of iron, when heated, absorbs a portion of heat from the system called latent heat, in order to allow the allotropic transformation to take place (however, in cooling, there is a transfer of latent heat from the bar of iron to the system). As a result, at the allotropic transformation temperature (at heating or at cooling), a discontinuity in the linear progression of the temperature is observed over time. A bit like what occurs with pure water, which undergoes evaporation at 100°C: at this temperature, the thermostatation of the system occurs, caused by the release of the latent heat of the phase change (from gas to liquid).*

[16] *At the dawn of scientific studies in the metallurgic field, it was mistakenly believed that at 770°C (critical point A_2), there was another allotropic transformation, stable up to 912°C, which was indicated as iron ß.*

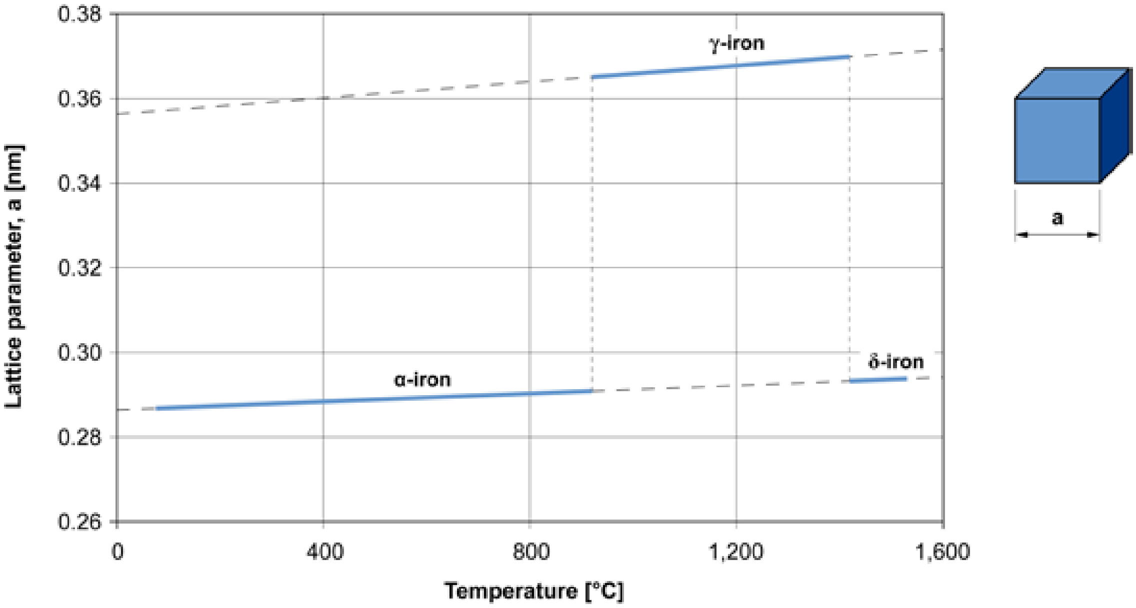

Figure 1.9 - The effect of temperature on the lattice paramiter *a* [from Onink et al.1993].

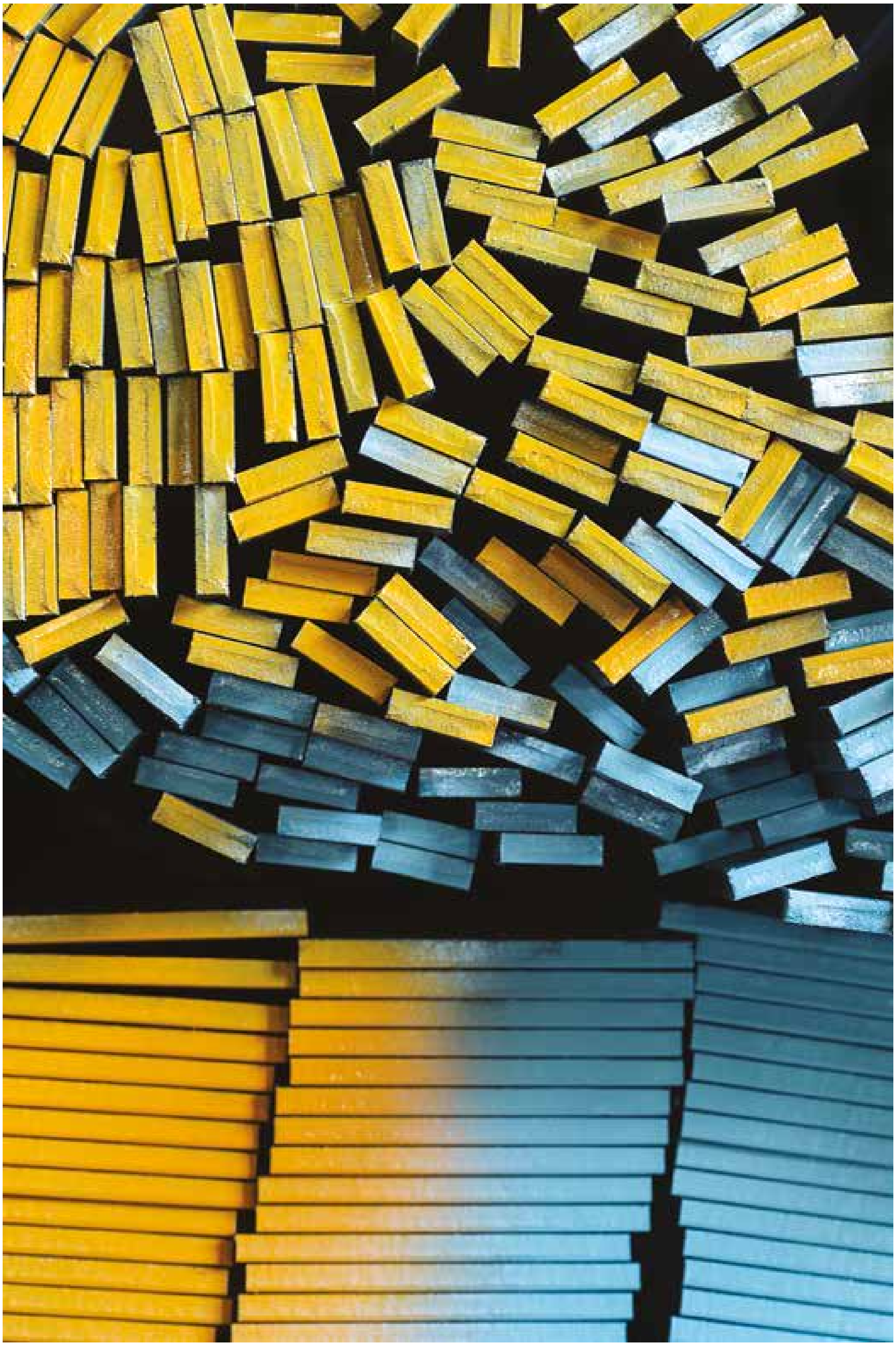

2. DEFECTS OF THE CRYSTAL LATTICE

2.1 Classification of crystal lattice defects

The crystal lattice of iron, as ideally shown in Chapter 1, should have a regular and orderly geometry in space. In practice, however, all metals and all real metal alloys always have a certain number of defects, namely areas where the original order of the lattice disappears[1].

Some types of lattice defects are a result of the entropy[2] of the system and, therefore, increase when the temperature increases: these defects are called "thermodynamic equilibrium defects". At absolute zero, thermodynamic equilibrium defects can be considered absent while, for temperatures that are on a constant increase, a progressive increase of their number is observed, as a consequence of the increase in energy of the system, that is, the thermal agitation of the atoms.

Most other defects, are deemed "not in thermodynamic equilibrium" and their numbers do not increase when temperature increases although, if required, their sized and distribution can be modified through appropriate heat treatments.

Another classification is related to the dimensional characteristics of lattice defects. Four different types can be distinguished:

- point defects (zero-dimensional defects);
- line defects (one-dimensional defects);
- surface defects (two-dimensional defects);
- volume defects (three-dimensional defects).

2.2 Point defects

Point defects are an atomic discontinuity and are normally associated with one or two atomic positions. All point defects are thermodynamic equilibrium defects.

The main types of point defects are:

- vacancies;
- substitutional atoms;
- interstitial atoms.

---

[1] *Generally, in common language, a negative connotation is given to the term "defect". In the case of crystal lattices, however, the term only indicates a lack of regularity. Sometimes, there are negative effects and, therefore, the defect is a defect in its full sense. In other cases, defects guarantees benefits to the metal mass.*

[2] *In statistical mechanics, entropy is a physical quantity of a system state indicated by the letter S. This represents a measure of the disorder of any system. An increase in the disorder of the system is associated with an increase in entropy, while a decrease in disorder leads to a decrease in entropy.*

A first kind of point defect is the vacancy, that is, a lack of an iron atom within the regular crystal lattice. The consequence of a vacancy is the movement of the surrounding atoms from their original position to compensate the electromagnetic vacuum, locally generating a distortion of the lattice (Figure 2.1).

Vacancies are point defects that originate mainly during solidification, plastic deformation, or heat treatment of steel.

The presence of vacancies, along with lattice interstitial sites, explains the movement of the atoms within the metal lattices.This phenomenon, called diffusion, is important for understanding many issues of a metallurgic nature[3].

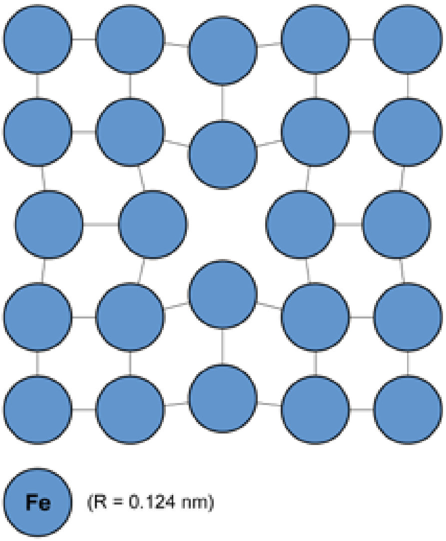

Figure 2.1 - Example a vacancy in a crystal lattice.

A second type of point defect is the substitutional atom. This defect is present when one or more atoms of the iron lattice are replaced with atoms of other chemical elements having an atomic radius comparable to the atomic radius of iron (R_{Fe} = 0.124 nm). Typical examples of substitutional atoms in the iron lattice are nickel (R_{Ni} = 0.124 nm), chromium (R_{Cr} = 0.125 nm), molybdenum (R_{Mo} = 0,136 nm), vanadium (R_V = 0.131 nm), manganese (R_{Mn} = 0.126 nm), aluminum (R_{Al} = 0.143 nm), and silicon (R_{Si} = 0.117 nm). The example of this defect is shown in Figure 2.2.

---

[3] *For a broad discussion on diffusion and subsequent phenomena, see Chapter 3.*

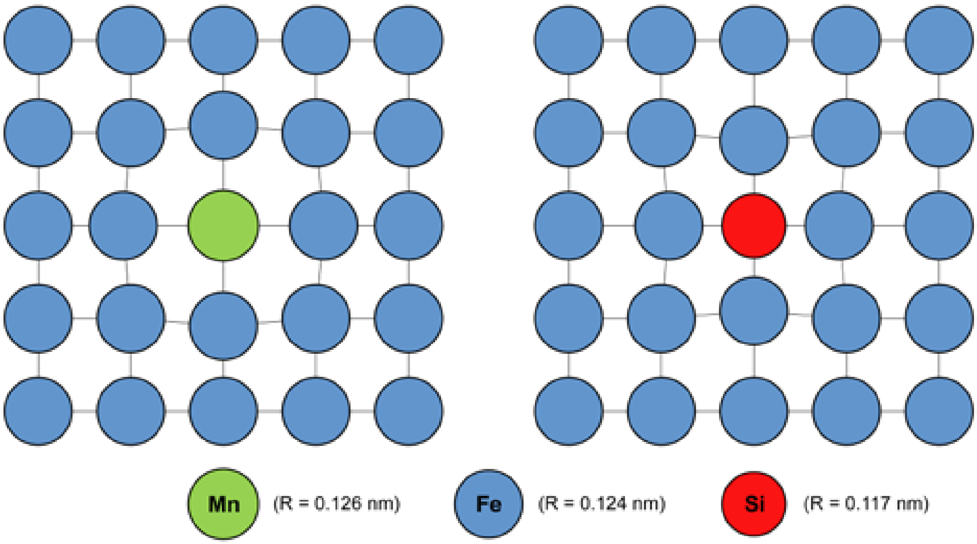

Figure 2.2 - Examples of substitutional atoms in the iron crystal lattice. Manganese, an atom that is larger than an iron atom (left); silicon, an atom that is smaller than an iron atom (right).

The last type of point defect to be examined is the interstitial atom. This defect is present when an atom outside the iron lattice slides into the lattice interstitial sites, that is, into the spaces left between the iron atoms.

The foreign atom must have an atomic radius much smaller than the atomic radius of iron, as is typical with carbon (R_C = 0.077 nm), nitrogen (R_N = 0.070 nm), oxygen (R_O = 0.066 nm), hydrogen (R_H = 0.030 nm). Only small atoms have the potential to occupy the interstitial spaces of F.C.C. or B.C.C. cells, i.e. the tetrahedral and octahedral interstitial sites in the iron lattice (Figure 2.3).

2.3 Solid solutions and compounds

Point defects (vacancies, substitutional atoms, and interstitial atoms) are important to explain the existence of steel and metal alloys, in general. Steel, as is known, is an alloy of iron and carbon. In many cases, in addition to carbon, it contains other alloying elements.

Let us understand how this can occur. Steel can be thought of as a lattice of iron atoms with interstitial atoms of carbon. One can imagine that iron is the solvent while carbon is the solute that dissolves in the iron lattice. This is somewhat like sugar that is dissolved in water, resulting in a more or less sweet water solution, depending on the greater or lesser quantity of sugar. It is no coincidence that, referring to steel, the solid solution of carbon in iron is mentioned.

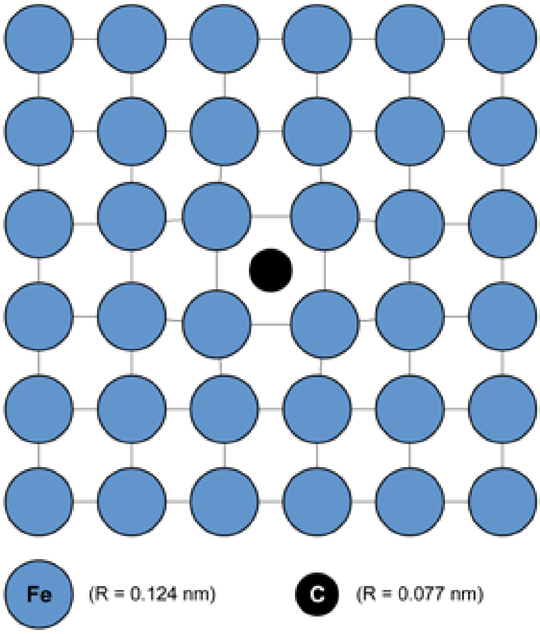

Figure 2.3 - Example of an interstitial atom in the crystal lattice of iron.

The presence of other alloying elements other than carbon, such as manganese, silicon, nickel, chromium, molybdenum, or vanadium, can be explained with the concept of the substitutional atom. Also in this case, iron is the solvent and the alloy elements are the solute that dissolves in the lattice.
Therefore, at a first approximation, steel can be conceived as a solid solution of carbon and other chemical elements in iron[4]. The iron lattice is partially filled with carbon in the form of interstitial atoms and partially replaced with other chemical elements in the form of substitutional atoms (Figure 2.4).

In addition, it should be noted that, as is the case for the liquid solution of water and sugar, even solid solutions have solubility limits for the solute in the solvent, depending on the temperature. Beyond the solubility limit, it is no longer possible to dissolve sugar in water and the sugar precipitates to the bottom of the container. Something similar is also true for the iron lattice when adding carbon and/or other alloying elements beyond the solubility limit.

---

[4] *This is true only at a high temperature (i.e. at 1,000°C), a condition where carbon, in the normal content of steel, is completely in solution in the lattice of γ-iron. When temperature decreases, the carbon solubility in the iron lattice is greatly reduced, and the schematic illustration indicated is no longer true.*

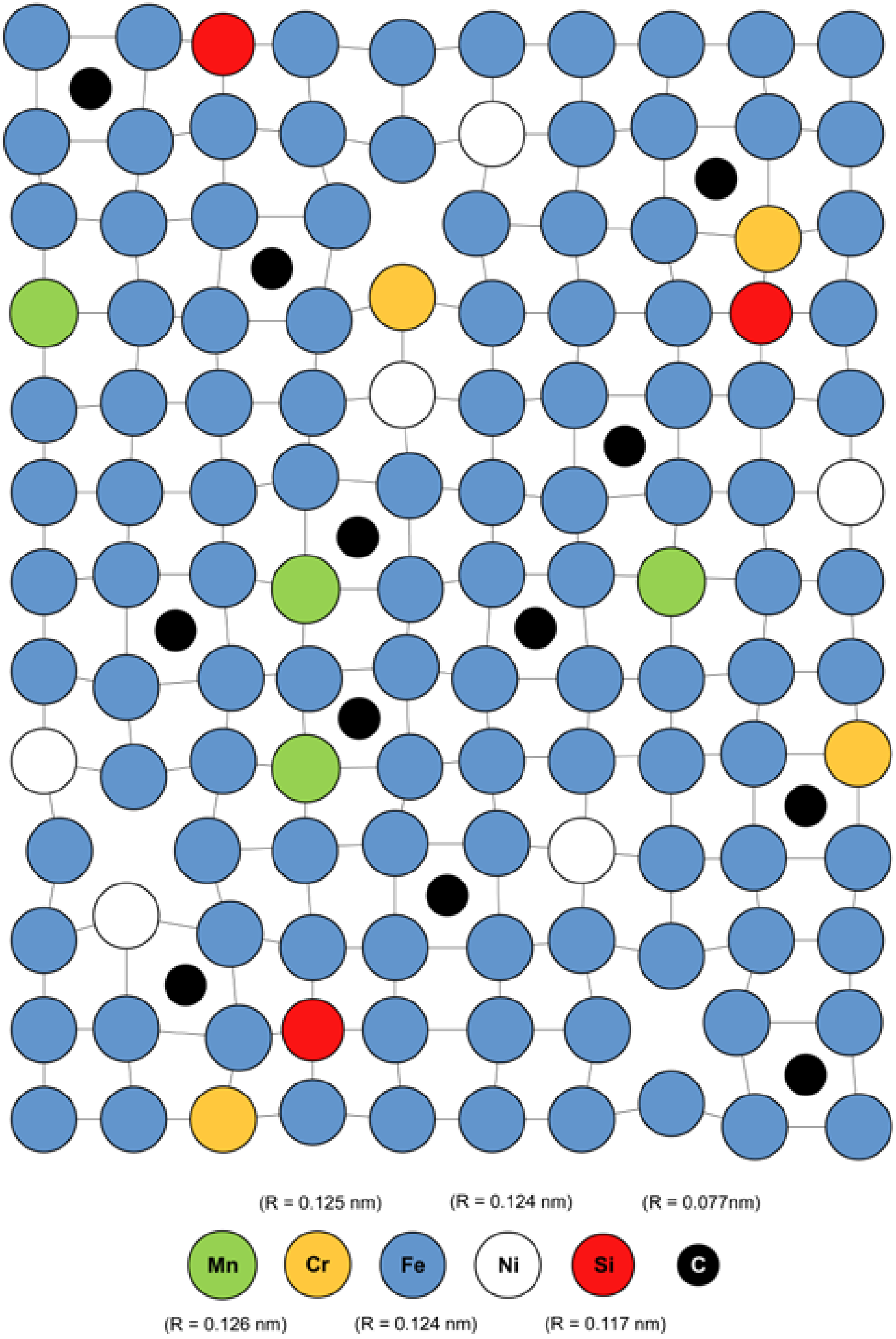

Figure 2.4 - Example of a solid solution of iron, carbon, and other alloying elements (steel).

The carbon case is typical. After exceeding a given composite threshold, it is no longer possible to insert additional carbon atoms into the iron lattice. Beyond the solubility limit, a chemical compound is formed between iron and carbon in the steel, called iron carbide, with stoichiometry Fe_3C.

The solubility of carbon in iron is highly dependent on the characteristics of the crystal lattice. In γ-iron (F.C.C. lattice), it is easier to fill carbon atoms because interstitial sites are larger than those of α-iron (B.C.C. lattice). The B.C.C. lattice has great difficulty in accepting carbon atoms inside it, precisely because the lattice interstitial sites are very small in size.

Consequently, the carbon solubility limit is higher for F.C.C. systems than for B.C.C. systems: at a temperature of 727°C, for example, the carbon solubility limit in γ-iron is equal to 0.77% and in α-iron it is equal to 0.02%[5]. Carbon solubility is also a function of temperature. As can be seen from Figure 2.5, the carbon solubility in the α-iron lattice at room temperature is virtually nil, while it is in the order of 0.02% at a temperature of 727°C.

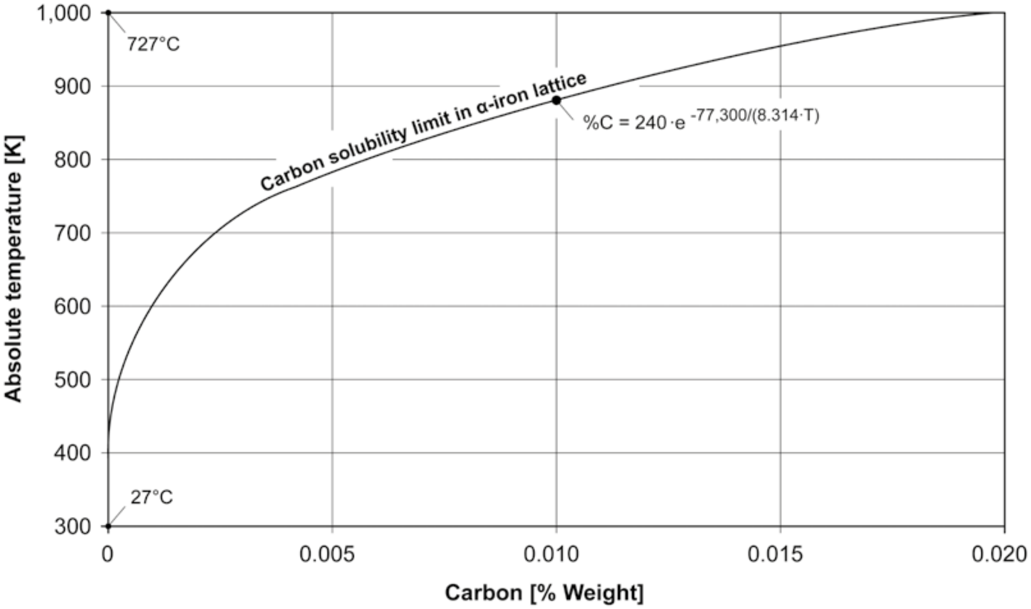

Figure 2.5 - Carbon solubility limit in α-iron lattice [from Abbaschian et al.2009].

---

[5] *The transformation of the steel from γ-lattice ($C = 0.77\%$) to α-lattice ($C = 0.02\%$) plus iron carbides of Fe_3C type ($C = 6.69\%$) occurs at 727°C.*

In addition to iron carbide, Fe_3C, many other chemical compounds[6] can also be present in steel.

The compounds are divided into two categories: interstitial compounds when formed between a metal and a non-metal, and intermetallic compounds when formed between two metals. Rather common in steel are interstitial compounds, such as carbides, nitrides, sulphides, and oxides. The case of intermetallic compounds is less common.

Iron can form all four types of interstitial compounds mentioned above: carbides, (Fe_3C, $Fe_{2,4}C$), nitrides (Fe_4N, $Fe_{2\text{-}3}N$), sulphides (FeS), oxides (FeO, Fe_2O_3, Fe_3O_4). In addition, many alloying elements may also form interstitial compounds, such as[7]:

- *Ti*, *V*, *Mo*, *W*, and *Cr* for the formation of carbides;
- *Ti*, *Al*, *V*, *Mo*, and *Cr* for the formation of nitrides;
- *Cr*, *Al*, *Si*, and *Mn* for the formation of oxides;
- *Mo*, *Cr*, and *Mn* for the formation of sulphides.

Frequently, compounds are not formed by only one metal and/or one non-metal. Two or more metals in combination with two or more non-metals can contribute to the formation of compounds, as in the case of iron carbonitrile, $Fe_{2\text{-}3}(CN)$, of iron-silicon oxide, $2(FeO)\cdot SiO_2$, or of manganese oxide sulphide, $MnS\cdot MnO$.

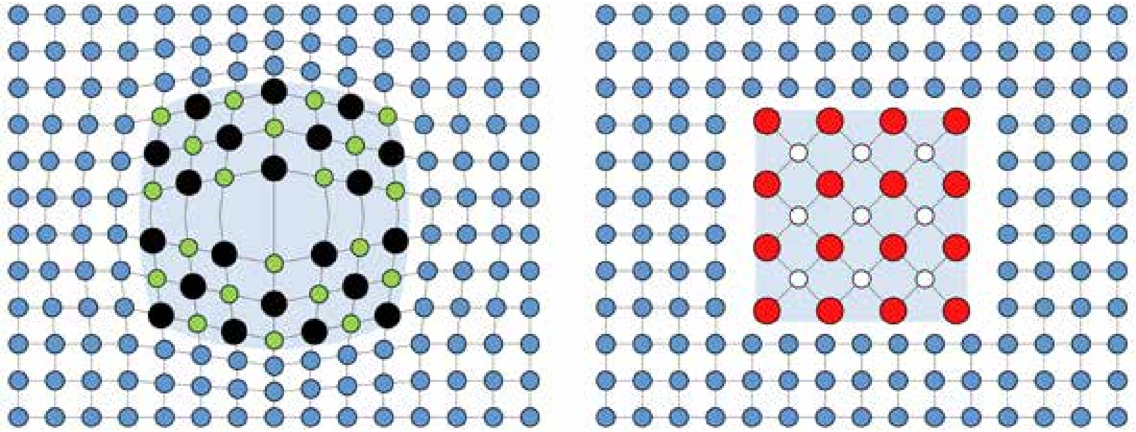

Figure 2.6 - Schematic representation of coherent compounds (left) and incoherent compounds (right).

---

[6] *All the chemical compounds present in metal materials have a predominantly ionic or covalent bond, in relation to the elements involved.*

[7] *The list proposed here has a indicative value and does not indicate a greater or lesser aptitude of the element in forming a compound (affinity).*

Another important classification of compounds is related to the characteristics of their crystal lattice. These are referred to as coherent compounds if the lattice of the compound has the same crystallographic orientation of the surrounding lattice, and incoherent otherwise (Figure 2.6).

From a last terminological consideration, it is common to call the compounds with the term precipitates. This derives from the analogy with liquids. When in a liquid sugar solution the solubility limit is reached, the sugar separates and precipitates to the bottom of the container. It is similar for precipitating compounds, when separating from the iron lattice, once the solubility limit of the solute in the solvent is reached.

2.4 Line defects

A typical line defect of metal lattices is dislocation. This is a defect that is not in thermodynamic equilibrium. Dislocations are discontinuities of the lattice that are formed during solidification and heat treatment, or due to mechanical stresses acting on the metal mass.

The most simple form of a dislocation is the so-called "edge dislocation" that consists in the lack of a crystallographic semi-planes within the lattice.

Through an example, let us try to understand how an edge dislocation is occurs (Figure 2.7).

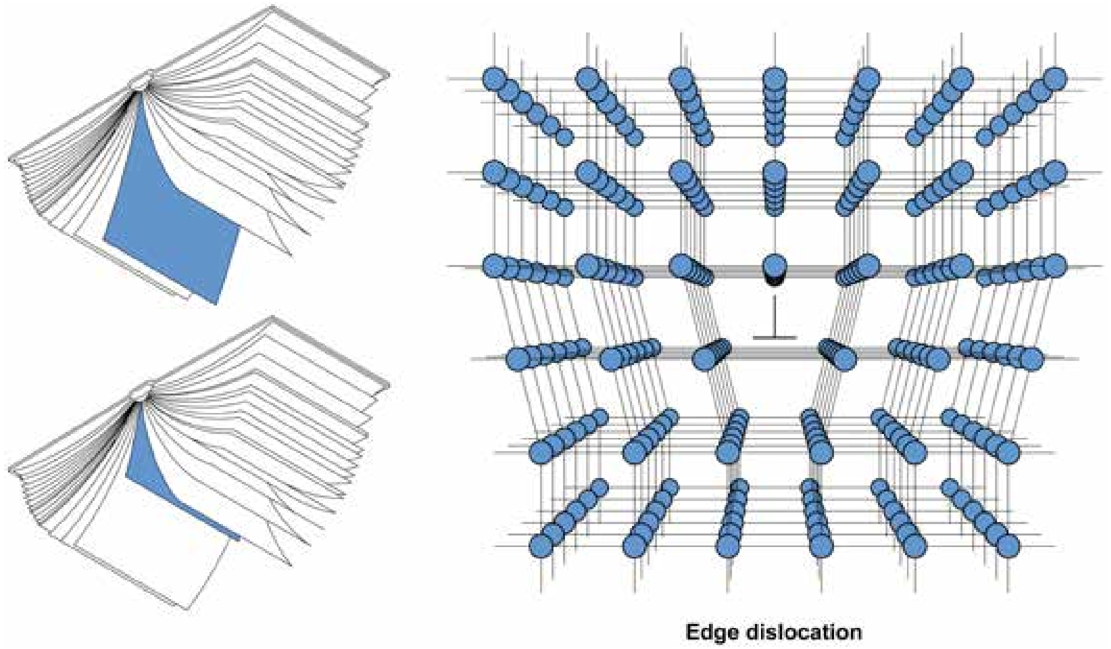

Figure 2.7 - Example of an edge dislocation and analogy with the pages of a book.

For convenience, the crystal lattice of iron can be thought of as a book. The pages of the book represent the planes, occupied by the atoms. The sum of all the pages, side-by-side, creates the book, that is, the three-dimensional crystal.

To create an edge dislocation, just take a page of the book and tear it lengthwise, leaving half the page attached to the book. Closing the book and placing the pages next to each other again, the book is put back together and the crystalline solid is reformed, without, however, a crystallographic semi-plane (i.e. the page torn in half). The end of the crystallographic semi-plane (the edge of the torn page) defines the dislocation line where the atoms are slightly shifted from their original position.

From a section of the crystal, perpendicular to the line of the dislocation, the defect appears as a point in the sectioning plane: this is indicated by an inverted letter *T* (⊥).

Edge dislocations are not the only type of line defects. Other types are screw dislocations or mixed[8] dislocations. These are linear irregularities, that make deformation of the metal mass easier (Figure 2.8).

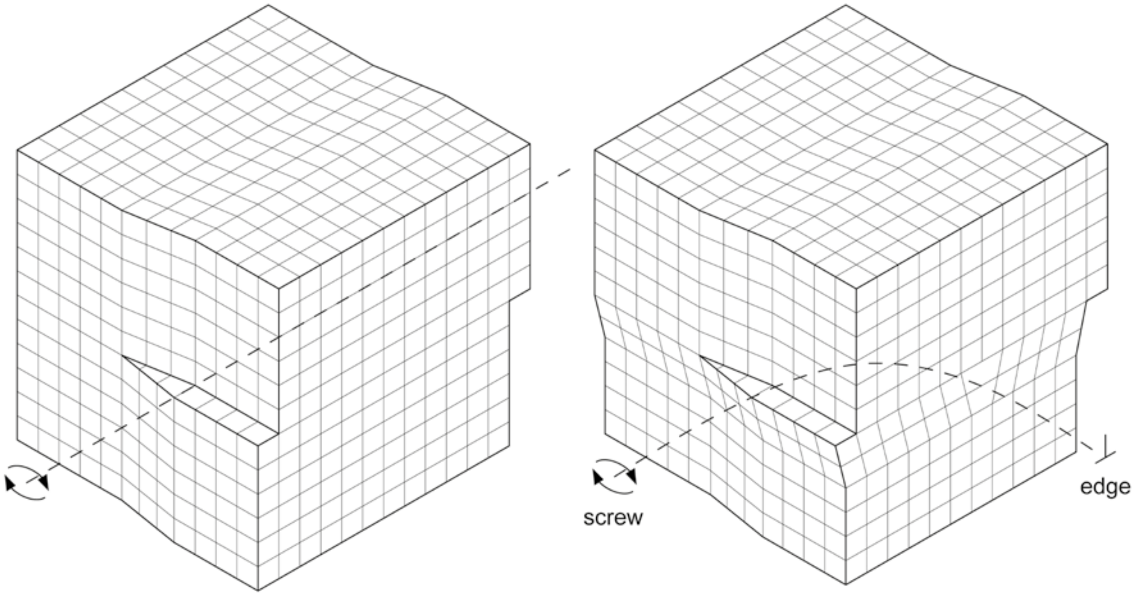

Screw dislocation **Mixed dislocation**

Figure 2.8 - Example of a screw dislocation and a mixed dislocation [from Campbell 2008].

---

[8] *Mixed dislocations derive from the sum between an edge dislocation and a screw dislocation.*

2.5 The dislocation motion and the deformability of metal lattices

Dislocations are very important because they explain the mechanical properties of iron, steel, and all metallic materials.

First of all, let us see how the plastic deformation of a metal lattice would occur if there were no dislocations. In order to deform the crystal, as indicated in Chapter 1, a shear stress τ must be applied on the lattice. Pure tensile stress applied to the lattice does not produce any permanent deformation[9].

If the lattice is ideal, i.e. if all the atoms are regularly arranged in space, by applying shear stress, a deformation occurs along the shear plane.

The deformation mechanism causes the breakage of the existing bonds between the atoms and the sliding of all the atoms along the shear plane[10] (Figure 2.9). It's important to note that all atoms slide forward one lattice step simultaneasly.

The shear stress τ required to deform the lattice can be theoretically calculated based on the bonding energies between the atoms. This results in:

$$\tau \cong \frac{G}{2\pi}$$

where G is the shear modulus of the material[11]. Since, in the case of steel, G is approximately 80-82 GPa, the theoretical stress is in the order of 13 GPa.

Let us now consider the deformation of the actual lattices.

If the crystal has an edge dislocation the deformation mechanism is different.

---

[9] *We are speaking of shear stress or tensile stress that acts on the crystal lattice (stress at lattice level), not of stress on the whole metallic mass. Very different is the case of a macroscopic tensile stress on a metallic bar as occurs, for example, during a mechanical tensile test. In this case, by effect of the tensile stress σ, a macroscopic shear stress τ is generated. The shear stress τ is maximum on directions at 45° with respect to the tensile direction. This stress condition gives rise to typical phenomena of macroscopic deformation of the specimen (elongation and necking).*

[10] *The notion of breaking the bonds between the atoms does not have to suggest that the bond is a sort of mechanical connection. It is rather an electromagnetic interaction: if the atoms approach each other, repulsing forces intervene, which tend to bring them back to their position of equilibrium. If they move away from each other, attracting forces are created that lead them back to their original position. The analogy with a mechanical spring is evident, even though there is no real physical connection between the atoms.*

[11] *The shear modulus G is related to the elastic modulus E through the Poisson's ratio υ according to the relation: $G = E/2\,(1+\upsilon)$. Remember that for steel, υ it is 0.27÷0.3.*

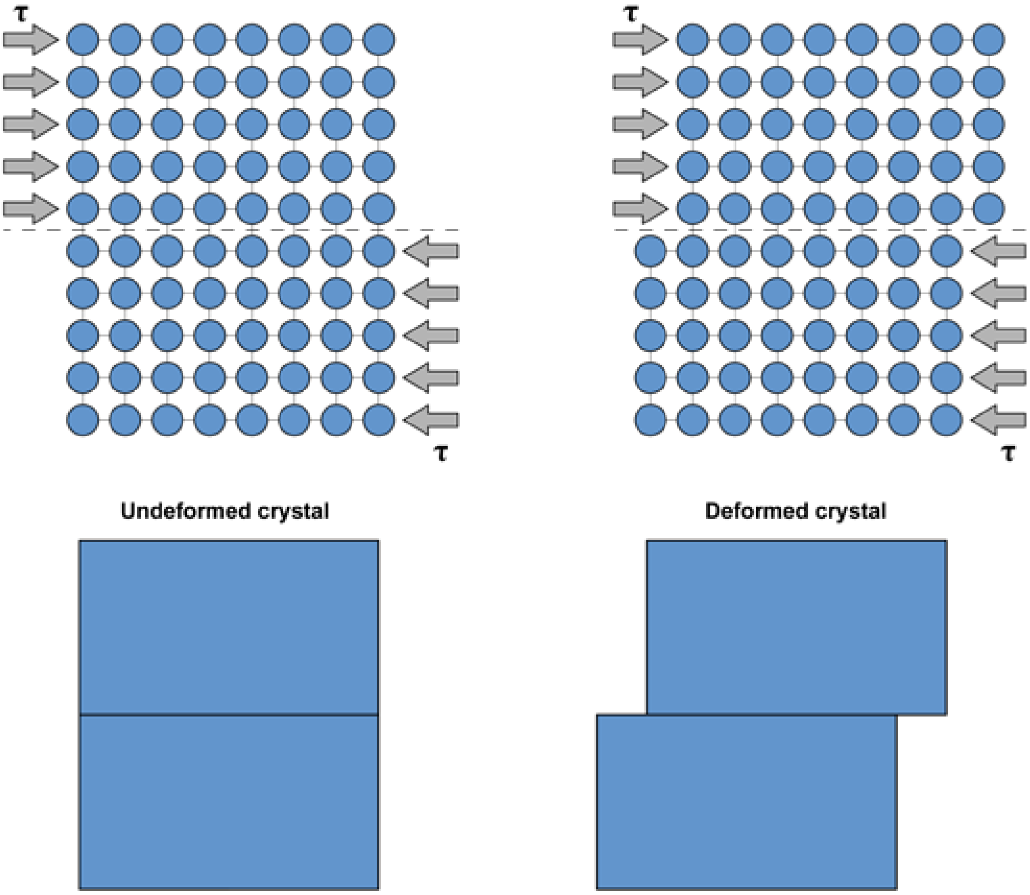

Figure 2.9 - Plastic deformation of an ideal crystal lattice. The dotted line represents the shear plane.

As a result of the applied stress τ, the sliding always takes place along the shear plane, yet, the dislocation significantly reduces the stress required to cause the crystal deformation. In fact, 5÷10 MPa are enough to start dislocations that require less energy input and not ~13 GPa, as previously evaluated according to theoretical models[12].

Let us see what is occurring in detail. Carefully observe Figure 2.10.

---

[12] *It is well understood that, in the event of dislocations, the term "defect" - in this case, line defect - should be taken as a positive meaning: without dislocations, the deformation of a crystal would be very difficult.*

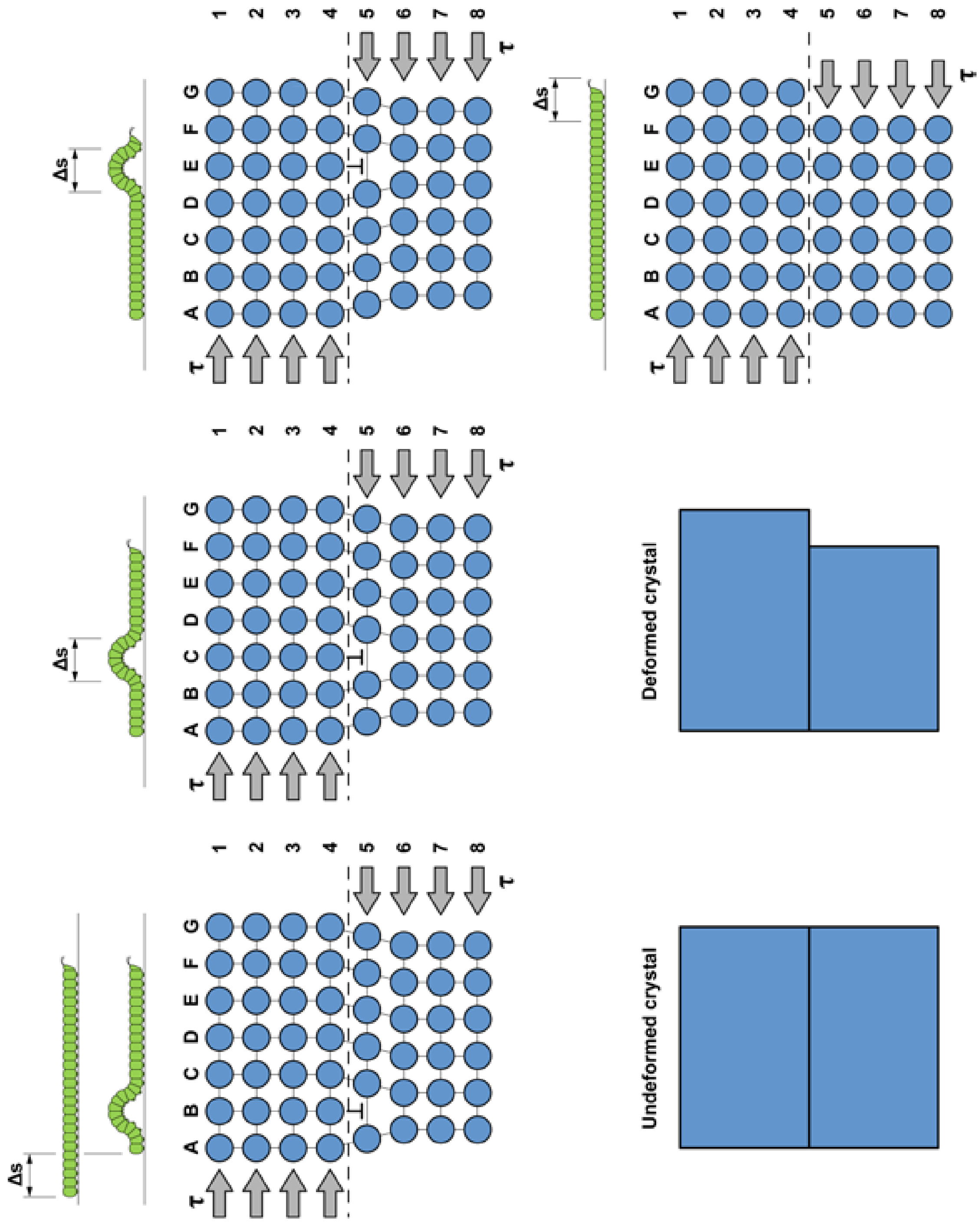

Figure 2.10 - Plastic deformation of a crystal lattice with an edge dislocation. The dotted line represents the shear plane.

When the stress τ is applied to the lattice, atom $C4$ progressively moves away from atom $C5$. Consequently, the link between the two atoms ($C4$ and $C5$) becomes more labile. At the same time, however, atom $B4$, at the end of the missing semi-plane of the dislocation, increasingly approaches atom $C5$. Therefore, it is progressively affected by the electromagnetic interaction that develops atom $C5$.

Once a certain energy threshold is passed (i.e. if the shear action τ is adequate), atom $C4$ frees itself from the bond it originally had with $C5$, and a new bond is created between $B4$ and $C5$. As a result, atom $C4$ becomes the end atom of the missing semi-plane and the dislocation has moved forward one lattice step.

The dislocation motion, one step at a time, causes the deformation of the lattice and, in the end, the defect emerges at the opposite end.

The movement described, one step at a time, is a bit like the motion of a caterpillar that has to cross a generic space Δs. The caterpillar does not move forward Δs because all its feet instantly increase by an amount equal to Δs. In contrast, the caterpillar moves itself because its legs, one after the other, move forward Δs: the sum of the individual advancement of the feet in succession, ultimately produces the overall movement Δs of the caterpillar.

The comparison of the two deformation mechanisms (perfect crystal and crystal with defects), clearly shows that the mechanical stress required to deform the lattice is much less when dislocations are present. For this reason, all metallic materials - some more, others less - are plastically deformable.

Dislocations also explains why, in metals and in alloys, the values of the shear stress required to deformation the lattices is lower than an order of magnitude than the theoretically calculated values for ideal crystals. Real crystals have a very high density of dislocations. This means that they contain a large number of line defects, which can be moved if correctly stressed: this promote deformability.

Mechanical resistance, as deformability, is also a direct consequence of the dislocation motion. While it is true that the lattice deformability is correlated to dislocation motions, it is equally true that also mechanical resistance - the opposite of deformability - is due to a limited dislocation motions.

In summary: the more the dislocations move, the more the lattice is deformed. The more the dislocation motion is limited, the less the lattice is deformed and the higher the mechanical strength of the metallic mass becomes.

2.6 Surface defects

Iron, steel, and all metal alloys have a polycrystalline structure, meaning a crystallite, which is the result of the solidification process. This means that any pure metal or metal alloy, if observed at a microscopic level, always shows an aggregate of irregular polygonal grains. Figure 2.11 shows the case of pure iron.

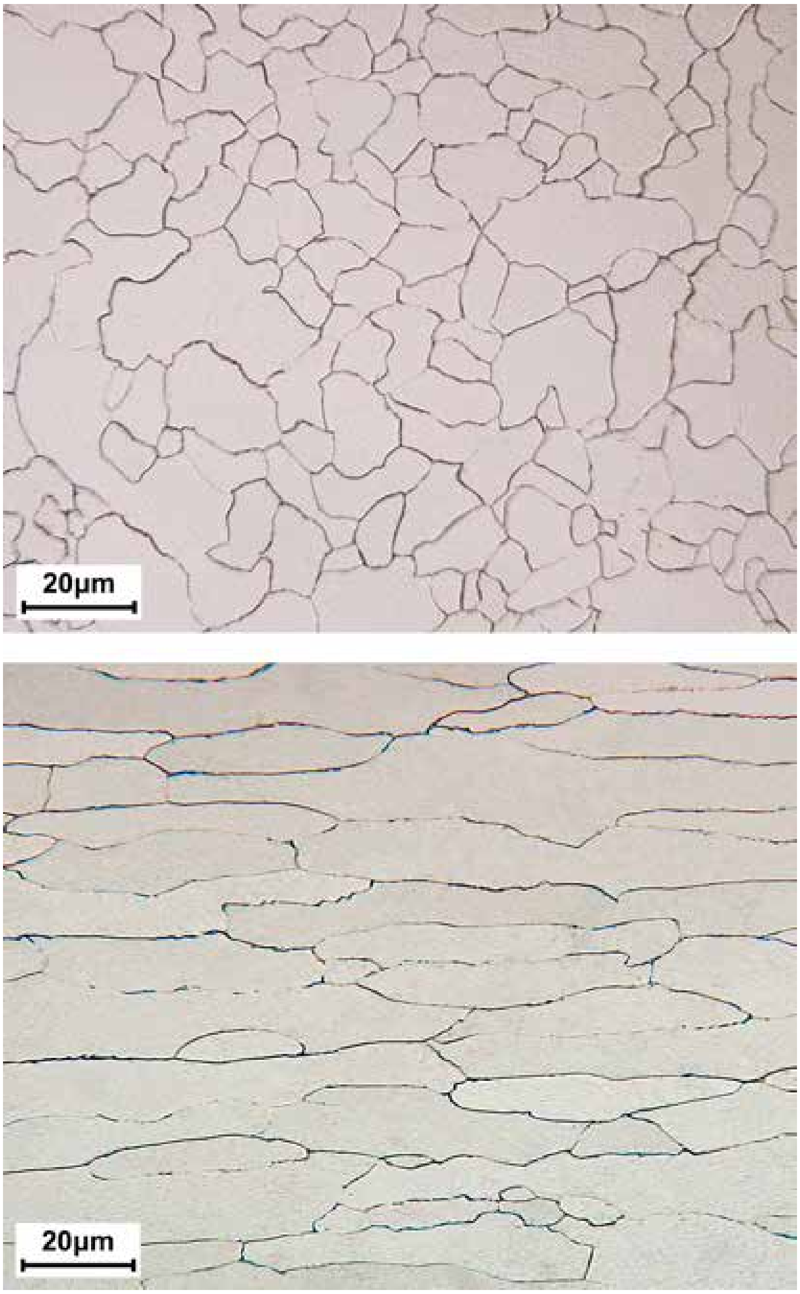

Figure 2.11 - Polycrystalline structure of pure ARMCO iron[13]: in the annealed state (above), and after cold work (below). Appearance under the metallographic microscope - Nital 2% etch. [Laboratori del Dipartimento di Meccanica del Politecnico di Milano - Milano].

---

[13] *Pure industrial iron with Fe > 99.8%, developed for the first time in 1909 by ARMCO (American Rolling Mill Company). The term, "Iron ARMCO", is now synonymous with pure industrial iron.*

Each grain has an homogeneous crystalline building, that is, a lattice of atoms that are uniformly oriented[14]. The crystalline lattice of each grain, however, has an orientation in space that is statistically different from the other grains. The problem then arises along the border area, where a transition between a lattice and the adjacent one is created, both regular but with different orientations.

Atoms located along the border area can not keep the smooth arrangement of the two contiguous crystalline lattices and are forced into an irregular shape. Locally, therefore, there is a distortion of the lattice, i.e. a defect, called "grain boundary" (see Figure 2.12).

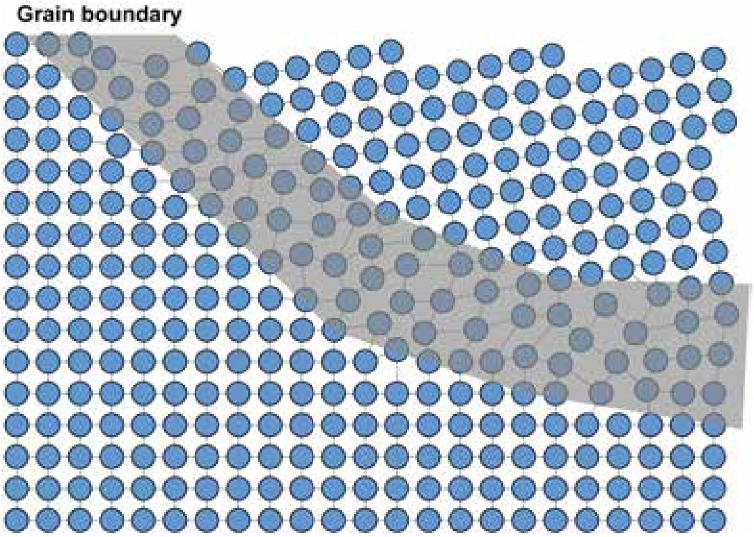

Figure 2.12 - Schematic representation of the boundary between two grains (grain boundary).

The grain boundaries have a typical extension of about 2-4 atomic diameters and they are surface defects (two-dimensional defects). Like dislocations, even grain boundaries are defects that are not in thermodynamic equilibrium.

Grain boundaries are areas characterized by a lower atomic density, and atoms located near grain boundaries have higher free energies than atoms located within the crystallite. Consequently, the grain boundary areas have a plastic deformation resistance that is greater as compared to the core of the grains themselves[15].

---

[14] *In many texts regarding material science, the uniformity of the crystalline lattice within individual grains is also defined as short-range regularity.*

[15] *An exception is the case of the grain boundary segregation of chemical elements that are harmful to steel (sulfur, phosphorous, hydrogen, etc.). In these cases, the grain boundary is subjected to embrittlement phenomena and intergranular type of fractures can occur.*

Moreover, the grain boundaries are much more responsive than the inner portion of the crystal lattice.Along the grain boundaries, diffusion phenomena[16] (oxidation, carburising, nitriding), precipitation of compounds, and segregation of impurities occur more easily.

2.7 Solidification

We will now analyze the metallurgic phenomena that occurs during for solidification. The solidification of a pure metal (iron) or a metal alloy (steel) always develops through a dual mechanism called nucleation and growth.

At first, the atoms of liquid metal gather to give origin to solid nucleus called nuclei, which subsequently increase their dimension through the aggregation of the atoms in the liquid phase. The process continues as long as the liquid has not completely used up. Only at this point the grains meet and interfere, creating the grain boundaries (Figure 2.13).

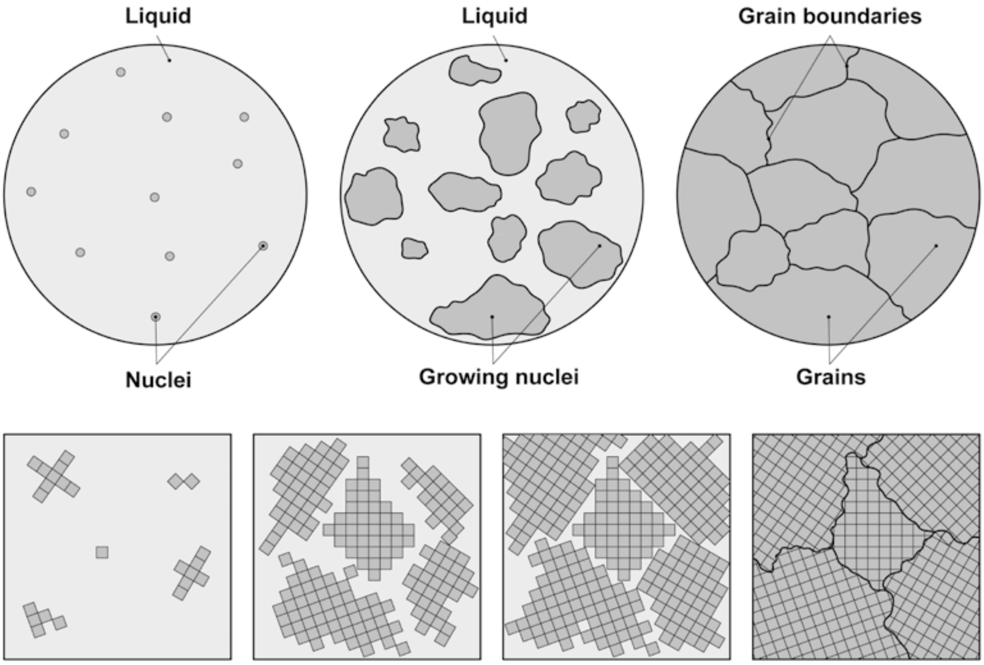

Figure 2.13 - Schematic representation of the solidification process of a generic metallic mass.

Initially consider the system in a liquid state. Atoms do not have a well-defined lattice shape, but are free to move at random.

---

[16] *For a broader discussion on diffusion phenomena, see Chapter 3.*

This occurs because, if the temperature is higher than the melting point, the kinetic energy of the atoms is enough to prevent the formation of solid bonds.

During the cooling phase, the movement of the atoms progressively decrease. Therefore, the probability that some atoms have a lattice configuration and a lattice distance equal to the crystal lattice of solid metal, increases even more. When the temperature falls below the melting point, this probability becomes so high and many solid nuclei form in the metallic bath. This method of nucleation is called homogeneous nucleation.

Homogeneous nucleation is very rarely in industrial practice. In almost all cases, solidification is characterized by the heterogeneous nucleation mechanism. Heterogeneous nucleation involves the formation of aggregates of atoms that solidify from the inner surface of the ingot mould and/or the solid impurities which act as trigger points for solidification[17].

For iron, as with all pure metals, solidification never occurs exactly at the melting point. For solidification to begin, there must always be subcooling: the liquid - before starting to solidify - must cool below its nominal solidification temperature.This phenomenon is called "undercooling".

Undercooling decreases the mobility of atoms and also promotes the solidification process. If undercooling is limited, also the number of nuclei is limited and the liquid solidifies forming a few coarse grains. However, if undercooling increases, the number of nuclei also increase and the liquid solidifies forming many small grains (Figure 2.14).

Similar considerations are also true for steel and for all alloys, in general. The main difference is that pure metals have a single liquid/solid transition temperature, instead, alloys solidify at a thermal interval (solidification interval)[18].

Undercooling also influences the morphology of the solidified microstructure. If the undercooling is limited, the solidification rate is very slow and the solid nuclei increase along all the directions in the space, in order to form crystallites of a planar or cellular type.

---

[17] *In the liquid metal phase, there are always microscopic solid impurities present.Typically, these are oxides and/or nitrides deriving from the preparation of the steel bath (Al_2O_3, SiO_2, MnO, AlN, TiN,, and so on).*

[18] *For a closer examination of this topic, see Chapter 5.*

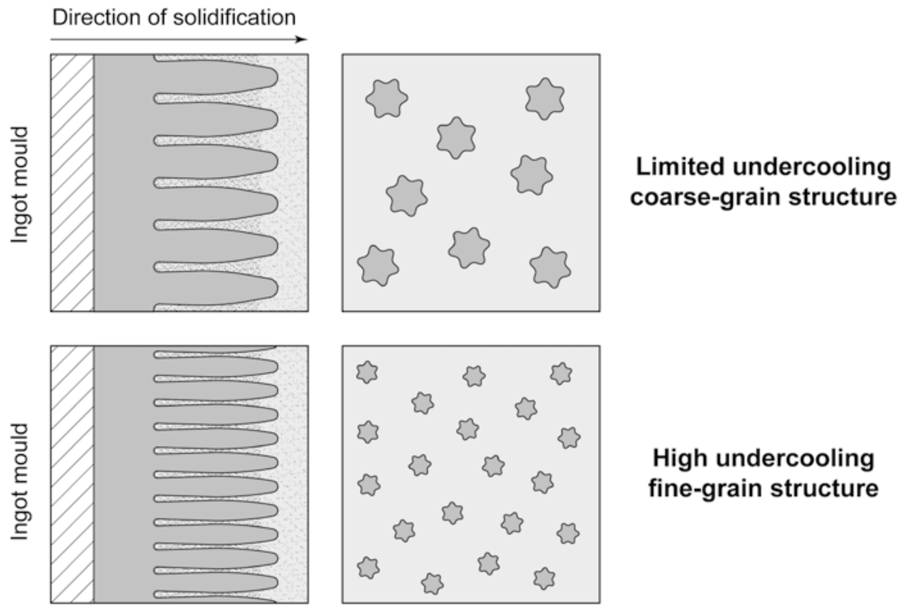

Figure 2.14 - The effect of undercooling on the nucleation mechanism.

If, on the other hand, the undercooling is high the growth is carried out along the direction of heat exchange with the formation of branched solid grains, called dendrites (Figure 2.15).

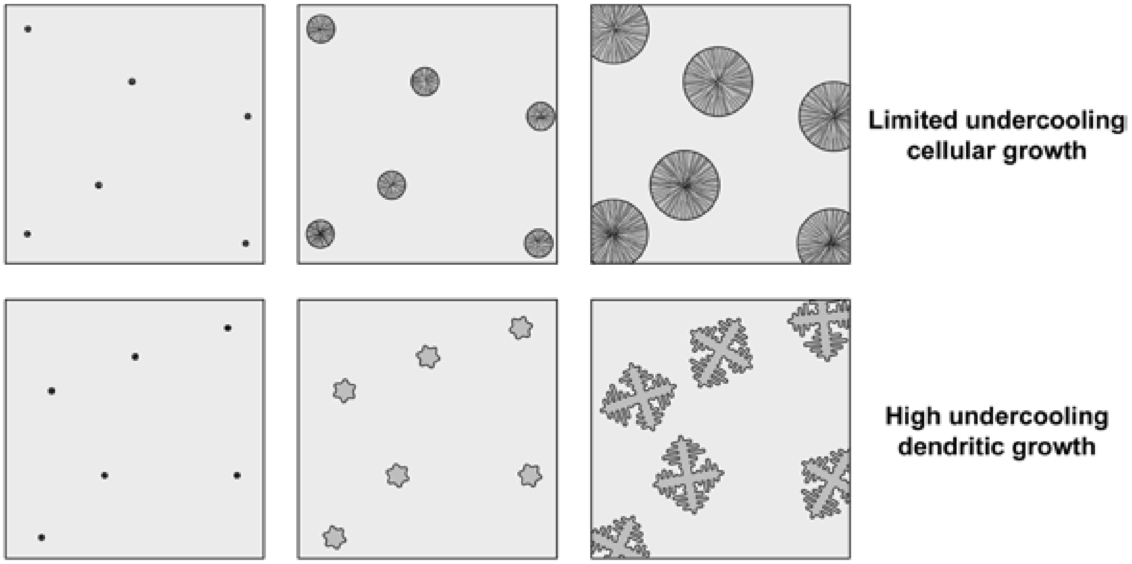

Figure 2.15 - Schematic representation of the cellular solidification process (limited undercooling) and the dendritic solidification process (high undercooling) [from Kurz and Fisher 1992].

The term "dendrite" comes from the Greek, *dendron* (tree) and derives from the tree-like shape formed by the crystallites during solidification. The secondary and tertiary branches of dendrites originate from the main grain when the lateral heat gradients also become appreciable. The size of the dendrites, measured through the average distance between the secondary branches, are closely related to of undercooling. A typical example of a dendritic structure is shown in Figures 2.16 and 2.17.

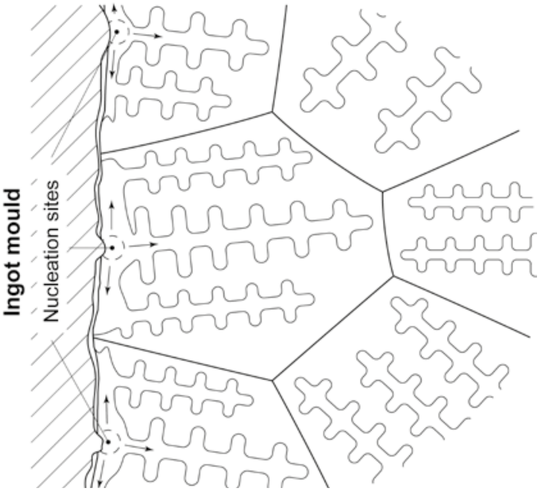

Figure 2.16 - Schematic representation of the dendritic solidification process [from Campbell 2003].

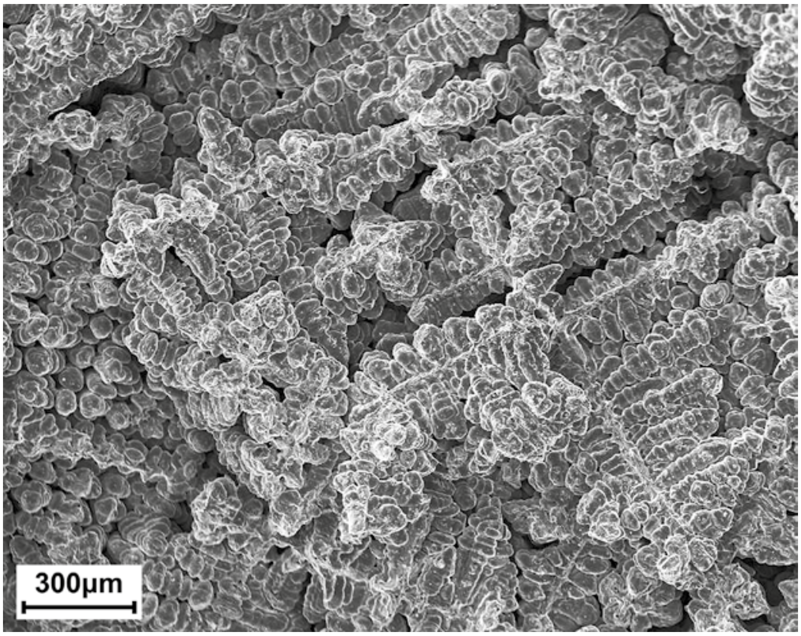

Figure 2.17 - Dendritic solidification structure. Appearance under the scanning electron microscope - without etching [Laboratori del Dipartimento di Meccanica del Politecnico di Milano - Milano].

2.8 Volume defects

Volume defects are three-dimensional discontinuities of the crystal lattice, not in thermodynamic equilibrium. There are essentially two categories of volume defects:

- micro-voids and macro-voids (shrinkage cavity, porosity, cracks, etc.);
- inclusions.

Micro-voids/Macro-voids

Micro-voids and macro-voids are three-dimensional or volume defects caused by the lack of atoms in the lattice. Macro-voids are visible to the naked eye, on the contrary, micr-voids are visible only under the metallografic microscope. Micro-voids and macro-voids develop during the solidification of steel, due to both the volumetric contraction of the liquid (shrinkage cavity), as well as to the entrapment of gaseous bubbles in the metallic mass (porosity).

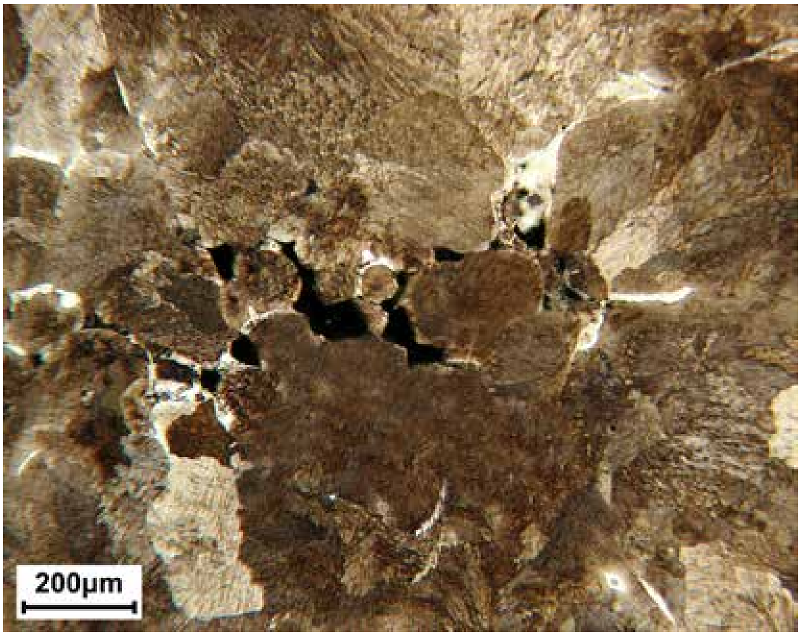

Figure 2.18 - Shrinkage cavities grouped in a continuous casting billet of an EN C45 steel with a pearlitic-ferritic microstructure. Appearance under the metallographic microscope - Nital 2% etch. [Laboratori del Dipartimento di Meccanica del Politecnico di Milano - Milano].

Cracks are also often considered as volume defects. They are caused by the action of external stress (mechanical, thermal, environmental, etc.) or due to of harmful chemical elements (i.e. hydrogen flakes).
Shrinkage cavities, porosity, and cracks always have a negative effect. Cracks reduce, in fact, both mechanical strength, as well as impact strength and fracture toughness of steel[19] (Figures 2.18 and 2.19).

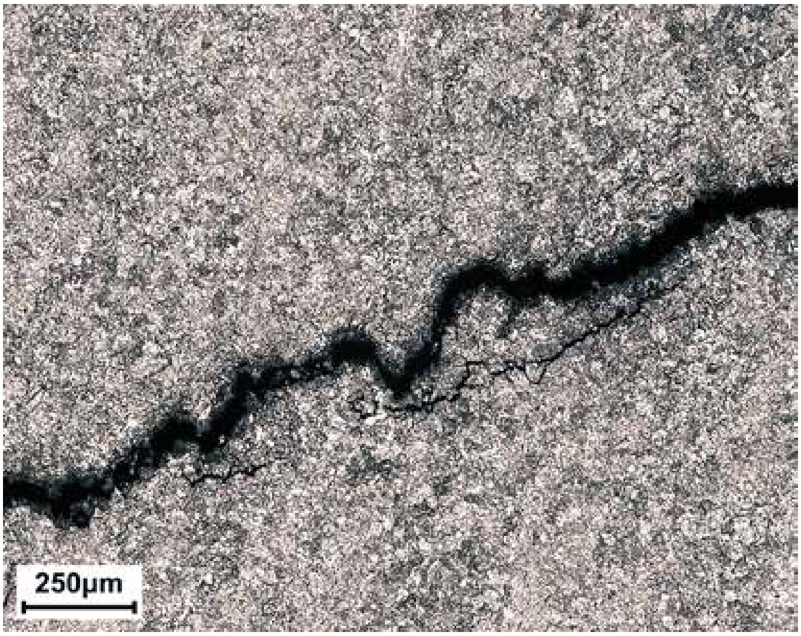

Figure 2.19 - Crack in an EN 34CrMo4 steel, with a tempered martensitic microstructure. Appearance under the metallographic microscope - Nital 2% etch. [Laboratori Hammer Srl, Rho - Milano].

Inclusions

Another important type of volume defect are inclusions. These are essentially interstitial compounds[20]. Inclusions show a different lattice than the surrounding metal.

---

[19] *The negative effect of macro-voids and/or micro-voids is evident both in static or quasi-static conditions (tensile strength) as well as in dynamic conditions (fatigue resistance, impact strength, fracture toughness).*

[20] *There are many types of steel inclusions: they range from particles that measure a few microns in diameter, up to defects that measure a few dozen millimeters.*

Inclusions are classified in endogenous (originating within the system) or exogenous (originating from outside). Endogenous inclusions are formed through separation from a liquid during the elaboration and refining phase for steel casting, for example during processes of deoxidation, dephosphorylation, desulphurization, and degassing. This is the case of the medium-small sized sulphides, oxides, and nitrides shown from Figures 2.20 to 2.23.

The term, exogenous inclusions, however, refers to particles outside steel that remain trapped in the solidifying metal. Typically, these are inclusions of refractory material, deriving from slag or from walls of the ingot mould (Figure 2.24).

In general, inclusions have a negative effect on steel, both since they reduce the resistant section of the components, and also because they represent preferred zones for cracks to occur. On the other hand, inclusions can also have positive effects. Just think of iron and/or manganese sulphides (FeS, MnS, or mixed $Fe_xMn_{1-x}S$), in free-machining steel. These inclusions decrease the impact strength and ductility of steel but greatly increase its machinability.

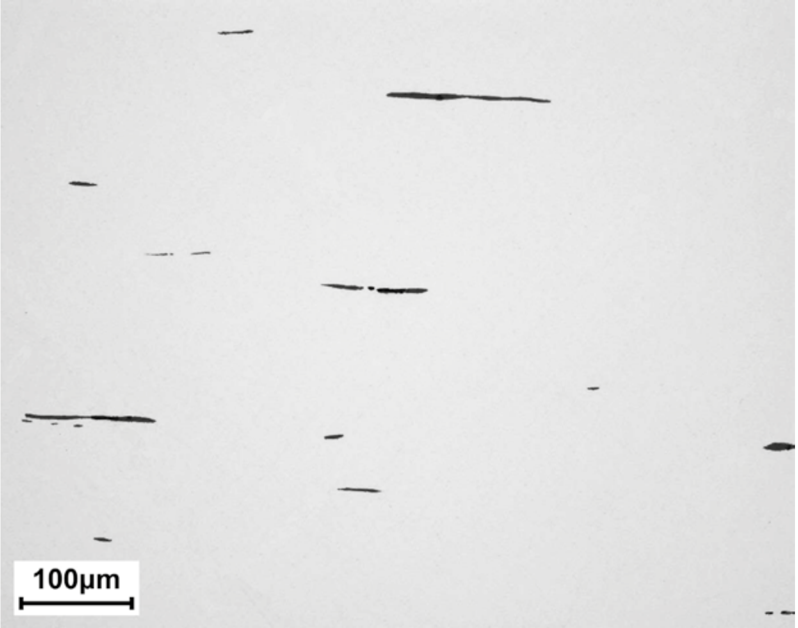

Figure 2.20 - Iron manganese sulphide inclusions in a special steel. Appearance under the metallographic microscope - without etching [Laboratori Omeco Srl, Monza - Monza Brianza].

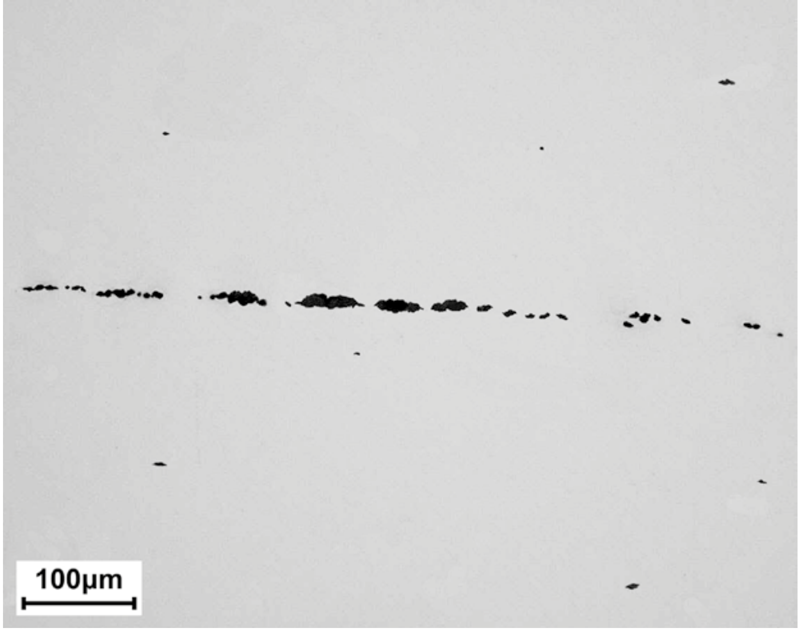

Figure 2.21 - Alumina inclusions in special steel. Appearance under the metallographic microscope - without etching [Laboratori Omeco Srl, Monza - Monza Brianza].

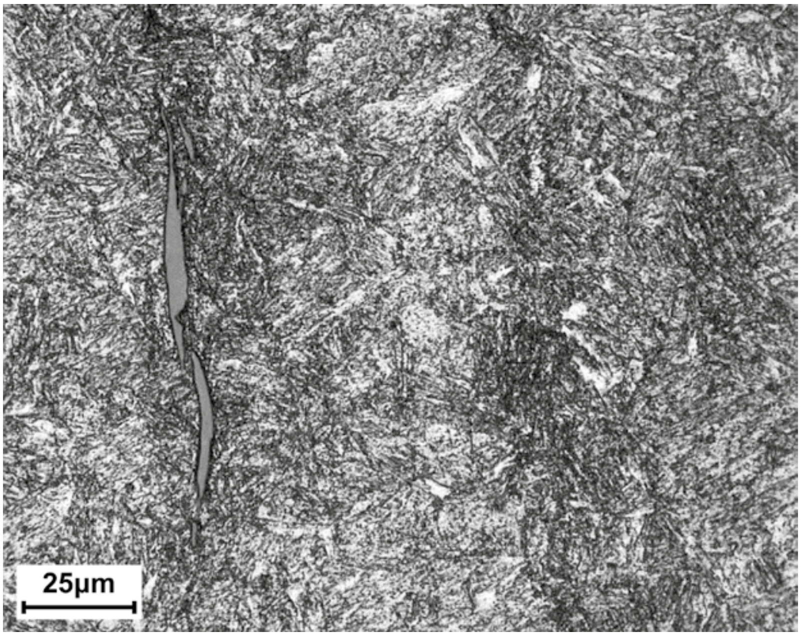

Figure 2.22 - Inclusion of iron/manganese sulphide in an EN 42CrMo4 steel with a tempered martensitic structure. Appearance under the metallographic microscope - Nital 2% etch. [Laboratori Hammer Srl, Rho - Milano].

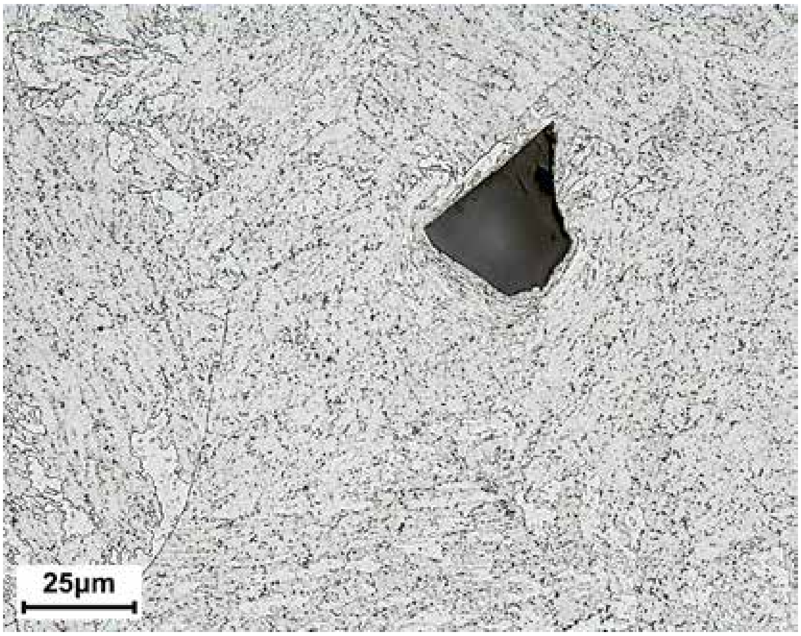

Figure 2.23 - Inclusion of titanium nitride in an ASTM SA336 F22V steel (2.25Cr-1Mo-0.25V) with a bainitic structure. Appearance under the metallographic microscope - Nital 2% etch. [Laboratori Hammer Srl, Rho - Milano].

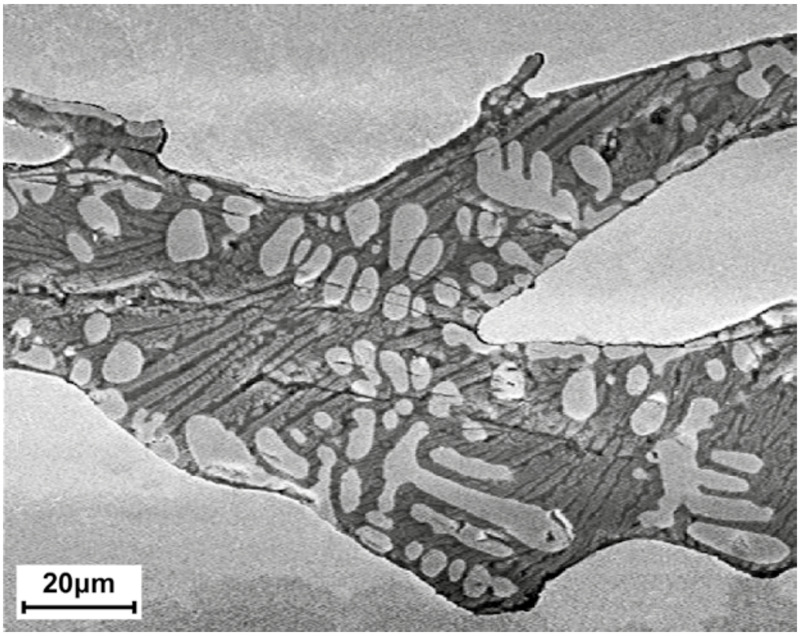

Figure 2.24 - Exogenous inclusion of ferrous scrap (iron, iron oxides, silicon oxides, calcium aluminates) in a 16th century artifact. Appearance under the scanning electron microscope - without etching [Laboratori del Dipartimento di Meccanica del Politecnico di Milano - Milano].

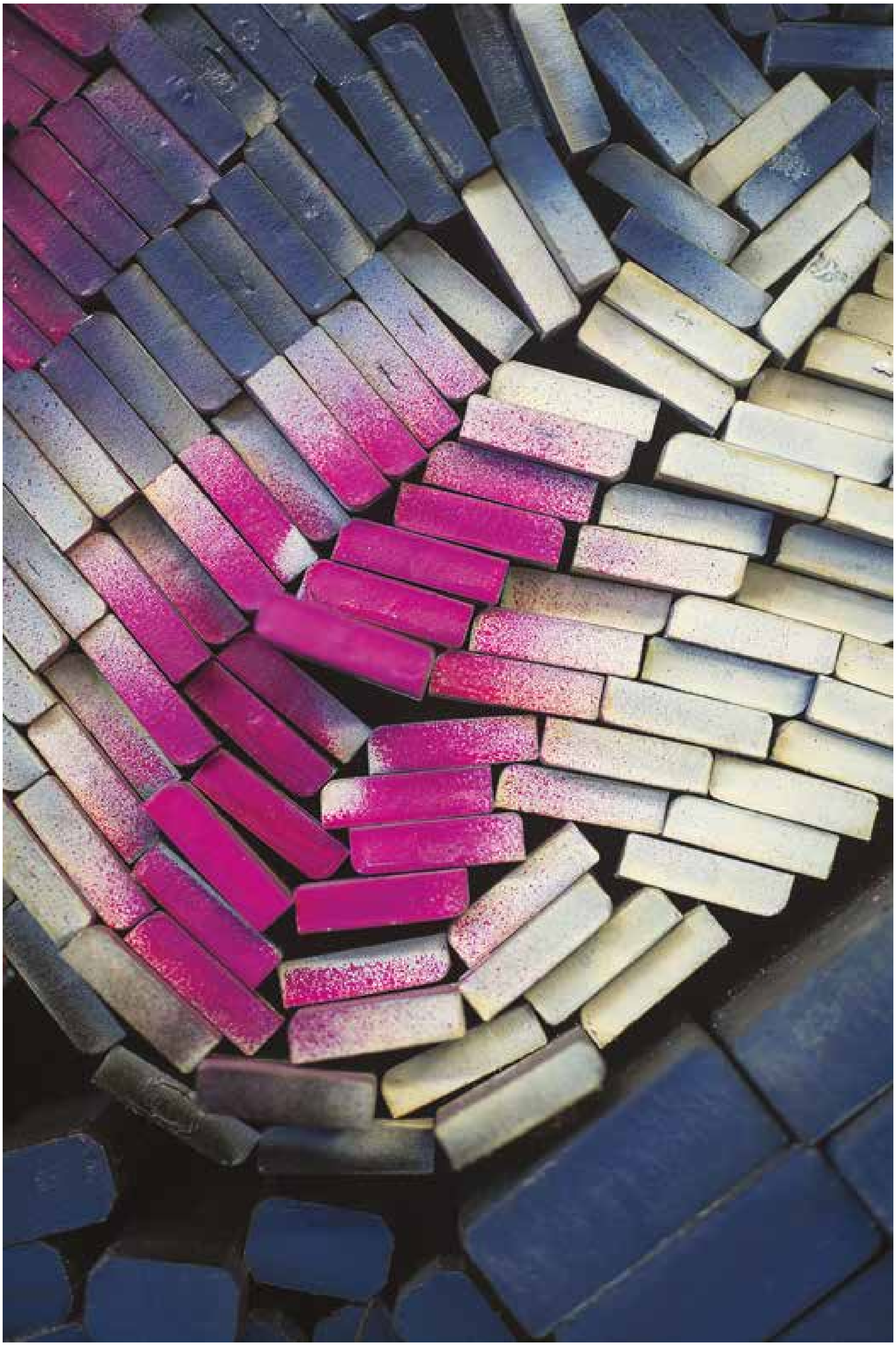

3. DIFFUSION

3.1 What is diffusion?

Diffusion is a mass transport phenomenon, a mechanism that allows the movement of atoms within matter. Diffusion represents the movement of the atoms within a system caused by their thermal agitation. Since the thermal energy of the atoms increases when temperature increases, even the diffusion rate increases when the temperature of the system increases. Diffusion can occur in gases, liquids, and solids and it is a function of temperature and time.

Diffusion is very important, since it explains a series of metallurgic phenomena, such as the formation of new phases, structural transformations, nucleation and growth mechanism of crystallites, recrystallisation, thermo-chemical treatments, creep, sintering, etc.

To understand the diffusion phenomenon one can use the simple example shown in Figure 3.1. This is a typical self-diffusion mechanism for vacancies, as can occur in a homogeneous crystalline solid, where the movement of atoms within the system takes place by the vacancies of the lattice.

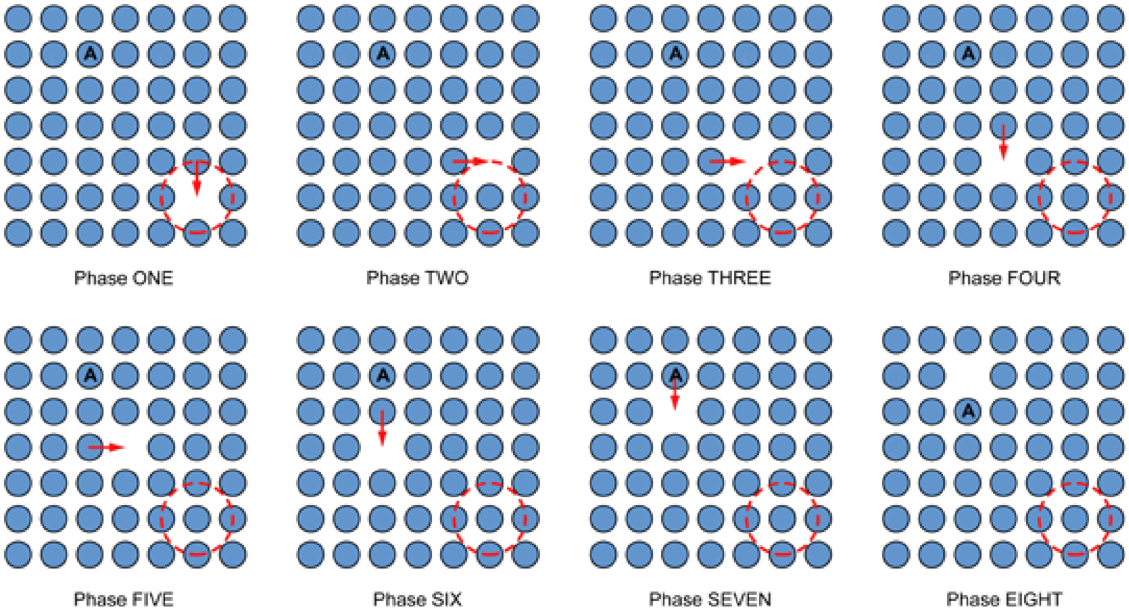

Figure 3.1 - Self-diffusion for vacancies in an homogeneous system. Note the original position of atom *A* and of the vacancy (dotted circle) and the movement that occurs as a result of diffusion.

Very often, diffusion occurs between different atoms of a different nature. In this latter case, we talk about inter-diffusion in heterogeneous systems.

If the atom of the diffusing species has dimensions comparable to the atoms of the system (such as, iron and nickel), diffusion occurs through vacancies (Figure 3.2). If, on the other hand, the diffusing chemical species has a much smaller atomic size (such as, iron and carbon), diffusion occurs by exploiting the interstitial sites in the crystal lattice (Figure 3.3).

In both cases, in addition to temperature and time, the diffusion mechanism is governed by the concentration of the diffusing chemical species within the heterogeneous system.

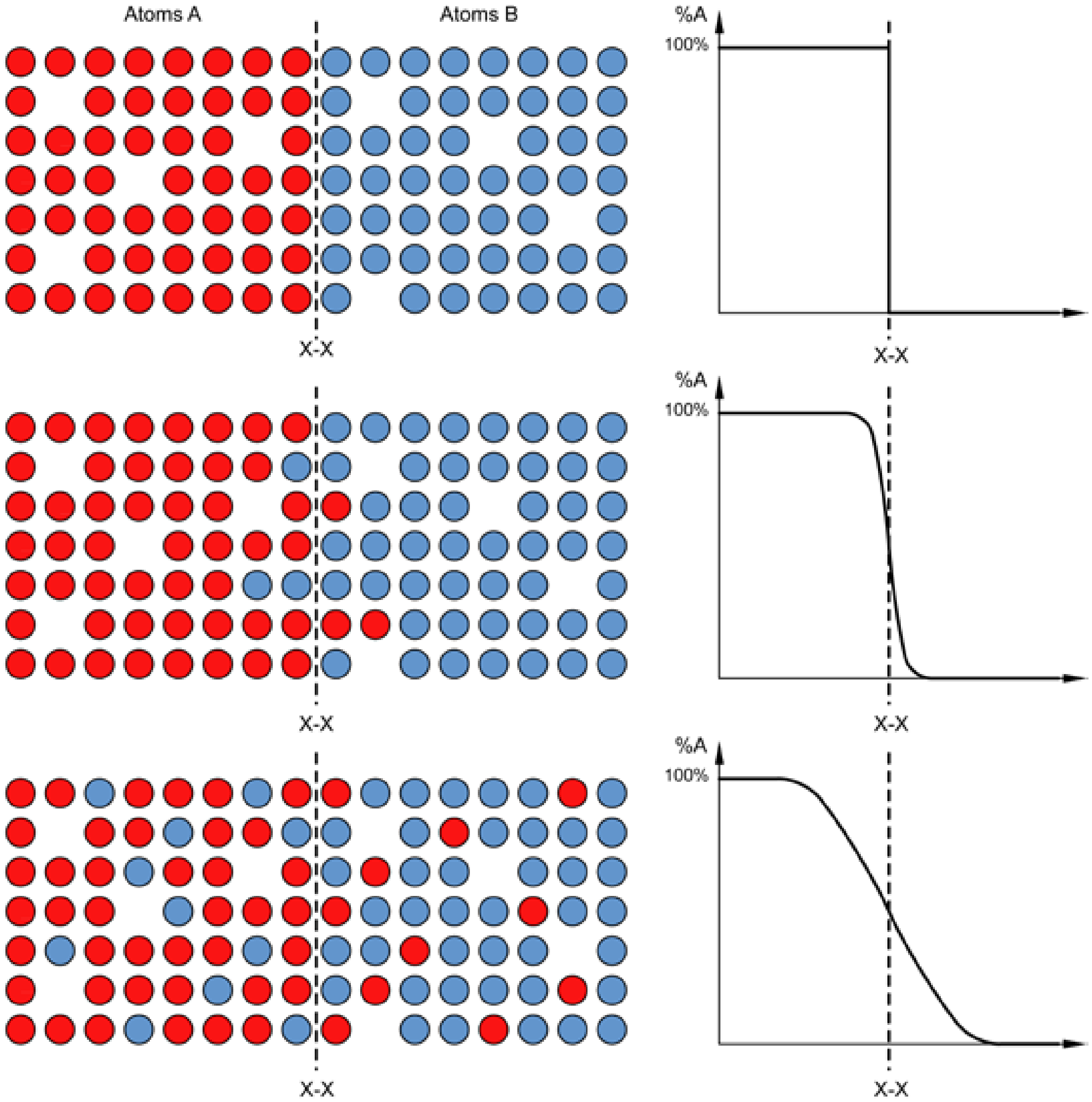

Figure 3.2 - Inter-diffusion for vacancies in a heterogeneous system between two crystalline solids.

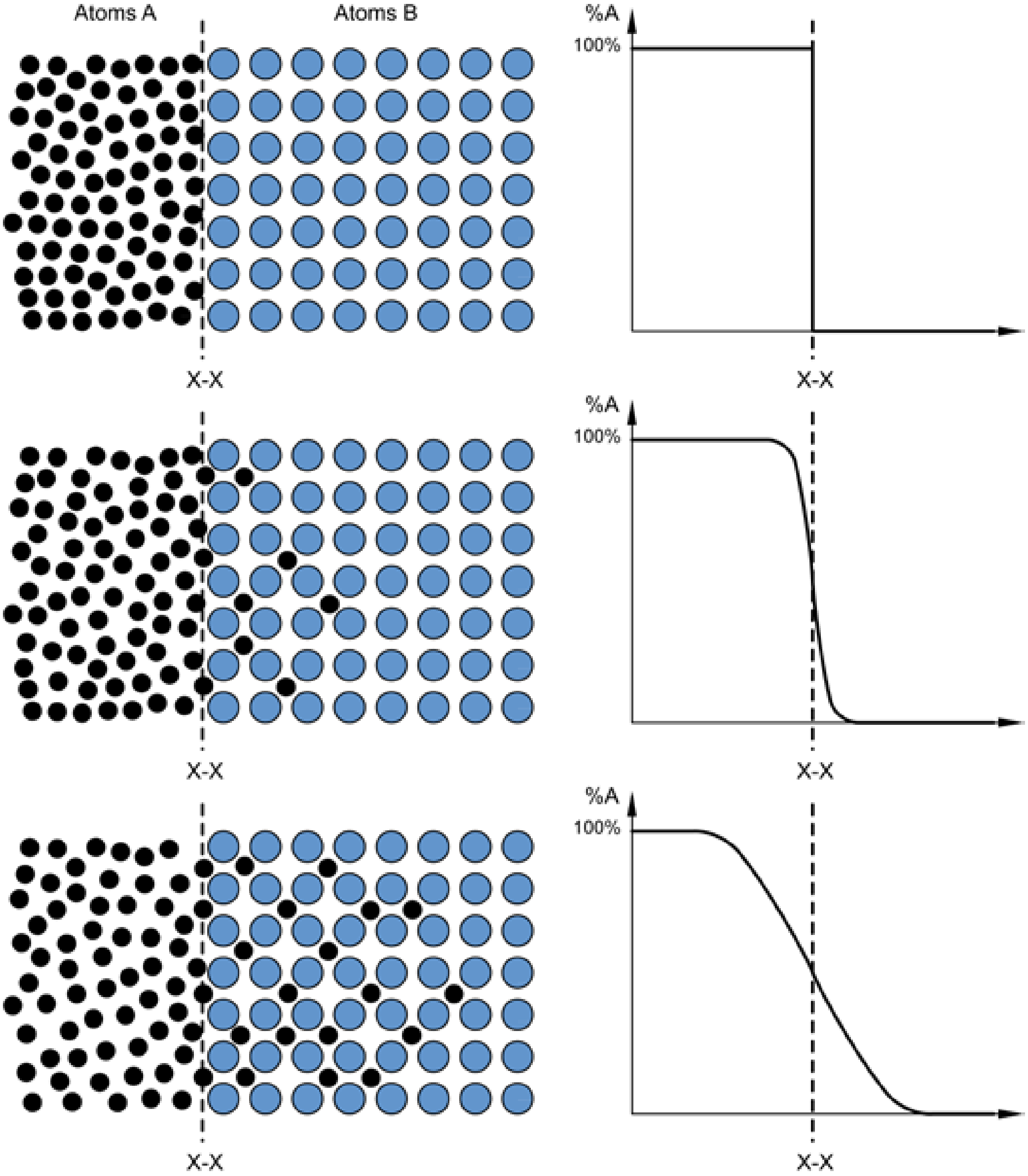

Figure 3.3 - Inter-diffusion for lattice interstitial sites in an heterogeneous system between a gas and a solid.

3.2 Mathematical model of the phenomenon

Diffusion mechanisms can also be treated quantitatively. In 1855, the physiologist, Adolf Eugen Fick, was the first to propose the two equations describing the phenomenon.

The two formulations proposed by Fick are based on the experimental observation that the diffusion of a chemical species is a function of both its different concentration in space, as well as of temperature and time.

A first type of problem to be evaluated is the rate of the diffusion process or, in other words, how quickly a given chemical species migrates from an area of greater concentration C_1 towards an area of lesser concentration C_2.

The described phenomenon is called diffusion flow and is indicated by the letter J. The unit of measurement is [atoms/m^2·s]. J Represents the amount of atoms that, in steady state, perpendicularly cross a surface A with a thickness of x in a unit of time t.

The Fick's first law can predict the diffusion flow J through the relation:

$$J = \frac{\partial C}{\partial t} = -D\frac{\partial C}{\partial x} \cong -D\frac{\Delta C}{\Delta x} = -D\frac{(C_2 - C_1)}{(x_2 - x_1)} \qquad [3.1]$$

where D [m^2/s] is the diffusivity and C [atoms/m^3] is the concentration of the chemical species along direction x. Equation 3.1 shows that the variation in time of C depends on the variation of C along direction x. The minus sign (-) indicates that the direction of the diffusion is opposite to the gradient of concentration, i.e. the atoms tend to move from areas where their concentration is greater (C_1) towards areas where their concentration is lower (C_2). To this respect, observe the schematic illustration in Figure 3.

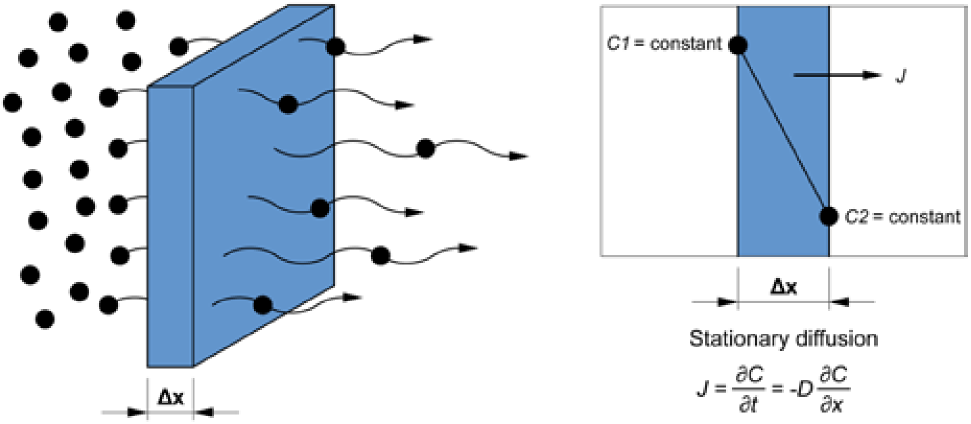

Figure 3.4 - Schematic representation of stationary diffusion (Fick's first law).

The diffusivity D greatly depends on temperature: approximately the value of D doubles for an increase in temperature of 20 degrees (°C or K).The equation to derive D as a function of T is an Arrhenius type of equation, namely:

$$D = D_0 e^{\left(-\frac{Q}{RT}\right)} \qquad [3.2]$$

where D_0 [m²/s] is the diffusion coefficient that depends on the diffusing chemical species and on the chemical species in which diffusion takes place, Q [J/mole] is the activation energy[1], T [K] is the temperature in Kelvin, and R is the gas constant equal to ~8.3145 J/mole·K.

Table 3.1 shows the values of the diffusion coefficient D_0 and the activation energy Q for several chemical species that are diffused in the iron lattice.

Diffusing chemical species	Chemical species through which diffusion occurs	Diffusion coefficient, D_0 [m²/s]	Activation energy, Q [J/mole]
Fe	γ-Fe	$5.0 \cdot 10^{-5}$	284,000
Fe	α-Fe	$2.8 \cdot 10^{-4}$	251,000
C	γ-Fe	$2.3 \cdot 10^{-5}$	148,000
C	α-Fe	$6.2 \cdot 10^{-7}$	80,000
N	γ-Fe	$3.4 \cdot 10^{-7}$	145,000
N	α-Fe	$6.6 \cdot 10^{-7}$	78,000
H	γ-Fe	$6.3 \cdot 10^{-7}$	43,000
H	α-Fe	$1.2 \cdot 10^{-7}$	15,000
O	α-Fe	$2.0 \cdot 10^{-7}$	86,000
Ni	γ-Fe	$5.0 \cdot 10^{-5}$	276,000
Mn	γ-Fe	$3.5 \cdot 10^{-5}$	282,000
Cr	γ-Fe	$5.4 \cdot 10^{-5}$	286,000

Table 3.1 - Diffusion coefficients D_0 and activation energies Q for several chemical species diffused in γ-iron and α-iron lattice.

Fick's first law (equation 3.1) is valid only when there are stationary diffusion phenomena, that is, in conditions where the gradient of concentration C remains unaltered over time (J constant).

More useful is the diffusion in a non-stationary mode, i.e. when the gradient of concentration C varies in space x, in relation to time.

In this second case, the diffusion equation, called Fick's second law, becomes:

$$J = \frac{\partial C}{\partial t} = -D\frac{\partial^2 C}{\partial x^2} \qquad [3.3]$$

where D, C, and x have the previously defined meaning (see Figure 3.5).

---

[1] *Activation energy Q is the minimum amount of energy needed to trigger a certain chemical reaction or a specific phenomenon in a system at equilibrium state.*

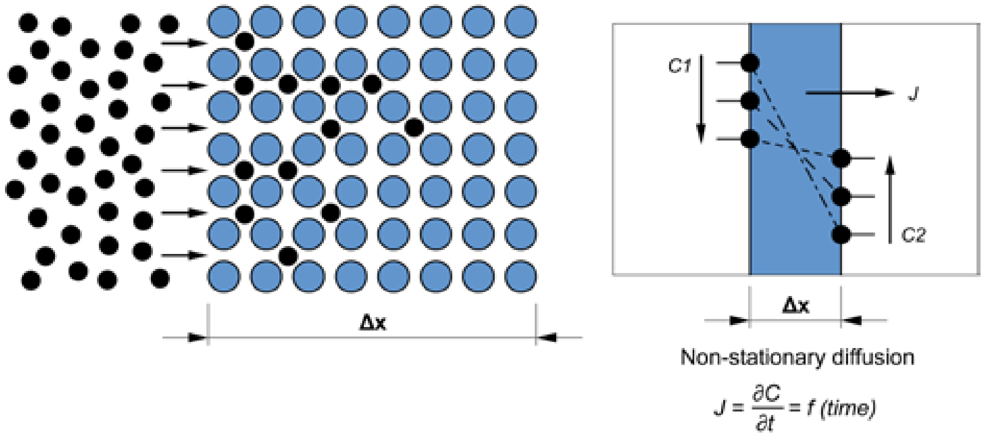

Figure 3.5 - Schematic representation of non-stationary diffusion (Fick's second law).

Equation 3.3 has been solved for some geometries that are of particular interest in the metallurgical field. Considering, for example, a semi-infinite solid, where the flow of the diffusing substance never reaches one of the two external surfaces[2], equation 3.3 can be solved as proposed by van Ostrand-Dewey:

$$C_x - C_0 = (C_s - C_0)\left[1 - erf\left(\frac{x}{2\sqrt{Dt}}\right)\right] \qquad [3.4]$$

where C_x is the concentration of the diffusing species at distance x from the exchange surface, while C_s e C_0 respectively represent the initial concentration of the diffusing chemical species and the initial concentration of the diffusing chemical species in the semi-infinite solid.
Erf (z) is the function of Gauss's error. It's values are listed in Table 3.2 as a function of the argument z.

---

[2] *It is the case of carburising and nitriding. In these surface heat treatments a gas-phase element (carbon or nitrogen) diffuses near the surface of a steel component.*

z	erf (z)	z	erf (z)	z	erf (z)
0	0	0.55	0.5633	1.3	0.9340
0.025	0.0282	0.60	0.6039	1.4	0.9523
0.05	0.0564	0.65	0.6420	1.5	0.9661
0.10	0.1125	0.70	0.6778	1.6	0.9763
0.15	0.1680	0.75	0.7112	1.7	0.9838
0.20	0.2227	0.80	0.7421	1.8	0.9891
0.25	0.2763	0.85	0.7707	1.9	0.9928
0.30	0.3286	0.90	0.7970	2.0	0.9953
0.35	0.3794	0.95	0.8209	2.2	0.9981
0.40	0.4284	1.0	0.8427	2.4	0.9993
0.45	0.4755	1.1	0.8802	2.6	0.9998
0.50	0.5205	1.2	0.9103	2.8	0.9999

Table 3.2 - Values of the *erf (z)* error function as a function of the argument $z = \frac{x}{2\sqrt{Dt}}$

3.3 Practical applications of diffusion equations

Several practical applications may be helpful in clarifying the use of the proposed equations. A reader not accustomed to metallurgical topics must keep in mind that the following examples refer to topics that will be better dealt with in the following chapters.

Case 1

Suppose you want to carburise a steel component with a carbon content of 0.18%, placing it in a furnace at 920°C in contact with a carburasing atmosphere equal to 0.9% of carbon.
You want to know how long the workpiece will have to stay in the furnace to achieve a carbon content of 0.4% in the steel at a distance of 0.5 mm from the surface[3] (See figure 3.6).

Using equation 3.4, the data to be included are:

from which: $C_x = 0.4\% \qquad C_s = 0.9\% \qquad C_0 = 0.18\%$

meaning:

$$0.4\% - 0.18\% = (0.9\% - 0.18\%)\left[1 - erf\left(\frac{x}{2\sqrt{Dt}}\right)\right]$$

$$erf\left(\frac{x}{2\sqrt{Dt}}\right) \cong 0.6944$$

---

[3] *A carbon content equal to 0.4% guarantees a martensitic structure after hardening, with a hardness of approximately 550 HV, i.e. the hardness at which the effective carburising depth is measured.*

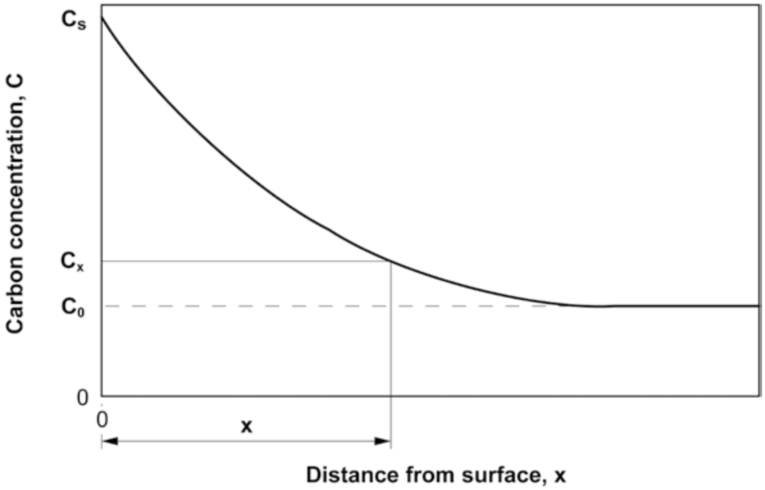

Figure 3.6 - The effect of carburising on carbon concentration [from Thelning 1975].

From Table 3.2, the value of the argument $\frac{x}{2\sqrt{Dt}}$ can be derived when the error function is 0.6944, and the result is:

$$\frac{x}{2\sqrt{Dt}} \cong 0.725$$

The diffusivity D of carbon in the γ-iron lattice at 920°C (1193 K) can be calculated with equation 3.2, using the appropriate values of D_0 and Q shown in Table 3.1.
This results is:

$$D = 2.3 \cdot 10^{-5} e^{\left(-\frac{148{,}000}{8.3145 \cdot 1193}\right)} \cong 7.617 \cdot 10^{-12} \quad [m^2/s]$$

Since the carbon content at 0.5 mm ($0.5 \cdot 10^{-3}$m) must be equal to 0.4%, the result is equal to:

$$\frac{x}{2\sqrt{Dt}} \cong 0.725 \qquad x = 1.45\sqrt{Dt}$$

$$0.5 \cdot 10^{-3} = 1.45\sqrt{7.617 \cdot 10^{-12} \cdot t}$$

$$t \cong 15{,}600\ s \cong 4\ h\ and\ 20\ min$$

This means that after approximately 4 hours and 20 minutes in contact with the carburising atmosphere at 920°C, the steel has reached a carbon content of 0.4% at a distance of 0.5 mm from the surface.

Case 2

Another application of equation 3.4 refers to the problems of steel decarburization. It is, in fact, well known that during normal heat treatments, the surface of semi-finished steel product may be depleted of carbon through a reaction with the oxygen in the atmosphere (oxidation). This phenomenon must be limited, since it may result in surface hardness levels below the technical standards.

Consider a round steel bar, of carbon steel, with $C = 0.4\%$. The heating process is performed in a furnace, operating in air, and holding is performed at 920°C for 2 hours. In the surface of the semi-finished piece, the carbon content is zero, due to decarburization.

You want to know at what distance x from the decarburated external surface the carbon content is at least equal to 0.36%, that is 10% less than the nominal value (see Figure 3.7).

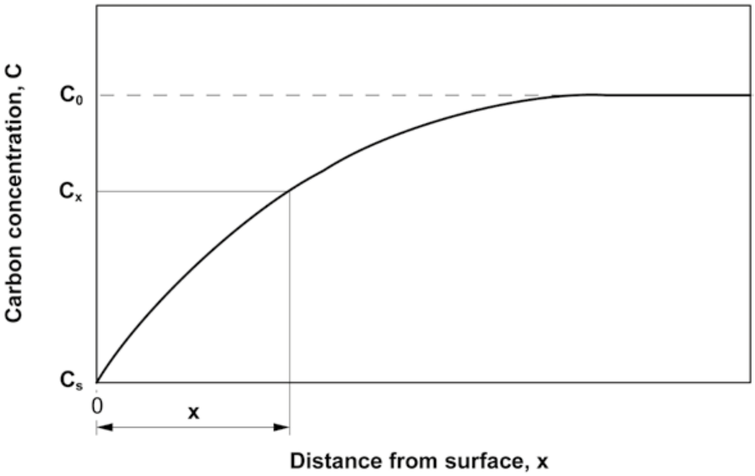

Figure 3.7 - The effect of decarburization on carbon concentration [from Thelning 1975].

To solve this problem, you can always use equation 3.4, but note that:

$$C_s = 0\%$$

therefore, equation 3.4 becomes:

$$C_x = C_0 erf\left(\frac{x}{2\sqrt{Dt}}\right)$$

Since $t = 7200$ seconds (2 hours), $C_x = 0.36\%$, and $C_0 = 0.4\%$, with a diffusivity value of $D = 7.617 \cdot 10^{-12}$ [m^2 / s] (identical to the previous example), the result is:

$$0.36 = 0.4 \cdot erf\left(\frac{x}{2\sqrt{7.617 \cdot 10^{-12} \cdot 7{,}200}}\right)$$

$$0.9 = erf\left(\frac{x}{2\sqrt{5.484 \cdot 10^{-8}}}\right)$$

$$1.165 = \frac{x}{2\sqrt{5.484 \cdot 10^{-8}}}$$

$$x \cong 0.00055\ m = 0.55\ mm$$

This means that, before using the bar, you have to remove about 0.6÷0.7 mm of material on the radius (1.2÷1.4 mm on the diameter) using a metalworking lathe, in order to ensure that the entire decarburated layer is removed. Or else, in the future, it will be more appropriate to perform the treatment in a non-oxidizing atmosphere (i.e. nitrogen atmosphere).

Case 3

The last interesting application related to Fick's laws refers to the problem of segregation in semi-finished steel products. As is well known, any semi-finished product is affected by a variability in its chemical composition along the section. The phenomenon is strictly dependent on the chemical composition of steel, the methods of solidification for the metallic mass (ingot or continuous casting billet), and the subsequent phases of hot working. In some cases, it is possible to reduce the effects of segregation through appropriate homogenization heat treatments at high temperatures.

Consider steel with a nominal carbon composition of 0.4% and manganese of 0.8%. As a result of segregation, the chemical composition is not constant but shows a fluctuation along the section with a regular spacing between segregation bands, l, equal to 100 μm ($0.1 \cdot 10^{-3}$ m): the carbon content fluctuates between 0.36% and 0.44% and the manganese content fluctuates between 0.72% and 0.88%, with a change in nominal value of ± 10% for both elements.

You want to know the duration of the homogenization treatment at 1,200°C to reduce the differences in chemical composition within the ± 2.5% interval of the nominal value of each element. In the case of carbon, the desired final variation is between 0.39% and 0.41%, and for manganese between 0.78% and 0.82%.

The diffusive phenomenon can be schematized as in Figure 3.8 in the hypothesis that the fluctuation of the chemical composition is of a sinusoidal type.

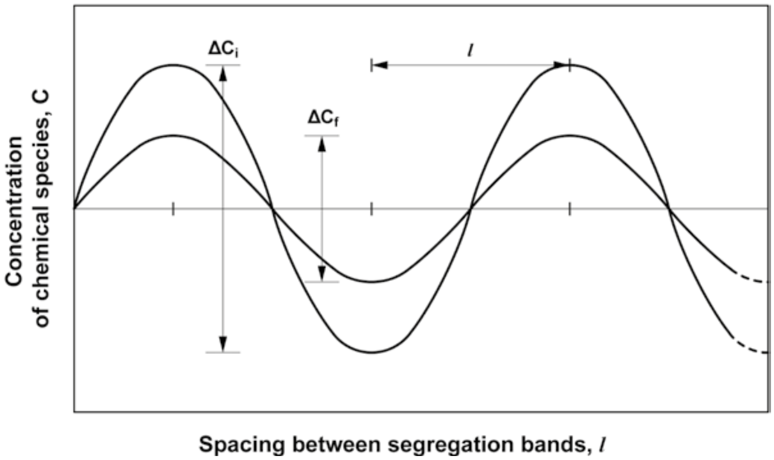

Figure 3.8 - The effect of homogenization heat treatment on concentration of a chemical species [from Hosford 2005].

The equation to use in this case is: $\boldsymbol{\Delta C_f = \Delta C_i e^{\left(-\frac{D\cdot t\cdot \pi^2}{l^2}\right)}}$

where ΔC_i and ΔC_f respectively represent the oscillation of the chemical composition before and after the homogenization treatment, D is the diffusivity of the element taken into consideration, t is time, and l is the spacing between two segregation bands.

First of all, the carbon and manganese diffusivity at 1,200°C (1473 K) should be calculated:

$$D_C = 2.3 \cdot 10^{-5} e^{\left(-\frac{148{,}000}{8.3145\cdot 1473}\right)} \cong 1.299 \cdot 10^{-10} \quad [m^2/s]$$

$$D_{Mn} = 3.5 \cdot 10^{-5} e^{\left(-\frac{282{,}000}{8.3145\cdot 1473}\right)} \cong 3.501 \cdot 10^{-15} \quad [m^2/s]$$

This simple calculation highlights that the diffusivity of carbon (interstitial element) is much higher than that of manganese (substitute element), and consequently, it is much easier to equalize the chemical composition of the first element than the second.

In order to make the chemical composition fall within ± 2.5% of their nominal value, the holding time for carbon is equal to:

$$0.02 = 0.08 e^{\left(-\frac{1.299\cdot 10^{-10}\cdot t\cdot \pi^2}{0.0001^2}\right)}$$

$$t_C \cong 10.8\ s$$

while for manganese, the holding time is equal to:

$$0.04 = 0.16 e^{\left(-\frac{3.501\cdot 10^{-15}\cdot t\cdot \pi^2}{0.0001^2}\right)}$$

$$t_{Mn} \cong 401{,}200\ s \cong 111\ h\ and\ 30\ min$$

Now, let us see what happens, if the spacing between the segregation bands was more limited, for example 20 μm ($0.02\cdot 10^{-3}$ m). In this case, the holding time for manganese is equal to:

$$0.04 = 0.16 e^{\left(-\frac{3.501\cdot 10^{-15}\cdot t\cdot \pi^2}{0.00002^2}\right)}$$

$$t_{Mn} \cong 16{,}048\ s \cong 4\ h\ and\ 30\ min$$

This example clearly shows how the effect of hot working is very important, in order to refine the segregation band structure and to homogenize the chemical composition during subsequent heat treatments.

The finer the segregation bands the easier it is to eliminate the segregation in the semi-finished product (forged, molded, laminated). In fact, reducing the spacing between the segregation bands by a fifth (100 μm as compared to 20 μm), the homogenization time is reduced by about 25 times.

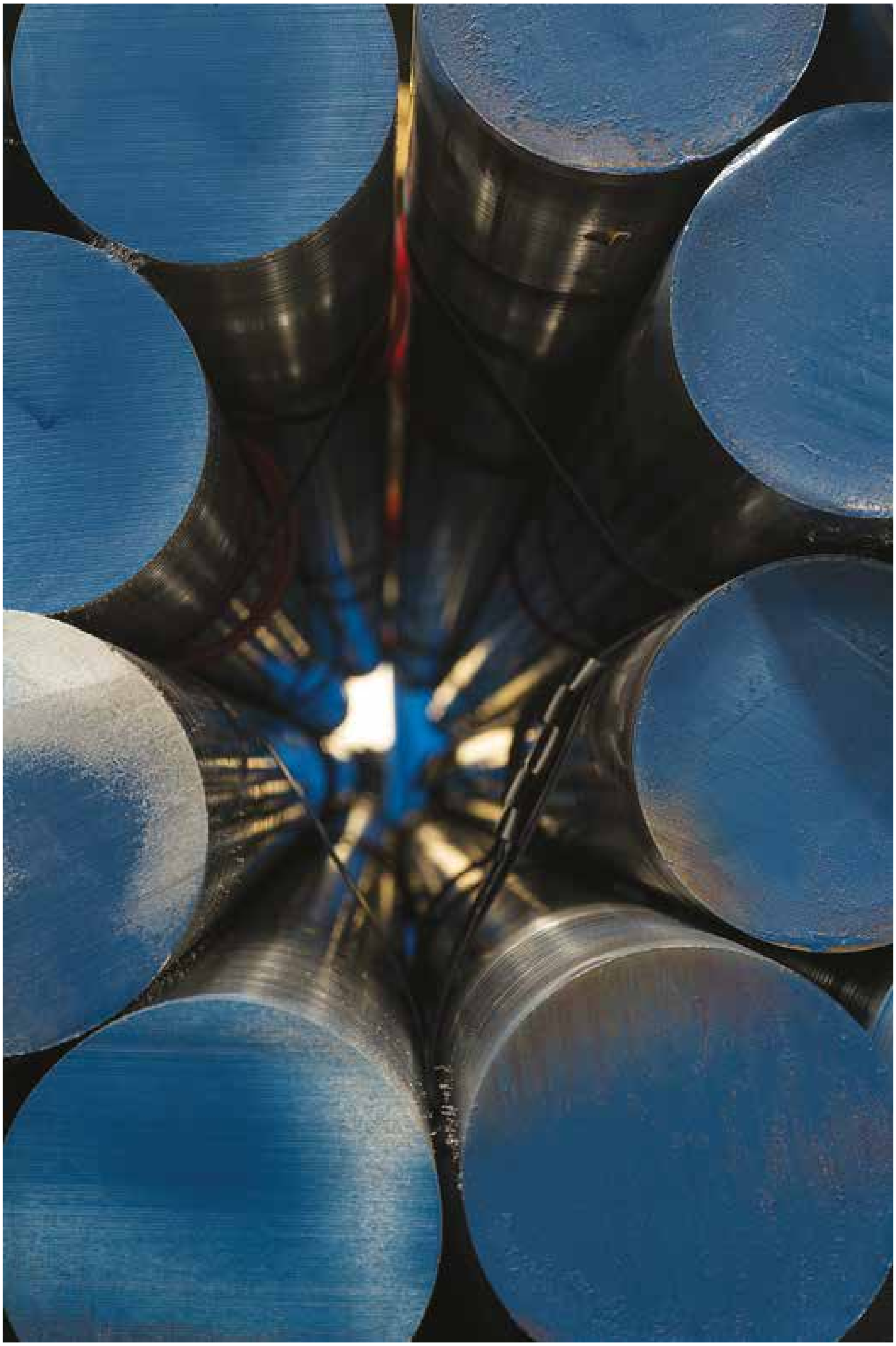

4. STRENGTHENING MECHANISMS OF STEEL

4.1 Classification of steel strengthening mechanisms

The considerations presented in Chapter 2 on crystal lattice defects are of fundamental importance for understanding the mechanisms that increase or decrease the mechanical strength of a basic iron alloy.

As we have seen, the aptitude towards the deformation of a metallic mass essentially depends on the mobility of the dislocations in the crystal lattice. Facilitating the dislocation motion means facilitating the deformability of steel. On the contrary, preventing the dislocation motion causes an increase in mechanical strength and hardness.

There are four methods to improve the mechanical strength of steel:

- add alloying elements (strengthening by alloying);
- Cold deformation of the metallic mass (strengthening by strain hardening);
- form precipitates inside the crystal lattice (strengthening by precipitation);
- reduce the mean grain size (strengthening by refining).

All of these mechanisms result in increased hardness, yield strength, and ultimate tensile strength of the steel by creating obstacles to the dislocation motion.

4.2 Strengthening by solid solution

The strengthening mechanism by alloying is based on the existence of point defects in the lattice, in particular, the substitutional atoms and the interstitial atoms.

Whatever the alloying element and the underlying mechanism (alloying by substitutional solid solution or interstitial solid solution), foreign atoms always generate a perturbation in the crystal lattice by locally creating a stress field. This phenomenon creates an obstacle to the dislocation motion as shown in Figure 4.1.

The actual increase in strength of the metallic mass depends on both the quantity of the alloying element in solution and its atomic size, that is, on the greater or lesser disruption action that a foreign atom creates in the iron lattice[1] (Figure 4.2).

---

[1] *Please note that the abnormality introduced in the lattice by the presence of foreign (substitutional or interstitial) atoms is not of a geometric but of an electromagnetic nature. It depends to the electronic configuration that is different for each chemical element (especially the outer orbital ones), and not to the size of foreign atoms with respect to iron atoms.*

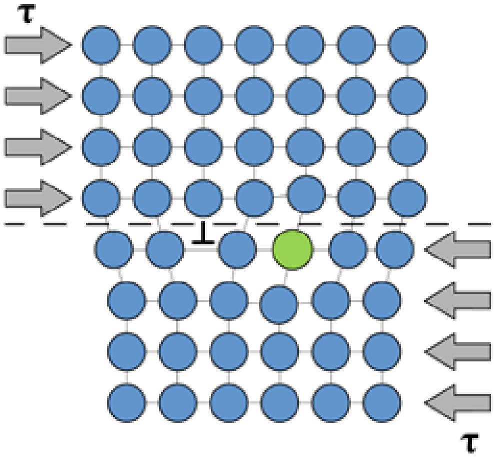

Figure 4.1 - The effect of substitutional atoms (left) and interstitial atoms (right) on dislocation motion.

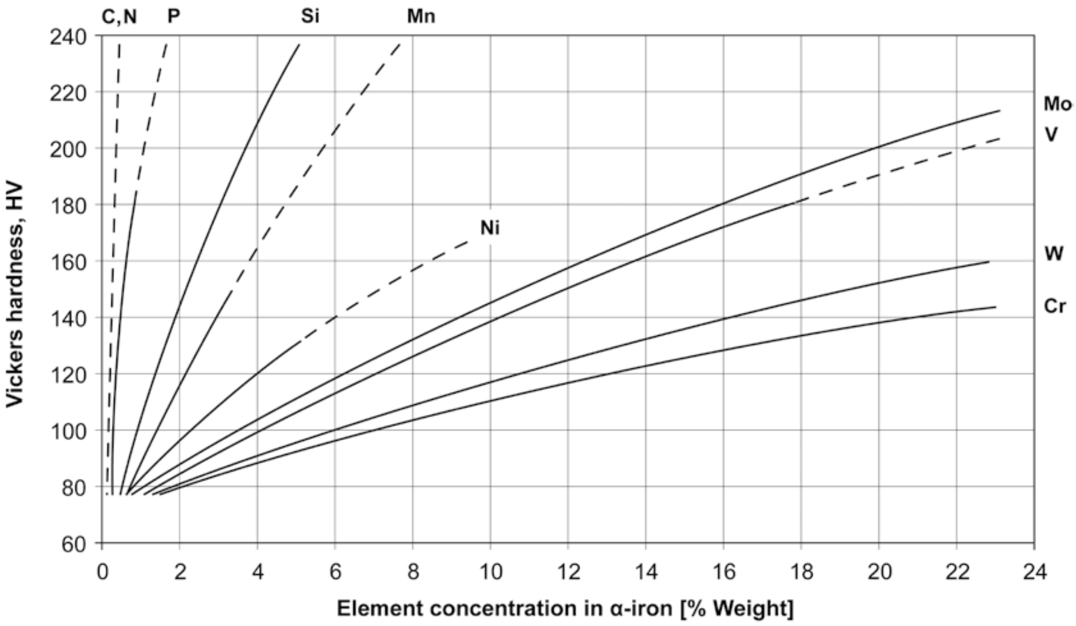

Figure 4.2 - The effect of substitutional and interstitial atoms on the hardness of α-iron lattice [from Bain and Paxton 1966].

In carbon steel and special steel, the most significant effect in terms of strength is related to interstitial elements, i.e. carbon or nitrogen. Instead, substitutional elements are less effective. The effect of the interstitial atoms is more consistent because the strengthening of the metallic matrix is related to a greater perturbation induced by small foreign atom that insinuates into the interstitial sites. Different is the case of the substitutional atoms which simply replace the iron atoms in their positions of equilibrium.

4.2 Strengthening by strain hardening

If a metal or alloy is subjected to cold deformation[2], it is normal to observe an increase in its strengthening characteristics (hardness, yield strength, and ultimate tensile strength). The higher is the degree of cold deformation, the greater the strengthening, that is, the increase in mechanical strength. Conversely, as the deformation increases, the residual ductility of the metallic mass decreases progressively. Along with the mechanical properties, cold deformation also modifies the shape and size of the crystallite, which is crushed and elongated in the direction of the main deformation.

This phenomenon is called strain hardening and occurs in all those cases where the shape and size of the metallic mass is modified through cold deformation. Typical technologies that allow a significant level of cold work are cold rolling, cold extrusion, drawing, deep drawing, and bending[3] (Figure 4.3).

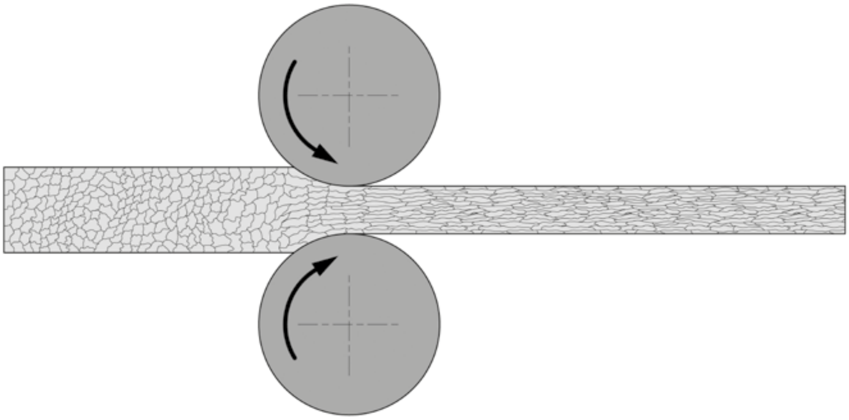

Figure 4.3 - The effect of cold rolling on the microstructure of the metallic mass.

---

[2] *A deformation process is said to be cold if the metallic mass is permanently modified when operating at room temperature or slightly higher. Many texts indicate 1/3 of the melting temperature in Kelvin degrees as the limit. In the case of low carbon steel, this value is equal to approximately 300°C.*

[3] *The term "cold" is indicated in cases where a misunderstanding might arise. For example for rolling and extrusion the term "cold" is specified while drawing or banding are generically indicated because usually work at room temperature or slightly above.*

The amount of strain hardening, is defined by the reduction of the section of the semi-finished product *S%*. The initial section is called A_0 and the final section is called A_f, while *S%*, equals:

$$S\% = \frac{A_0 - A_f}{A_0} \cdot 100 \qquad [4.1]$$

The effects of cold deformation in a low-carbon steel are shown in Figure 4.4.

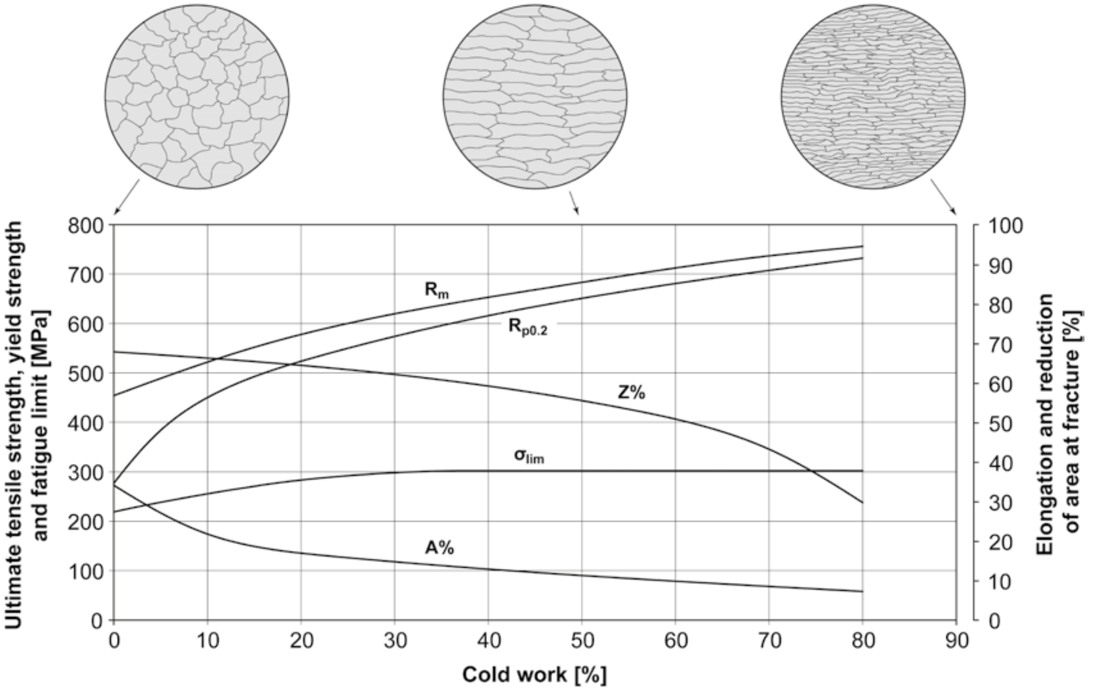

Figure 4.4 - The effect of strain hardening on the strengthening and deformability of an EN C15-type steel with a pearlitic-ferritic structure [from Dieter 1988].

The efficiency of the process is not only a function of the strain hardening level, but it also depends on the type of steel structure.

As a result of the strain hardening induced in semi-finished products that are cold-finished, residual stresses[4] are always present. Residual stresses are nothing more than macroscopic mechanical forces that remain in the component when the external forces used to deform it have been eliminated.

---

[4] The residual stresses were self-balancing inside a workpiece that was not subjected to any external applied strength. Typically, residual stresses are caused by the processes of plastic deformation (hot or cold), from machinig, as a result of massive or superficial heat treatments, during solidification of castings, or the creation of welded joints. Residual stresses are always difficult to evaluate and, very often, affect the behavior of mechanical components. Residual stresses are combined with the stress states induced by the operating stress and may also lead to fracture of the component.

Residual stresses are a direct consequence of the heterogeneous distribution of strain hardening in the metallic mass (Figure 4.5).

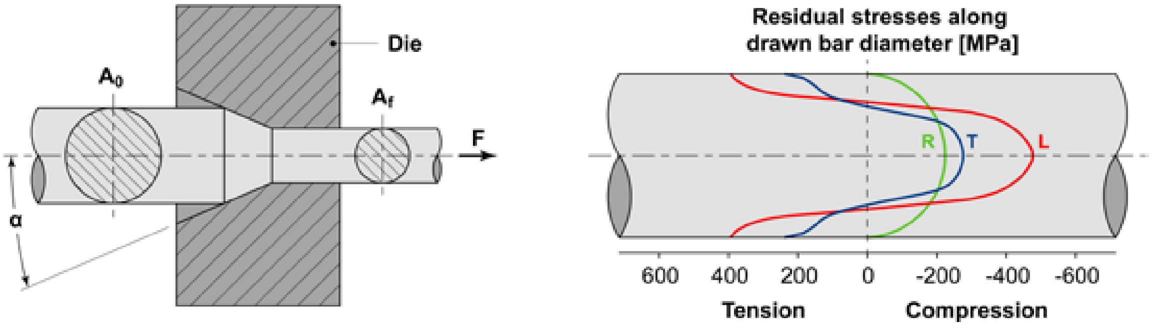

Figure 4.5 - The effect of drowing process on residual stresses of a bar of EN C45 steel (drawing angle α = 20°; section reduction *S%* = 11.6%). Stresses in longitudinal *L*, radial *R* and tangential *T* direction [from Rocha et al. 2012].

Plastic deformation and strain hardening are directly related to the dislocation motion and their progressive multiplication and stacking in the crystal lattice.

It is the dislocation motion that causes their multiplication: deforming the metallic mass, that is, putting the dislocations in motion, also means increasing their number. For example, the density of dislocations in low carbon steel in the annealed state[5] is equal to $10^9 \div 10^{10}$ m/m^3, while after strain hardening, it is in the order of $10^{16} \div 10^{17}$ m/m^3.

The multiplication of the dislocations is understood by considering what happens, for example, to an edge dislocation when its movement is blocked at the extremities (Frank-Read mechanism). This phenomenon occurs if the line defect is anchored to obstacles, such as crystal lattice irregularities, impurities, precipitates, other dislocations, etc. In such cases, the continuous application of shear stresses produces a curvature of the advancing edge of the dislocation. In the end, the dislocation closes on itself and forms a new dislocation. As movement proceeds, there is a continuous multiplication of dislocations that increase in number as the deformation increases (Figure 4.6).

---

[5] *Dislocation is a line defect, measured in units of length. Therefore, in order to have a defect density, the total length of the defects must be indicated, with respect to the volume.*

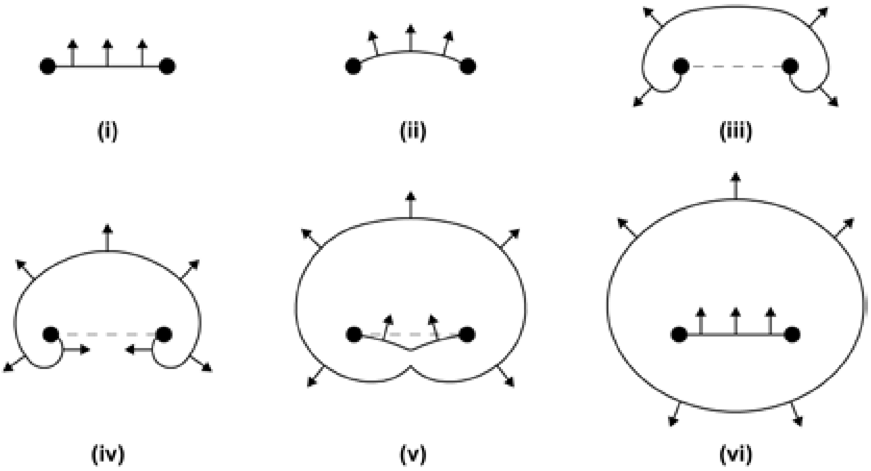

Figure 4.6 - Schematic representation of the Frank-Read Mechanism [from Campbell 2008].

The direct consequence is the creation of an ever increasing amount of obstacles to the dislocation motion. Generating new dislocations that move in every direction means forming a growing number of obstacles to their movement. By moving and multiplying, dislocations tend to obstruct each other: this progressively reduces their mobility, meaning it decreases the deformability of the metallic mass, while increasing hardness and mechanical strength.

What has been described explains what happens during the plastic deformation of a steel. In order to deform the metallic mass, the application of increasing forces is required. When they are deformed, metals and alloys tend to gradually become work-hardened, that is, it is increasingly difficult to continue to deform them, since their strength increases: this effect is due to the dislocation motion. Once the ductility of the metallic mass is exhausted, further deformation cause the ductile fracture of the component.

4.3 Strengthening by precipitation

The third steel strengthening mechanism is due to nano-particles[6] of a second phase distributed in the metallic matrix.

These precipitates lead to the strengthening of steel both by hindering the dislocation motion and also by favoring their continuous multiplication. In both cases, the effect is to reduce the deformability and to increase the mechanical strength of the metal.

The mechanisms involved when the nano-particles are coherent or incoherent with the metallic matrix are different (Figure 4.7).

---

[6] *Particles that favor the strengthening by precipitation of metallic materials are also called dispersoids.*

If the precipitates are coherent, that is, with the same orientation of the surrounding lattice, the dislocation slows down, while it cuts in half the particle that obstructs its movement (Friedel-Fleischer effect). When the precipitates are incoherent with the lattice of the matrix, that is, they cannot be directly crossed by dislocation, both the mobility reduction of the defect and its multiplication (Orowan mechanism) are observed.
In either case precipitates reduce the dislocation motion and increase the mechanical strength of the steel.

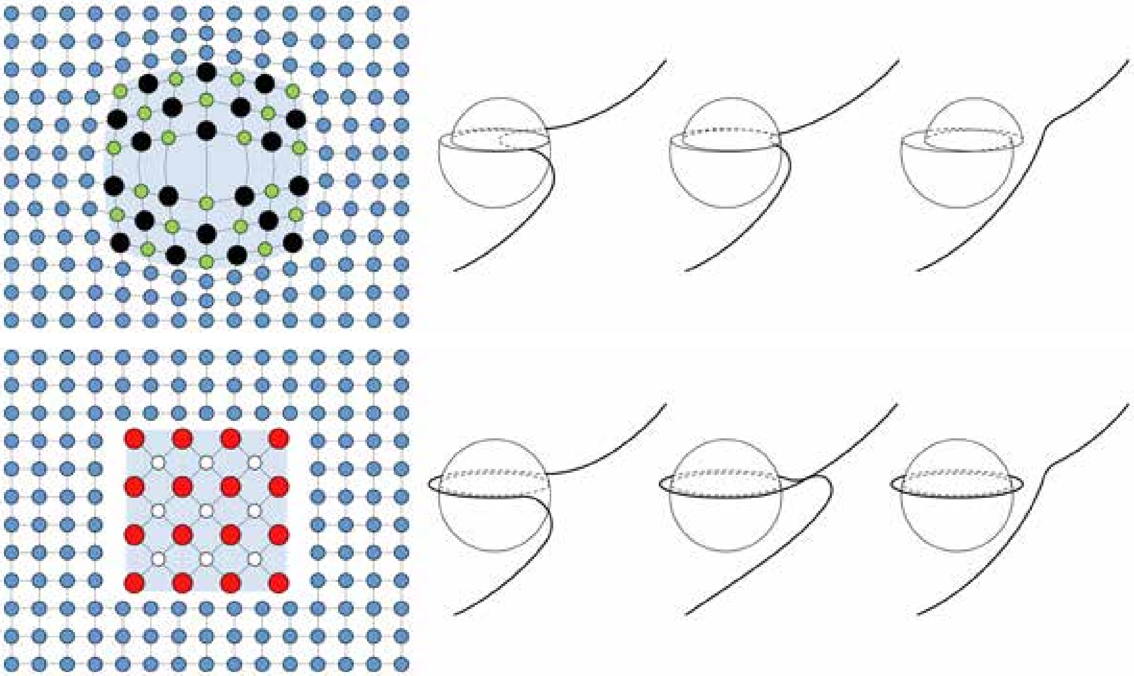

Figure 4.7 - Obstruction to dislocation motion caused by nano-particles: Friedel-Fleischer effect, in the case of coherent precipitations (above) and Orowan mechanism in the case of incoherent precipitates (below) [from Gerold 1979].

Phenomena of this type are observed in steel with a particular chemical composition, that is, if there are alloying elements present, such as titanium, vanadium, and niobium in a very small quantity (0.05÷0.15%)[7]. During the hot working of semi-finished products, these chemical elements form very fine precipitates[8], which block the dislocation motion (Figure 4.8).

---

[7] *Steels of this type are also called micro-alloyed steels or HSLA: High-Strength Low-Alloy (Steel).*

[8] *Micro-alloyed steels include carbides and niobium carbonitrides,* Nb_4C_3 *and* $Nb(C, N)$*, nitrides and vanadium carbides,* VN *and* V_4C_3*, titanium carbides,* TiC*. These precipitates are formed during hot working deformation of coils, plates, bars, forged components, and so on.*

For these materials, the increase of the ultimate tensile strength ($\Delta\sigma_m$ in MPa), caused by nano-particles precipitation, can be estimated with the Ashby-Orowan formula:

$$\Delta\sigma_m = \frac{A \cdot \sqrt{V_f}}{\bar{d}} \ln\left(B \cdot \bar{d}\right) \qquad [4.2]$$

A and B are two constants that depend on the material, V_f the volumetric fraction of the nano-particles, and $\bar{d}$ their average diameter in µm[9]. As is evident in equation 4.2, the finer the nano-particles and the greater is thair volumetric fraction, the more effective is strenghtening by precipitation (optimum size is in the order of 5÷30 nm).

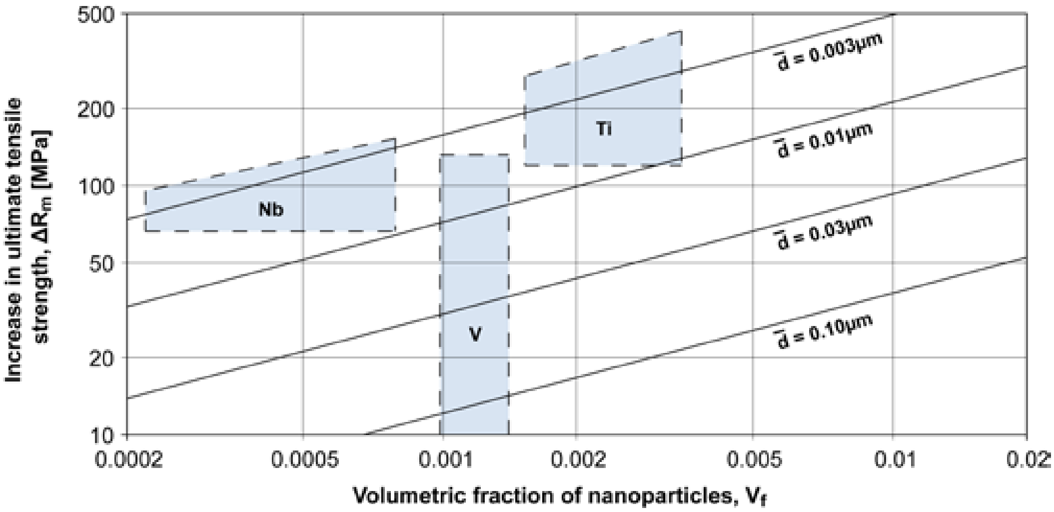

Figure 4.8 - The effect of the volumetric fraction of nano-particles , V_f , and their average size , $\bar{d}$, on strengthening by precipitation. Comparison of the Ashby-Orowan model (continuous lines) and the experimental results on High Strength Low Alloy Steel (colored areas) [from Ginzburg 2005].

4.5 Strengthening by grain refinement

The fourth strengthening mechanism is grain refinement: the grain boundaries are one of the most effective obstacles for the dislocation motion. Steel with many grain boundaries per unit of volume, that is, with small grains, has a mechanical strength, higher than steel with coarse grain.

---

[9] *In the case of HSLA steels, A is equal to 5.9, while B is 4000 [Ginzburg 2005].*

As seen previously in Chapter 2, the dislocations do not move randomly within the grain, but they always follow the lattice orientation. Since each grain has a uniformly arranged lattice inside it, the path of the dislocations is generally defined and delimited by the grain boundaries. Once they have reached the grain boundary, the dislocations stop their movement (Figure 4.9) and there is a progressive buildup of defects in these areas, which increases as the lattice deformation increases.

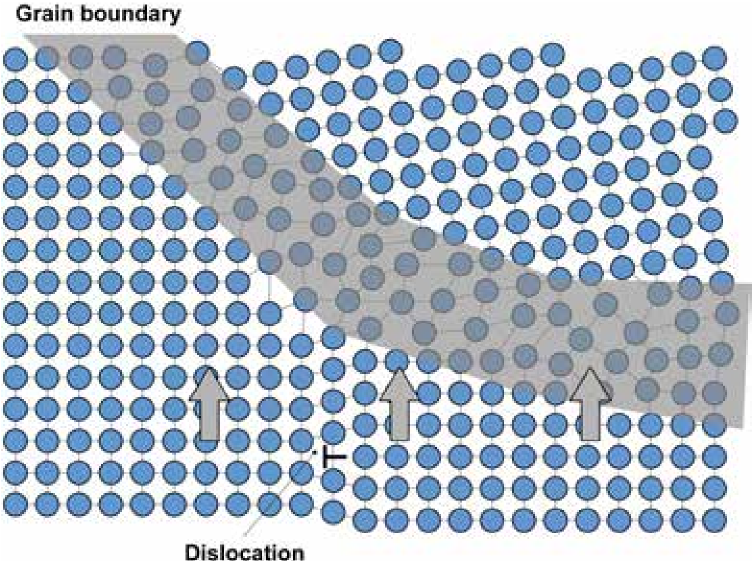

Figure 4.9 - The effect of grain boundary on dislocation motion.

Therefore, the mean grean size has important implications on the mechanical strength of steel and metal alloys. A decrease in the mean grain size creates more grain boundaries, that is, more obstacles for the dislocation motion. This reduces the deformability and increases the mechanical strength of steel.

If, instead, the crystallite is coarse, that is, there are few grain boundaries, the mean free path of dislocations is large. Consequently, deformability is facilitated and mechanical strength is lower (Figure 4.10).

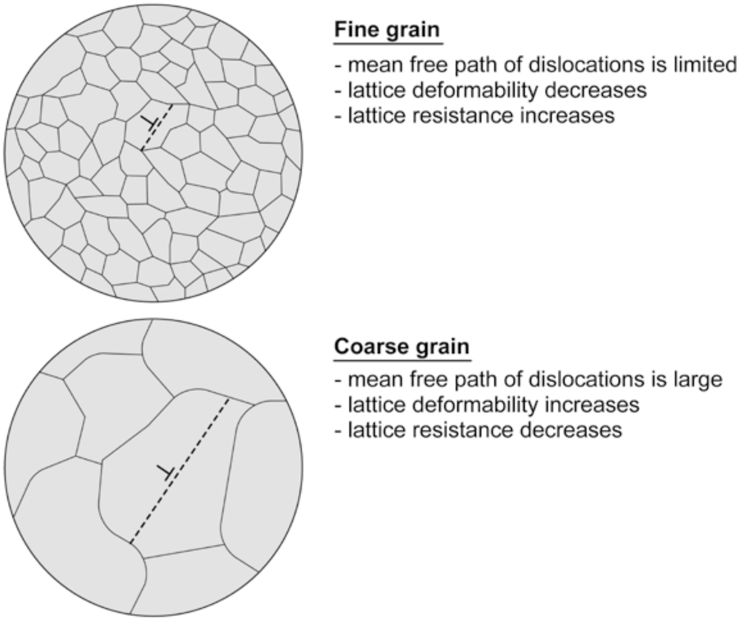

Figure 4.10 - The effect of mean grain size on mechanical strength and deformability of a metal.

There is an experimental correlation, called Hall-Petch's relation, between yield strength and mean grain size. The relation is expressed by the following formula:

$$\sigma_{sn} = \sigma_0 + kd^{-1/2} \qquad [4.3]$$

where σ_{sn} is the yield strength, k is a coefficient that depends on the material (called Hall-Petch constant), σ_0 is the minimum stress required to trigger the dislocation motion, and d is the average diameter of a crystallite[10]. The graphic representation of Equation 4.3 is shown in Figure 4.11.

Even if, theoretically, an infinite increase in strength could be obtained by decreasing the mean grain size to nanometric values ($d \longrightarrow 0$), actually, it is experimentally observed that Hall-Petch's relation is valid only up to grain size of 10μm. Below these values, the deformation mechanism is no longer ruled by the dislocation motion but by the sliding of the grain boundaries, and even the yield strength begins to diminish.

---

[10] *In the case of low carbon steel σ_0, it is equal to 70 MPa, while k is 0.74 MPa $\sqrt{m}$ [Smith & Hashemi 2006].*

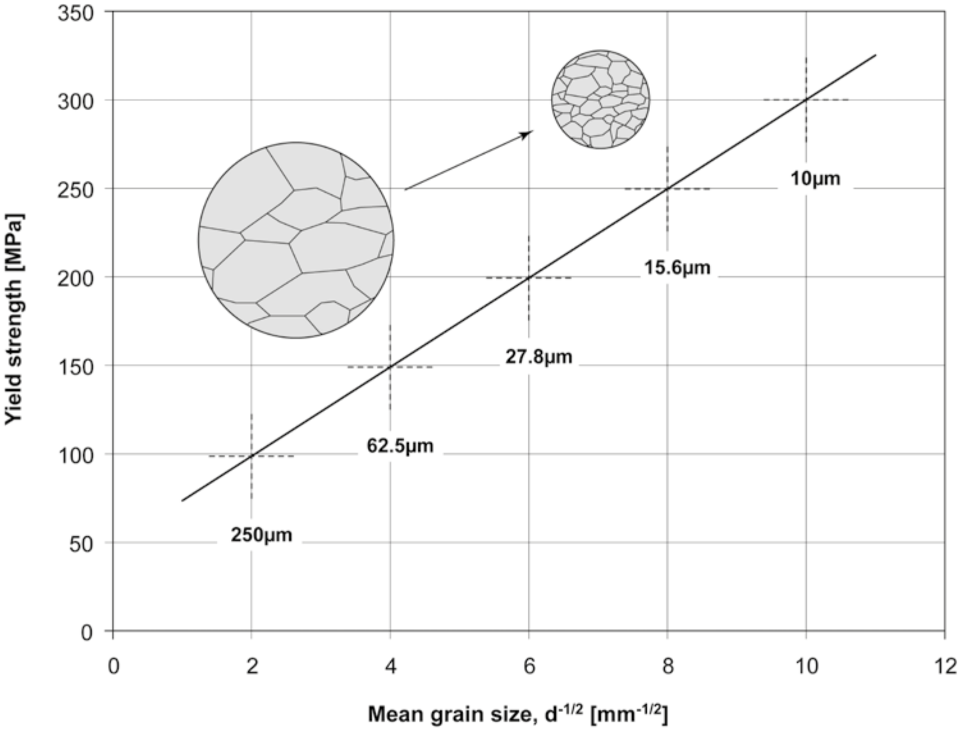

Figure 4.11 - Hall-Petch's relation for low carbon steels [from Campbell 2008].

4.5 Recovery, recrystallisation and grain growth

Let us now see what happens if a heat treatment is performed on a semi-finished product that has been strengthened by one or more of the mechanisms previously discussed.

By exposing the metallic mass to a high temperature, three metallurgic phenomena can be observed (Figure 4.12):

- recovery
- recrystallisation
- grain growth

Recovery

Cold deformation occurs mainly due to the motion and multiplication of the dislocations. At the same time, crystallites are extended in the direction of the deformation and residual stresses originate in the semi-finished product. These phenomena accumulates a large amount of mechanical energy in the material, inducing thermodynamic instability in the lattice.

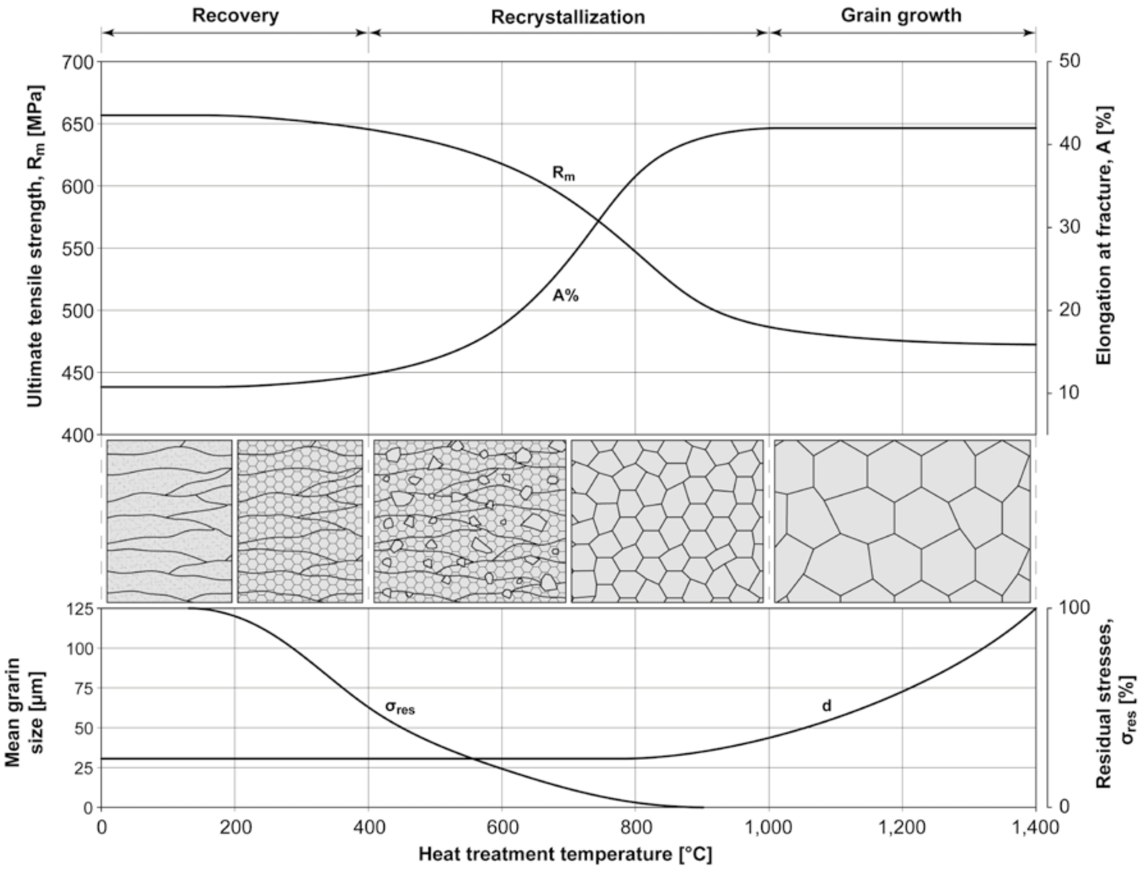

Figure 4.12 - Schematic representation of the microstructural and mechanical evolution of a strain hardened EN C15 steel, subjected to heat treatment (recovery, recrystallisation, and grain growth phenomena).

When the metallic mass is warmed up at temperatures below the minimum recrystallisation temperature[11], there is a progressive redistribution of the mechanical energy accumulated in the system during plastic deformation.The phenomenon occurs because at these temperatures atoms move by diffusion from high energy positions to positions of equilibrium. This phenomenon favors a reassembly of the mechanical stresses in both crystal lattices and in the metallic mass as a whole, inducing a more stable thermodynamic state with respect to strain hardened material.

---

[11] *For the definition of the recrystallisation temperature, see the next point of this paragraph.*

Recovery is accompanied by a significant reduction in the dislocation density through their reorganization according to mechanisms on a lattice level (Figure 4.13). These are mainly phenomena of annihilation (cancellation of two opposing dislocations), polygonization, and formation of sub-grains (transformation of a curved grain caused by strain hardening in two polygonal sub-grains), and dislocation climb (progressive climb over an obstacle).

During the recovery phase, the mechanical strength of steel do not change significantly, even if the decreasing of the residual stresses improves fatigue strength and physical properties of the metallic mass (for example, electrical and heat conductivity).

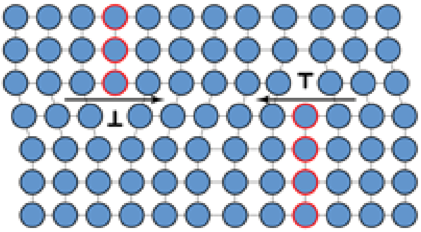

a) **Annihilation**

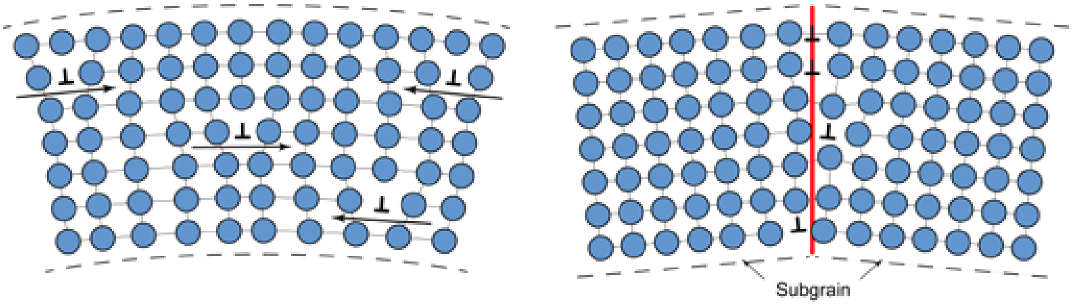

b) **Polygonization and subgrain formation**

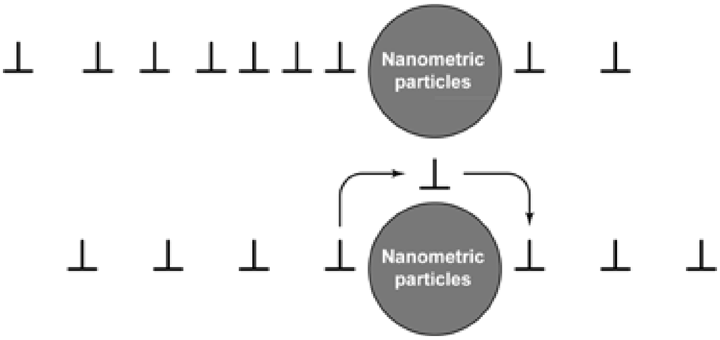

c) **Dislocation climb**

Figure 4.13 - Schematic representation of lattice phenomena that favor recovery: a) annihilation of dislocations; b) polygonization and formation of sub-grains; c) dislocation climb.

Recrystallisation

If the heat treatment temperature exceeds a minimum threshold, the recrystallisation phenomenon also occurs. Activated by an increase in temperature and through the mechanical energy still stored in the metallic mass, the cold deformed grains transform into new homogeneous and equal-sized grains, without stress and strain hardening.

Recrystallisation takes place according to a nucleation and growth mechanism and, over time, the new grains completely replace the initial microstructure. When recrystallisation has ended, the microstructure has completely recovered the original deformability level (Figure 4.14).

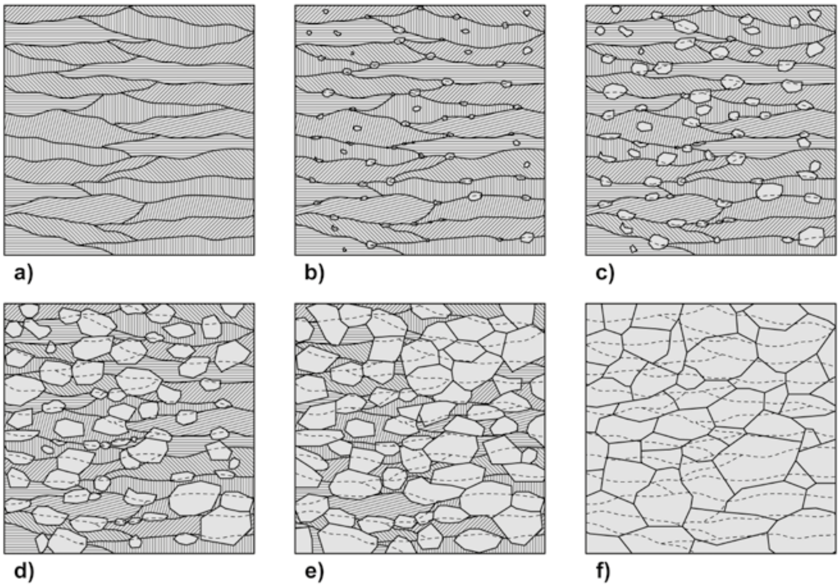

Figure 4.14 - Recrystallisation phases in steel: a) metallic mass in the strain hardened state; b) recrystallisation with formation of new grains; (c-e) growth of new grains at the expense of the original structure; f) completed recrystallisation [from Higgins 1993].

Recrystallisation is controlled through various parameters: process temperature, chemical composition of the metallic mass, degree of strain hardening and mean size of the original grains.

The minimum recrystallisation temperature, T_r, is in the order of 0.4÷0.5 of melting point of the material in Kelvin[12]. If temperature increases, the rate of recrystallisation also increases.

---

[12] *The recrystallisation temperature is the minimum temperature that, after one hour of time, causes complete transformation of the strain hardened grains into new homogeneous and equally-sized crystallites.*

In pure metals, T_r is low: ARMCO iron, for example, is recrystallized at about 400°C. The presence of atoms in solid solution (even if in a limited quantity) increases the recrystallisation temperature by many degrees: in low carbon steel T_r, it is in the order of 500°C÷550°C.

As the strain hardening increases, the recrystallisation temperature gradually decreases. It should also be noted that is required a minimum level of colled deformation (5-10%) so that recrystallisation takes place.

Finally, consider the effect of the mean size of the original grains. Since recrystallisation is a nucleation and growth phenomenon, it is faster in fine-grain materials as compared to coarse-grain materials. Also, if the starting microstructure is very work-hardened, the size of the grains at the end of recrystallisation is smaller with respect to the undeformed materials, which have coarser crystallites.

Grain growth

The increase in heat treatment temperature causes the progressive enlargement of the grain size. Some crystallites, in order to further reduce their energy level, increase in size at the expense of adjacent grains. Consequently, a coarse-grain structure is produced, with respect to the fine grains at the end of recrystallisation.

The driving force of the growth is the surface energy of the grains, proportional to the total surface of the grains. During of growth, the polycrystalline structure tends to evolve in the direction that leads to a decrease in the surface energy of the system, i.e. a reduction in the total surface of the grain boundaries. This is the case if the holding temperature is sufficiently high or if the holding time is prolonged, in order to favor the diffusion movement of the atoms. This allows for several crystallites to grow homogeneously, at the expense of others (Figure 4.15).

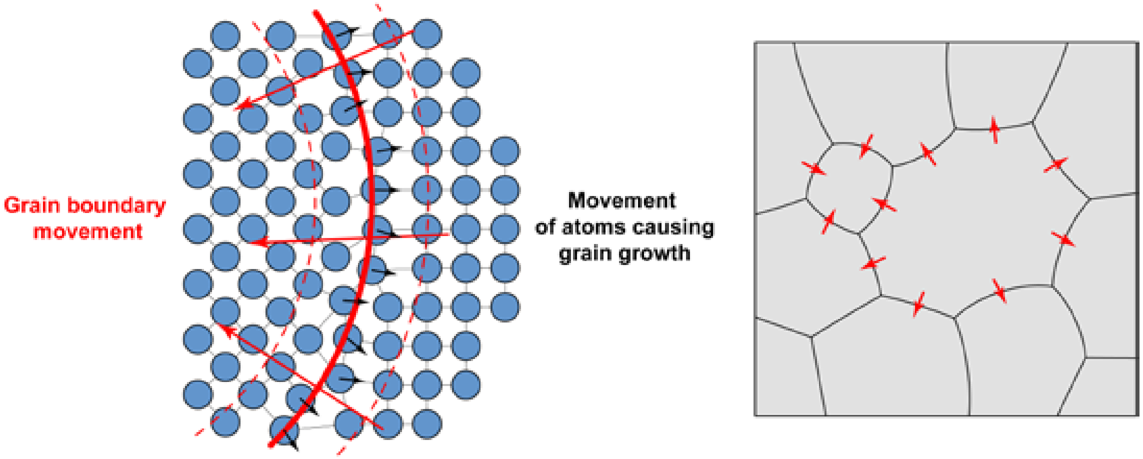

Figure 4.15 - Shematic representation of the grain growth mechanism [from Singh 1999].

Grain growth in a metallic mass may be continuous or discontinuous[13].

In the first case, all the growing crystallites increase in size homogeneously. In the second case, the growth occurs only in some points of the microstructure, with the formation of abnormal grains at the expense of others that remain small in size (Figure 4.16).

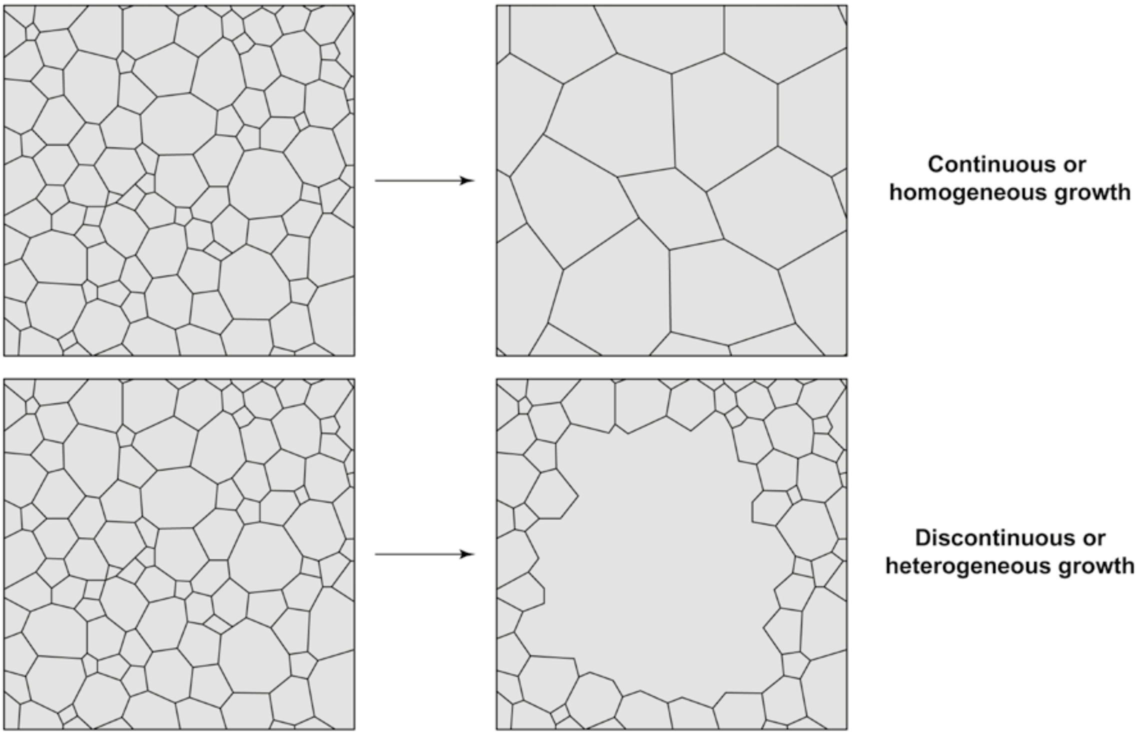

Figure 4.16 - Example of crystallite growth: a) continuous growth; b) discontinuous growth [from Thompson 1985].

The phenomenon of discontinuous growth occurs when normal recrystallisation is inhibited by very small inclusions. A typical case is killed steel, where small aluminum oxides (Al_2O_3) and/or small nitrides (AlN), force the crystallites to remain within limited sizes. However, if the heating temperature is very high or the holding time is prolonged the secondary particles begin to coalesce or even solubilize in some areas. The crystallite explosion occurs in these points, while the surrounding grains remain small because their growth is inhibited by the inclusions still present (Figure 4.17).

---

[13] *These two methods are also called primary (or continuous) growth and secondary (or discontinuous) growth.*

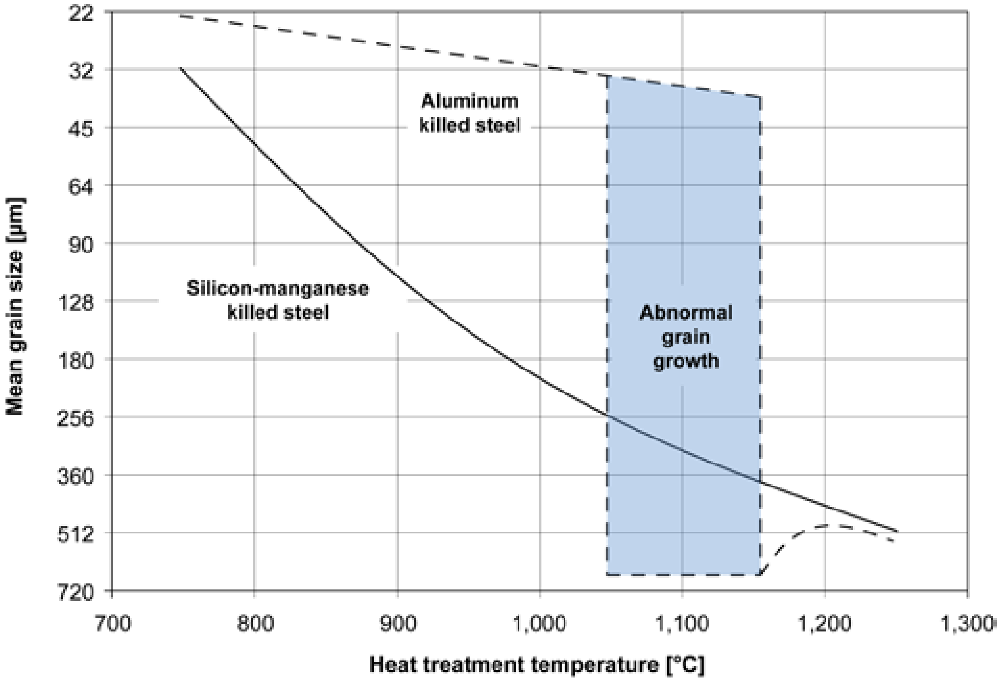

Figure 4.17 - The effect of temperature on continuous or discontinuous grain growth for silicon-manganese killed steel and aluminum killed steel [extracted from Gladman 2004].

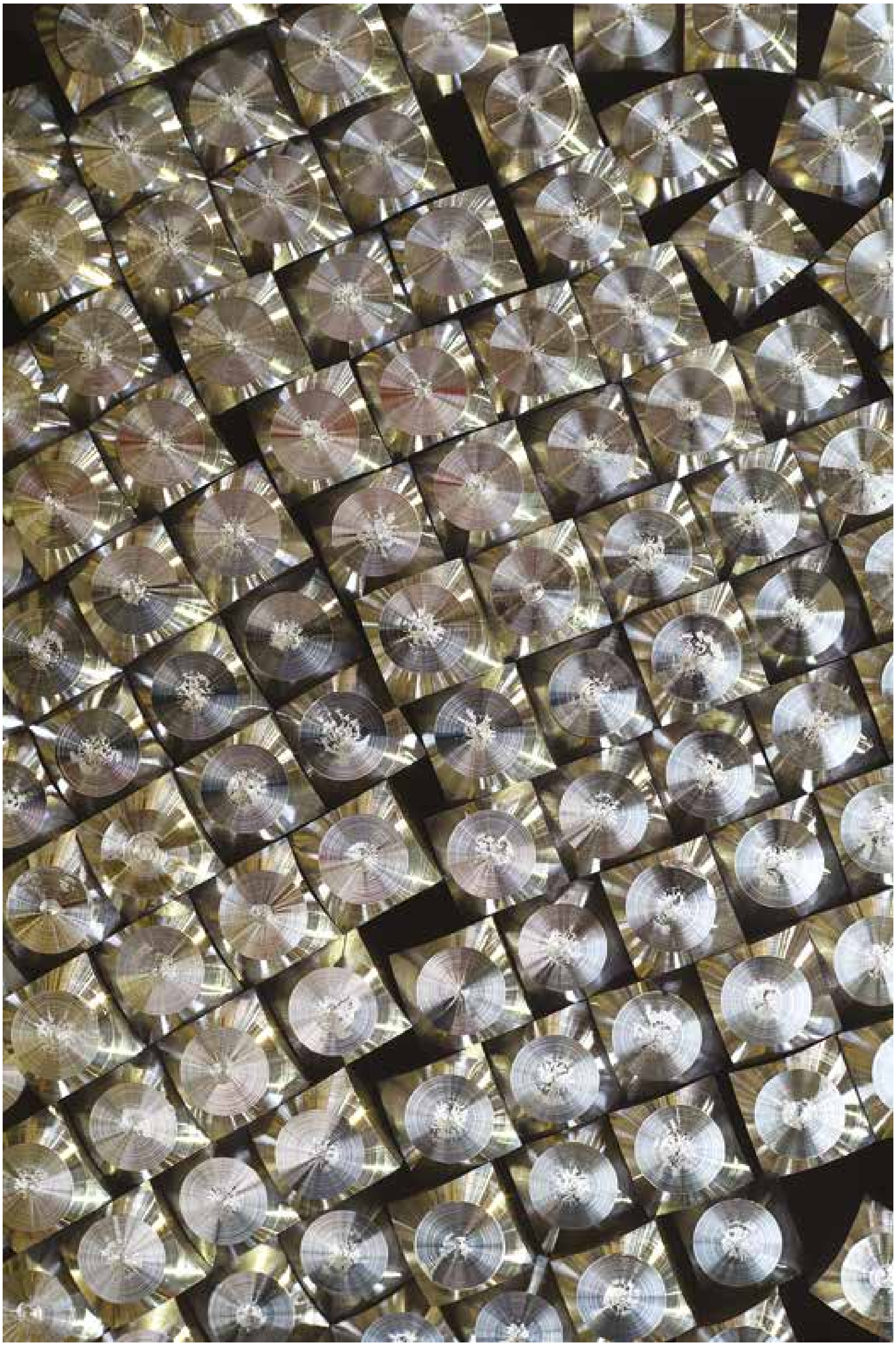

5. PHASE DIAGRAMS

5.1 Phase diagrams for pure substances

A phase is defined as any portion of a chemical system that is homogeneous in chemical composition, state of aggregation, pressure, and temperature.

To understand the phase concept, consider the case of a glass of water at atmospheric pressure (1 atm) and room temperature (20°C). In this situation, the water in the glass is completely liquid, is homogeneous in temperature and pressure, and its chemical composition is constant because it is a pure substance: all the water present in the glass is, therefore, a single phase. Something similar is obtained if the temperature is set at -5°C and the pressure remains atmospheric: the iced water in the glass is a single phase. The two situations described above can be replicated infinitely by changing the temperature and pressure values from time to time. It is, therefore, possible to define all the conditions in which the water is aggregated in a solid, liquid, or gaseous form. Graphic representation of what is experimentally obtained is shown in Figure 5.1.

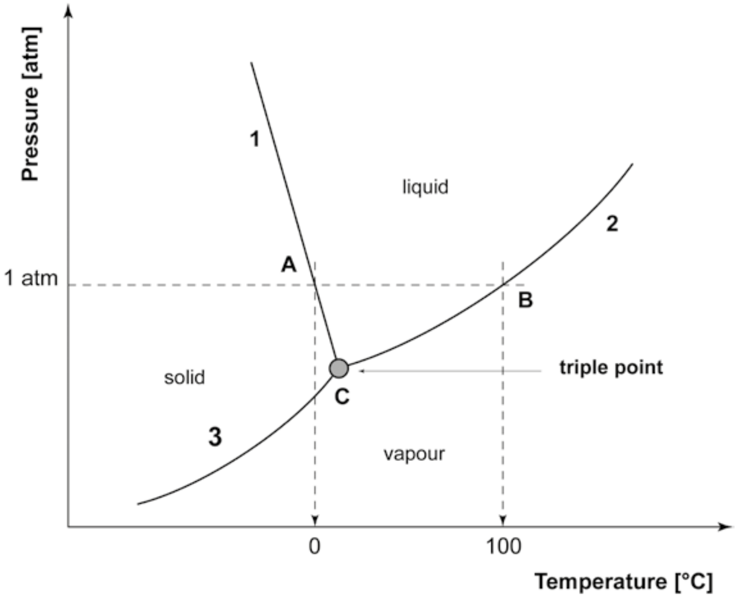

Figure 5.1 - Phase diagram for pure water: points, *A* and *B*, are respectively the solidification temperature and the boiling temperature at atmospheric pressure, *C*, the triple point.

Figure 5.1 is a typical phase diagram for a pure substance, that is, a graph that represents the phases of the system in conditions of thermodynamic equilibrium, when temperature and pressure vary. Remember that any chemical system is defined as being in thermodynamic equilibrium if all the thermodynamic variables that contribute to describing it (pressure, temperature, and chemical composition) are indicated in a completed manner and do not change over time. In the case of water, the chemical composition is constant and, therefore, only the pressure and temperature may vary.

Curve 1 in Figure 5.1 indicates the equilibrium between the solid and the liquid, that is, the condition where solidification occurs at cooling and melting occurs at heating. Along this line, there are two distinct phases (solid phase and liquid phase) corresponding to the two different aggregation states of the system.

Similarly, curve 2 and curve 3 respectively show the equilibrium between liquid and vapour (condensation/evaporation) and between solid and vapor (deposition/sublimation).

Considering, for example, pure water at atmospheric pressure, solidification/melting occurs at 0°C (point *A*) and condensation/evaporation at 100°C (point *B*). If the pressure is modified (increased or decreased), the temperatures at which the aggregation state transitions occur also change. Furthermore, water, like many pure substances, has a triple point (point *C*), that is, a point where the three aggregation states (liquid phase, solid phase, and gaseous phase) coexist: this point is uniquely defined by a single pressure and temperature value (p = 4.58 mmHg; T = 0.01°C).

The pure iron phase diagram, shown in Figure 5.2, is similar to the water phase diagram. Note that, in this case, as is typical of metals, the axes are reversed: abscissa for the pressure, ordinate for the temperature.

The fields of iron in vapour state, liquid state, and solid state are also on the diagram in Figure 5.2. It is interesting to note that, for the solid state, the allotropic transformation temperatures are also indicated: α-iron (B.C.C.), γ-iron (F.C.C.), and δ-iron (B.C.C.).

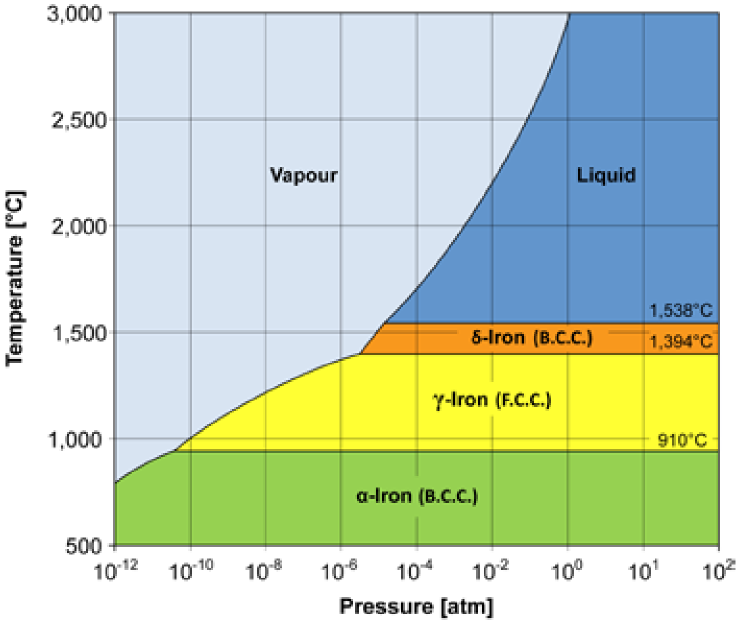

Figure 5.2 - Pure iron phase diagram.

5.2 The Gibbs Phase Rule

Before proceeding further with examining phase diagrams, it is necessary to introduce a very important rule related to the systems of equilibrium: this is the so-called "Gibbs Phase Rule"[1]. It allows to predict the equilibrium state of an homogeneous or heterogeneous chemical system (as, for example, a phase diagram) when there is a change in temperature, pressure, and concentration of the individual chemical species[2] that form the phases of the system.

The Phase Rule is expressed as follows:

$$V = C_i + M - F \qquad [5.1]$$

where V is the variance, C_i is the number of independent chemical components, M is the number of efficient physical factors, and F is the number of phases.

Let us see the meaning of the various parameters of equation 5.1.

The variance, or number of degrees of freedom of the system, is the number of independent variables (pressure, temperature, and concentration of chemical species present in each single phase), which can be arbitrarily chosen, for which the other variables also assume well-determined values.

The independent chemical components, C_i , are the chemical species needed to uniquely identify the composition of all the phases that form the system. C_i is obtained from the following relation:

$$C_i = C_t - r \qquad [5.2]$$

where C_t is the total number of chemical species in the system (total chemical components), while r represents the number of reversible reactions that bind these chemical species and the stoichiometric constraints between substances that form each phase[3].

The number of efficient physical factors, M, that is, the physical parameters that have an effect on changing the equilibrium of the system, is equal to two: temperature and pressure. However, it should be noted that in many applications involving metals and metal alloys, the pressure is constant and is equal to the atmospheric pressure.

---

[1] *Josiah Willard Gibbs, an American Chemical Engineer, is one of the founders of thermodynamics and modern chemistry-physics. His main contribution is related to the definition of free enthalpy, (commonly known as Gibbs free energy) witch allows to predict the spontaneity of a chemical reaction. He is also known for the Phase Rule which was developed in 1876.*

[2] *The term, "chemical species", is used to define a generic chemical substance, regardless of the number of atoms or molecules that constitute it. A chemical species can be defined only if the nature, proportion, and disposition of the chemical elements that constitute it are known. Examples of chemical species are simple substances, chemical compounds, reagents, products, and intermediates of any chemical reaction. Phases and mixtures, on the other hand, cannot be considered chemical species, since more than one chemical species of a different nature can coexist within them.*

[3] *Take, for example, the dissociation reaction for calcium carbonate:* $CaCO_{3(s)} \leftrightarrow CaO_{(s)} + CO_{2(g)}$. *The total chemical components are 3 (*$CaCO_{3(s)}$, $CaO_{(s)}$, $CO_{2(g)}$*), there is a single chemical reaction, and there are no stoichiometric constraints between* $CaO_{(S)}$ *and* $CO_{2(g)}$. *The independent chemical components are, therefore, equal to 2 (*C_i*= 3-1 = 2).To define the composition of the three phases that make up the system, two chemical species must, therefore, be chosen, for example* $CaO_{(s)}$ *and* $CO_{2(g)}$.

Consequently, for metals and metal alloys, M, it is always equal to one.
Finally, the number of phases F: this represents the number of portions of the system with an identity of chemical composition, aggregation state, pressure, and temperature.

Let us now apply the Gibbs Phase Rule to the case of the water phase diagram (Figure 5.1). Regardless of the pressure and temperature values, there is always only one independent chemical component, $C_i = 1$, since water is a pure substance.
Let us also assume that the chosen temperature and pressure values define a generic point in a one-phase field (liquid, solid, or gaseous): in these areas, the number of efficient physical factors, M, is equal to two (pressure and temperature) and the phase, F, is one. Therefore, the calculation of variance, V, becomes:

$$V = 1 + 2 - 1 = 2$$

This shows how one-phase fields are characterized by two degrees of freedom ($V = 2$). There are two parameters (specifically pressure and temperature) that can be altered within certain limits, without altering the equilibrium of the system (water remains in the same phase: liquid, solid, or gaseous).
Always with reference to Figure 5.1, let us now consider the case of the curves marked by numbers 1, 2, and 3. These lines represent the temperature and pressure conditions in which the system changes its state, that is, where two phases coexist ($F = 2$). According to the Gibbs Phase Rule:

$$V = 1 + 2 - 2 = 1$$

This means that it is possible to vary the temperature (or pressure) and, as a result, the value of the pressure (or temperature) that describes that particular condition is uniquely defined. There is only one degree of freedom of the indipendent variables (pressure, temperature) so that the two states of aggregation coexist simultaneously.
Finally, let us look at the triple point case C where all three phases are present ($F = 3$). The variance of the system is:

$$V = 1 + 2 - 3 = 0$$

Since the variance is zero, the system has no degree of freedom. Therefore, only one condition of independent variables (pressure, temperature) exists that allows the system to have three phases in equilibrium (p = 4.58 mmHg; T= 0.01°C). Similar conclusions can be reached by applying the Gibbs Phase Rule to pure iron phase diagram in Figure 5.2.

5.3 Binary phase diagrams for metal alloys

Phase diagrams for metal alloys, in their simplest formulation, are characterized by two chemical elements, generally indicated as A and B. This is why they are called binary phase diagrams.

The diagrams show the temperature in ordinate and the chemical composition of the alloy in abscissa. The pressure is a variable that is normally not considered because in many applications it is constant and is equal to the atmospheric pressure. Therefore, the system at equilibrium is completely described if temperature and chemical composition of the phases are defined.

Furthermore, in currently used phase diagrams, temperature is limited to the condition where the system is completely in a liquid phase.The vapor phase is not usually indicated.

In order to better understand the above, and to examine real alloys in detail, let us consider the example of two liquids that are perfectly soluble between themselves: water and mint syrup (Figure 5.3).

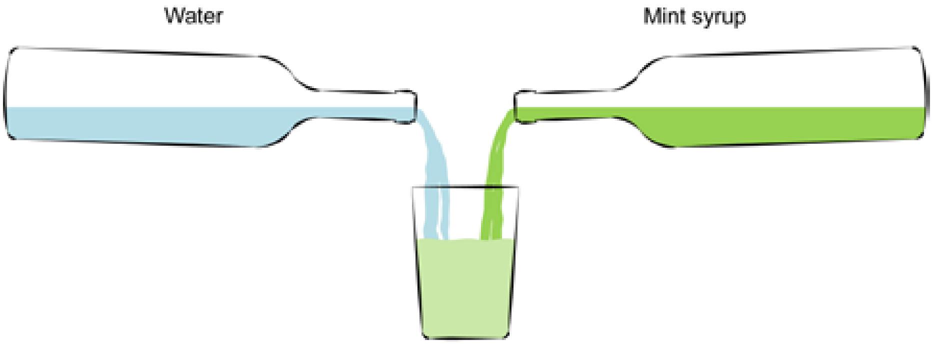

Figure 5.3 - Liquid solution between water and mint syrup: the two liquids are perfectly soluble.

By mixing water and mint syrup in a glass, a homogeneous liquid solution is obtained. As is well-known, water and mint syrup are perfectly soluble and, depending on the relative quantities, a drink that is more or less rich in mint syrup will be obtained.The color of the beverage is also an index of the greater or lesser presence of the two substances: the greater the amount of mint syrup is used, the greener the color of the liquid will be.

The system obtained is homogeneous: the temperature is well-defined and the amount of water and mint syrup is defined; the liquid solution has, at any point, the same chemical composition, aggregation state, pressure, and temperature. Moreover, since it is homogeneous, the system consists of a single phase, that is, it is a one-phase system.

The terms of the problem do not change if the temperature is changed: by cooling to a temperature below 0°C, the system solidifies and, the greater the amount of mint is used, the greener the popsicle obtained will be.

Even the mint popsicle is an homogeneous solid system (it is a single phase) because it has an identity of chemical compostion state of aggregation, pressure, and temperature at all points.

In several cases, something analogous occurs also among metals.

Consider gold and silver. If they are mixed together in a crucible and then solidified, the two metals behave exactly like water and mint syrup. Both in their liquid state and in their solid state, gold and silver are perfectly soluble with each other. The liquid solution between gold and silver is homogeneous and, when cooled, solidification occurs with the formation of an homogeneous system.The metal alloy obtained is a solid substitutional solution[4] in which the gold lattice is partially replaced by silver atoms[5].

Even a gold-silver alloy, like the mint popsicle, has a color that vibrates between bright yellow (color of gold) and brilliant metallic gray (color of silver), depending on the quantity of the two metals. The aptitude of the gold-silver alloy to form homogeneous solid solutions is not an isolated case. For example, copper-nickel, molybdenum-niobium, niobium-tantalum, and silver-palladium alloys have a similar behavior.

The graphic representation of what is described is shown in Figure 5.4: this is the phase diagram for gold-silver.The temperature is in ordinate, while the chemical composition of the alloy is in abscissa as a percentage in weight of silver. The percentage in weight of gold is, obviously, the complement to one hundred.

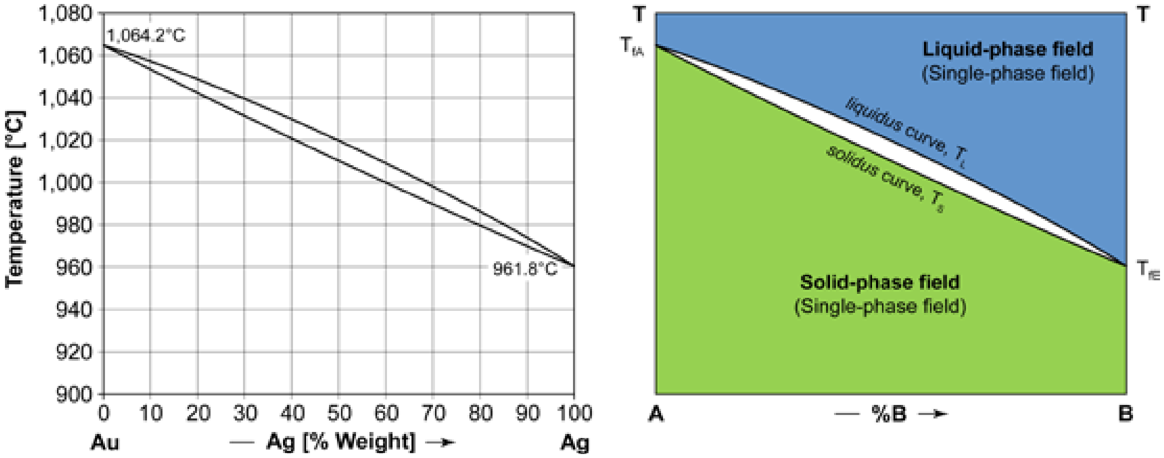

Figure 5.4 - Gold-silver phase diagram (*Au-Ag*) [from ASM-H.3 1992] and its schematic representation.

---

[4] *See Paragraph 2.3 of Chapter 2.*

[5] *Note that both gold and silver have a body-centered cubic lattice: gold has an atomic radius of 0.144 nm, silver of 0.153 nm.*

Figure 5.4 shows the gold-silver phase diagram: the one-phase fields of the homogeneous liquid phase (blue) and the homogeneous solid phase (green) are highlighted in color.

The diagram indicates the melting point of gold (T_{fA}) along the left vertical axis and the melting point of silver (T_{fB}) along the right vertical axis. There are also two lines called "liquidus" and "solidus" that connect T_{fA} with T_{fB}: these lines delimit the field (white color) where the alloy solidifies. Above the liquidus line (T_L), the system is completely in liquid phase[6]; under the solidus line (T_S), the system is completely in solid phase. Between liquidus and solidus lines, the system consists of two phases, since both the liquid and the solid phase coexist.

Let us apply the Gibbs Phase Rule to the binary phase diagram of Figure 5.4. Equation 5.1 is always valid, i.e:

$$V = C_i + M - F$$

In case of binary metal alloys, the number of independent chemical components, C_i, is always equal to 2, since the total chemical components are 2 (A and B[7]) and, between them, no reversible reactions or stoichiometric constraints exist ($C_i = 2 - 0 = 2$). The efficient physical factor is only one: temperature ($M = 1$). In order to define the variance value V, it is necessary to establish the number of phases in the system:

$$V = C_i + M - F = 2 + 1 - F$$

If temperature and chemical composition detect a point in a single-phase field (blue or green color), variance is equal to two ($V = 2 + 1 - 1 = 2$). If, however, it falls within the two-phase field (white color), the variance is equal to one ($V = 2 + 1 - 2 = 1$).

This result is of general validity for all binary metal alloys: one-phase fields have always $V = 2$, and two-phase fields have always $V = 1$.

---

[6] *It should be noted that, aside from very particular situations, in metal alloy phase diagrams, the two elements, A and B, are completely soluble at liquid state.*

[7] *The generic solid solution between A and B cannot be considered a chemical because it does not have a well-defined "chemical nature" and cannot be described by a chemical formula. A solid solution is, in fact, an homogeneous mixture in which one or more chemical species are uniformly mixed in the available space, so that the solution at each point has the same composition.*

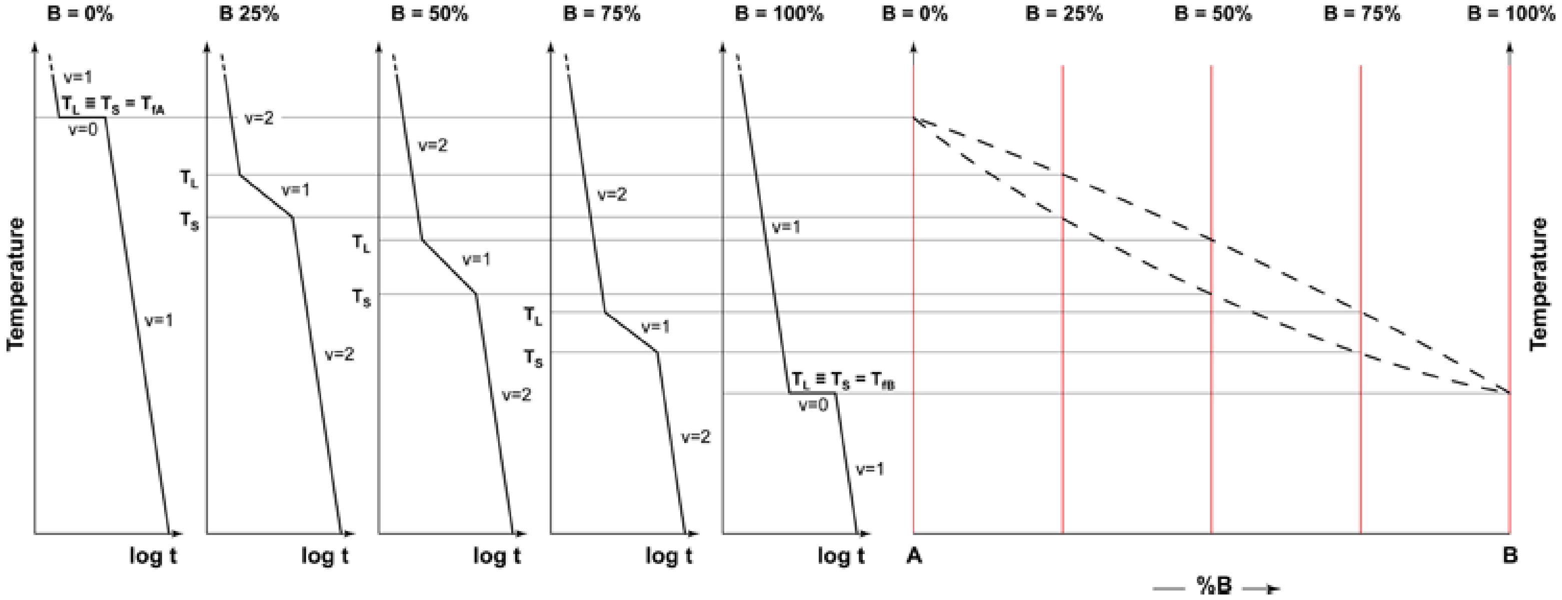

Figure 5.5 - Schematic representation of the construction method of a binary phase diagram.

5.4 Equilibrium cooling curves for binary alloys

The binary phase diagram in Figure 5.4 is obtained experimentally. It is, in fact, obtained starting from the equilibrium cooling curves[8] that can be traced by considering alloys with a composition of *B*, which gradually grows. In Figure 5.5, observe the trend of these curves[9] on a temperature - logarithm of time diagram and the construction method of the phase diagram.

Above T_L (system in completely liquid phase) or below T_S (system in completely solid phase), the cooling curves are all almost parallel: this means that the cooling rate is similar. This result depends to the homogeneous aggregation state (all liquid or all solid) of the system. In these cases, the cooling rate is expressed by the equation:

$$Q_S = c \cdot m \cdot \Delta T \qquad [5.3]$$

where the amount of heat extracted from the system, Q_s, is equal to the specific heat of the substance, *c*, times the mass of the system itself, *m*, times the temperature variation that results from that heat extraction. Heat, Q_s, calculated with equation 5.2, is called sensible heat[10] and represents the heat transferred by the chemical system when no phase transformations occurring. Note that the specific heat, *c*, varies with temperature but, both for the liquid state and the solid state, it is of the same magnitude. In the case of iron, the specific heat in a liquid state (melting point) is 0.82 kJ /kg · K, while in a solid state (room temperature) it is 0.45 kJ /kg · K.

On the contrary between T_L and T_S the slope of the cooling curve is lower. This phenomenon is typical of any phase transition (in this case from liquid to solid) and is common to most alloys[11].

To pass from T_L to T_S it is necessary to subtract the so-called "latent heat of solidification", Q_l[12], in addition to the sensible heat Q_s.

---

[8] *With reference to the equilibrium transformations, see note 13 of Chapter 1.*

[9] *Cooling curves are quite similar to those shown for pure iron in Figure 1.8 even if only cooling is represented.*

[10] *The sensible term is related to the real possibility of appreciating the heat extracted from the system.*

[11] *Exceptions to this rule are eutectic composition alloys. To this regard, see Paragraph 5.9.*

[12] *In relation to the type of change in state, a latent solidification/melting heat or latent evaporation/condensation heat occurs.*

The latent heat of solidification, Q_l, is a quantity of heat that varies from one chemical species to another and is proportional to the mass of the system according to the relation:

$$Q_l = \lambda \cdot m \quad [5.4]$$

where λ is the latent specific heat and m the mass of the chemical system. Q_l represents the amount of energy that, when it is subtracted from a liquid system, it causes solidification at a constant temperature. The effect of heat subtraction from the system does not induce a decrease in temperature but a transformation of the physical state of the matter through the re-aggregation of the atoms (transition from liquid to solid)[13]. For iron, the specific latent heat λ is equal to 272kJ /kg · K: as can be seen, being equal to the same substance considered (iron), the value of λ is some orders of magnitude greater than the value of the specific sensible heat, c.

The set of concepts previously expressed can be summarized as follows:
a) at temperatures higher than T_L or less than T_S, to cool the system, it is necessary to subtract sensible heat Q_s;
b) at temperatures between T_L and T_S, to cool the system, it is necessary to subtract both sensible heat Q_s, as well as latent heat Q_l.
Consequently, in the case of equilibrium cooling, in case a) the cooling rate is faster than in case b), since the amount of heat to be subtracted is less: Q_s in case a) and $Q_s + Q_l$ in case b). Therefore, if the temperatures are higher than T_L or less than T_S, the slope of the cooling curve is higher than in the portion between T_L and T_S.

Pure metals A (B = 0%) and B (B = 100%) show different cooling curves. As long as pure metal (A or B) is liquid ($T > T_L \equiv T_S$) or solid ($T < T_L \equiv T_S$), the slope of the cooling curve is the same of a completely liquid or solid system. In fact it is only necessary to subtract the sensible heat Q_s.
At a solidification temperature, however, thermostatation of the system occurs for a certain length of time, that is, until the transition to a state (in this case, from liquid to solid) has occurred. This phenomenon is typical of all pure substances: solidification occurs at a well-defined temperature and not in a thermal range, as is normal for most metal alloys.

Finally, a consideration relevant to the variance V of the system.

---

[13] *Just as a latent solidification/melting heat exists a latent condensation/evaporation heat also exists and it refers to the transition from vapor state to a liquid state, and vice versa. Latent condensation/evaporation heat is of little interest to metallic alloys and is normally not mentioned.*

Since the phase diagram is binary, the independent chemical components, C_i, are 2. The efficient physical factor on the equilibrium of the system, M, is the only temperature[14], and the phases, F, are those that can be read on the phase diagram. Therefore, the following occurs:

- for temperatures greater than T_L or less than T_S, ($F = 1$): $V = C_i + M - F = 2 + 1 - 1 = 2$
- for temperatures between T_L and T_S, ($F = 2$): $V = C_i + M - F = 2 + 1 - 2 = 1$

Other exceptions are the cases of pure metal A and pure metal B[15]. At temperatures greater than $T_L \equiv T_S$ or less than $T_L \equiv T_S$, the variance is equal to 1 ($V = C_i + M - F = 1 + 1 - 1 = 1$) while, during the liquid-solid state transition ($T = T_L \equiv T_S$) the result is $V = C_i + M - F = 1 + 1 - 2 = 0$ with consequent thermostatation of the system as long as solidification is not completed.

5.5 Complete solid solution phase diagram

The binary phase diagram shown in Figure 5.4 is a classic diagram of complete solid solution.

To understand its usefulness, we study, as an example, the case of an alloy containing 30% of B (Figure 5.6) indicated by the vertical axis that passes through 30% of B.

The points of intersection of the vertical line at 30% of B, with liquidus and solidus lines, represent the starting and ending temperature for alloy solidification (i.e. approximately 1,040°C and 1,030°C[16]).

To establish the phases on the diagram, simply draw a horizontal line in correspondence of the selected temperature, perpendicular to the vertical line indicating the chemical composition: the point of intersection between the two straight lines represents the system as a whole. If this point falls in the field of existence of a single phase, the system at equilibrium is a one-phase system. Otherwise, the system is a two-phase system.

Figure 5.7 shows the schematic illustration of a complete solid solution phase diagram. For the alloy at 30% of B, let us consider three points: X, Y, and Z respectively defined by temperatures T_X, T_Y e T_Z.

---

[14] See Paragraph 5.2 of this chapter.

[15] In the case of pure substances $C_i = 1$.

[16] Refer to Figure 5.4.

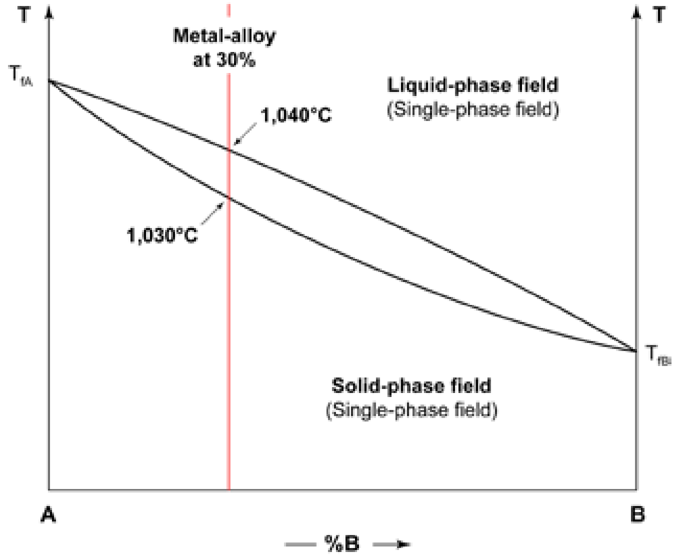

Figure 5.6 - Schematic representation of a generic complete solid solution phase diagram and graphic representation of an alloy at 30% of *B* and at 70% of *A*.

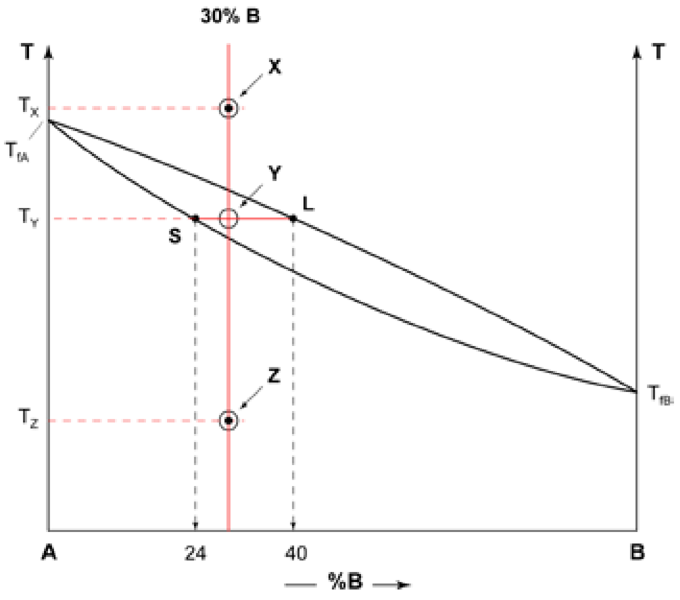

Figure 5.7 - Schematic representation of a generic complete solid solution phase diagram and graphic representation of an alloy at 30% *B*.

The chemical system, i.e. the intersection of the two straight lines, is indicated by an empty circle (○), while the phase is represented by a full dot (•). Since both point X and point Z fall within one-phase fields, the full dot coincides with the circle. This means that in point X the system consists of an homogeneous liquid (one phase), while at the point Z the system consists of an homogeneous solid (one phase).

Different is the case of point Y, which lays between the line of the *liquidus* and that of the *solidus*. Here, the field is not one-phase. To find the phases present at that temperature, it is necessary to move along the horizontal line traced in correspondence of T_Y until it meets the one-phase fields of the liquid L and of the solid S. Therefore, at temperature T_Y, there will be two phases: phase L (liquid) and phase S (solid). The chemical system as a whole is always indicated by an empty circle (point Y) in correspondence of the intersection between the vertical line of the alloy at 30% of B and the horizontal line passing through T_Y. Instead, the two phases, that is, the two full dots (L and S) are positioned where the two one-phase fields are delimited by the liquidus and solidus lines. The field between these two lines is, therefore, a two-phase field.

5.6 Chemical composition of the phases

Phase diagrams are useful to define the chemical composition of the phases starting from the chemical composition of the alloy and the temperature.

The chemical composition of a phase can be easily determined: it is sufficient to descend vertically from the full dot and read the value of the chemical composition on the abscissa axis.

Let's look at a simple example. Take in consideration Figure 5.7 and focus on point X at temperature T_X.

The system has a chemical composition equal to 30% of B and 70% of A. The only phase present at that temperature is the liquid phase, which has a chemical composition equal to 30% of B and 70% of A. The system coincides totally with the only phase present and, therefore, the system and phase have the same chemical composition (the empty circle ○ and the full dot • coincide). Similar conclusions are reached by considering point Z.

Different is the case of point Y, which is in a two-phase field, that is, at a temperature at which solidification is taking place. While the system described by Y (empty circle) always has a chemical composition equal to 30% of B, the two phases, L and S (full dots), have a different chemical composition. Liquid phase L has a composition equal to 40% of B and 60% of A, while the solid phase S has a composition equal to 24% of B and 76% of A: the empty circle (○) and the two full dots (•) no longer coincide.

5.7 The lever rule

The number of phases at a given temperature can be calculated through the phase diagram, as well.

When the system is one-phase, the problem does not arise (Figure 5.7): at points X and Z, the system is comprised 100% by a single phase: at T_X, the system is entirely in an homogeneous liquid phase; at T_Z, it is entirely in an homogeneous solid phase.

The problem arises when the system is two-phase, such as at temperature T_Y. At T_Y, the chemical composition of the system and of the individual phases is known (see Paragraph 5.6 above), but it does not seem possible to determine how much of the 100% of the system is already solid and how much is still liquid.

To obtain this data, the so-called "lever rule" is used. This is a simple mathematical relationship based on the principle of mass conservation. Starting from the assumption that, in a two-phase system, the sum of the phases is always equal to 100%, the lever rule states that the quantity of the two phases (Q_L and Q_S) is inversely proportional to the distance from the point of equilibrium of the system.

This is an application of Archimede's Law of the first type Lever. The system represents the fulcrum (the position of the circle ○), while the number of phases are the weights at the two ends (the dots •) at appropriate distances, in order to ensure equilibrium (Figure 5.8).

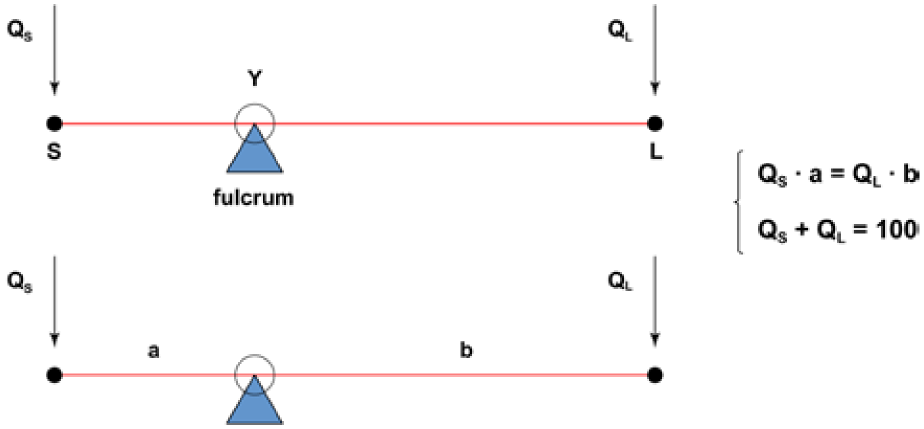

Figure 5.8 – Schematic representation of the lever rule: Q_S and Q_L represent the quantities of the solid phase S and the liquid phase L, point Y is the equilibrium of the system.

Segment $\overline{SY}$ is called a, and segment $\overline{YL}$ is called b; the quantity of the solid phase Q_S and the quantity of the liquid phase Q_L can be calculated using the following formulas:

$$Q_S = \frac{b}{a+b} \cdot 100\% \qquad Q_L = \frac{a}{a+b} \cdot 100\% \qquad [5.5]$$

Applying Equation 5.5 to temperature T_Y, Q_S and Q_L are equal to:

$$Q_S = \frac{40-30}{40-24} \cdot 100 = 62.5\% \qquad Q_L = \frac{30-24}{40-24} \cdot 100 = 37.5\%$$

This means that, at temperature T_γ, the quantity of the solid phase is 62.5%, while the quantity of the phase that is still solid is 37.5%.

5.8 Phases and structural constituents (or microstructures)

Another important element to be taken into account in the study of phase diagrams is the fundamental distinction between phases and structural constituents.

While the phase is the portion of a chemical system that is identified as a chemical composition, state of aggregation, pressure and temperature, the structural constituent (or microstructure) is, instead, represented by the aggregation of one or more phases within an homogeneous or heterogeneous crystallite[17].

Let us take into consideration the simple case of the complete solid solution phase diagram. Let us suppose to observe the solidification process under a microscope.

The system solidifies in the form of single phase homogeneous crystals following the nucleation and growth mechanism[18].

Figure 5.9 shows a schematic representation of the solidification process. Note that the grains are homogeneous and are all identical: the phase is only one (green) but is repeated identically in the various crystallites. The microstructure can, therefore, be described as green homogeneous crystallites in a solid state.

5.9 Eutectic phase digram

Not all metallic alloys are formed from chemical elements that have a complete solubility at a solid state. In many cases, the two elements, A and B can only be mixed together up to a certain content. A solubility gap occurs beyond this limit and, for example, a eutectic horizontal may appear on the phase diagram. Examples of metal alloys with partial solubility at a solid state and a eutectic transformation are aluminum-silicon, iron-carbon, copper-silver, and lead-tin alloys (Figure 5.10).

---

[17] *In the complete solid solution phase diagram the difference between phase and microstructure may not seem relevant. In this case, there is a perfect identity between the phase and the structural constituent. However, keep in mind that this distinction becomes fundamental in the case of complex structural constituents (with heterogeneous crystallites), such as those of the iron-carbon phase diagram.*

[18] *To this respect, see what is described in Paragraph 2.7 of Chapter 2.*

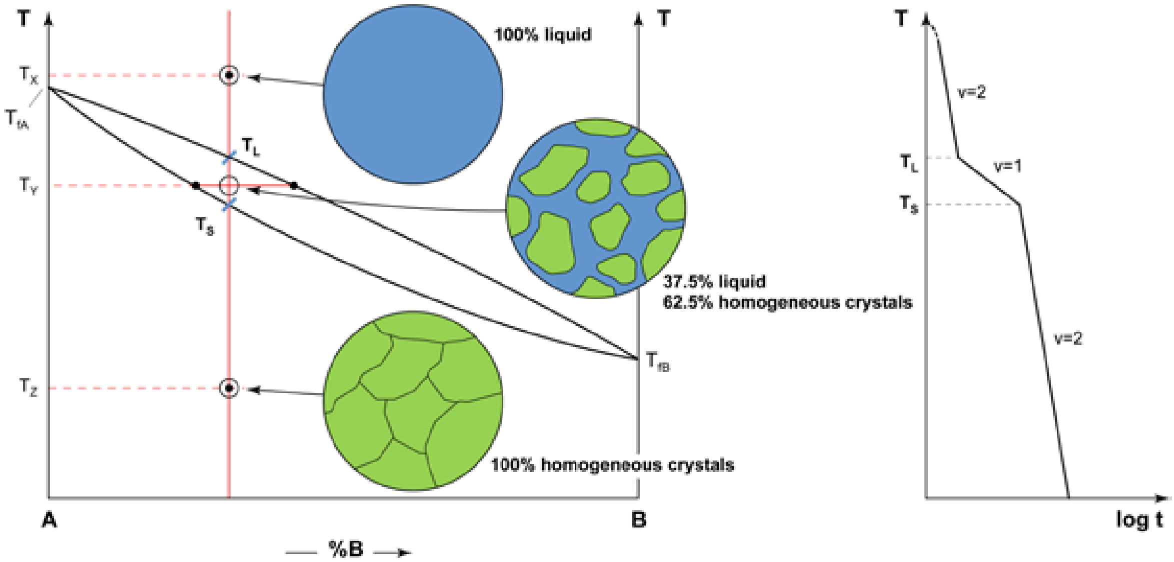

Figura 5.9 – Schematic representation of a generic complete solid solution phase diagram. Graphic representation of an alloy at 30% of B and its equilibrium cooling curve.

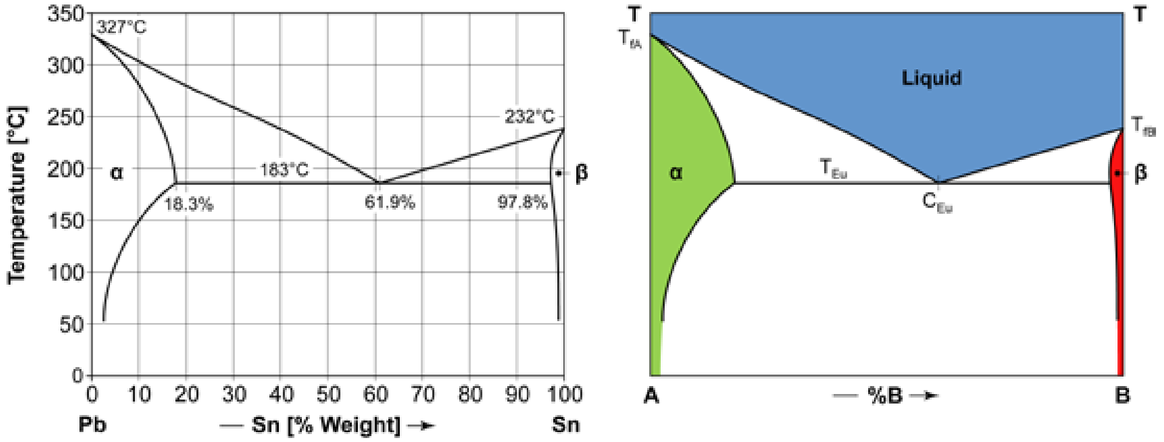

Figure 5.10 - Lead-tin phase diagram (*Pb-Sn*) [from ASM-H.3 1992] and its schematic representation.

Let us now look at the schematic illustration of the phase diagram shown in Figure 5.10. The melting temperature of lead (T_{fA}= 327°C) is placed along the left vertical axis, and the melting temperature of the tin (T_{fB} = 232°C) along the right vertical axis. The horizontal line at temperature T_{Eu} is called eutectic horizontal (183°C), while C_{Eu} indicates the composition of the eutectic alloy (61.9% of B).

In the upper part of the diagram, the one-phase field of the liquid (blue) is always present, while the one-phase fields of existence of the two solid phases are indicated near the right and left vertical axes: to the left, green: the phase that is rich in A, to the right, red: the phase that is rich in B. The two solid state one-phase fields are indicated by the Greek letters α and β, depending on how they relate to the solid phase rich in *A* (α-phase) or rich in *B* (β-phase). We clearly notice how the solubility of *A* and *B*, does not apply to any chemical composition but is limited at a interval, function of the temperature. At the eutectic temperature, for example, the solubility limit of *B* in α-phase is 18.3%, while the solubility limit of *A* in β-phase is 2.2%[19].

Let us examine the different types of alloys that can be obtained by equilibrium cooling. For each alloy, the phases and structural constituents are evaluated at various temperatures. To this regard, observe the diagram in Figure 5.11 (different from that of Figure 5.10): for this diagram, the eutectic composition C_{Eu} is equal to 56% of *B* and the solubility limits of α-phase and β-phase are between 10% and 32% of *B* and between 88% and 93% of *B*.

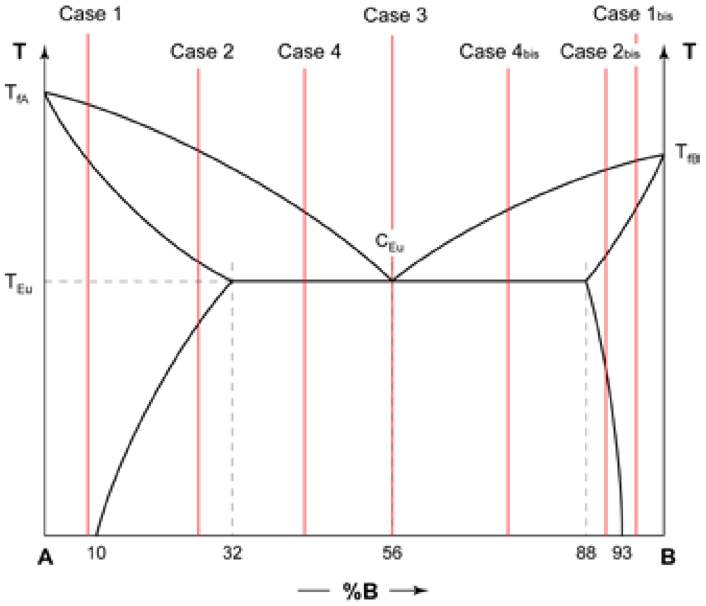

Figure 5.11 - Schematic representation of a generic eutectic phase diagram.

Case 1 (alloys with *B* <10%)

First consider an alloy that falls completely into the α-phase field, that is, an alloy with a composition in *B* lower than the solubility limit of *B* in α-phase at room temperature (10%): this occurs if, for example, the chemical composition is equal to 8% of *B* (Figure 5.12).

When solidification ends, there is complete solubility of the chemical element *B* in the lattice of α-phase.

---

[19] *The solubility limit of B in β-phase is equal to 97.8%, that is, 2.2% of A. Since β-phase is rich in B (from 97.8% to 100%), solubility should be expressed in terms of the content of A in β-phase.*

This condition remains unaltered until room temperature is reached. The result obtained is perfectly consistent with what has already been observed for the complete solid solution phase diagram and, therefore, the alloy is made up of homogeneous crystallites of α-phase (green). The equilibrium cooling curve is also similar to that of the complete solid solution phase diagram.

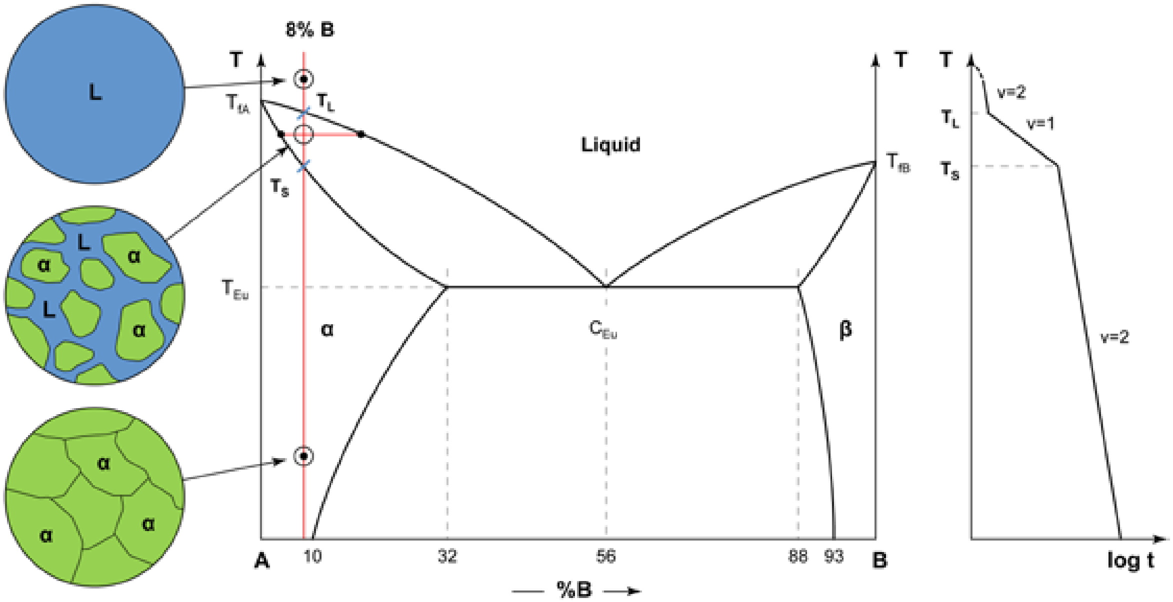

Figure 5.12 - Schematic representation of a generic eutectic phase diagram. Graphic representation of microstructure and equilibrium cooling curve of an alloy at 8% of *B*.

Case 2 (alloys with 10% < *B* <32%)

Let us now consider the alloy with a content of *B* equal to 24%, that is, an alloy with a content of *B* between the solubility limit of *B* in α-phase at room temperature (10%) and the solubility limit of *B* in α-phase at a eutectic temperature (32%). The proposed example is valid for any chemical composition in the interval between 10% and 32% (Figure 5.13).

In this second case, there is the important difference of the solubility limit. Up to the temperature of the solubility limit, T_{Sol}, the alloy is homogeneous and solidification takes place in the form of homogeneous crystals of α-phase, all identical to each other and green in color, similar to the alloy at 8% of *B*. Below T_{Sol} the amount of *B* in excess in α-phase forms plates of β-phase at the grain boundary (red color). At room temperature, therefore, the alloy consists of homogeneous crystals of α-phase surrounded by plates of β-phase at the grain boundary.

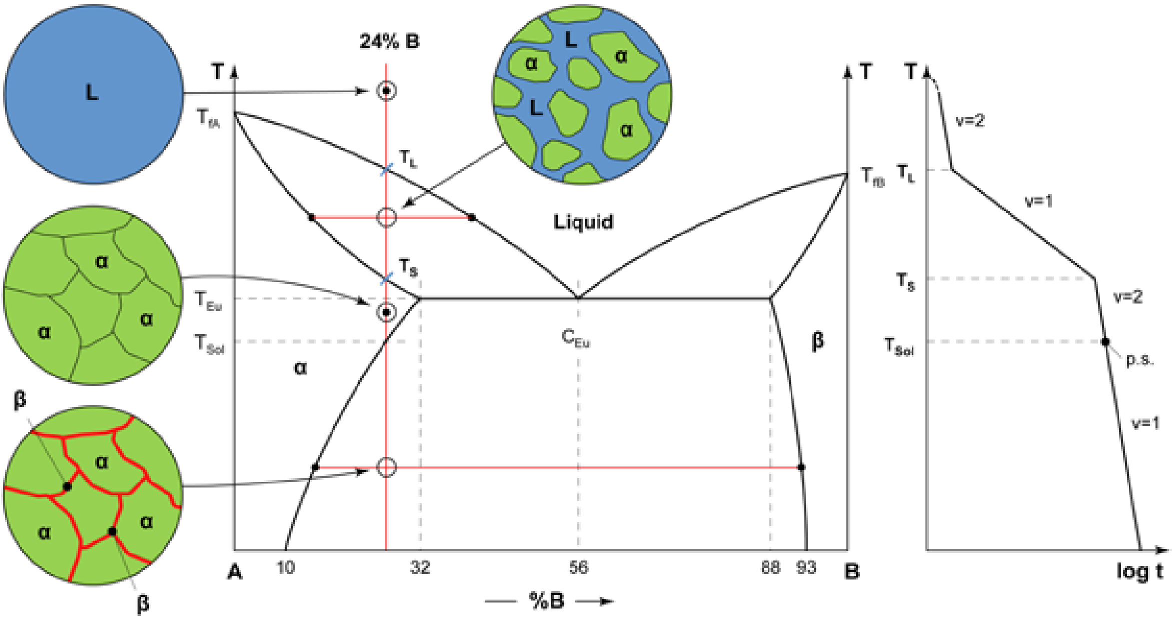

Figure 5.13 - Schematic representation of a generic eutectic phase diagram. Graphic representation of microstructure and equilibrium cooling curve of an alloy at 24% of *B*.

It should be noted that the presence of a limit of solubility in metallic solid alloys is quite similar to the existence of a limit of solubility between a solute and a liquid solvent, as occurs in the case of sugar in tea. The amount of sugar that can be dissolved in a given amount of tea is limited. This is the function of temperature: the hotter the tea, the greater the amount of sugar can be dissolved. Once the sugar solubility threshold in the tea is exceeded, the excess sugar separates, depositing on the bottom of the container.
Something similar occurs for metallic alloys. The solubility limit of one element in one phase is a function of the temperature and, once the solubility threshold is exceeded (in the case of Figure 5.13 temperature T_{Sol}), the excess of *B* forms plates of β-phase on grain boundary.
The quantity of the two phases at room temperature can be calculated with the lever rule. The quantity of homogeneous crystallites of α-phase and plates of β-phase is:

$$Q_{\alpha\, homogeneous\ crystals} = \frac{93-24}{93-10}\cdot 100 \cong 83.1\% \qquad Q_{\beta\, plates\ at\ grain\ boundary} = \frac{24-10}{93-10}\cdot 100 \cong 16.9\%$$

The cooling curve is not very different from the cases seen earlier (Figure 5.9 and Figure 5.12). The only difference is the discontinuity point at T_{Sol} (singular point p.s. on the equilibrium cooling curve).

This represents a slight variation in slope of the equilibrium cooling curve and is the consequence of the β-phase formation on grain boundary[20].

Case 1bis (alloys with *B* > 93%) and 2bis (alloys with 88% < *B* < 93%)

Similar conclusions to in case 1 and case 2 are obtained for the alloys that fall in the field of existence of β-phase. The behavior of alloys with *B* > 93% is comparable to those of alloys with *B* <10%, being careful, however, to reverse the phases (β with α). Similarly, the solidification method for alloys with 88% < *B* <93% is similar to that of alloys with 10% < *B* < 32% (but always with inverted phases).

In the case, for example, of an alloy with 95% of *B* at room temperature (Figure 5.14), the microstructure is totally formed of homogeneous grains of β-phase (red color). For an alloy with 90% of *B* (Figure 5.15) the microstructure is formed instead of homogeneous crystals of β-phase (red color) surrounded by plates on the grain boundary of α-phase (green color).

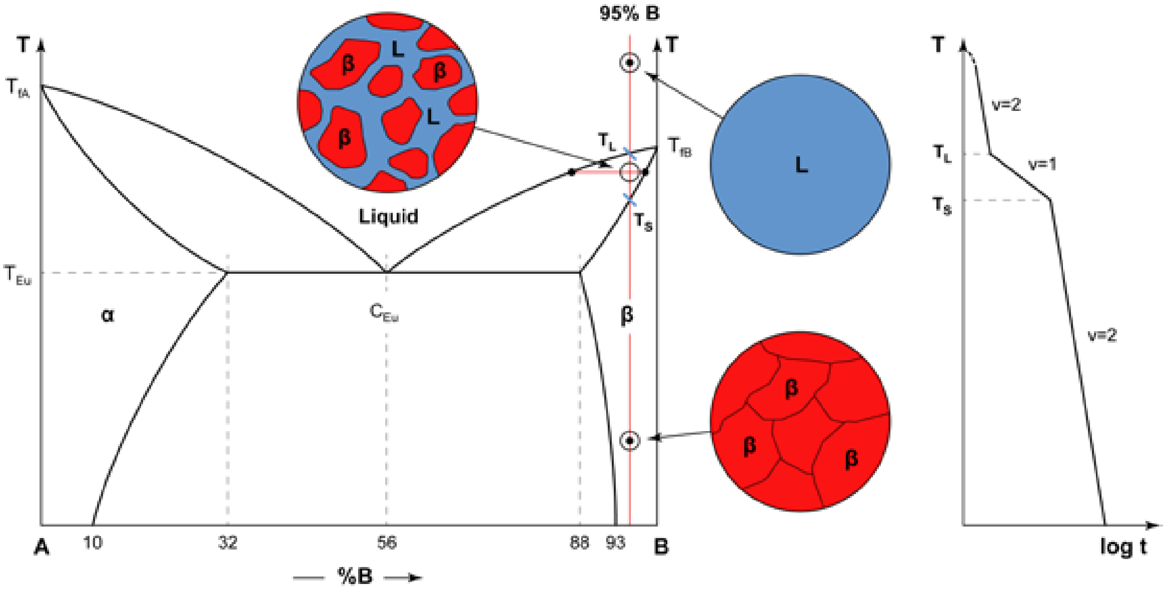

Figure 5.14 - Schematic representation of a generic eutectic phase diagram. Graphic representation of microstructure and equilibrium cooling curve of an alloy at 95% of *B*.

---

[20] *Since the passage is from a one-phase system (homogeneous crystals of α-phase) to a two-phase system (homogeneous crystals of α-phase and plates on the grain boundary of β-phase), the value of the specific sensible heat , c , changes minimally and produce a slight variation in slope of the equilibrium cooling curve. The alteration is not appreciable graphically and it is common practice to indicate a singular point on the equilibrium cooling curve.*

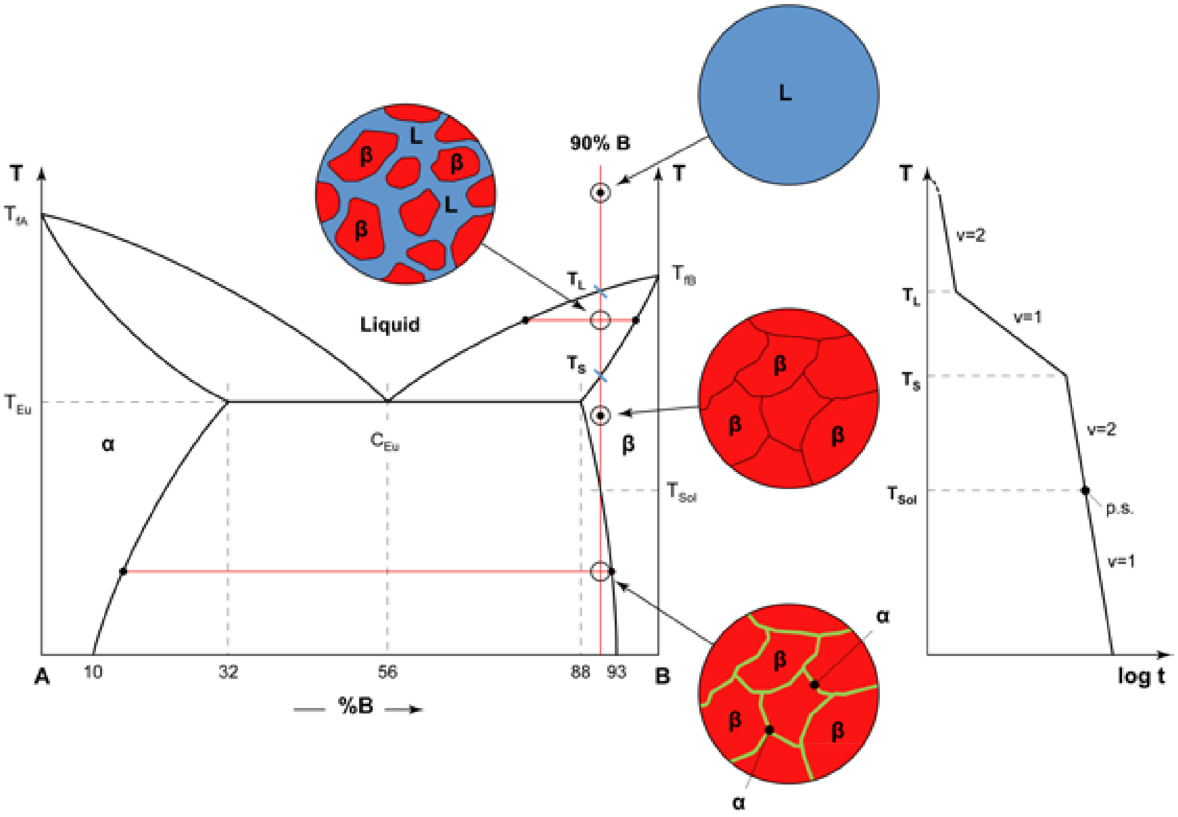

Figure 5.15 - Schematic representation of a generic eutectic phase diagram. Graphic representation of microstructure and equilibrium cooling curve of an alloy at 90% of *B*.

Case 3 (eutectic alloy, *B* = 56%)

Now, let us consider what happens when the alloy intercepts the eutectic horizontal at T_{Eu} during solidification, that is, when on the phase diagram in Figure 5.11, the amount of *B* is between 32% and 88%. The eutectic horizontal has a peculiarity: it represents the lowest temperature at which alloy solidification can take place[21]. Let us first examine the eutectic composition alloy C_{Eu} (*B* = 56%): the various stages of solidification are shown in Figure 5.16.

---

[21] *The term, "eutectic", derives from the Greek, "eútēktos", which means "easy melting" and indicates the fact that a eutectic alloy melts at a lower temperature as compared to the alloying elements.*

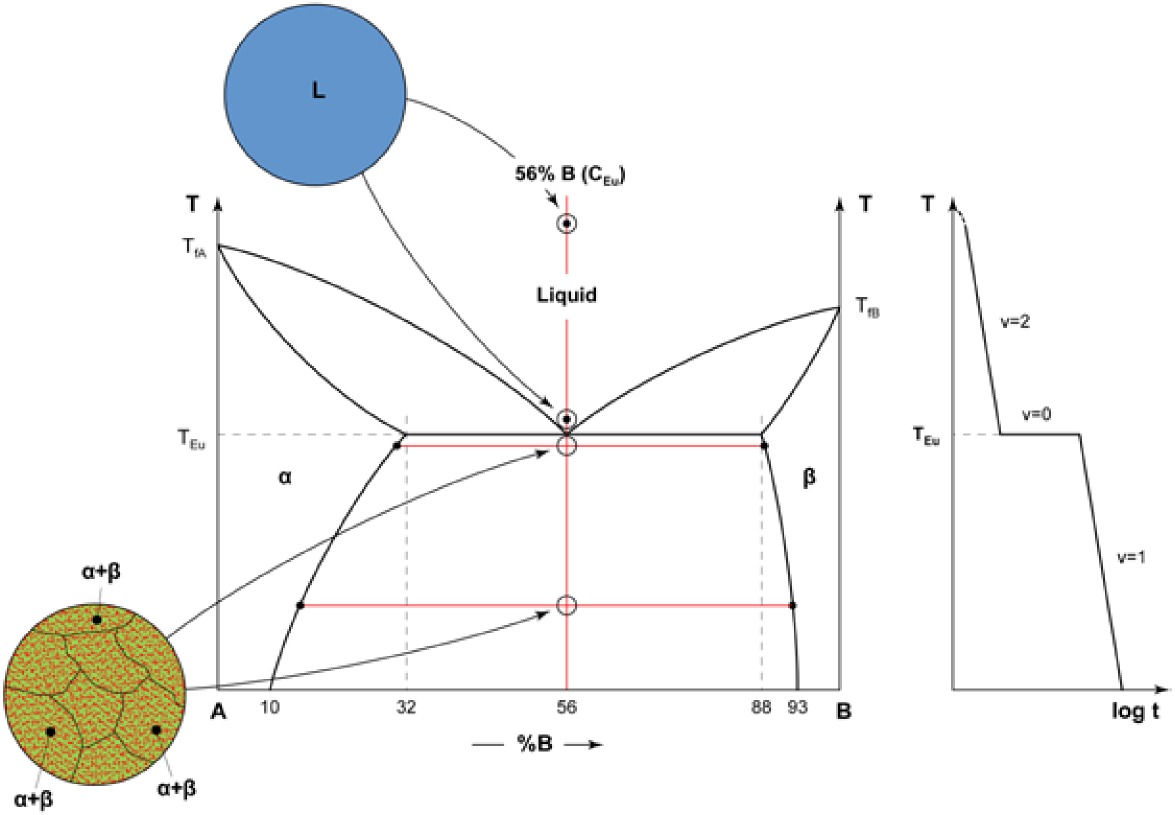

Figure 5.16 - Schematic representation of a generic eutectic phase diagram. Graphic representation of microstructure and equilibrium cooling curve of an alloy at 56% of *B*.

Up to an infinitesimal of a degree above the eutectic temperature, the system is completely liquid. Therefore, once T_{Eu} is reached, the alloy solidifies and, through nucleation and growth, forms a crystalline structure characterized by α and β phases. At the temperature of a infinitesimal degree below T_{Eu} the system is completely in solid phase.

The microstructure obtained through this method of solidification is called eutectic structure. In the eutectic microstructure the two phases, α and β, are not separated into homogeneous grains but are connected to each other within each single grain. Therefore, heterogeneous crystallites of α and β phases are formed. As shown in Figure 5.17, the eutectic structure may have a lamellar (the most typical), globular, or acicular shape, depending on the alloy.

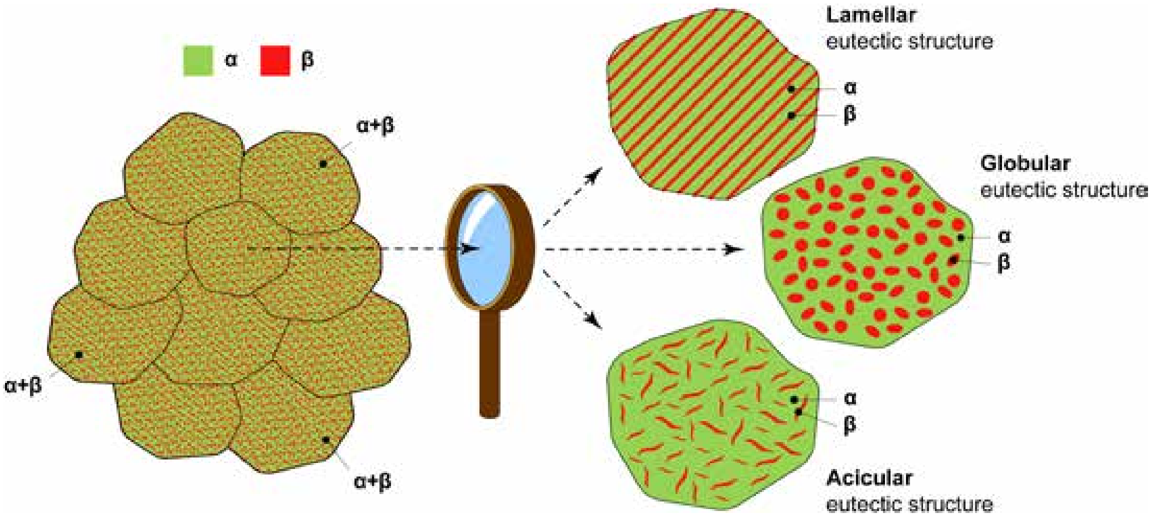

Figure 5.17 - Graphic representation of the eutectic microstructures.

An infinitesimal of a degree below T_{Eu}, the alloy at 56% B is made up of 100% eutectic crystals. The amount of the two phases within the eutectic grains can be calculated with the lever rule. The result is:

$$Q_{\alpha\, in\, eutectic\, crystals} = \frac{88-56}{88-32} \cdot 100 \cong 57.1\% \qquad Q_{\beta\, in\, eutectic\, crystals} = \frac{56-32}{88-32} \cdot 100 \cong 42.9\%$$

Assuming that the eutectic crystals are of a lamellar nature, this means that 57.1% of the lamellae is comprised of α-phase and 42.9% of β-phase.

In the transition from eutectic temperature to room temperature, there is a change in the solubility of B in α-phase (that goes from 32% to 10%) and of A in β-phase (that goes from 12% to 7%). Consequently, there is a variation in the amount of the two phases in the eutectic crystals. At room temperature, the lever rule gives the following result:

$$Q_{\alpha\, in\, eutectic\, crystals} = \frac{93-56}{93-10} \cdot 100 \cong 44.6\% \qquad Q_{\beta\, in\, eutectic\, crystals} = \frac{56-10}{93-10} \cdot 100 \cong 55.4\%$$

At room temperature the system is always comprised of 100% lamellar crystals but the amount of the phases is slightly different: 44.6% of α and 55.4% β.

During the eutectic transformation, the equilibrium cooling curve undergoes a substantial modification. While at temperatures above or below T_{Eu} the cooling law follows a well-known trend[22], thermostatation always occurs at the eutectic horizontal.

---

[22] *The trend of the cooling curves above and below the eutectic horizontal is similar to that observed for chemical systems with homogeneous aggregation state (all liquid or all solid).*

This depends to the variance value that equals[23]:

$$V = C_i + M - F = 2 + 1 - 3 = 0$$

which implies maintaining the temperature at constant levels until solidification is complete (the system has no degree of freedom). An isothermal arrest is typical of all eutectic horizontal and is similar to what occurs during the solidification of pure metals (Figure 5.5).

Case 4 (hypoeutectic alloys with 32% < *B* < 56%) and Case 4bis (hypereutectic alloys with 56% < *B* < 88%)[24]

We now come to the case of hypoeutectic and hypereutectic alloys. We first see the evolution of the hypoeutectic alloy at 40% of *B* during equilibrium cooling (see Figure 5.18).

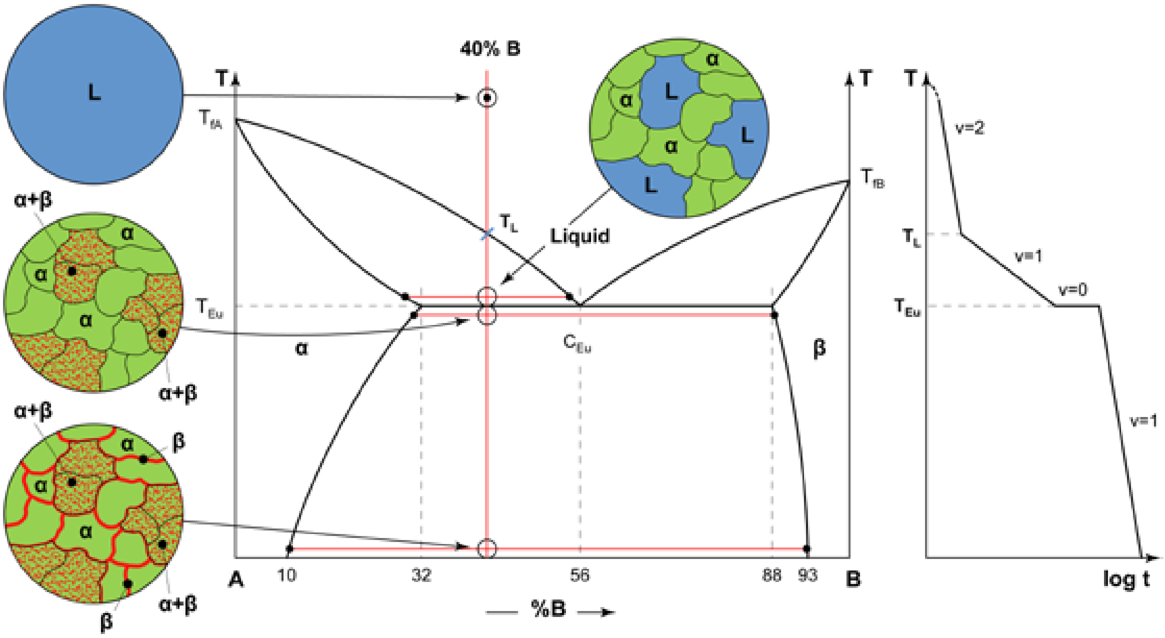

Figure 5.18 - Schematic representation of a generic eutectic phase diagram. Graphic representation of microstructure and equilibrium cooling curve of an alloy at 40% of *B*.

---

[23] *Note that, during solidification, three phases coexist: α-phase, β-phase, and the liquid.*

[24] *The prefixes "hypo" and "hyper" derive from Greek and are often used to indicate lower or higher conditions to a level considered normal. In this case, the reference is the eutectic alloy.*

The alloy in Figure 5.18 contains a percentage of 60% of A that is, greater than the content of A in the eutectic alloy (44% of A and 56% of B). Therefore, before a eutectic transformation at T_{Eu} occurs, the alloy must change its chemical composition and reduce the amount of A in excess. This phenomenon occurs during the initial phase of solidification, between temperatures T_L and T_{Eu}, when a solid fraction of homogeneous crystals of α-phase (i.e. the phase rich in A) separates from the liquid. Consequently, after reaching an infinitesimal of a degree above the eutectic temperature, the system is partially formed by homogeneous crystals of α-phase and, in part, from the liquid that has reached the composition C_{Eu}[25].

At T_{Eu}, an eutectic transformation occurs: this only involves the liquid that forms the eutectic microstructure. Following the eutectic transformation, the system is comprised of homogeneous grains of α-phase formed between T_L and T_{Eu} and from eutectic grains of α-phase and β-phase, formed at T_{Eu} from the liquid that remained at that temperature.

Let us calculate, using the lever rule, the phases present upstream and downstream of the eutectic temperature. At an infinitesimal of a degree above T_{Eu}, the result is equal to:

$$Q_\alpha = \frac{56-40}{56-32} \cdot 100 \cong 66.7\% \qquad Q_{liquid} = \frac{40-32}{56-32} \cdot 100 \cong 33.3\%$$

where the α-phase is in homogeneous crystals.

Since the eutectic transformation involves only the liquid, the quantities of structural constituents downstream of T_{Eu} are:

- 66.7% of homogeneous crystals of α-phase;
- 33.3% of eutectic crystals of α+β phases.

At an infinitesimal of a degree below T_{Eu}, the result is the following:

$$Q_\alpha = \frac{88-40}{88-32} \cdot 100 \cong 85.7\% \qquad Q_\beta = \frac{40-32}{88-32} \cdot 100 \cong 14.3\%$$

The quantities of α and β phases, represent the totality of the phases at that temperature (i.e. an infinitesimal of a degree below T_{Eu}).Therefore, at the end of the eutectic transformation, the distribution of the phases in the two structural constituents is:

- 66.7% of homogeneous crystals (66.7% of α-phase)
- 33.3% of eutectic crystals containing 19%[26] of α-phase and 14.3% of β-phase[27].

---

[25] *The crystallites that separate from the liquid before the eutectic transformation are also called pro-eutectic crystals.*

[26] *α-phase, in the eutectic structural constituent (19%), is obtained as the difference between the total of α-phase calculated at an infinitesimal of a degree below T_{Eu} (85.7%) less the part of α-phase that is already present in homogeneous crystals (66.7%). This can be performed because the lever rule allows to calculate the totality of the phases at a given temperature.*

[27] *All the percentages of the phases calculated with the lever rule refer to the totality of the chemical system and not to the individual structural constituents.*

Finally, in the transition from the eutectic temperature to room temperature, there is a change in the solubility of B in α-phase and of A in β-phase. This entails a twofold alteration of the structure:

- homogeneous crystals of α-phase form plates of β-phase on the grain boundary (as was observed for the alloy in Figure 5.13)
- the amount of the two phases in the eutectic grains changes (as was observed for the allow in Figure 5.16).

Therefore, at room temperature, the alloy at 40% of B is comprised of:

- homogeneous crystals of α-phase,
- plates of β-phase at the grain boundary of the homogeneous crystals of α-phase,
- eutectic crystals of $\alpha + \beta$ phases.

For this latter condition (room temperature), the calculation of the phases amount within structural constituents was omitted: this calculation presents some issues that are out of the discussion of this text.

It is now necessary to discuss the equilibrium cooling curve of the alloy at 40% of B: this brings together, in a single graph, the characteristics that have already been examined for the alloy at 24% of B (Figure 5.13) and the alloy at 56% of B (Figure 5.16).

Above T_L the equilibrium cooling curve is equal to that of a system at a liquid state ($V = 2$), then an initial solidification occurs with the formation of homogeneous crystals of α-phase between T_L and T_{Eu}. In this area, the phases are 2 ($V = 1$), and the slope of the equilibrium cooling curve becomes lower.

At T_{Eu}, variance becomes nil ($V = 0$) and thermostatation occurs until solidification is completed. Subsequently, the alloy cools down to room temperature with a slope similar to that at the liquid state (the system is completely at a solid state). Note that the variance in this latter area is 1 ($V = 1$) because the α and β phases[28] are simultaneously present.

The case of hypereutectic alloys is similar to that of hypoeutectic alloys, making sure to reverse the phases of the system. Consider, for example, the generic hypereutectic alloy at 70% of B (Figure 5.19).

The only difference with hypoeutectic alloys is the excess of B as compared to the eutectic alloy (70% of B in the hypereutectic alloy against 56% of B of the eutectic alloy). Consequently, during solidification, the system between T_L and T_{Eu} separates the homogeneous crystals of β-phase (the phase rich in B) to give origin, at T_{Eu} to a liquid of eutectic composition.

---

[28] *This latter specification is rather important because underlines that the slope of the equilibrium cooling curve should never correlated to the variance value. The case of Figure 5.18 is symbolic: the equilibium cooling curve has the same slope when the system is completely liquid or completely solid, but in the first case the variance value is two and in the second case the variance value is one.*

At T_{Eu}, liquid is transformed into the eutectic microstructure, while the homogeneous crystals of β-phase remain unchanged.

Finally, during equilibrium cooling to room temperature, homogeneous crystals of β-phase form plates on the grain boundaries and lamellae of α and β phases modify its relative quantities within the eutectic grains.

At room temperature, a generic hypereutectic alloy has the following microstructures:

- homogeneous crystals of β-phase,
- plates of α-phase at the grain boundary of the homogeneous crystals of β-phase,
- eutectic crystals of α + β phases.

The equilibrium cooling curve is equal to that of the hypoeutectic alloy at 40% of *B*.

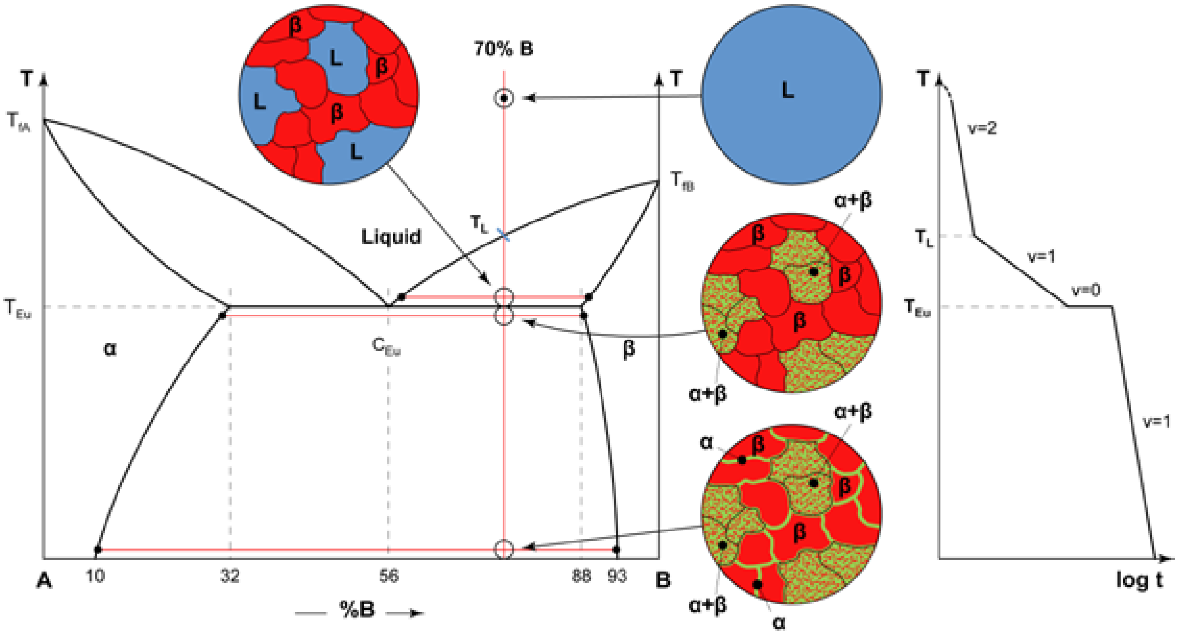

Figure 5.19 - Schematic representation of a generic eutectic phase diagram. Graphic representation of microstructure and equilibrium cooling curve of an alloy at 70% of *B*.

5.10 Peritectic phase diagram

In diagrams of partial solubility at solid state, the so-called "peritectic transformation" may be present, as an alternative to the eutectic transformation. Examples of metal alloys with peritectic transformation are copper-zinc, iron-carbon, and platinum-silver alloys (Figure 5.20).

The schematic representation in Figure 5.20 shows the one-phase fiel of the liquid at the top of the diagram (blue color). The one-phase field of the to solid phases are also indicated to the left, α-phase rich in *A* (green color), and to the right, β-phase rich in *B* (red color). Horizontal line at temperature T_{Pe} is called peritectic horizontal (1186°C), while C_{Pe} is the alloy of peritectic composition (44.7%).

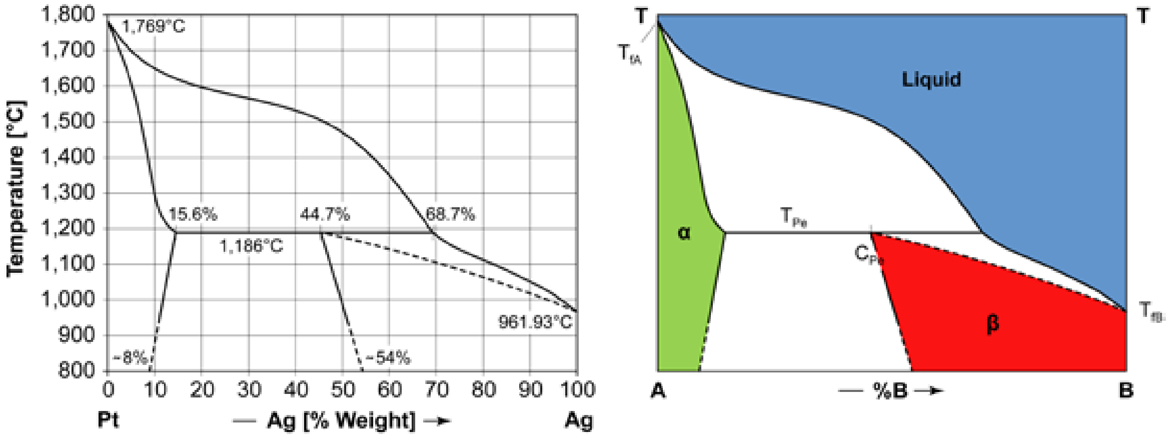

Figura 5.20 – Platinum-silver (*Pt-Ag*) phase diagram [from ASM-H.3 1992] and its schematic representation.

Let us now examine the different types of alloys that can be obtained by equilibrium cooling. For each alloy, the phases and structural constituents are evaluated at the various temperatures. To this regard, observe the diagram in Figure 5.21 (different from that of Figure 5.20). For this diagram, the peritectic composition C_{Pe} is equal to 57% of *B* and the solubility limits are between 4% and 12% of *B* for and between 52% and 57% of *B* for β-phase.

Case 1 (alloys with *B* < 4%)

Alloys with a content of *B* less than 4% do not intercept the peritectic horizontal: their equilibrium cooling curves are quite similar to that of Figure 5.12 (Case 1 of the eutectic phase diagram).

Case 2 (alloys with 4% < *B* < 12%)

Also alloys with a content of *B* between 4% and 12% do not intercept the peritectic horizontal: their equilibrium cooling curves are quite similar to that of Figure 5.13 (Case 2 of the eutectic phase diagram).

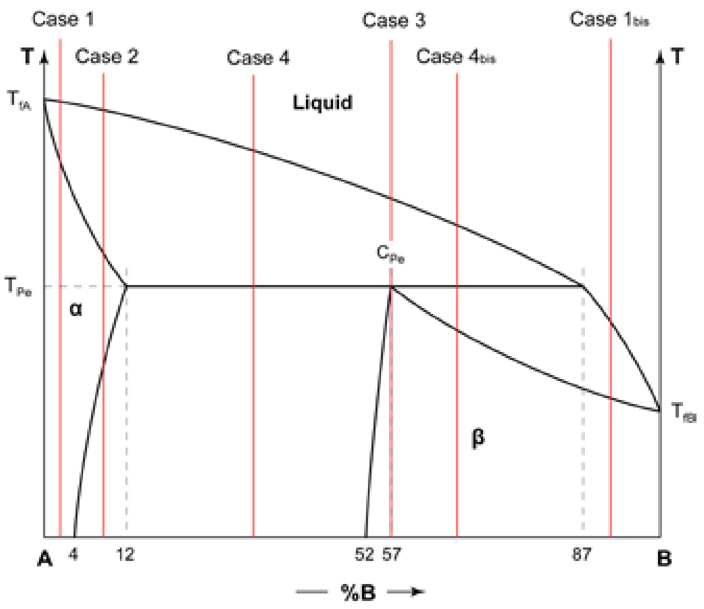

Figure 5.21 - Schematic representation of a generic peritectic phase diagram.

Case 1bis (alloys with B > 87%)

Also alloys with a content of B greater than 87% do not intercept the peritectic line: their equilibrium cooling curves are quite similar to that of Figure 5.14 (Case 1bis of the eutectic phase diagram).

Case 3 (peritectic alloy with B = 57%)

The first case refers to the peritectic alloy with B = 57% (Figure 5.22).

The alloy begins to solidify starting from temperature T_L with the formation of homogeneous crystals of α-phase. Solidification continues to an infinitesimal of a degree above T_{Pe}; at this temperature the system is comprised of homogeneous crystals of α-phase and liquid, their quantities can be calculated with the lever rule:

$$Q_\alpha = \frac{87-57}{87-12} \cdot 100 \cong 40\% \qquad Q_{liquid} = \frac{57-12}{87-12} \cdot 100 \cong 60\%$$

At T_{Pe} the peritectic transformation occurs, similar to a sort of "chemical reaction" between reagents and products[29]. Liquid and α-phase in homogeneous crystals act as reagents that give origin, as a product, to β-phase in homogeneous crystals. In summary, we have:

$$liquid + \alpha \rightarrow \beta$$

---

[29] *In fact, during the peritectic transformation, no chemical reaction occurs: this concept has been used to point out that phases and structural constituents before the peritectic transformation have nothing in common with phases and structural constituents after the transformation.*

It should be noted that the microstructure formed during peritectic transformation is always composed of homogeneous crystals.

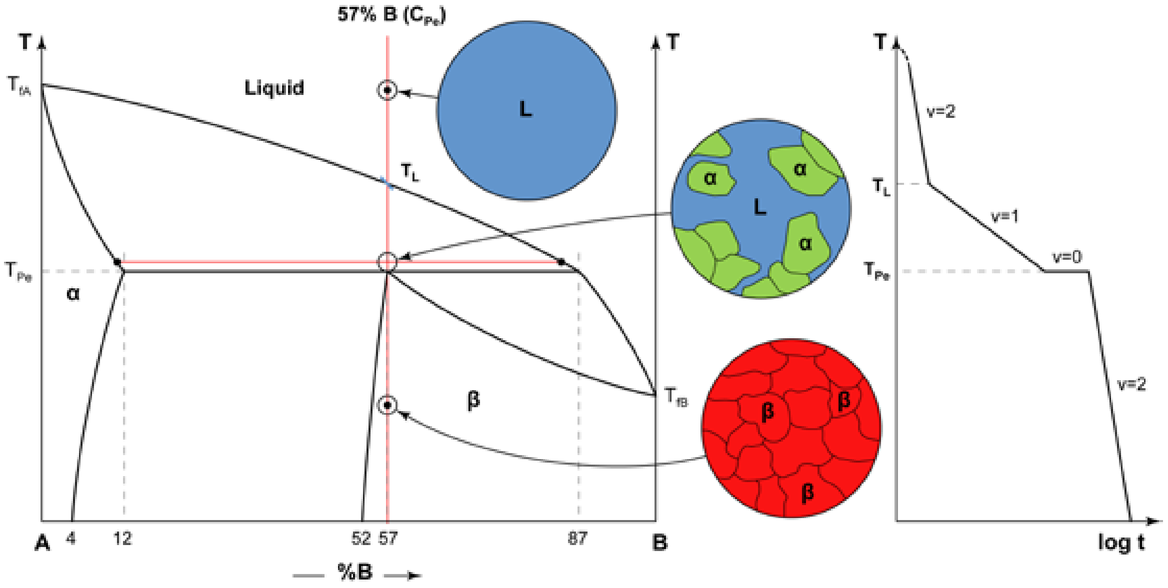

Figure 5.22 - Schematic representation of a generic peritectic phase diagram. Graphic representation of microstructure and equilibrium cooling curve of an alloy at 57% of *B*.

The equilibrium cooling curve is similar to that of the alloys in Figure 5.18 or 5.19. Above T_L, the equilibrium cooling curve is typical of a liquid state system ($V = 2$). Subsequently, between T_L and T_P, there is partial solidification ($V = 1$): the cooling curve slope becomes lower, due to the latent heat of solidification Q_l. At peritectic temperature T_{Pe}, the variance is:

$$V = C_i + M - F = 2 + 1 - 3 = 0$$

and temperature stops until solidification is completed. Finally, when the system is completely solid, the alloy cools down to room temperature, with a cooling rate equal to that in the liquid state.

Case 4 (alloy with 12% < *B* <52%)[30]

We consider the chemical composition at 32% of *B* (Figure 5.23). As in the previous case, the alloy starts solidifying at T_L, forming homogeneous crystals of α-phase. Their amount increases until the peritectic horizontal is reached. Upstream of T_{Pe}, the amount of the two phases is:

$$Q_\alpha = \frac{87-32}{87-12} \cdot 100 \cong 73.3\% \qquad Q_{liquid} = \frac{32-12}{87-12} \cdot 100 \cong 26.7\%$$

while downstream, the system is formed by both α-phase and by β-phase in the following quantities:

$$Q_\alpha = \frac{57-32}{57-12} \cdot 100 \cong 55.6\% \qquad Q_\beta = \frac{32-12}{57-12} \cdot 100 \cong 44.4\%$$

The peritectic transformation can be schematized as follows:

$$liquid + \alpha \rightarrow \alpha + \beta$$

where solid α and β phases are both in homogeneous crystals.

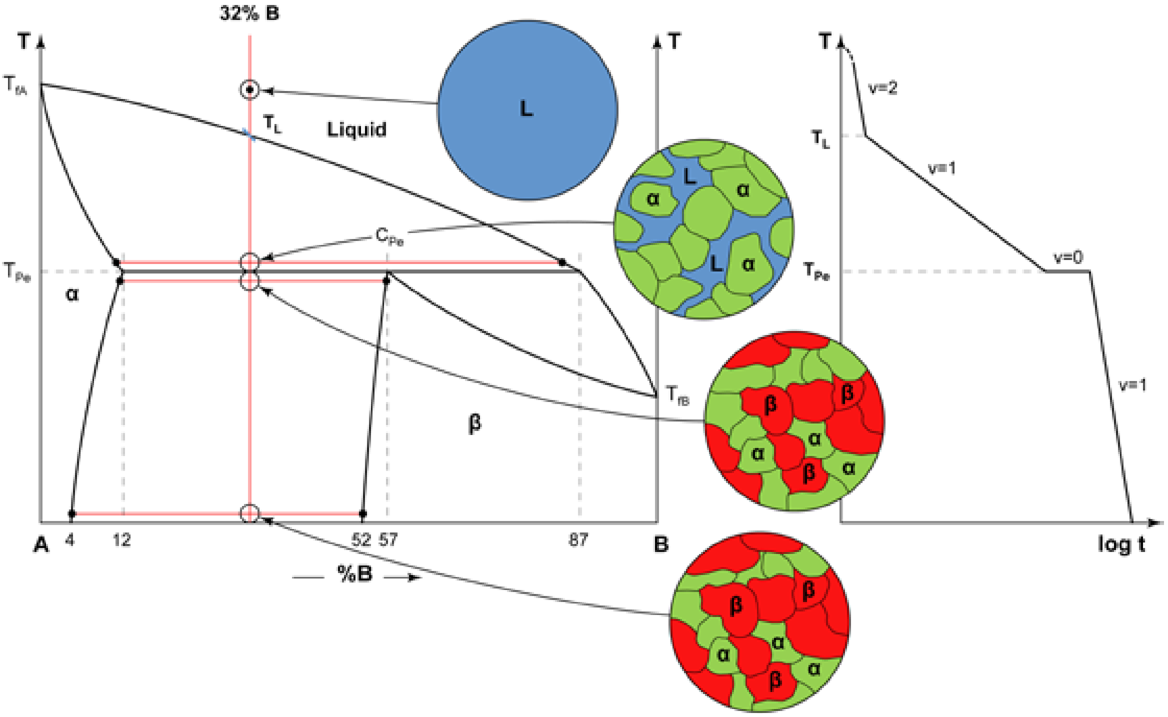

Figure 5.23 - Schematic representation of a generic peritectic phase diagram. Graphic representation of microstructure and equilibrium cooling curve of an alloy at 32% of *B*.

---

[30] *In the case of the peritectic horizontal, the prefixes, hypo- and hyper-, are not used to indicate chemical composition alloys that are lower or greater than the peritectic value.*

Solubility variation of α and β phases is observed from peritectic temperature to room temperature. In this case, since both phases are present at T_{Pe}, no new phase is formed. The quantities of the phases at room temperature are equal to:

$$Q_\alpha = \frac{52-32}{52-4} \cdot 100 \cong 41.7\% \qquad Q_\beta = \frac{32-4}{52-4} \cdot 100 \cong 58.3\%$$

The amount of the two structures at room temperature (homogeneous crystals of α-phase and homogeneous crystals of β-phase) is, as can be seen, slightly different from what is calculated downstream T_{Pe}.
The equilibrium cooling curve is similar to that of Case 3[31].

Case 4bis (alloy with 57% < *B* < 87%)

The alloy used as a reference has 70% of *B* (Figure 5.24).
The alloy begins to solidify starting from temperature T_L with the formation of homogeneous crystals of α-phase. An infinitesimal of a degree above T_{Pe}, the amount of liquid and of α-phase in homogeneous crystals is:

$$Q_\alpha = \frac{87-70}{87-12} \cdot 100 \cong 22.7\% \qquad Q_{liquid} = \frac{70-12}{87-12} \cdot 100 \cong 77.3\%$$

At T_{Pe}, a peritectic transformation occurs. Liquid and homogeneous crystals of α-phase give origin to liquid and homogeneous crystals of β-phase, according to "reaction":

$$liquid + \alpha \rightarrow liquid + \beta$$

Once the peritetic transformation has ended the system is still partially liquid. As a result of the cooling, the alloy completes its solidification at temperature T_S in the form of homogeneous crystals of β-phase.

The equilibrium cooling curve shows a thermostatation at the peritectic temperature.

Between T_L - T_{Pe} and T_{Pe}-T_S, the slope of equilibrium cooling curve is similar and it is lower than the slope observe for temperature above T_L or below T_S . The change in slope betwen T_L - T_{Pe} and T_{Pe}-T_S is due to latent heat, Q_l.

---

[31] *Downstream of T_{Pe}, the equilibrium cooling curve has the same pattern for both Case 3 and Case 4, since the system is completely solid. The change invarians, V = 2 in case 3 and V = 1 in case 4 as no effect on the slope of the equilibrium cooling curve.*

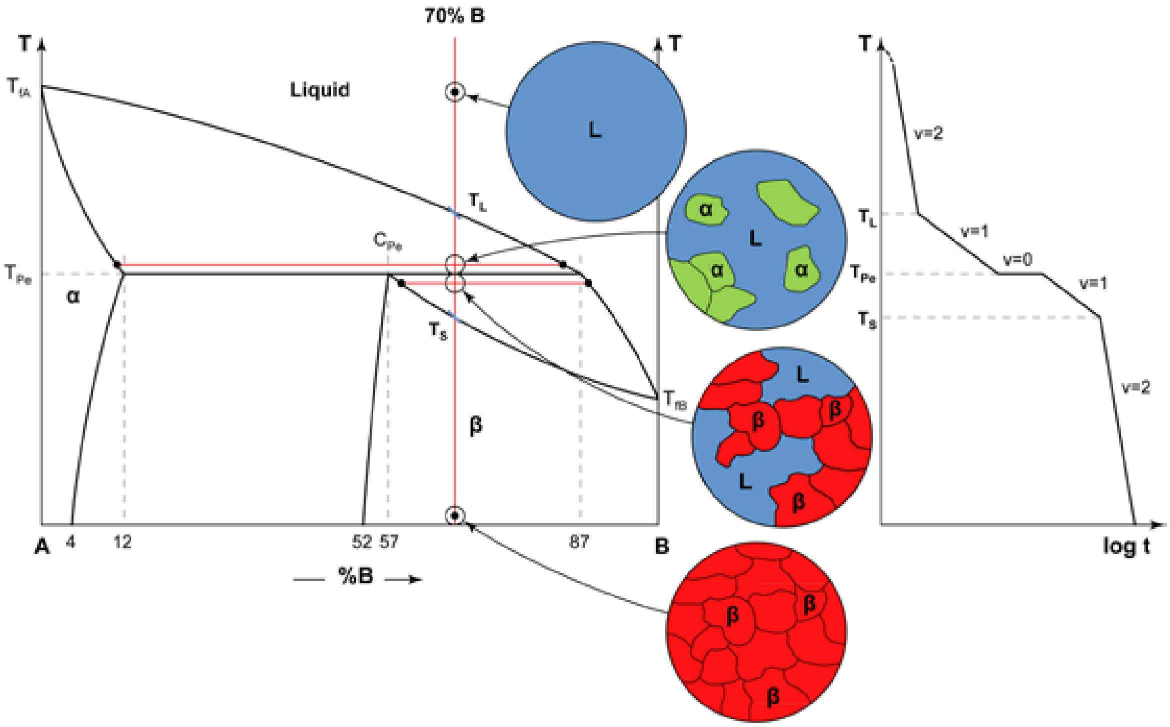

Figure 5.24 - Schematic representation of a generic peritectic phase diagram. Graphic representation of microstructure and equilibrium cooling curve of an alloy at 70% of *B*.

5.11 Intermediate phases

Often, binary phase diagram are more complex than those seen in previous paragraphs: they normally highlight various structural transformations, not just one[32]. These structural transformations are related to of phases of an intermediate chemical composition between pure metal *A* and pure metal *B*[33].

A typical example is the copper-zinc phase diagram (Figure 5.25). In addition to the liquid phase (blue), α-phase (green, rich in copper) and η-phase (red, rich in zinc) there are also β, γ, δ and ε phases (all represented in yellow): these intermediate phases have different chemical composition, depending on the temperature and, in the specifical case, derive from various peritectic structural transformations.

---

[32] *The phase diagrams studied in the previous paragraphs have always considered a single structural transformation (eutectic or peritectic).*

[33] *The phase diagrams studied in the previous paragraphs have always considered the existence of a single solid phase (diagram of complete solubility at solid state) or of two solid phases (diagram of partial solubility at solid state), respectively rich in metal A (α-phase) and metal B (β-phase).*

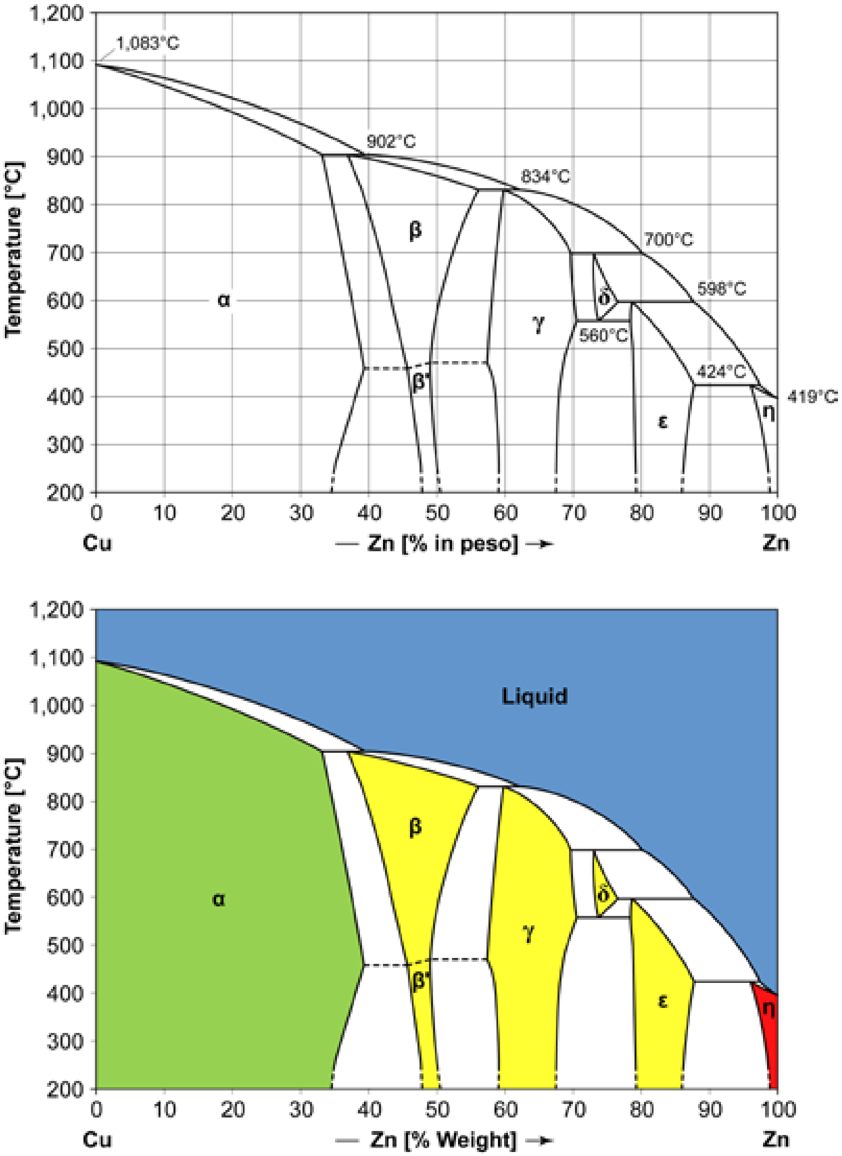

Figure 5.25 - The copper-zinc phase diagram (*Cu-Zn*) [from ASM-H.3 1992] and its schematic representation.

On the contrary when the chemical composition of the intermediate phases is uniquely defined, we speak of compounds (intermetallic or interstitial[34]). These are represented on the phase diagram by a vertical line in correspondence of the stoichiometric chemical composition of the compound. A typical example is the magnesium-lead phase diagram (Figure 5.26).

---

[34] *To this regard, see Paragraph 2.3 of Chapter 2.*

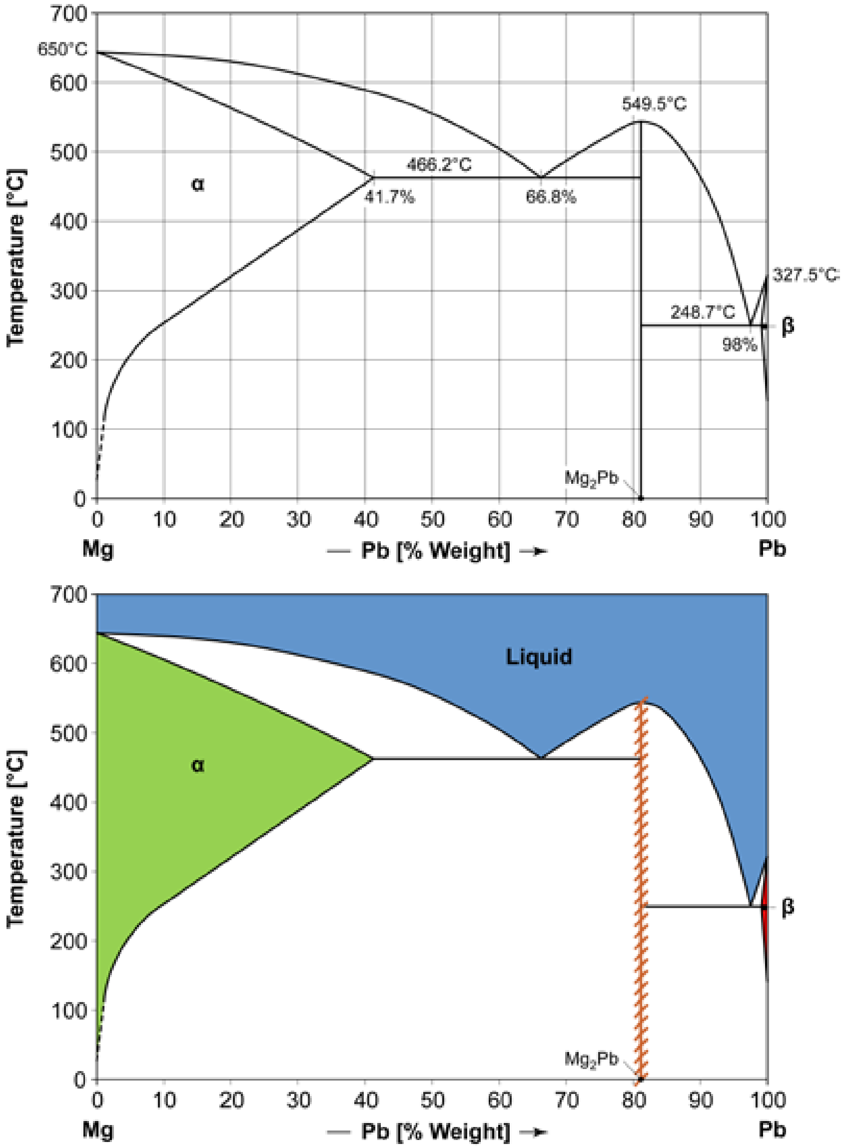

Figure 5.26 - Magnesium-lead phase diagram (*Mg-Pb*) [from ASM-H.3 1992] and its schematic representation.

In the *Mg-Pb* diagram phase Mg_2Pb exists from room temperature to melting temperature (549.5°C) and it is limited to the single vertical line containing 81% of lead (outlined in light brown).

Phase Mg_2Pb is properly called an intermetallic compound, since it consists of two metallic elements (*Mg* and *Pb*) in specific stoichiometric ratios (two magnesium and one lead atom).

The intermetallic compound Mg_2Pb also acts as a limit between two eutectic horizontal lines, one on the left (466.2°C) and the other on the right (248.7°C) of the vertical line at 81%.

The presence of a compound (intermetallic or interstitial) does not modify the considerations regarding the quantitative evaluations of the phase diagram in Figure 5.26 (chemical composition, Gibbs Phase Rule, lever rule, structural constituents, etc.): the compound Mg_2Pb is treated as a one-phase field with an extension that has been reduced to a vertical line.

Figure 5.27, shows the solidification of a hypoeutectic alloy at 52% of Pb. As can be seen, the structural constituents are similar to those of the alloy in Figure 5.18, making sure to replace β-phase with the intermetallic compound Mg_2Pb.

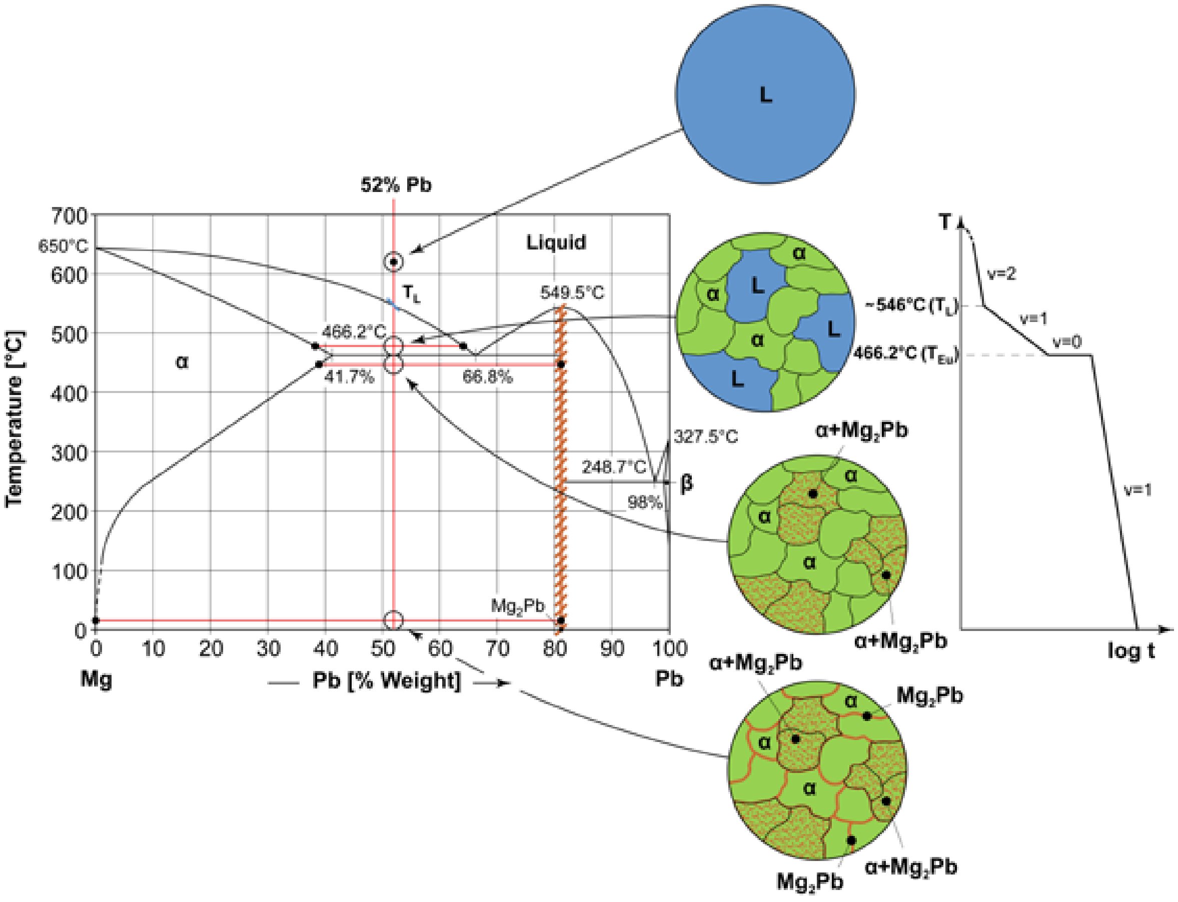

Figure 5.27 - Magnesium-lead phase diagram (Mg-Pb) [from ASM-H.3 1992] and schematic representation of the equilibrium cooling curve of an alloy at 52% of Pb.

5.12 Solid state transformations

The eutectic and peritectic transformations are not exclusive to liquid phase systems, but they can also occur in the solid state.

If they occur at a solid state, they are called eutectoid or peritectoid transformations: the only difference is the aggregation state of the phase undergoing transformation, which is in a solid state rather than a liquid state. Consider the example in Figure 5.28 that shows two simple phase diagrams arranged one over the other.

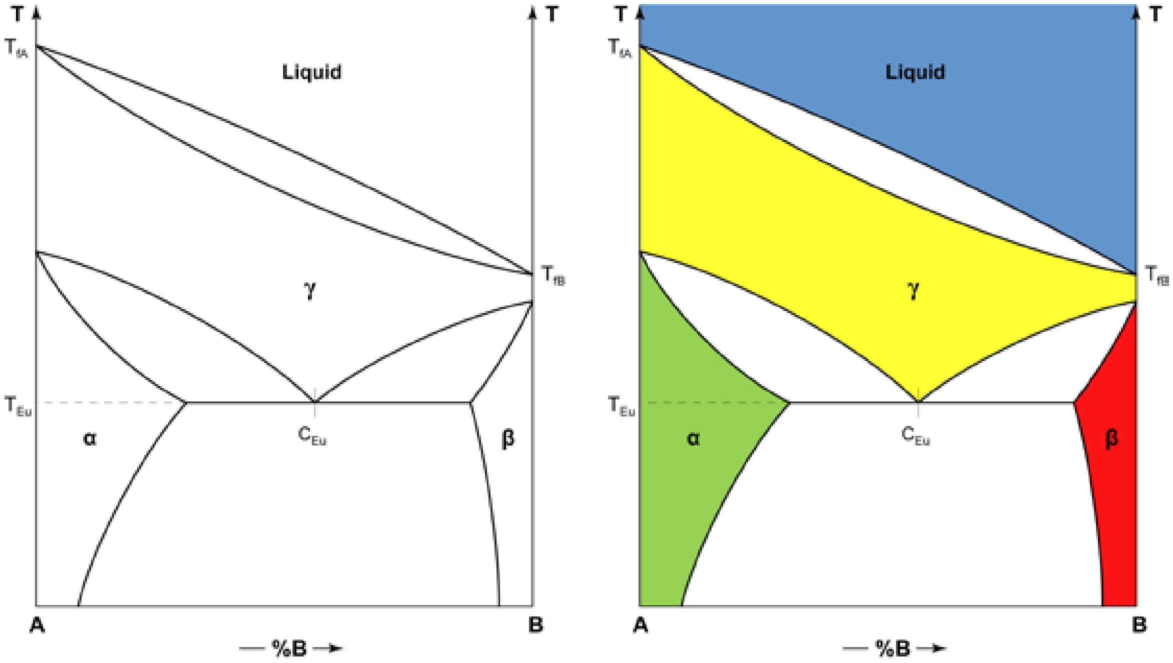

Figure 5.28 - Generic binary phase diagram with an eutectoid transformation.

This diagram is elementary and derives from what is seen on simple phase diagrams.

Considering a generic alloy at 70% of B (Figure 5.29), that is, an hypereutectoid alloy[35]. Solidification always occurs with the formation of homogeneous crystals of γ-phase (yellow) that, when cooled, go towards a partial transformation in homogeneous crystals of β-phase (red). Once the T_{Eu} line, has been reached, a eutectoid transformation occurs, similar to the eutectic transformation in Figure 5.19: in case of eutectic horizontal, the transformation occurs on liquid, while in case of eutectoid horizontal the transformation occurs, on the solid state γ-phase. The eutectoid transformation is, therefore, analogous to the eutectic transformation, even if it involves the solid state γ-phase and not the liquid state.

---

[35] *Just as there are hypoeutectic and hypereutectic alloys, hypoeutectoid and hypereutectoid alloys may also exist.*

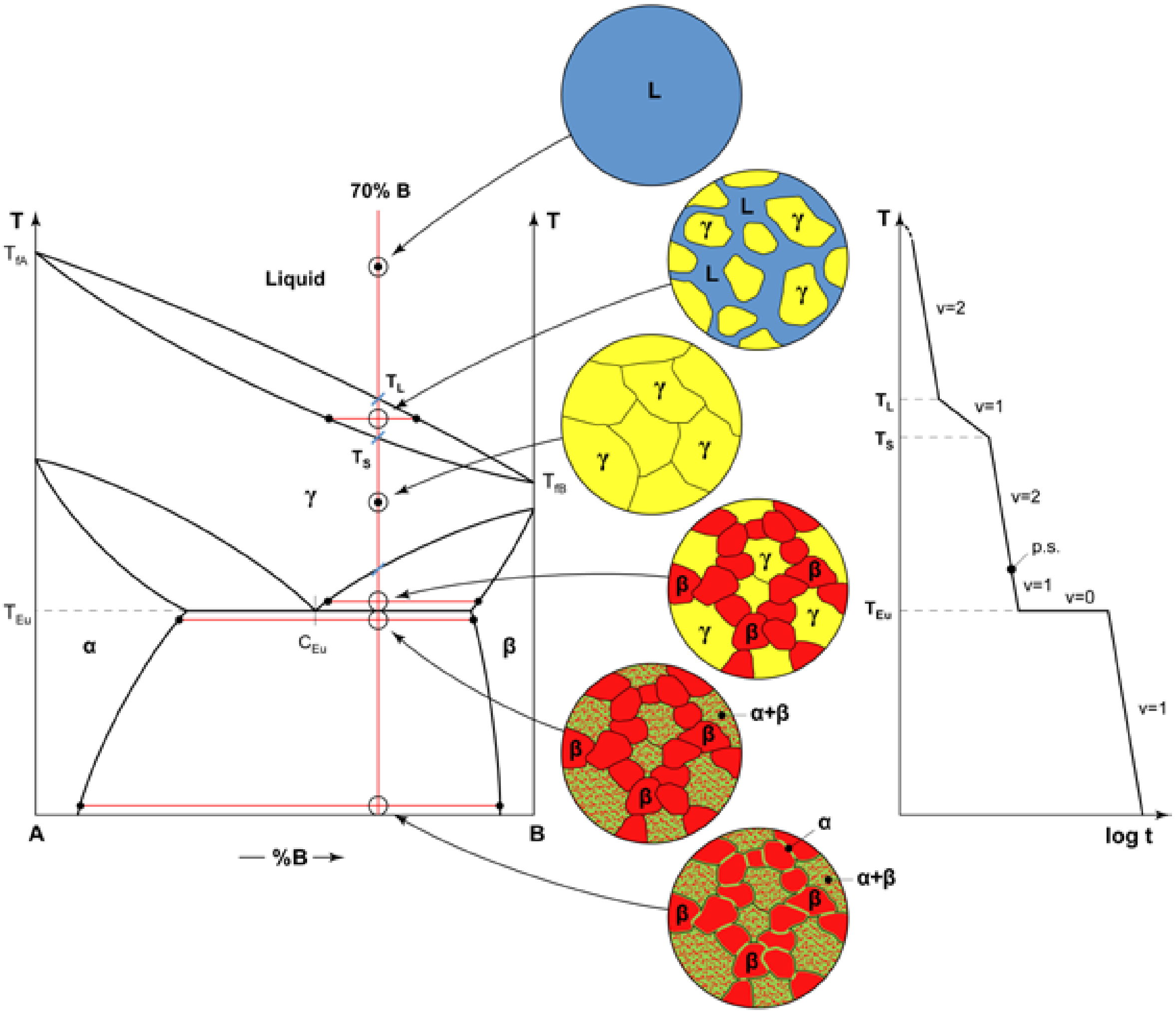

Figure 5.29 - Generic binary phase diagram with an eutectoid transformation and schematic representation of the equilibrium cooling curve of an alloy at 70% of *B*.

The eutectoid transformation forms a lamellar structure:

$$liquid \rightarrow \alpha_{lamellar} + \beta_{lamellar} \;\; (eutectic\ transformation)$$
$$phase\ \gamma \rightarrow \alpha_{lamellar} + \beta_{lamellar} \;\; (eutectoid\ transformation)$$

The result of a peritectoid transformation is:

$$liquid + \alpha \rightarrow \beta_{homogeneous\ crystals} \;\; (peritectic\ transformation)$$
$$\alpha + \gamma \rightarrow \beta_{homogeneous\ crystals} \; (peritectoid\ transformation)$$

The set of liquid state and solid state transformations are showed in Figure 5.30.

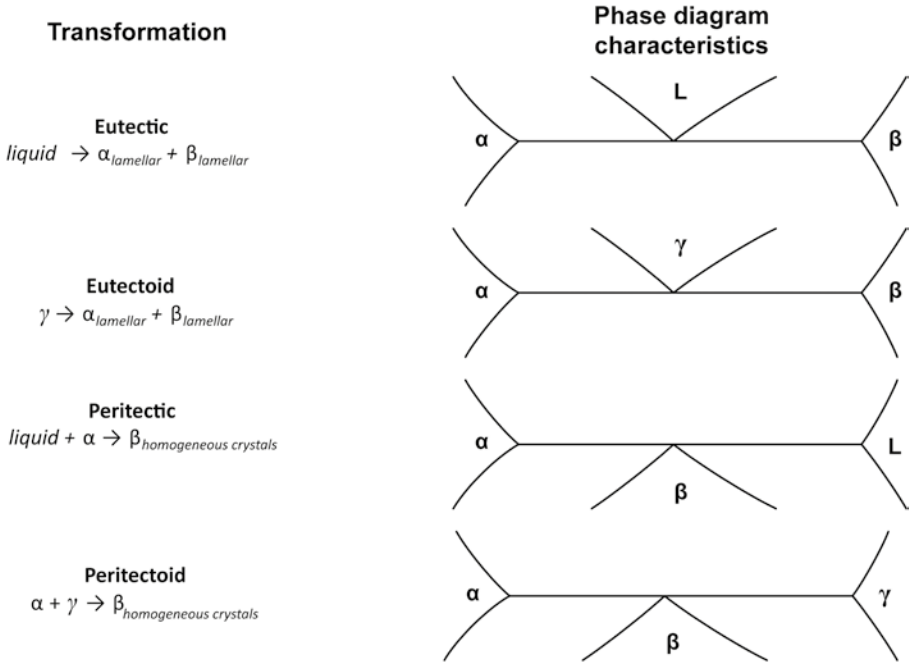

Figure 5.30 - Example of liquid state (eutectic and peritectic) and solid state (eutectoid and peritectoid) transformations in phase diagrams.

6. IRON-CARBON PHASE DIAGRAM (*Fe-C*)

6.1 Why is the *Fe-C* phase diagram required?

The starting point for the steel study is the iron-carbon phase diagram (Figure 6.1). It shows - as temperature[1] and carbon content changes - the phases[2] of the alloy under conditions of thermodynamic equilibrium.

The *Fe-C* phase diagram has three structural transformations ($V = 0$): peritectic transformation at 1,495°C, eutectic transformation at 1,148°C, and eutectoid transformation at 727°C.

In addition to the liquid, the one-phase fields of the *Fe-C* phase diagram are four:

- α-phase (light green), with a very limited amplitude, at the bottom left of the diagram, from 912°C up to room temperature, and a maximum solubility in carbon (0.02%) at 727°C;
- γ-phase (yellow), with a large extension on the diagram, between 1,394°C and 912°C, and a maximum solubility in carbon (2.11%) at 727°C;
- δ-phase (light brown), with a very limited amplitude, top left on the diagram, between melting temperature at 1,538°C and 1394°C, and a maximum solubility in carbon (0.09%) at 1,495°C;
- Fe_3C phase (red), on the vertical axis to the left of the diagram, with a constant carbon composition of 6.69%, from melting temperature to room temperature.

Conventionally, the *Fe-C* alloys are divided into steel and cast iron: steel, if the carbon content is less than 2.11%, cast iron if higher.

The *Fe-C* phase diagram has several peculiarities. It is truncated at 6.69% of carbon, i.e. the stoichiometric percentage of carbon in iron carbide (Fe_3C). Beyond this value, the alloys that do not have any practical use, since the excess carbon separates from the iron in the form of graphite.

Another peculiarity is related to the solubility of iron and carbon in the liquid state: it is assumed that carbon is soluble in the liquid throughout the entire extension of the phase diagram. Practically, however, the solubility of carbon in iron is limited to about 5%[3]. This is why the liquidus curve, at the top right in the *Fe-C* phase diagram, is indicated with a dotted line.

Finally, iron carbide (Fe_3C) is a metastable compound, i.e. non-stable: it tends to decompose into iron and graphite carbon (g) according to the reaction [6.1]:

$$Fe_3C \rightarrow 3Fe + C_{(g)} \quad [6.1]$$

---

[1] As already observed in Chapter 5, the cooling rate of an alloy on the phase diagram is always very slow (equilibrium cooling). This allows the system, at each infinitesimal variation in temperature, to return to equilibrium, that is, to uniformize the temperature and the chemical composition of the phases at all points of the system (see also note 13 of Chapter 1).

[2] For the phase definition, see paragraph 5.1 of Chapter 5.

[3] Over 5%, carbon separates from the liquid in the form of graphite.

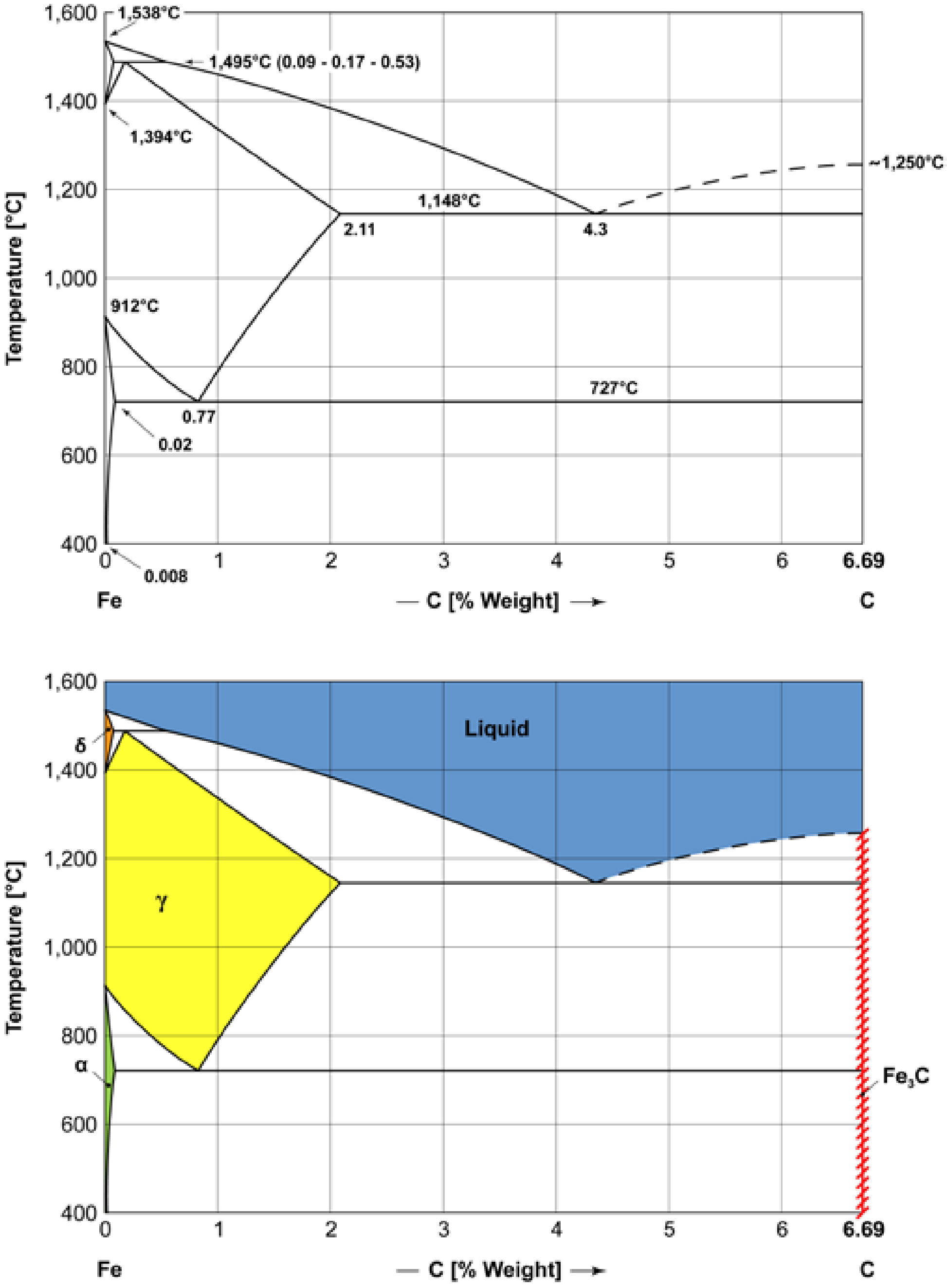

Figura 6.1 – *Fe-C* phase diagram. The one-phase fields are highlighted with different colors [from ASM-H.3 1992].

Since the decomposition of iron carbide takes place over a very long period of time, the reaction [6.1] can be neglected. This is particularly true for steel and for cooling rate used in industrial applications. However, graphite is to be considered for cast iron, especially in case of elements that promote graphitization.

6.2 Eutectoid, hypoeutectoid, and hypereutectoid steel

The cooling of *Fe-C* alloys can be studied by dividing the different types of steel into two families:

- hypoeutectoid steel, if $C < 0.77\%$,
- hypereutectoid steel, if $C > 0.77\%$,

since steel with $C = 0.77\%$ is the eutectoid alloy that divides the two.

Case 1: Eutectoid steel ($C = 0.77\%$)

Let us first consider the case of eutectoid steel ($C = 0.77\%$) and study the trend of its phases during equilibrium cooling, from the melting temperature to room temperature, as provided by the *Fe-C* phase diagram (see Figure 6.2).

Initial solidification occurs between T_L and T_S (temperature of *liquidus* and *solidus*) and involves the formation of homogeneous crystals of γ-phase. Subsequently the alloy goes towards the eutectoid transformation at 727°C.

The eutectoid transformation is similar to the eutectic one, already described in Chapter 5. The only difference is related to the phase that changes: during the eutectic, it is the liquid phase while, during the eutectoid, it is the γ-phase at solid state.

The eutectoid of the *Fe-C* phase diagram is particular and always involves the transformation of homogeneous crystals of γ-phase in crystals of a lamellar nature, with alternating lamellae of α and Fe_3C phases.

Therefore, at an infinitesimal of a degree less than 727°C, the structure of eutectoid steel consists of 100% of crystals with alternating lamellae of α-phase and of Fe_3C phase (Figure 6.3).

During the final cooling, from the eutectoid temperature to room temperature, the system is always composed of 100% of lamellar crystals.

The quantity of the two phases (α and Fe_3C) at 20°C can be calculated with the lever rule[4]:

$$Q_\alpha = \frac{6.69 - 0.77}{6.69 - 0.008} \cdot 100 \cong 88.6\% \qquad Q_{Fe_3C} = \frac{0.77 - 0.008}{6.69 - 0.008} \cdot 100 \cong 11.4\%$$

---

[4] At 727°C the quantity of α-phase is ~88,8% and the amount of Fe_3C phase is ~11,2%. The difference compared to the same quantities calculated at 20°C depends on the variation of carbon solubility in α-phase.

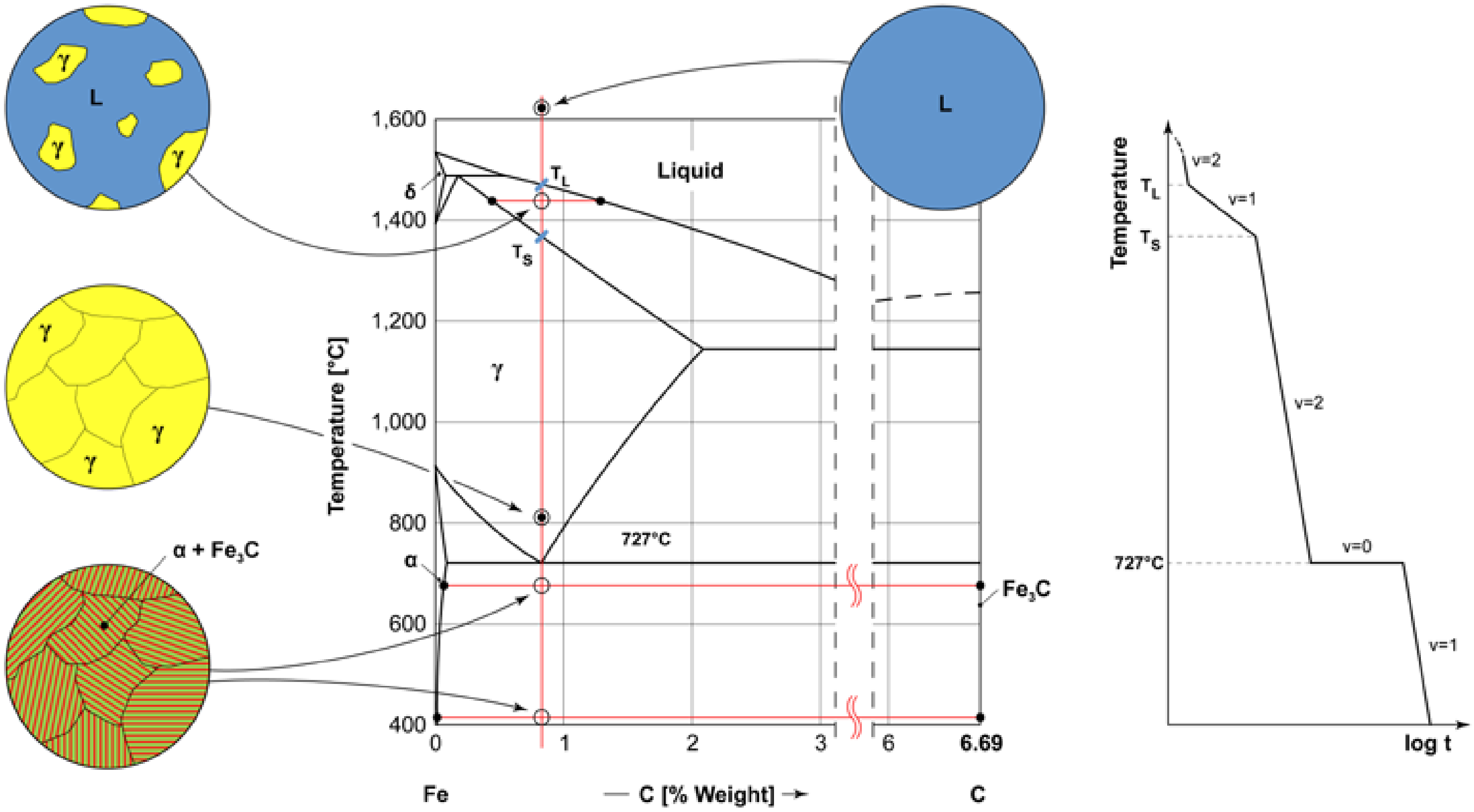

Figure 6.2 - *Fe-C* phase diagram. Graphic representation of microstructure and equilibrium cooling curve of an eutectoid steel ($C = 0,77\%$).

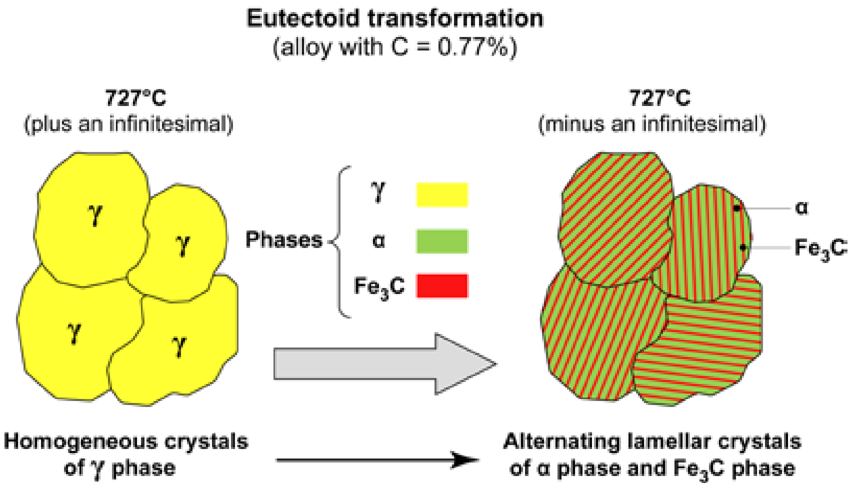

Figure 6.3 - Graphic representation of the eutectoid transformation of the alloy with $C = 0.77\%$.

Case 2: Hypoeutectoid steel ($0.02\% < C < 0.77\%$)

Let us now consider the case of hypoeutectoid steel, i.e. *Fe-C* alloys with carbon contents less than 0.77% (Figure 6.4).

A generic hypoeutectoid steel, during solidification between T_L and T_S, crosses the area of the peritectic horizontal at 1,495°C. In particular:

- alloys with $0.02\% < C < 0.09\%$ solidify in homogeneous crystals of δ-phase and then turn completely into homogeneous crystals of γ-phase;
- alloys with $0.09\% < C < 0.53\%$ undergo a peritectic transformation and, then give rise to a system consisting entirely of homogeneous crystals of γ-phase;
- alloys with $0.53\% < C < 0.77\%$ solidify in homogeneous crystals of γ-phase.

As can well be observed, below a certain temperature level, the system is entirely formed of homogeneous crystals of γ-phase. Consider, for example, what happens to any hypoeutectoid alloy at 1,300°C: from that temperature[5] and up to temperature T_1, the system consists of 100% of homogeneous crystals of γ-phase.

---

[5] *Note that hypoeutectoid alloys consist of homogeneous crystals of γ-phase, even for temperatures above 1,300°C. The numeric indication of 1,300°C has no specific value: it is only a purely indicative value (it could have also been 1,200°C or 1,350°C) to make the reader aware that the system is fully in γ-phase for a wide temperature range.*

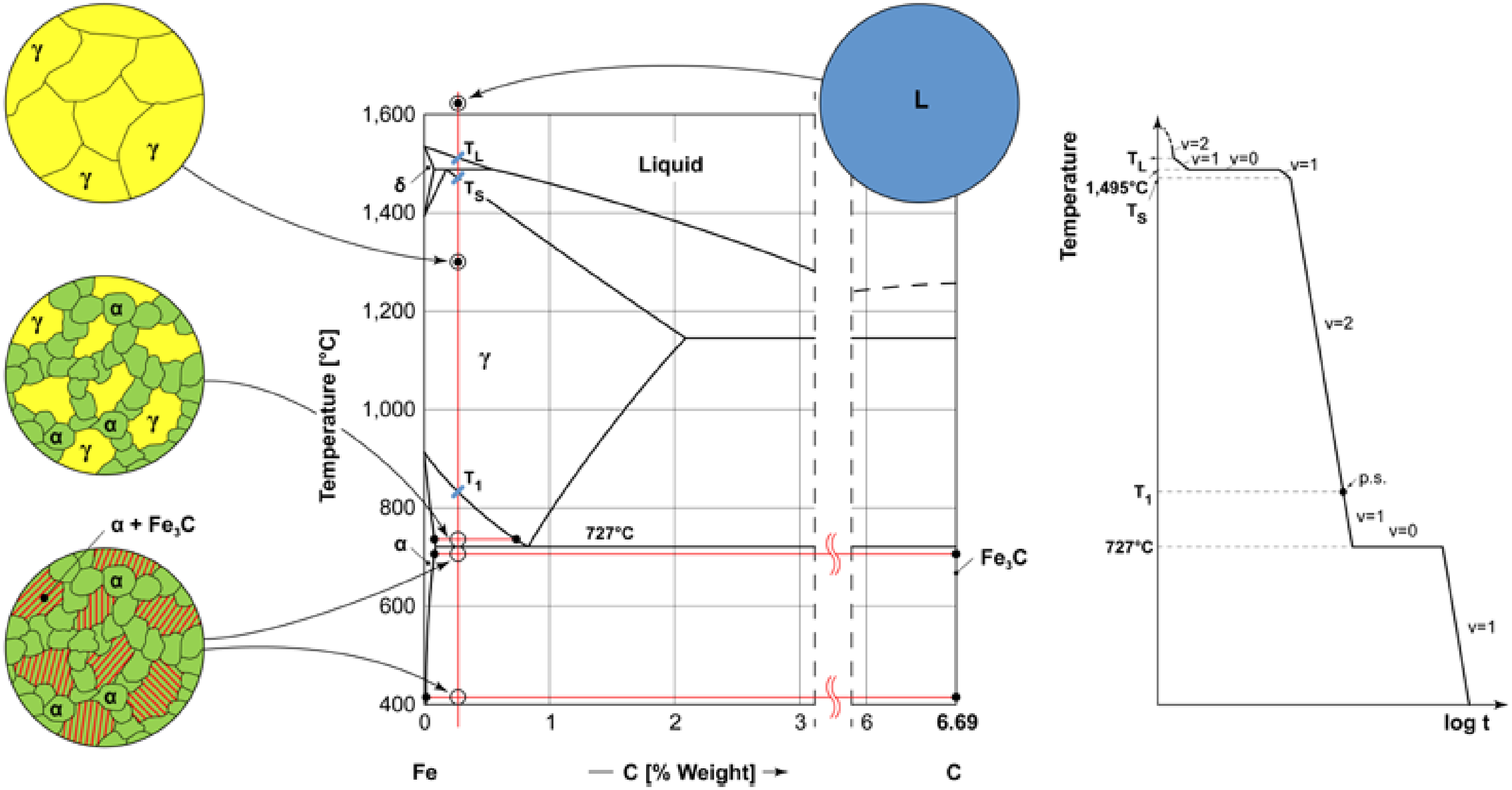

Figure 6.4 - *Fe-C* phase diagram. Graphic representation of microstructure and equilibrium cooling curve of a generic hypoeutectoid steel.

To understand the transformations that occur at the eutectoid horizontal, it is necessary to consider, what has been seen for steel with $C = 0.77\%$.

The hypoeutectoid alloy has carbon contents lower than 0.77%; consequently its iron content is greater than alloy with $C = 0.77\%$. Thus, before the eutectoid transformation can take place, the alloy must reduce the excess iron between T_1 and 727°C, and it forms α-phase in homogeneous crystals.

An infinitesimal of a degree above 727°C, that is, a moment before the eutectoid transformation begins, the alloy is composed of homogeneous crystals of α-phase and homogeneous crystals of γ-phase.

The greater is the amount of homogeneous crystals of α-phase, the lower is the percentage of carbon in the alloy. For $C = 0.02\%$ you have 100% of homogeneous crystals of α-phase, while for $C = 0.77\%$, the quantity of α-phase in homogeneous crystals is zero (eutectoid alloy). At intermediate chemical compositions, homogeneous crystals of α-phase is inversely proportional to the carbon content.

At 727°C, as is typical for all alloys in the *Fe-C* phase diagram, the homogeneous crystals of γ-phase transform into lamellar crystals composed of alternating layers of α-phase and Fe_3C phase; on the contrary homogeneous crystals of α-phase remains unchanged (Figure 6.5).

Finally, during very slow cooling to room temperature, the structure does not undergo significant modifications and remains comprised of homogeneous crystals of α-phase and lamellar eutectoid crystals[6].

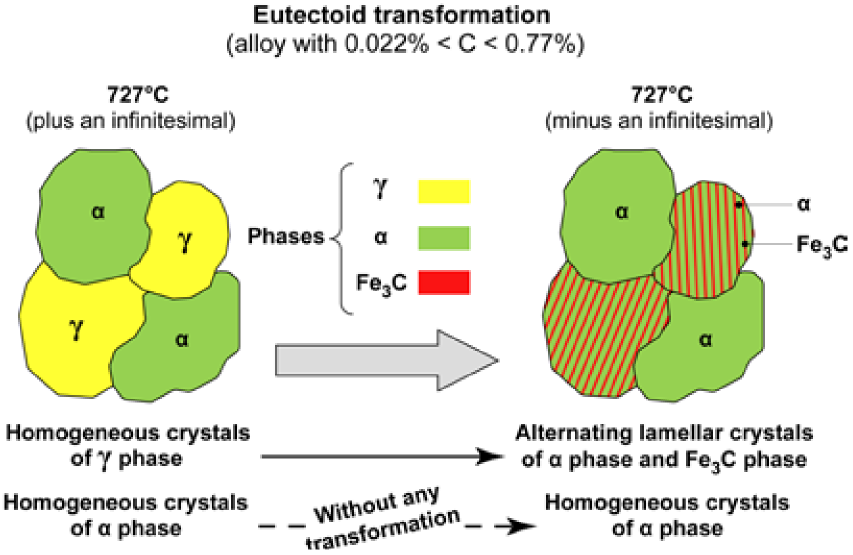

Figure 6.5 - Graphic representation of the eutectoid transformation of a generic hypoeutectoid alloy ($0.02\% < C < 0.77\%$).

---

[6] *In cooling from 727°C to 20°C, hypoeutectoid alloys form plates of phase Fe_3C on the grain boundary of homogeneous crystals of α-phase. Plate formation is due to the solubility variation of carbon in α-phase. However, the quantity is very limited (less than 0.3%) and can practically be neglected.*

Case 3 Hypereutectoid steel (0.77% < *C* < 2.11%)

Lastly, the case of steel with a carbon content greater than 0.77%. Hypereutectoid steel forms homogeneous crystals of γ-phase without crossing the peritectic horizontal at 1495°C or the eutectic horizontal at 1148°C (Figure 6.6).

This steel family has a higher carbon content than eutectoid steel. Therefore, before the eutectoid transformation occurs, excess carbon is reduced between T_1 and 727°C, forming plates of Fe_3C phase on the grain boundary of homogeneous crystals of γ-phase.

The higher the carbon content, the greater the quantity of plates on the grain boundary. The maximum amount plates on the grain boundary is for the alloy with $C = 2.11\%$. The result is equal to:

$$Q_{Fe_3C} = \frac{2.11 - 0.77}{6.69 - 0.77} \cdot 100 \cong 22.6\% \qquad Q_\gamma = \frac{6.69 - 2.11}{6.69 - 0.77} \cdot 100 \cong 77.4\%$$

For carbon contents less than 2.11%, of plates on grain boundary are proportionally lower than 22.6%, up to zero at $C = 0.77\%$.

The transformation of the homogeneous grains of γ-phase to lamellar grains composed of alternating layers of α-phase and Fe_3C phase, takes place at the eutectoid temperature; F_3C phase, previously deposited on the grain boundary, does not undergo any change (Figure 6.7).

Lastly, during the very slow cooling to room temperature, the structure does not undergo any further change.

6.3 Structural constituents of the *Fe-C* phase diagram

The study of equilibrium cooling of the *Fe-C* alloys allows to determine phases and microstructures in equilibrium at each temperatures.

With reference to steel, there are three types of microstructures[7]:

- homogeneous grains,
- lamellar grains,
- plates on grain boundary,

formed by the phases shown by Fe_3C phase diagram (γ, α and/or Fe_3C phases).

---

[7] *In metallurgy, the terms "crystallites", "crystals", and "grains" are used indistinctly and interchangeably.*

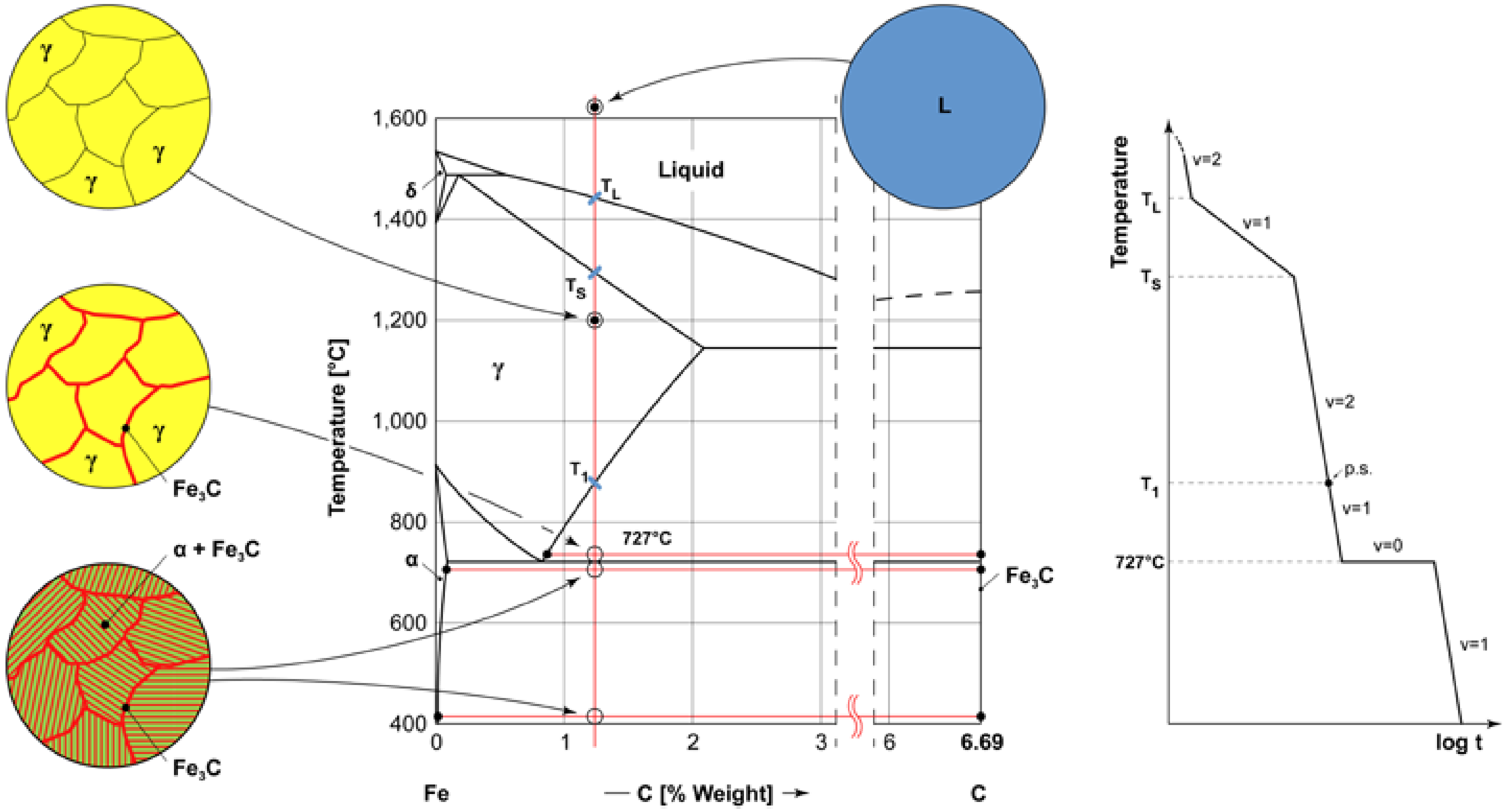

Figure 6.6 - *Fe-C* phase diagram. Graphic representation of microstructure and equilibrium cooling curve of a generic hypereutectoid steel.

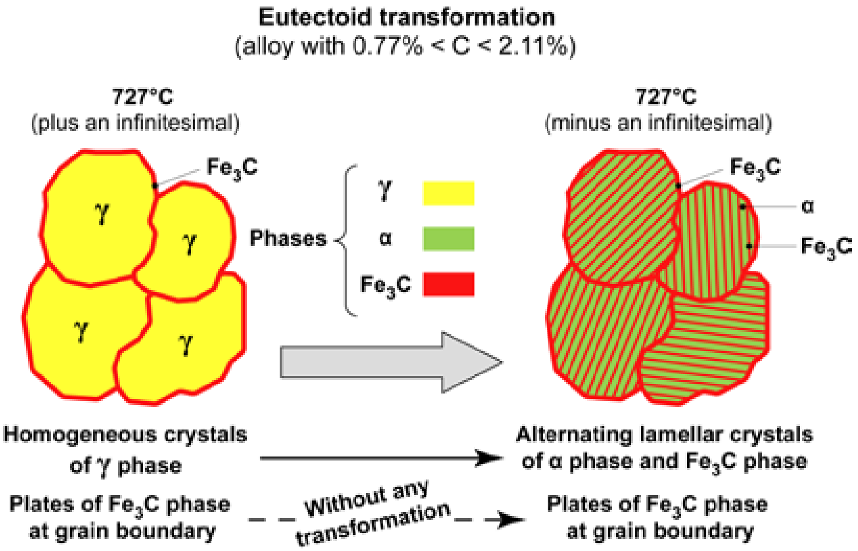

Figure 6.7 - Graphic representation of the eutectoid transformation of a generic hypereutectoid ($0.77\% < C < 2.11\%$).

Conventionally, phases and microstructures of steel[8], are usually indicated with a specific denomination:

- austenite with reference to homogeneous grains of γ-phase;
- ferrite (or α-ferrite[9]) with reference to homogeneous grains of α-phase;
- pearlite with reference to lamellar grains composed of alternating layers of α-phase and Fe_3C phase;
- cementite with reference to plates of Fe_3C phase at the grain boundary of homogeneous crystals or lamellar crystals.

As it is well understand, it is much easier to speak of ferrite and pearlite rather than microstructures with homogeneous grains of α-phase and alternating lamellar grains of α-phase and of Fe_3C phase.

Also remember that microstructure of the *Fe-C* phase diagram are always comprised of one or more phases, aggregated in a particular form. For example, ferrite is not simply α-phase but it is α-phase aggregated in the form of homogeneous crystals.

---

[8] *In metallurgy, the terms "structures", "microstructures" and "structural constituents" are used interchangeably.*

[9] *The therm α-ferrite is used to distinguish this microstructure from δ-ferrite, which exists near the melting temperatures, for very low carbon contents. In particular, α-ferrite consists of homogeneous crystals of α-phase, while δ-ferrite consists of homogeneous crystals of δ-phase. The term used to define the structure is the same (ferrite) because the crystal lattice is body-centered cubic for both phases (α and δ), as is aggregation in homogeneous crystals.*

The distinction is not just formal: α-phase, in fact, is not present only in homogeneous grains but also in the form of lamellae in pearlite grains. In the latter case, however, it is not possible to speak of lamellar ferrite (erroneous term) but of α-phase in lamellae, aggregated to the Fe_3C phase in lamellae[10].

Therefore, for the three families of steel described above, at 20°C and in conditions of thermodynamic equilibrium, the microstructures are:

- eutectoid steel ($C = 0.77\%$): pearlite,
- hypoeutectoid steel ($0.02\% < C < 0.77\%$): ferrite and pearlite (the quantities of the two microstructures are function of the carbon content),
- hypereutectoid steel ($0.77\% < C < 2.11\%$): pearlite and cementite (the quantities of the two microstructures are function of the carbon content).

The amounts of the microstructures can be calculated with the lever rule. The result is shown in Figure 6.8.

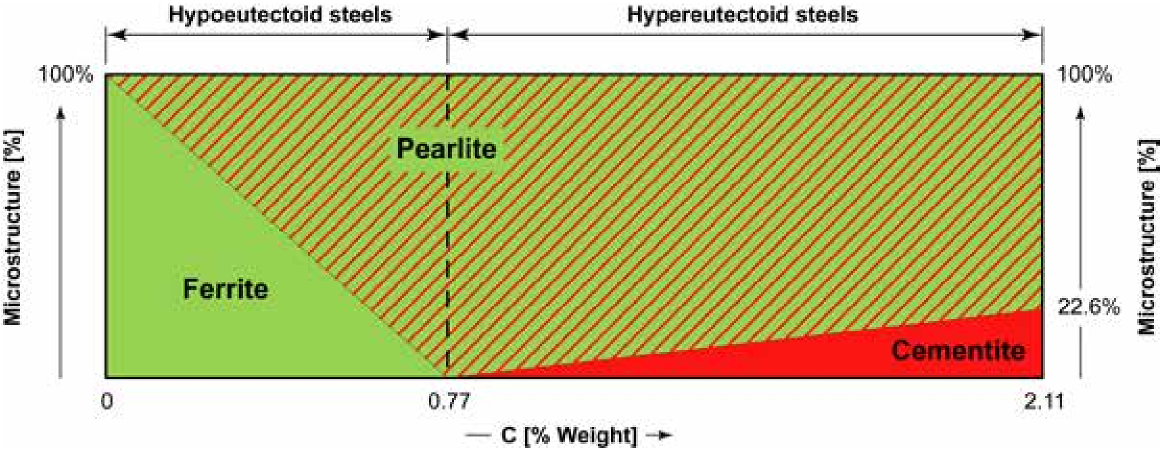

Figure 6.8 - The effect of carbon content on steel microstructure at room temperature.

---

[10] *The distinction between phases and microstructures, although it may seem sophisticated, is significant. Unfortunately, in many books, it is written that pearlite is a lamellar aggregate of ferrite and cementite. This definition is incorrect, since a microstructure (pearlite) cannot be described as an aggregate of two other microstructures (ferrite and cementite). Pearlite is a structural constituent and it must be defined by one or more phases, aggregated according to a certain method. For this reason, pearlite is an aggregate in lamellar crystals composed of alternating layers of α-phase and Fe_3C phase. Similarly, ferrite is an aggregate in homogeneous crystals of α-phase, while cementite is Fe_3C phase in the form of plates on the grain boundary.*

6.4 Critical points of the *Fe-C* phase diagram

As seen in the previous paragraph, steel undergoes an important transformation at the solid state: γ-phase, turns completely into α-phase and Fe_3C phase. This important phenomenon must be taken into account when explaining the microstructural changes that occur during industrial heat treatments[11].

The critical points indicate the trasformation of γ-phase and are defined according to the carbon content (see Figure 6.9)[12]:

- critical point A_3: points on the *Fe-C* diagram where γ-phase in homogeneous crystals (austenite) transforms into α-phase in homogeneous crystals or, more simply, where austenite transforms into ferrite;
- critical point A_1: points of the *Fe-C* diagram where γ-phase in homogeneous crystals (austenite) transforms into lamellar crystals composed of alternating layers of α-phase and Fe_3C phase or, more simply, where austenite becomes pearlite;
- critical point A_{cm}: points on the *Fe-C* diagram where γ-phase in homogeneous crystals (austenite) transforms into Fe_3C phase in plates on the grain boundary, or, more simply, where austenite transforms into cementite.

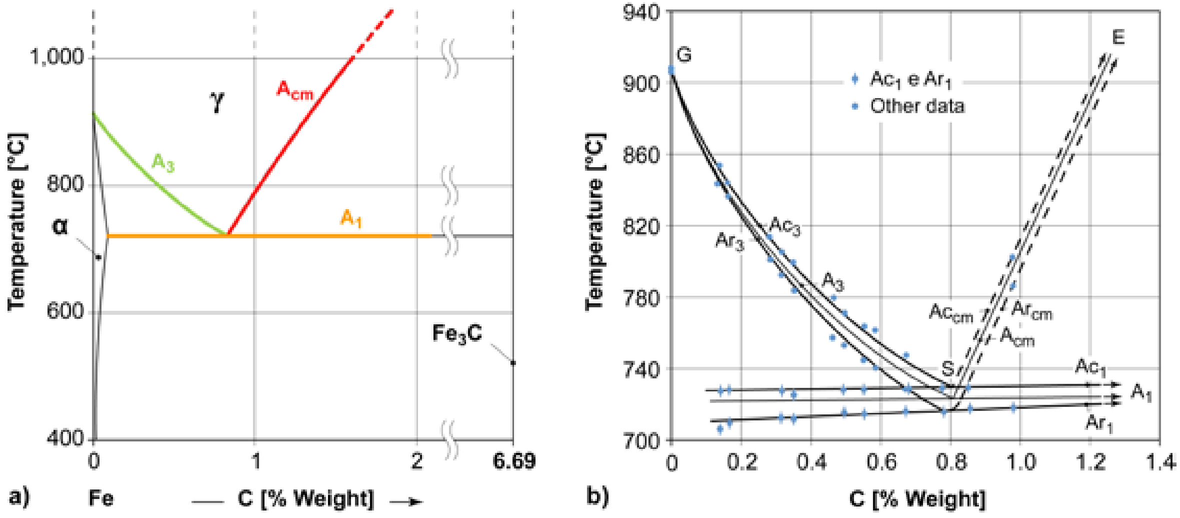

Figure 6.9 - Critical points of the *Fe-C* phase diagram: a) definition of critical points; b) real position of critical points at equilibrium, heating, and cooling [from Bain and Paxton 1966].

---

[11] The transformation of austenite is typical of steels and involves the possibility of having very different mechanical/metallurgical properties, in relation to the heat treatment performed. Other alloys, such as aluminum alloys or copper alloys, do not have this peculiarity.

[12] Critical points are always designated by the letter A (arrêter) followed by a number (1, 2, 3, 4) or letters (cm).

The critical points are determined in conditions of thermodynamic equilibrium and in their description, letter e (A_{e1}, A_{e3}, A_{ecm}) should always be present, yet this information is often omitted.

Critical points can also be measured in conditions of non-equilibrium, i.e. in conditions of continuous heating or cooling: in these cases are used letter c (A_{c1}, A_{c3}, A_{ccm}) or letter r (A_{r1}, A_{r3}, A_{rcm})[13].The position of critical points at heating (A_c) or at cooling (A_r) is different from equilibrium (A_e). This depends to the thermal hysteresis of the system when the condition of equilibrium are missing. Thermal hysteresis causes an increase in critical points with respect to equilibrium in the heating phase, or a decrease in the cooling phase.

Critical points are useful for describing the transformations of steel without indicate the temperature. Considering, for example, any hypereutectoid steel, it can be stated that austenite begins to transform into cementite at the temperature of A_{cm}. Therefore, at temperature of A_{c1}, the remaining austenite transforms into pearlite.

6.5 The effect of alloying elements

All types of steel, even the most commonly used, is not simply iron and carbon. In addition to carbon, there are always other alloying elements: sometimes as residue of the steel production process, other times because they are added to obtain specific properties.

In all types of steel, for example, traces of silicon and manganese are always detectable, both used in steel making due to the elimination of unwanted chemical species[14]. Sulfur and phosphorus are also systematically present as residue of the iron ore used as raw material.

Finally, manganese, chromium, nickel, molybdenum, vanadium, and silicon can be found as alloying elements that are added.

Steel alloying elements cause substantial changes to the Fe-C phase diagram. Their effect can be classified into two categories:

- austenitizing chemical elements,
- ferritizing chemical elements.

The first group includes manganese (Mn), nickel (Ni), carbon (C), nitrogen (N), copper (Cu): these are called austenitizing because they tend to expand γ-phase field and close α-phase field of the Fe-C diagram (Figure 6.10).

---

[13] *In practice, reference is always made to critical points measured in condition of continuous heating, i.e.* A_{c1} *and* A_{c3}*. Critical point* A_{ccm} *is, however, only indicated as* A_{cm}*.*

[14] *Silicon and manganese are used to neutralize oxygen. Manganese, in combination with calcium, favors the separation of sulfur present in the liquid steel bath. Oxygen and sulfur are two highly damaging chemical elements for steel, since they induce a significant reduction of impact strength and fracture toughness.*

Ferritizing elements (Figure 6.10), such as titanium (*Ti*), chromium (*Cr*), molybdenum (*Mo*), vanadium (*V*), silicon (*Si*), tungsten (*W*), aluminum (*Al*) boron (*B*), tantalum (*Ta*), and niobium (*Nb*). Have opposite effects (contraction of γ-phase field and expansion of α-phase field).

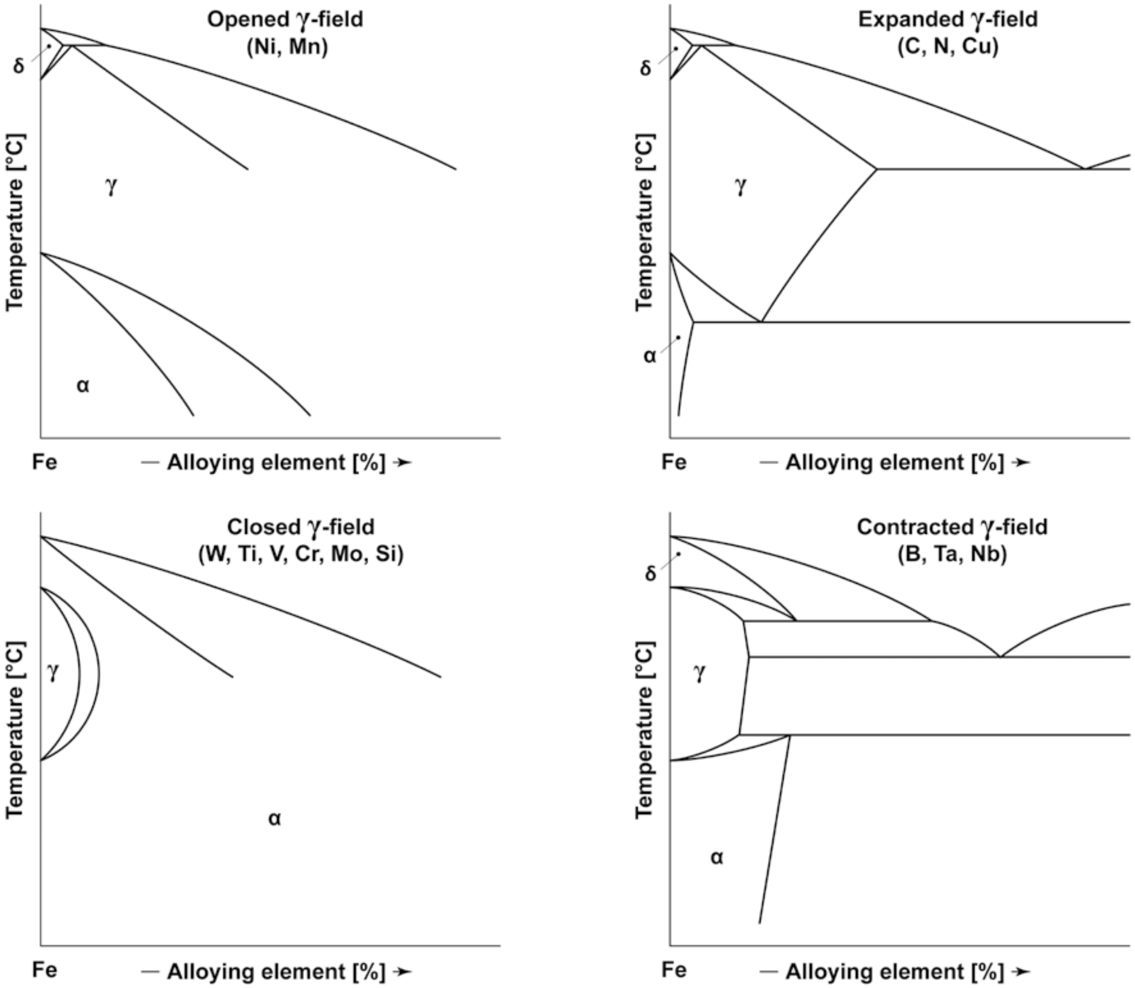

Figura 6.10 - Schematic representation of the types of phase diagrams that iron forms with austenitizing and ferittizing alloying elements [from Bain and Paxton 1966].

The austenitizing or ferritizing action of the alloying elements is not only function of the alloying elements content, but it also depends on the alloying elements type (see Figure 6.11). For example, the ferritizing effect of titanium is much higher than chromium: 0.8% titanium is enough to have a closed γ-phase field while, with a 5% of chromium, γ-phase field is only slightly narrower.

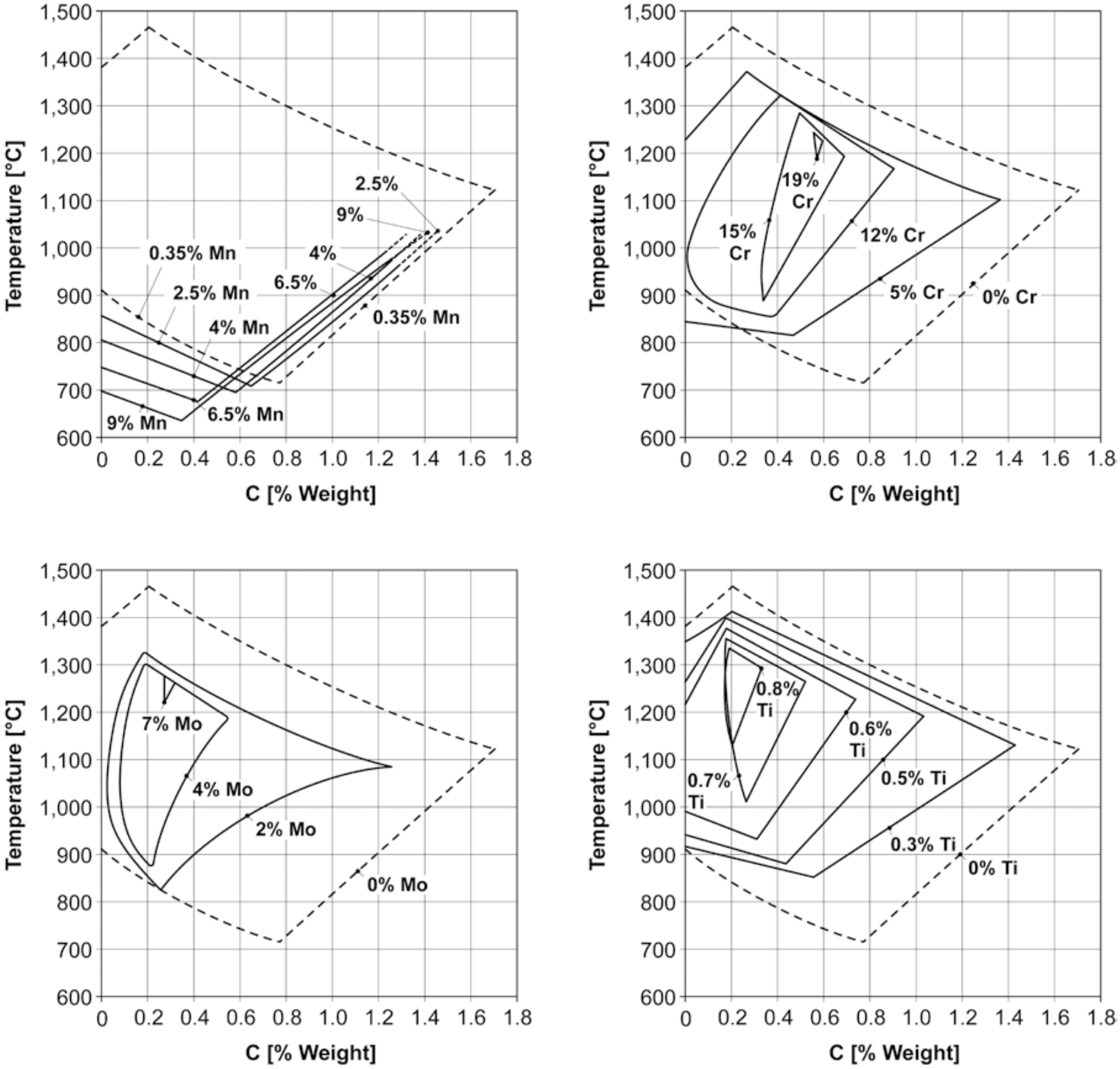

Figure 6.11 - The effect of manganese, chromium, molybdenum, and titanium on amplitude of γ-phase field of the *Fe-C* phase diagram [from ASM-H.4 1991].

The alloyng elements can raise (ferritizing elements) or lower (austenitizing elements) the eutectoid temperature. On the contrary, the carbon content of the eutectoid alloy (that for *Fe-C* equals 0.77%) is always reduced by the addition of any alloying element (Figure 6.12).

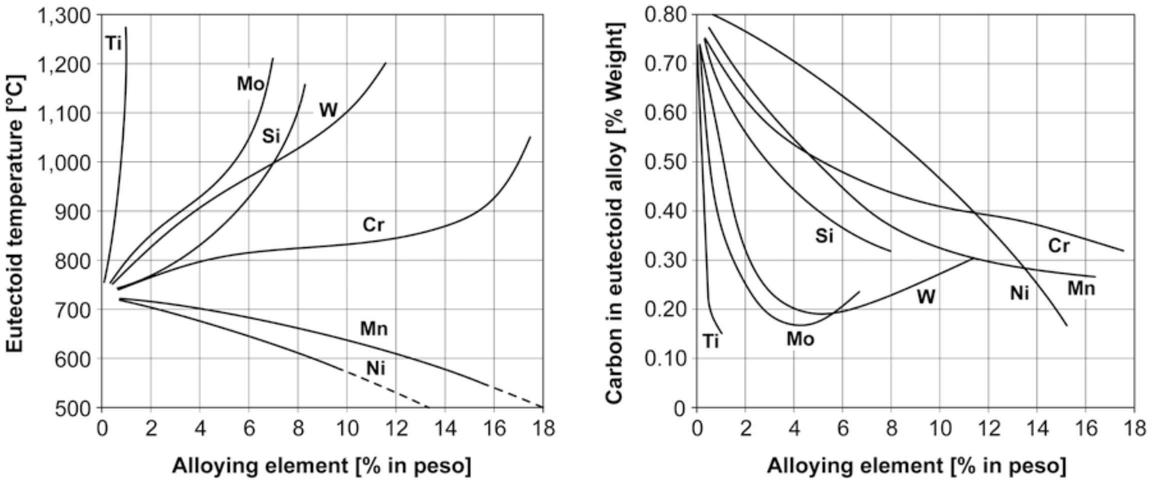

Figure 6.12 - The effect of alloying elements on the eutectoid temperature and on the carbon content of the eutectoid steel [from Bain and Paxton 1966].

The critical points as it is modified by alloying elements, can be calculated through various empirical formulas. The most commonly used are listed in [Andrews 1965], valid for low carbon steel with $C < 0.6\%$ [6.2; 6.3]:

$$Ae_1[°C] = 723 - 10.7Mn - 16.9Ni + 29.1Si + 16.9Cr + 290As + 6.38W \quad [6.2]$$

$$Ae_3[°C] = 910 - 203\sqrt{C} - 30Mn + 44.7Si - 15.2Ni - 11Cr - 700P + 31.5Mo + 104V - 20Cu + 460Al + 13.1W + 120As \quad [6.3]$$

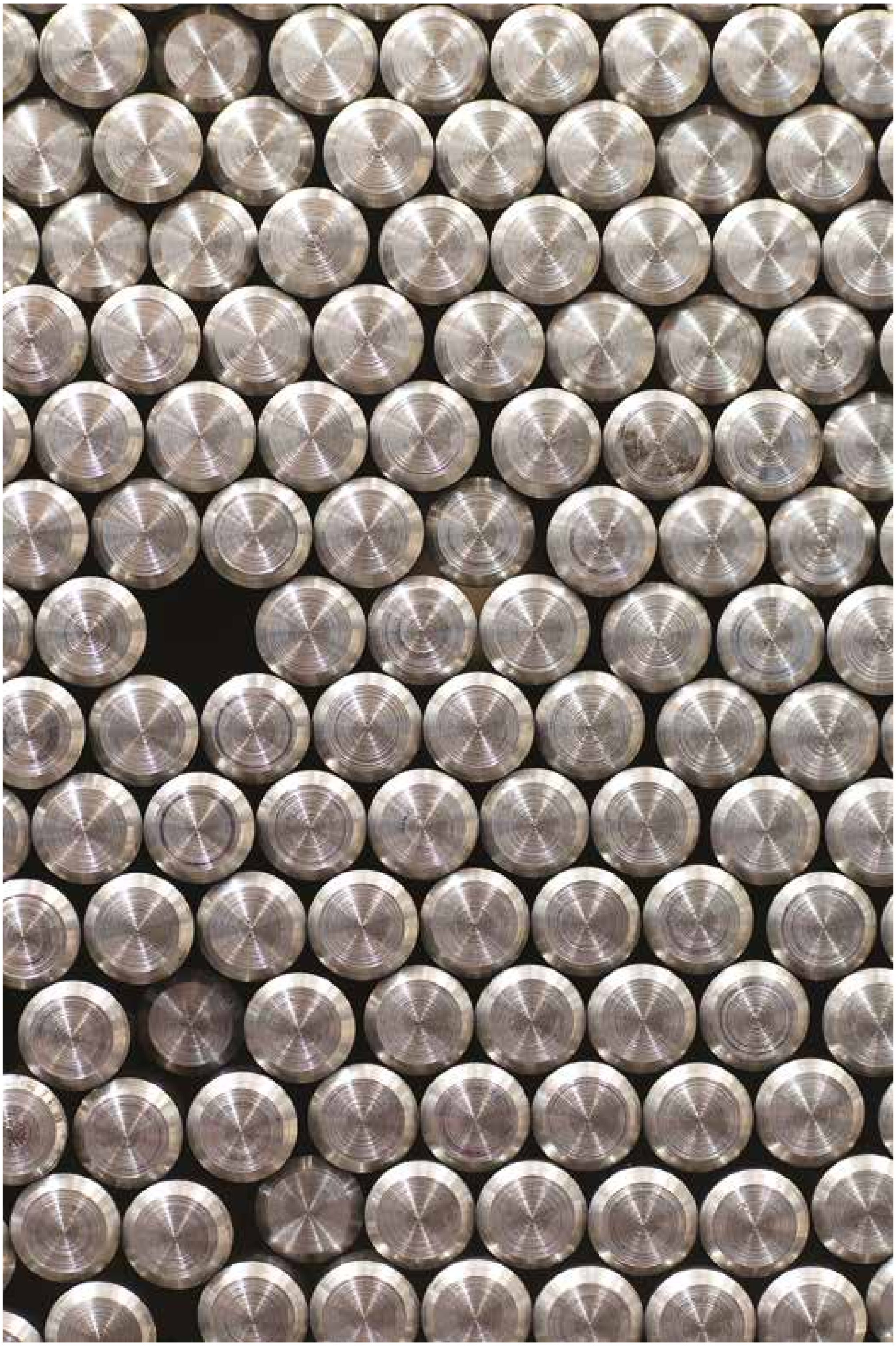

7. T.T.T. AND C.C.T. DIAGRAMS

7.1 What are the T.T.T. and C.C.T. diagrams?

The *Fe-C* phase diagram is very important because it provides information regarding the steel microstructures in conditions of thermodynamic equilibrium, i.e. the microstructures at the end of equilibrium cooling.

In industrial practice, however, the cooling curves used for heat treatments are different from equilibrium cooling[1]. At most, only a very slow cooling in the furnace can be generally assimilated to equilibrium cooling. When cooling curves are different from equilibrium cooling, it is no longer possible to refer to the *Fe-C* phase diagram and, to predict the microstructures at the end of the heat treatment, other diagrams are needed. To solve the problem of austenite transformations under conditions of non-equilibrium, there are two types of diagrams: the isothermal transformation diagrams and the continuous cooling diagrams. These diagrams show the austenite transformations and the microstructure at the end of the heat treatment in relation to cooling curves. Usually, these diagrams show the temperature in ordinate and the logarithmic scale of time in abscissa[2].

Normally, the isothermal transformation diagrams and the continuous cooling diagrams are simply called T.T.T. diagrams (Time Temperature Transformations) and C.C.T. diagrams (Continuous Cooling Transformations).

7.2 Bain's Experiences. T.T.T. diagram and C.C.T. diagram for eutectoid steel.

The T.T.T. and C.C.T. diagrams were originally developed in the 1930s by E. C. Bain[3] and E. S. Davenport. Later, these diagrams were corrected by M. Cohen, who indicated the martensitic transformation.

The T.T.T. and C.C.T. diagrams are born on the evidence that, according to the cooling curve, austenite can form:

- structures such as ferrite, pearlite, and cementite, as typical for *Fe-C* phase diagram;
- new structures such as bainite and martensite, not present on the *Fe-C*.

---

[1] *Keep in mind that, during the actual heat treatments, the heating curves are different from equilibrium heating.*

[2] *The logarithmic scale of time is a mathematical operator used to reduce the extension of the abscissa.*

[3] *Edgar Collins Bain (1891-1971), American chemist and metallurgist (BSc and MSc from Ohio State University). He interrupted his PhD to work at the Goodrich Company. After a short pause in the American Army's technical department (Sub-liutenant at the Chemical Warfare Service), in 1919 he joined the General Electric Company, dealing with the use of X-rays in metallurgy. In 1924, he moved to the laboratories of Union Carbide and Carbon Corporation. From 1928 until his retirement in 1957, he worked for the US Steel Corporation in Pittsburgh, Pennsylvania. Famous worldwide for his research in the field of steel heat treatments and the effect of alloying elements, Bain is also remembered for having discovered bainite.*

Case 1 (T.T.T. diagram for eutectoid steel)

The simplest example refers to eutectoid steel ($C = 0.77\%$). In this steel, if you consider the *Fe-C* phase diagram, austenite would transform completely into pearlite due to equilibrium cooling.

Let us see, however, what transformations occur if the same alloy is subjected to an actual cooling curve.

First consider the case of an isothermal cooling curve (Figure 7.1).

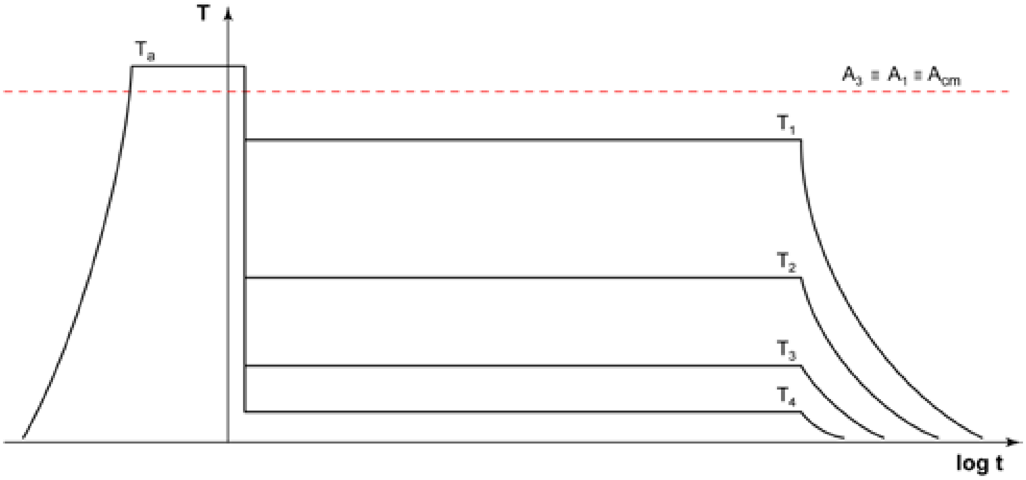

Figure 7.1 - Schematic representation of isothermal cooling curves (T_1, T_2, T_3 or T_4).

The alloy is heated above the critical point[4], in order to have the complete transformation of the microstructure into austenite (temperature T_a). After being in the austenitic field for a certain period, steel is abruptly cooled to a given temperature (in this case, T_1, T_2, T_3 or T_4). The temperature is then kept constant (isothermal holding), in order to evaluate the structural changes that steel undergoes over time.

At the end, the system is air cooled to room temperature.

The idea behind this particular cooling method is quite simple. After austenitization, an abrupt cooling of the steel is required, in order to have non-equilibrium conditions in the system and to prevent, at 727°C, the transformation into pearlite, as expected by the *Fe-C* phase diagram. Rapid cooling freezes the austenitic microstructure and brings it virtually unchanged to temperature T_1, T_2, T_3 or T_4. At these temperatures, we want to observe the microstructures and the time when the transformation begins and ends[5].

---

[4] *As seen in Chapter 6, an eutectoid steel has only one critical point ($A_3 \equiv A_1 \equiv A_{cm}$) that, in conditions of equilibrium, corresponds to 727°C.*

[5] *The isothermal cooling method is sometimes also used in the industrial field, as is the case, for example, of isothermal annealing (see Chapter 10).*

The isothermal transformation curves of austenite for steel with $C = 0.77\%$ is shown in Figure 7.2: it is the so-called "T.T.T. diagram"[6] for eutectioid steel.

In the graph, there are two red curves in the form of C joined at the bottom with two horizontal lines, also red, defined by the letters M_s and M_f. The first C and the horizontal line at M_s represent the beginning of the transformation of the austenite, while the second C and the horizontal line at M_f represent the end of the transformation of austentite into a new microstructure.

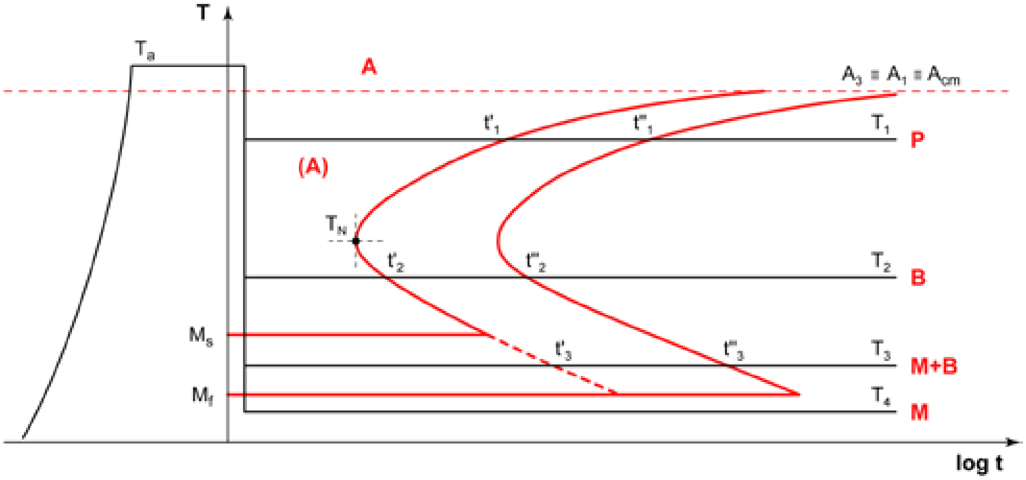

Figure 7.2 - The T.T.T. diagram (red lines) for eutectoid steel; the cooling curves are black.

Consider the trajectory characterized by isotherm T_1 (in black). Above the critical point, steel has a stable austenitic microstructure (letter A). As a result of abrupt cooling up to T_1 austenite becomes unstable (letter A in parentheses), i.e. it is in thermodynamic conditions that allow its transformation.

At temperature T_1, the austenite transformation is not immediate but occurs with a certain delay: it begins at time t'_1 (first curve at C, red) and ends with time t''_1 (second curve at C, red). Similar for the isotherm at T_2 (in black), where austenite begins to transform at t'_2 and ends at t''_2.

As can be observed in Figure 7.2, the C curves have a nose shape, that is, they show a temperature T_N, that minimized the starting time of the austentite transformation. This temperature is very important for defining the final microstructure of the steel: above T_N, austentite transforms into pearlite (letter P), instead, under T_N, the transformation forms a different microstructure called bainite (letter B). Bainite is considered a non-equilibrium microstructure because it does not exist on the Fe-C phase diagram. In conclusion: at temperature T_1, 100% of austenite becomes 100% of pearlite. At temperature T_2, 100% of austenite turns into 100% of bainite.

---

[6] *Oftentimes, the T.T.T. diagrams are called C curves or S curves due to their shape.*

Let us now examine the last two isothermal trajectories (T_3 and T_4), simply starting from T_4.

The isotherm at T_4 (in black) intercepts the field limited by the two red horizontal lines M_s and M_f (i.e. martensite *start* and martensites *finish*) during the initial cooling. This is the area of transformation of austenite into martensite.

Martensite is a steel microstructure, not present on the *Fe-C* phase diagram, that is, a non-equilibrium microstructure. In summary, at the end of the isotherm T_4, the microstructure is completely martensitic. It should be noted that the transformation of austenite into martensite is completed when the initial cooling curve meets the horizontal line M_f. The isothermal holding at T_4 is non influential to the microstructural changes.

A little more complex is the case of the isotherm at T_3. The cooling curve (in black) initially intercepts the field limited by the red horizontal line of M_s without arriving to M_f. In this area, the microstructure is only partially transformed into martensite, while there is still a certain amount of austenite. Subsequently, the isotherm at T_3 crosses the red dotted line. Here, at point t'_3, begins the modification of austenite in bainite, which ends in t''_3. The final microstructure consists of martensite and bainite.

Case 2 (C.C.T. diagram for eutectoid steel)

Now observe what occurs by subjecting eutectoid steel ($C = 0.77\%$) to continuous cooling.

Let us first consider the cooling curve. After heating and holding at T_a, steel is subjected to continuous cooling (according to trajectories T_1, T_2, T_3 or T_4). The cooling curves are very different with respect to the isothermal cooling. This time, the temperature varies continuously from the austenitization temperature (T_a) to room temperature, according to different cooling curves that become increasingly abrupt (from T_1 to T_4)[7].

---

[7] *The anisothermal cooling method is the most common in industrial heat treatments. Steel components cooled in a furnance, in air, in oil, or in water are subjected to anisothermal cooling (see Chapter 10).*

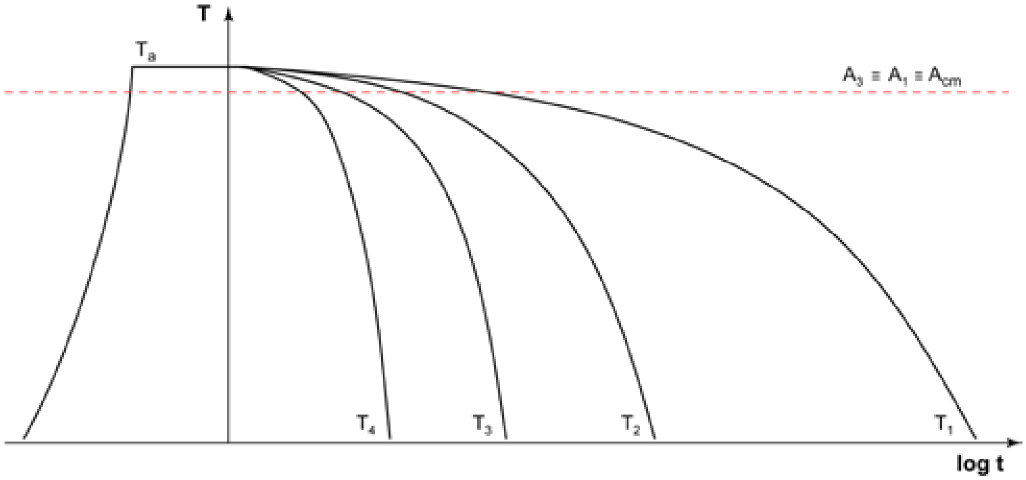

Figure 7.3 - Schematic representation of continuous cooling curves (T_1, T_2, T_3 or T_4).

Figure 7.4 shows a schematic representation of C.C.T. diagram for eutectoid steel (red lines).

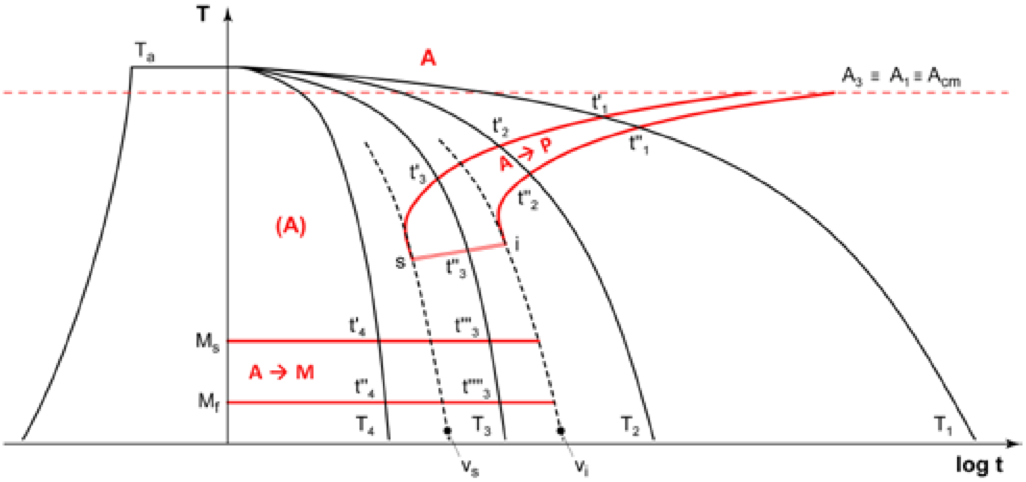

Figure 7.4 - C.C.T. diagram (red lines) for eutectoid steel; the cooling curves are black.

Following the cooling curve T_1, austenite begins to transform at time t'_1 and ends at time t''_1, transforming completely into pearlite.

Similar is the trajectory described by T_2, which intercepts the same field as the previous one. In this case as well, the austenite forms 100% of pearlite between t'_2 and t''_2 .

A bit more complex is the cooling curve indicated with T_3. At t'_3 austenite begins to transform into pearlite.

This transformation ends at t''_3, when only a part of the austenite is transformed. The austenite not yet transformed becomes martensite, due to the cooling between M_s ed M_f (from time t'''_3 to time t''''_3). The amount of pearlite and martensite is due to the cooling rate.

The more the trajectory T_3 approaches i, the greater the amount of pearlite and the lesser the amount of martensite; the contrary if T_3 is close to s[8]. The double thin red line, found between s and i in Figure 7.4, is an area of arrest for the austenite transformation. On the contrary, the other red curves of the diagram are drawn with thick lines, since they represent the beginning and end of the austentite transformations.

In the case of the cooling curve indicated by t'_4 austenite transforms completely into martensite when crossing the two horizontal lines (M_s and M_f) between t'_4 and t''_4.

The cooling curve passing through s is the slowest one that forms only martensite[9]. Similarly the cooling curve passing through i is the fastest cooling curve that forms only pearlite[10].

7.3 T.T.T. diagrams and C.C.T. diagrams for hypoeutectoid steels

After the case of eutectoid steel, it is necessary to consider a hypoeutectic steel when subjected to isothermal (T.T.T. diagrams) or continuous (C.C.T. diagrams) cooling.

The typical diagrams are shown in Figures 7.5 and 7.6. As you can see, the two diagrams are very similar to those of eutectoid steel. The only differences are related to the fields of transformation of austenite into ferrite (both in T.T.T. and C.C.T. diagrams) and the presence of the so-called "bainitic island" (only for C.C.T. diagrams).

---

[8] *If trajectory T_3 passes through i, the system forms 100% of pearlite, instead if trajectory T_3 passes trough s, the system forms 100% of martensite.*

[9] *If the cooling curve has a slower rate, system forms other microstructures in addition to martensite.*

[10] *The concept of higher or lower critical rate is not related to the value of the cooling rate but by the shape of the curve. For example, the curve for lower critical rate (v_i) for a eutectoid steel is the fastest cooling curve that forms 100% of pearlite: this curve is positioned on the temperature-time axis, lower and to the left with respect to the other cooling curves that form 100% of pearlite.*

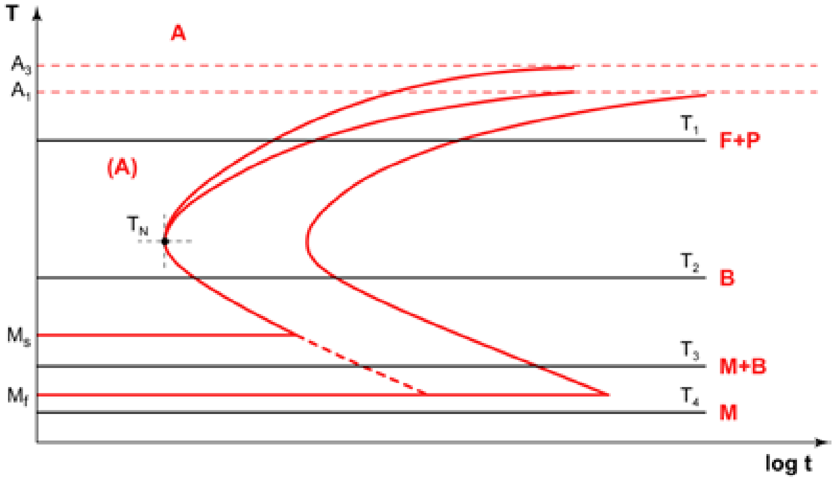

Figure 7.5 - Example of a T.T.T. diagram for a generic hypoeutectoid steel ($C < 0.77\%$).

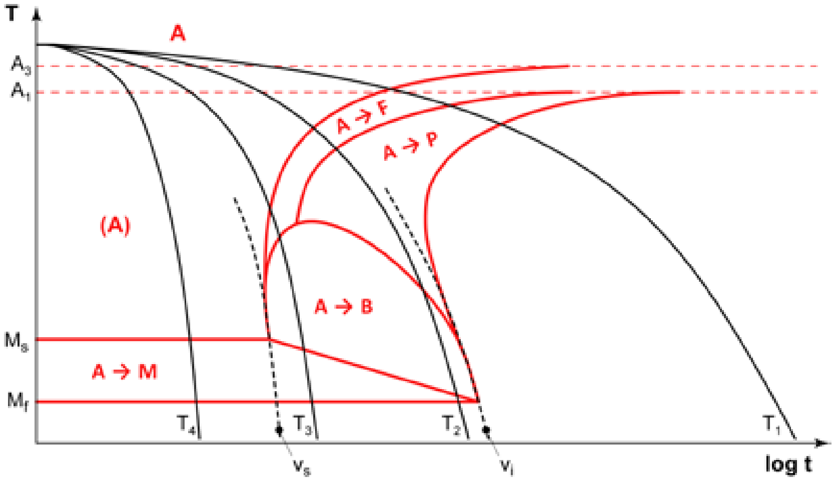

Figure 7.6 - Example of a C.C.T. diagram for a generic hypoeutectoid steel ($C < 0.77\%$).

Consider four isothermal cooling curves on the T.T.T. diagram in Figure 7.5. The result is:

- at the end of the horizontal line at T_1, the microstructure is ferritic-pearlitic;
- at the end of the horizontal line at T_2, the microstructure is bainitic;
- at the end of the horizontal line at T_3, the microstructure is martensitic-bainitic;
- at the end of the horizontal line at T_4, the microstructure is martensitic.

Similarly, for the four continuous cooling curves of the generic C.C.T. diagram in Figure 7.6, the result is:

- at the end of cooling curve T_1, the microstructure is made up of ferrite and pearlite;
- at the end of cooling curve T_2, the microstructure is made up of ferrite, pearlite, bainite, and martensite;
- at the end of cooling curve T_3, the microstructure is made up of ferrite, bainite, and martensite;
- at the end of cooling curve T_4, the microstructure is made up of martensite.

The curves indicated with V_s and V_i, also in this case represent two limit conditions: V_s is the slower cooling rate that forms only the martensitic microstructure; V_i is the fastest cooling rate that forms only ferrite and pearlite.

The Figures 7.5 and 7.6 show schematic representations of T.T.T. and C.C.T. diagrams. In a real case for each steel, there are only one T.T.T. diagram and only one C.C.T. diagram.

In particular, the shape and position of the T.T.T. and C.C.T. diagrams varies with various parameters. The addition of alloying elements, including carbon, causes a delay in the austenite transformation. As a result, the more the amount of alloying elements, the more moved down and right are T.T.T. and C.C.T. diagrams[11]. Similar effects are caused by increasing the austenitization time and the austenitization temperature[12] (Figure 7.7).

The forward shift of the T.T.T. and C.C.T. diagrams explains why it is easier to form martensite in steel containing alloying elements, in addition to carbon.

Figures 7.8 to 7.10 show some examples of T.T.T. and C.C.T. diagrams for hypoeutectic steels.

Note how in real T.T.T. and C.C.T. diagrams there are many useful informations to evaluate microstructure and its characteristics at the end of the heat treatment.

All T.T.T. diagrams show the hardness value on the right and vertically. In many cases, the percentage of microstructure is also indicated. For example, in Figure 7.8 the isothermal cooling curve at 600°C forms 25% of ferrite and 75% of pearlite with a hardness of 29 HRC (number inside the circle). Similarly, in Figure 7.10, the isothermal cooling curve at 400°C forms 100% of bainite with a hardness of 40 HRC.

The C.C.T. diagrams show similar informations. In this case, the hardness values are reported at the end of the cooling curves.

---

[11] An exception to this general rule of validity is cobalt, which moves T.T.T. and C.C.T. diagrams to the top and left.

[12] An increase in austenitization time and austenitization temperature causes an increase of the mean grain size and a delay of the austenite transformation.

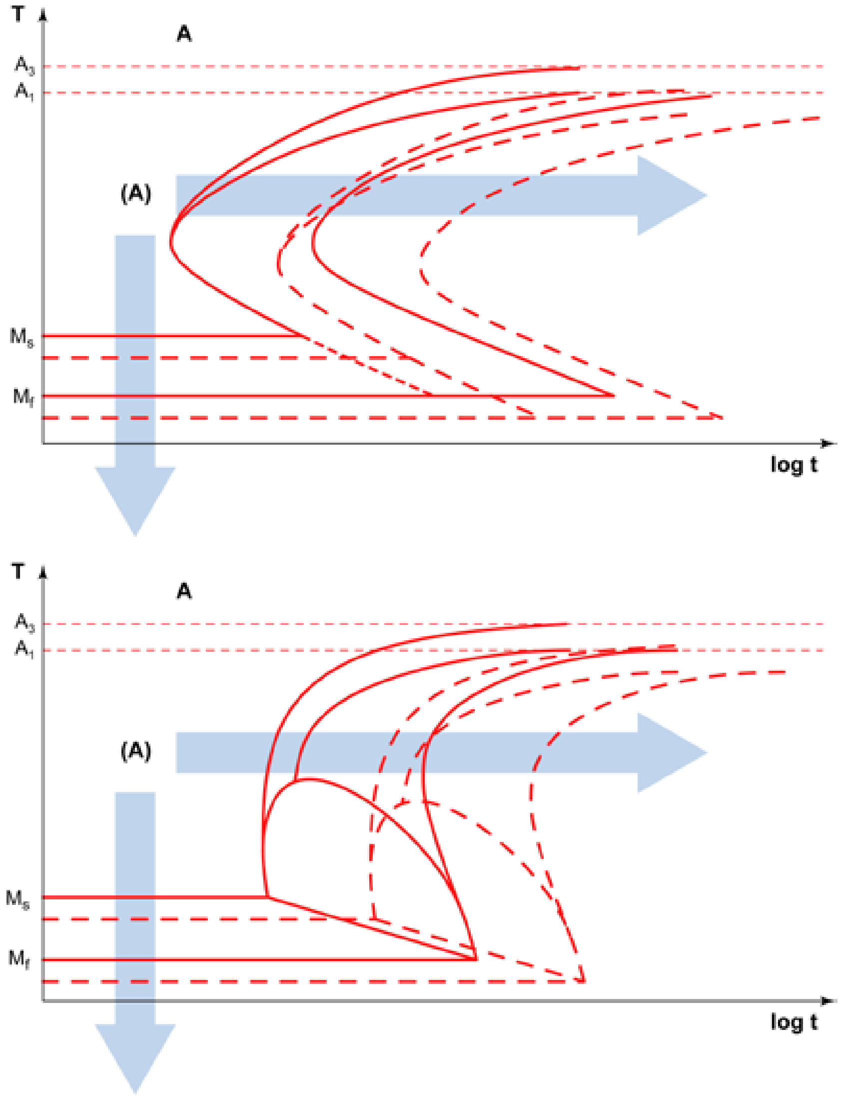

Figure 7.7 - Example of the shift of T.T.T. (top) C.C.T. (bottom) diagrams caused by the addition of alloying elements or the increase in the austenitization temperature and/or austenitization time.

For example, in Figure 7.9, as a result of the slower cooling curve the microstructure are formed of 40% of ferrite and 60% of pearlite with a hardness of 200 HV. The slowest and the fastest cooling curve in Figure 7.10 form 2% of ferrite and 98% of pearlite (22 HRC), and 100% of martenstite (57 HRC) respectively[13].

---

[13] *A three-digit hardness value refers to Vickers hardness scale (HV), while a two-digit hardness value refers to Rockwell C hardness scale (HRC).*

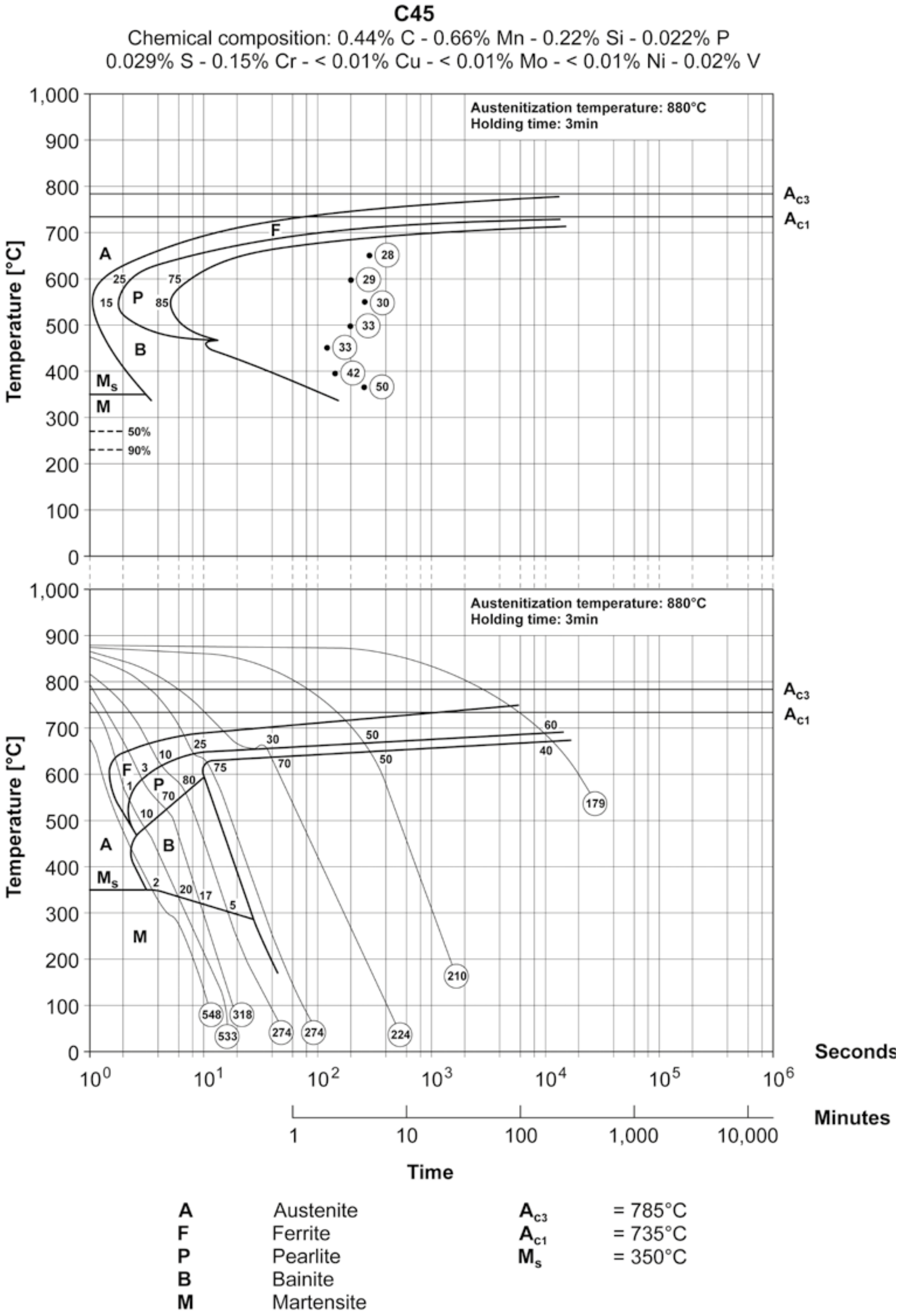

Figure 7.8 - T.T.T. and C.C.T. diagrams for EN C45 steel (0.44%C; 0.22%Si; 0.66%Mn; 0.022%P; 0.029%S; 0.15%Cr; 0.02%V - austenitized at 880°C for 3 minutes) [from Wever et al.1954/56/58].

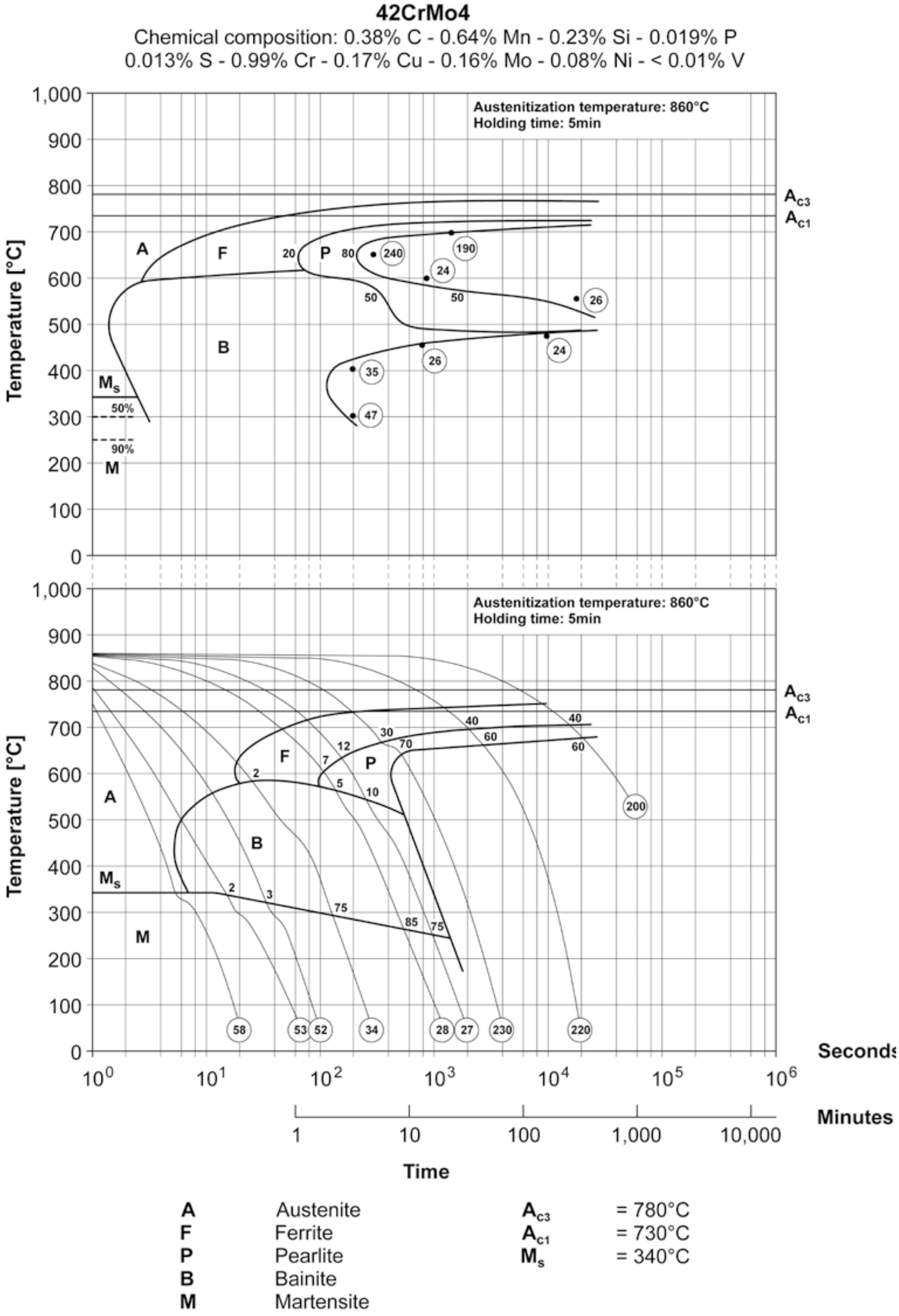

Figure 7.9 - T.T.T. and C.C.T. diagrams for EN 42CrMo4 steel (0.38%C; 0.23%Si; 0.64%Mn; 0.019%P; 0.013%S; 0.99%Cr; 0.08%Ni; 0.16%Mo; 0.17%Cu <0.01%V - austenitized at 860°C for 5 minutes) [from Wever et al.1954/56/58].

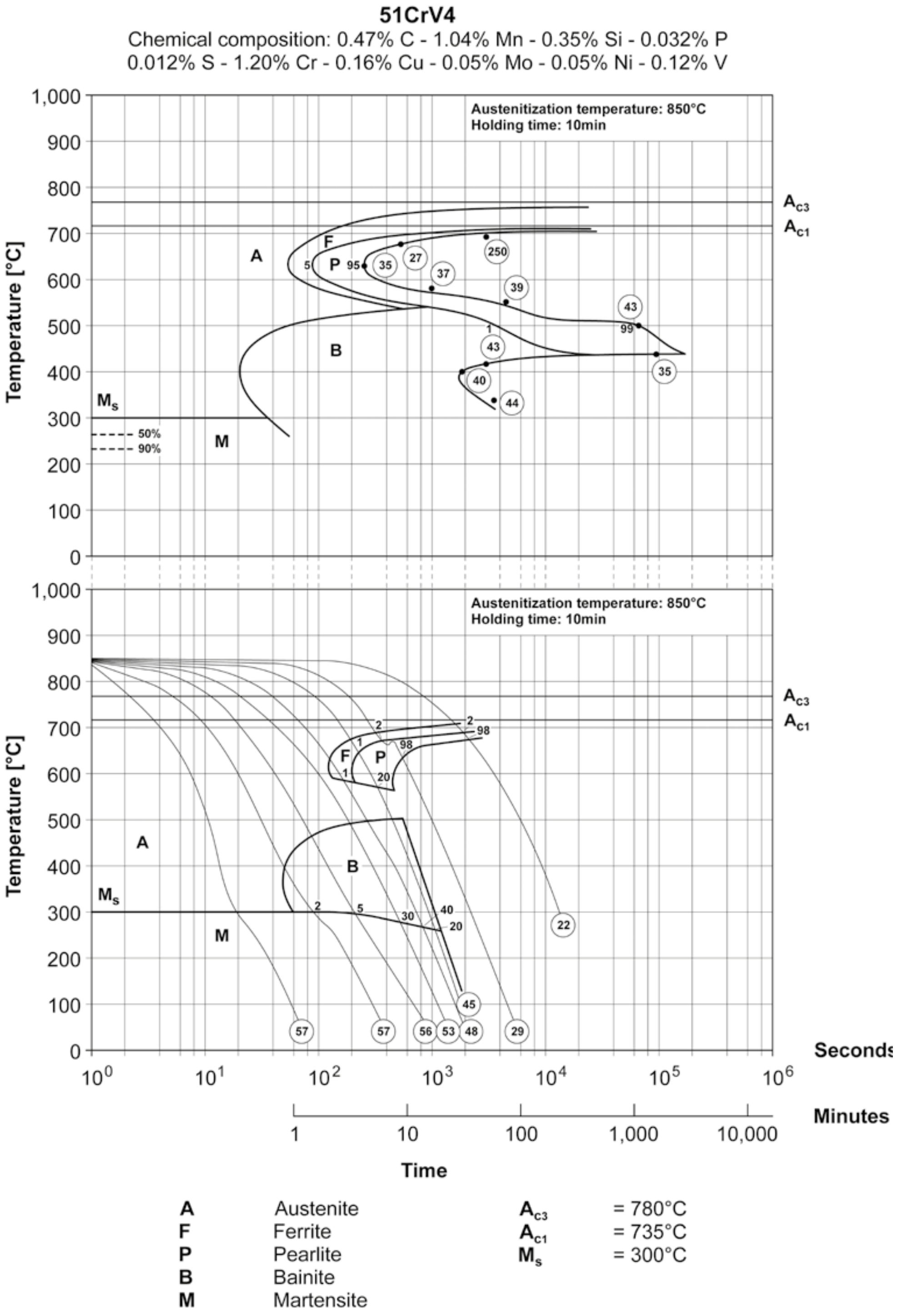

Figure 7.10 - T.T.T. and C.C.T. diagrams for EN 51CrV4 steel (0.47%C; 0.35%Si; 1.04%Mn; 0.032%P; 0.012%S; 1.20%Cr; 0.05%Ni; 0.05%Mo; 0.16%Cu, 0.12%V - austenitized at 850°C for 10 minutes) [from Wever et al.1954/56/58].

7.4 T.T.T. diagrams and C.C.T. diagrams for hypereutectic steels

Let us now consider a generic hypereutectoid steel: typical T.T.T. and C.C.T. diagrams are shown in Figures 7.11 and 7.12.

The shape of the diagrams does not change with respect to hypoeutectoid steel. The only changes are the critical point at the highest temperature that becomes A_{cm} and the transformation into cementite/carbide (C) instead of into ferrite.

For the four isothermal cooling curves on the T.T.T. diagram in Figure 7.11, the result is:

- at the end of the horizontal line at T_1, the microstructure is made up of cementite and pearlite;
- at the end of the horizontal line at T_2, the microstructure is made up of bainite;
- at the end of the horizontal line at T_3, the microstructure is made up of martensite and bainite;
- at the end of the horizontal line at T_4, the microstructure is made up of martensite.

while for the four continuous cooling curves on the C.C.T. diagram in Figure 7.12, the result is:

- at the end of cooling curve T_1, the microstructure is made up of cementite and pearlite;
- at the end of cooling curve T_2, the microstructure is made up of ferrite, pearlite, bainite, and martensite;
- at the end of cooling curve T_3, the microstructure is made up of cementite, bainite, and martensite;
- at the end of cooling curve T_4, the microstructure is made up of martensite.

The cooling curve indicated by V_s has the same significance as in Paragraph 7.3, while V_i is the fastest cooling curve that forms only pearlite and cementite.

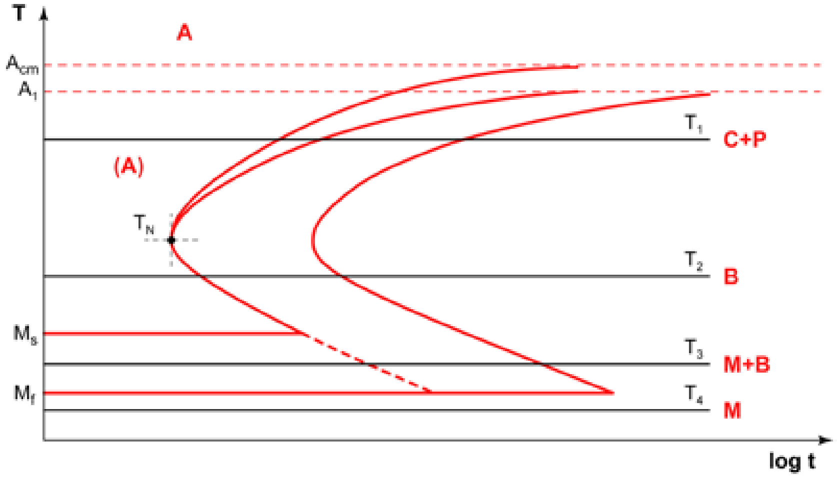

Figure 7.11 - Example of T.T.T. diagram for a generic hypereutectoid steel ($C > 0.77\%$).

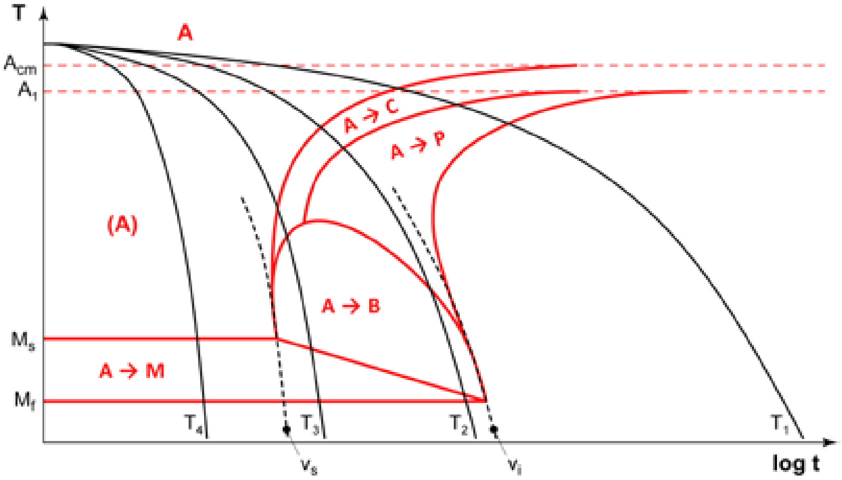

Figure 7.12 - Example of the C.C.T. diagram for a generic hypereutectoid steel ($C > 0.77\%$).

The Figures 7.11 and 7.12 show schematic representations of T.T.T. and C.C.T. diagrams. Two real examples of T.T.T. and C.C.T. diagrams for hypereutectic steel are shown in Figures 7.13 and 7.14. The wording $A + C$ indicates that a certain amount of carbides is always present.

Also in the case of hypereutectoid steel, the alloying elements, as well as the increase in austenitization time and/or austenitization temperature cause a shift to the right and bottom of the T.T.T. and C.C.T. diagrams, i.e. a delay in the austenite transformation.

7.5 Absence of martensite finish, M_f on T.T.T. and C.C.T. diagrams.

The horizontal line of martensite finish, M_f, is not usually present in real T.T.T. and C.C.T. diagrams, especially in the case of high carbon content or low alloy steel. In fact, in these types of steel M_f are near or below room temperature.

The addition of carbon and other alloying elements leads to a gradual lowering of the horizontal lines of M_s and M_f (Figure 7.15). For this reason, in the case of hypoeutectoid and hypereutectoid steels, it is normal not to find the indication of M_f (Figures 7.8, 7.9, 7.10, 7.13, and 7.14). In these cases, if M_f is absent and if the cooling curve forms martensite, a certain percentage of non-transformed austenite is normal. The indication *RA*[14] at the end of the cooling curves, followed by a number, indicates the percentage of non-transformed austenite, known as retained austenite.

---

[14] *Retained Austenite.*

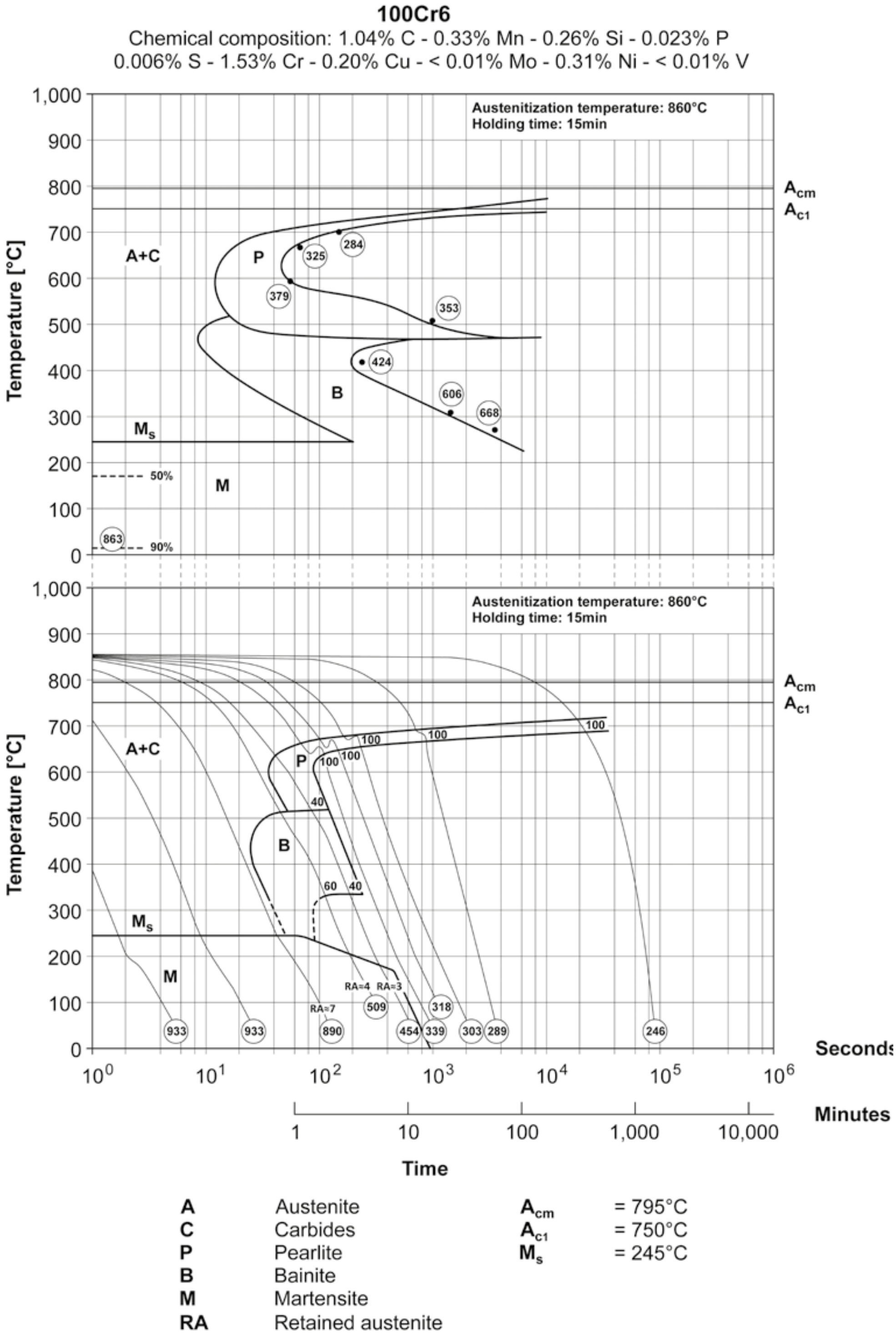

Figure 7.13 - T.T.T. and C.C.T. diagrams for EN 100Cr6 steel (1.04%C; 0.26%Si; 0.33%Mn; 0.023%P; 0.006%S; 1.53%Cr; 0.20%Cu; 0.31%Ni; <0, 01%Mo; <0.01%V - austenitized at 860°C for 15 minutes) [from Wever et al.1954/56/58].

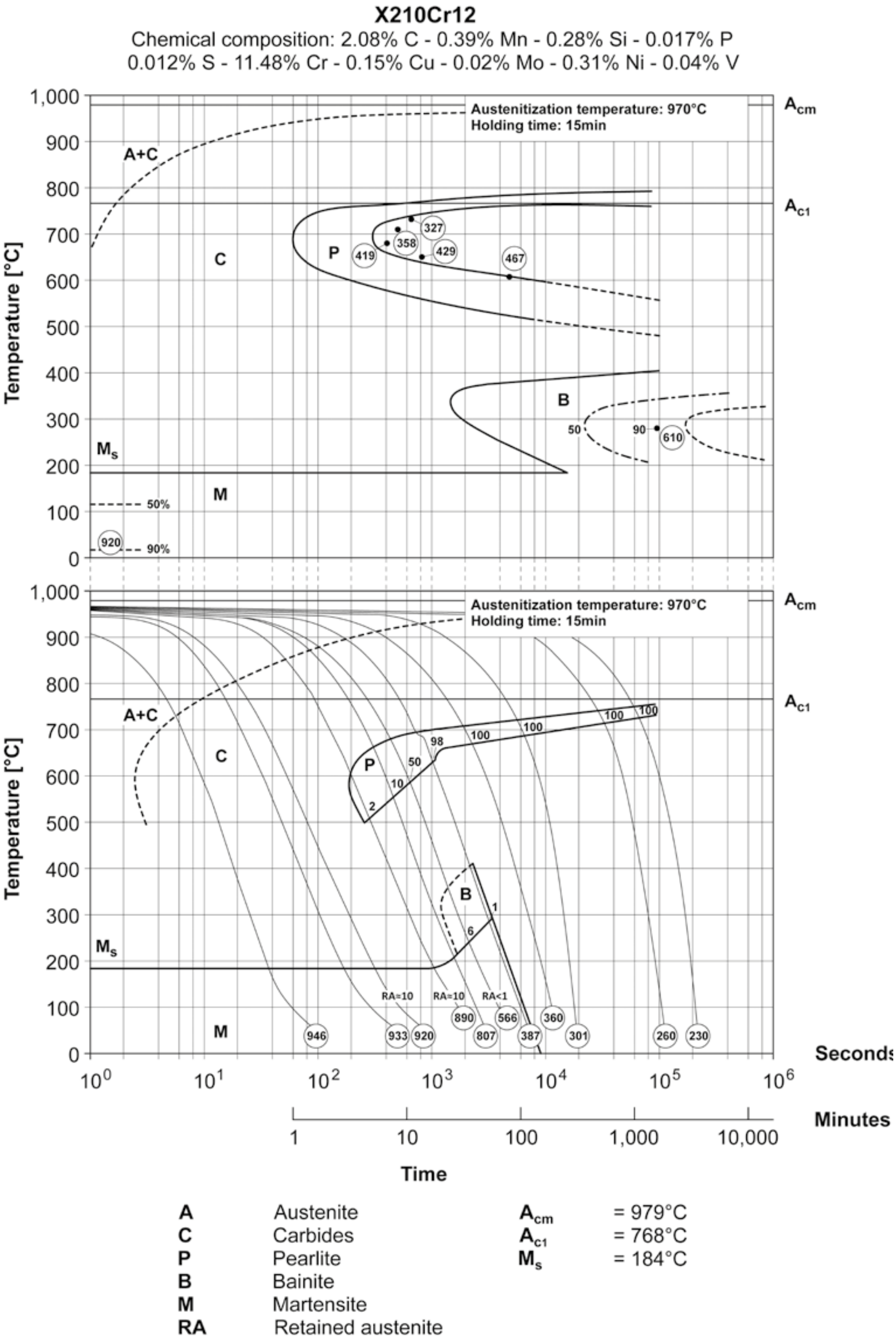

Figure 7.14 - T.T.T. and C.C.T. diagrams for EN X210Cr12 steel (2.08%C; 0.28%Si; 0.39%Mn; 0.017%P; 0.012%S; 11.48%Cr; 0.31%Ni; 0.02%Mo; 0.15%Cu: 0.04%V - austenitized at 970°C for 15 minutes) [from Wever et al.1954/56/58].

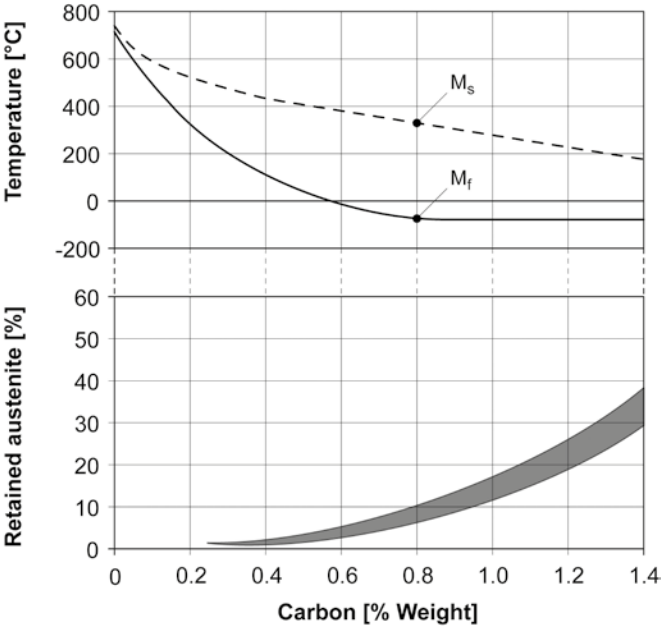

Figure 7.15 - The effect of carbon content on the amount of retained austenite at room temperature and on the shift downward of M_s and M_f temperatures [from Totten 2006].

The retained austenite is due to the rapid cooling. Various empirical formulas estimate the shift of M_s and M_f caused by alloying elements. A simplified formula is that proposed by [Steven and Haynes 1956]:

$$M_s = 561 - 474C - 33Mn - 17Cr - 17Ni - 21Mo \qquad [7.1]$$

$$M_{10} = M_s - 18 \qquad [7.2]$$

$$M_{50} = M_s - 85 \qquad [7.3]$$

$$M_{90} = M_s - 185 \qquad [7.4]$$

$$M_f = M_{100} = M_s - 387 \qquad [7.5]$$

M_x is a temperature in Celsius degrees and it aindicates the volumetric fraction x of martensite already transformed at that tempeature (for example, at temperature M_{50}, the 50% of austenite is already transformed into martensite). The equations from 7.1 to 7.5 demonstrate that retained austenite cannot be avoided, even for medium carbon steel (for example, C40 steel); in fact for these steels the value of M_f is approximately -30°C.

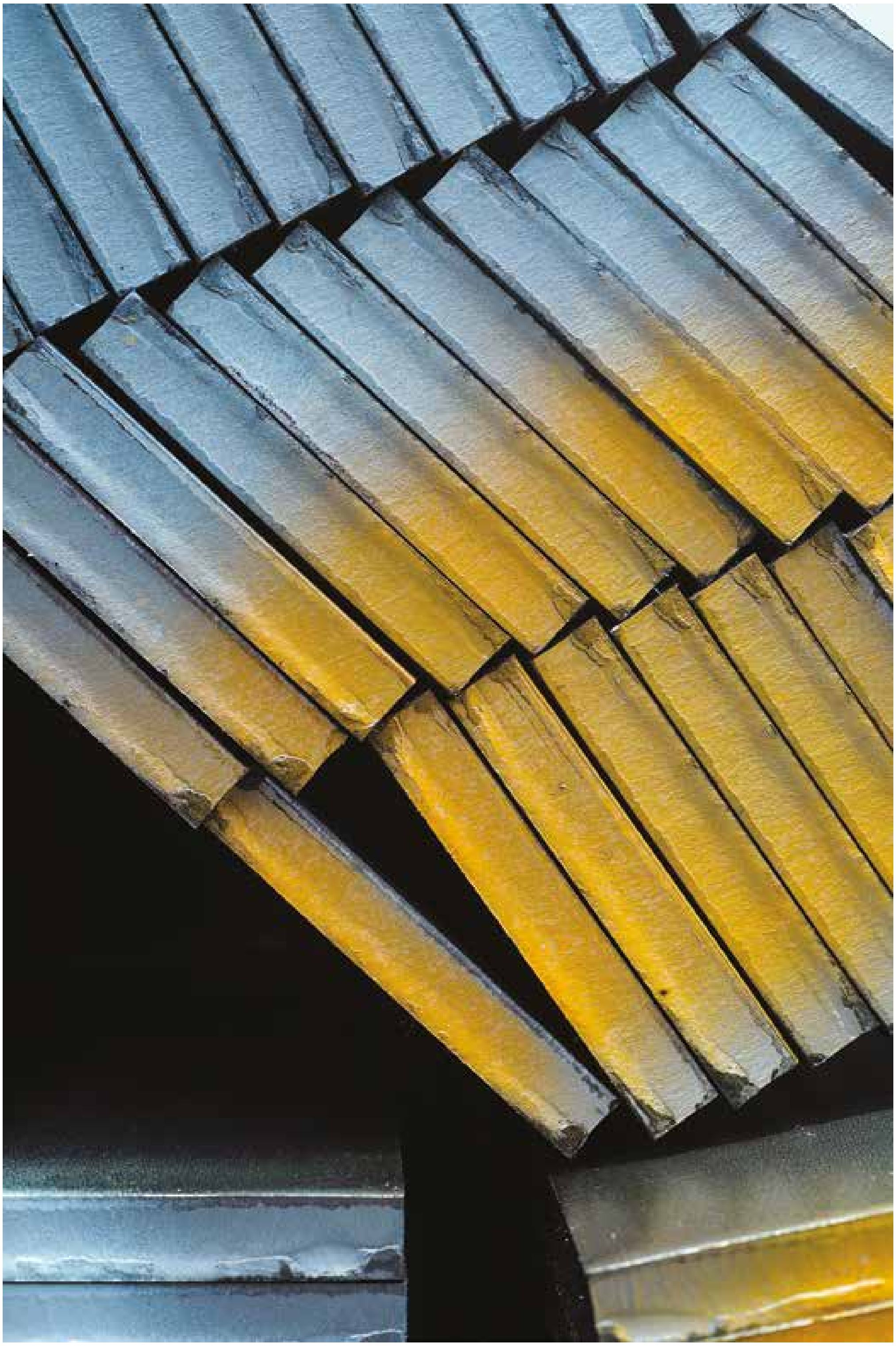

8. STEEL MICROSTRUCTURES

8.1 Equilibrium microstructures and non-equilibrium microstructures

The *Fe-C* phase diagram and T.T.T. or C.C.T. diagrams highlight how steel may have different microstructures: this depends on both the chemical composition and the cooling methods.

Downstream of solidification or as a result of heating, steel, whatever its carbon content ($0\% < C < 2.11\%$), always passes through the field of γ-phase. At these temperatures, the microstructure is therefore austenitic.

Austenite, if subjected to a slow equilibrium cooling, as provided by the *Fe-C* phase diagram, transforms into:

- pearlite if steel is eutectoid ($C = 0.77\%$);
- ferrite and pearlite if steel is hypoeutectoid ($0\% < C < 0.77\%$);
- pearlite and cementite if steel is hypereutectoid ($0.77\% < C < 2.11\%$).

The same austenite, on the other hand, as a result of non-equilibrium cooling, as provided by T.T.T. or C.C.T. diagrams, transforms into:

- pearlite, bainite and/or martensite if steel is eutectoid;
- ferrite, pearlite, bainite and/or martensite if steel is hypoeutectoid;
- cementite, pearlite, bainite and/or martensite if steel is hypereutectoid[1].

In general, the microstructures formed during equilibrium cooling are microstructures of equilibrium, while the microstructures formed during non-equilibrium cooling are microstructures of non-equilibrium.

This classification is important because ferrite, pearlite, and cementite are often spoken of as equilibrium microstructures and bainite and martensite as non-equilibrium microstructures.

While in the case of bainite and martensite, the definition is certainly correct (bainite and martensite are always non-equilibrium microstructures), for other microstructures, the definition is not correct. For example, ferritic-pearlitic microstructures can be formed in conditions of equilibrium (as a result of a very slow cooling, as provided by the *Fe-C* phase diagram), or in conditions of non-equilibrium (as a result of cooling according to T.T.T. or C.C.T. diagrams). This is similar for cementite and pearlite microstructures.

---

[1] *For a description of the microstructures formed as a result of non-equilibrium cooling, see Chapter 7. The list of the microstructures is only and example. If, for example, steel is hypereutectoid, it can have cementite-pearlite or cementite-pearlite-bainite or cementite-pearlite-bainite-martensite or bainite-martensite or only martensite, in relation to the cooling curve. Finally, do not forget the possible formation of retained austenite.*

A more appropriate classification of steel microstructures refers to austenite transformation mechanisms. In this case, we speak of:

- microstructures that are formed by austenite through nucleation and growth mechanisms due to carbon diffusion;
- microstructures that are formed from austenite for instant transformation without carbon to diffusion.

The first group refers to the transformation of austenite into pearlite, ferrite, cementitite or bainite[2]. The second refers to the transformation of austenite into martensite.

8.2 Transformations through nucleation and growth

As seen in the previous paragraph, ferrite, pearlite, cementite, and bainite are microstructures formed through nucleation and growth from austenite, due to carbon diffusion[3].

A simplification of the mechanism leading to the nucleation of the new microstructures and their growth, at the expense of the original austenitic microstructure, is shown in Figure 8.1.

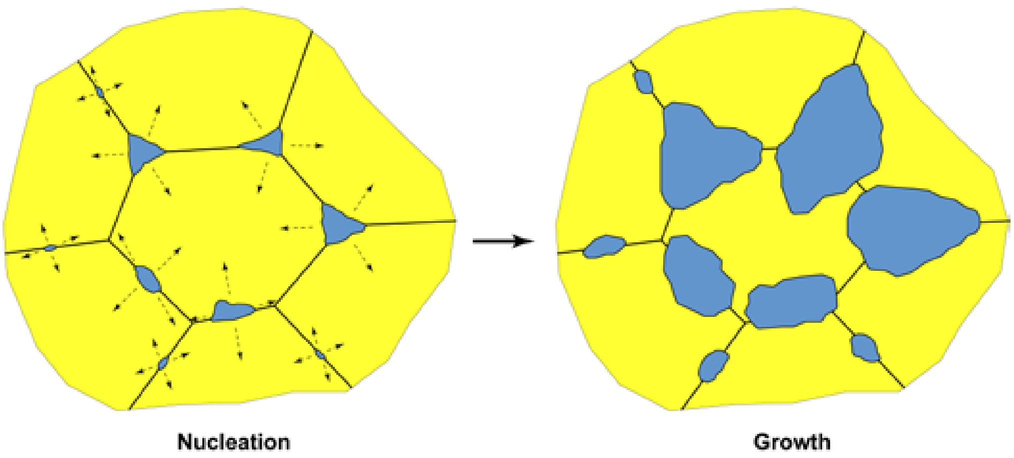

Figure 8.1 - Example of the nucleation and growth mechanism of steel microstructures. The yellow grains represent the original microstructure (austenite), instead the blue grains represent the new microstructure (pearlite, ferrite, cementite or bainite).

---

[2] *To avoid confusion, the metallurgical theory of bainitic transformation as a diffusional transformation was preferred. A second theory of bainitic transformation exists (displacive theory), such as lattice transformation with mechanism similar to the martensitic transformation.*

[3] *Austenite is also a microstructure formed through nucleation and growth. Austenite nucleates and grows starting from liquid and/or from homogeneous crystals of δ-phase, in relation to the carbon content of steel. The mechanism is described in Paragraph 2.7 of Chapter 2.*

Now let us see what happens if increases or decreases the number of nuclei.

Consider Figure 8.2. It is evident that if the nucleation phase is favored, the growth is limited and the final microstructure has very fine grains. On the contrary, if few nuclei are formed, the growth is facilitated and the final microstructure has coarse grains. What happens is typical of all the microstructures formed by nucleation and growth: the more nucleation is favored, the more the final microstructure is fine-grained. The more growth is favored, the more the final microstructure is coarse-grained.

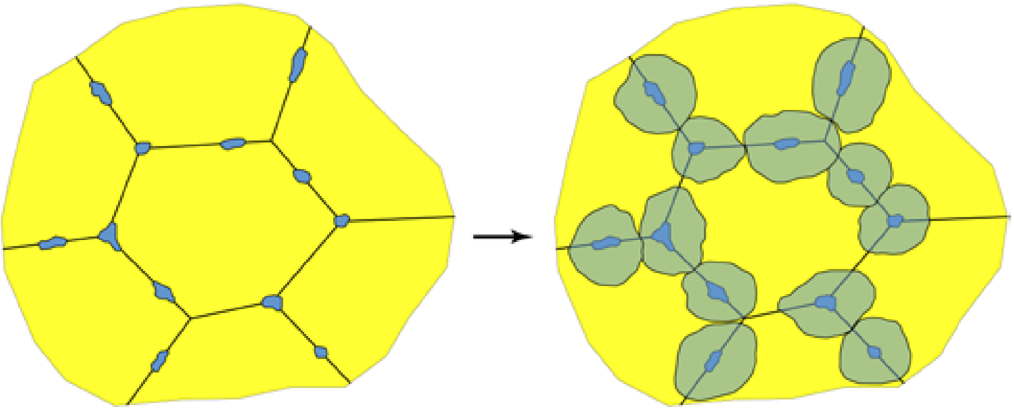

Nucleation (many nucleation sites)

Growth (limited growth)

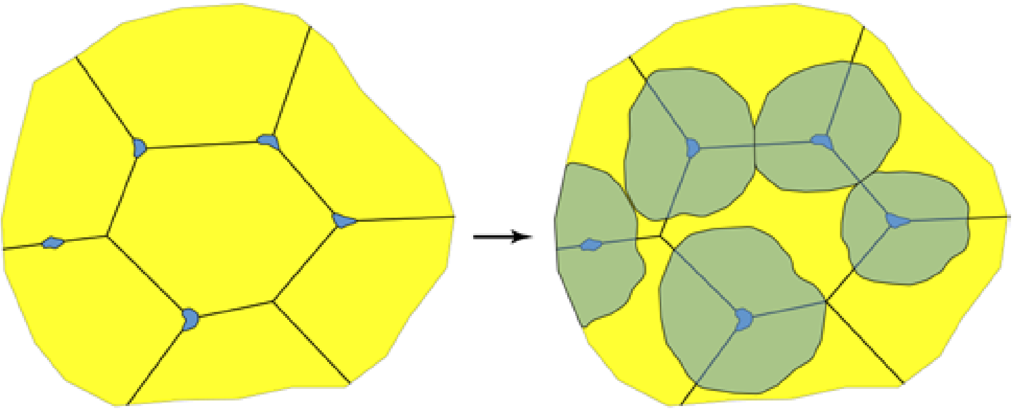

Nucleation (few nucleation sites)

Growth (large growth)

Figure 8.2 - Examples of the nucleation and growth mechanism if the nucleation is favored (at the top) or if the nucleation is limited (at the bottom). The yellow grains represent the original microstructure (austenite), instead the blue grains represents the new microstructure (pearlite, ferrite, cementite or bainite).

The phenomenon of microstructural transformations through nucleation and growth is always a function of temperature: austenite transformation at high temperature is dominated by growth (carbon diffuses faster); when temperature decreases, nucleation predominates (carbon diffuses more slowly).

Taking into account the same microstructure that transforms from austenite:

- the final microstructure is finer if it nucleates and grows at a low temperature,
- the final microstructure is coarser if it nucleates and grows at high temperatures.

Observe, for example, the case of transformation through the nucleation and growth of pearlite (Figure 8.3): at high temperatures, close to 700°C growth is prevalent ($V_G > V_N$), while at lower temperatures, such as at 600°C, nucleation prevails ($V_N > V_G$)[4].

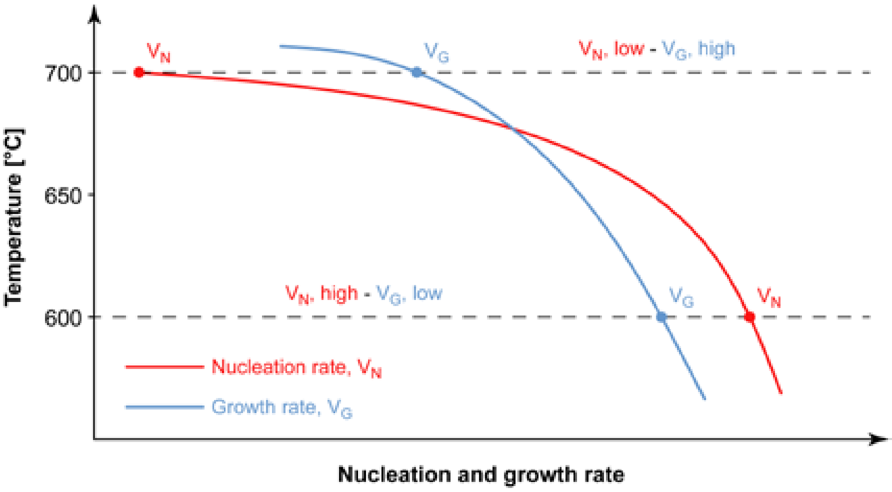

Figure 8.3 - Correlation between temperature and nucleation rate V_N or growth rate V_G of the transformation of austenite into pearlite.

---

[4] *Both the rate of nucleation and the rate of growth, increase when temperature decreases. What is important is whether one or the other predominant. Although the example refers to the nucleation/growth of pearlite, it has a general validity (transformation of austenite into pearlite, ferrite, cementite, and bainite).*

8.3 Pearlite

Let us consider the austenite-pearlite transformation[5] governed by carbon diffusion and the nucleation and growth phenomena. Pearlite (lamellar crystallites composed of alternating layers of α-phase and Fe_3C phase) is formed from austentite (homogenous crystallites of γ-phase) when, as provided by the *Fe-C* phase diagram or by the T.T.T./C.C.T. diagrams, γ-phase must transform into α-phase and into Fe_3C phase. As long as the system is in γ-phase, carbon is in a solid solution in the iron lattice. When, instead, the transformation from γ-phase to α-phase must occurs, the solubility of carbon is reduced drastically and Fe_3C phase must be formed. In fact, the diffusion of carbon atoms cause the concentration of carbon in several areas (lamellae of Fe_3C phase) and the impoverishment of carbon in other areas (lamellae of α-phase).

If the transformation occurs at a high temperature, carbon diffuses from wide areas of γ-lattice (large-scale diffusion) and the lamellae of Fe_3C phase and of α-phase have a large size. If, however, the transformation takes place at a low temperature, carbon has a more limited diffusion path (short-range diffusion) and the lamellae of Fe_3C phase and of α-phase have a smaller size.

In the first case, the final microstructure consists of coarse pearlite colonies. In the latter case, however, the final microstructure is comprised of fine pearlite colonies (see Figure 8.4).

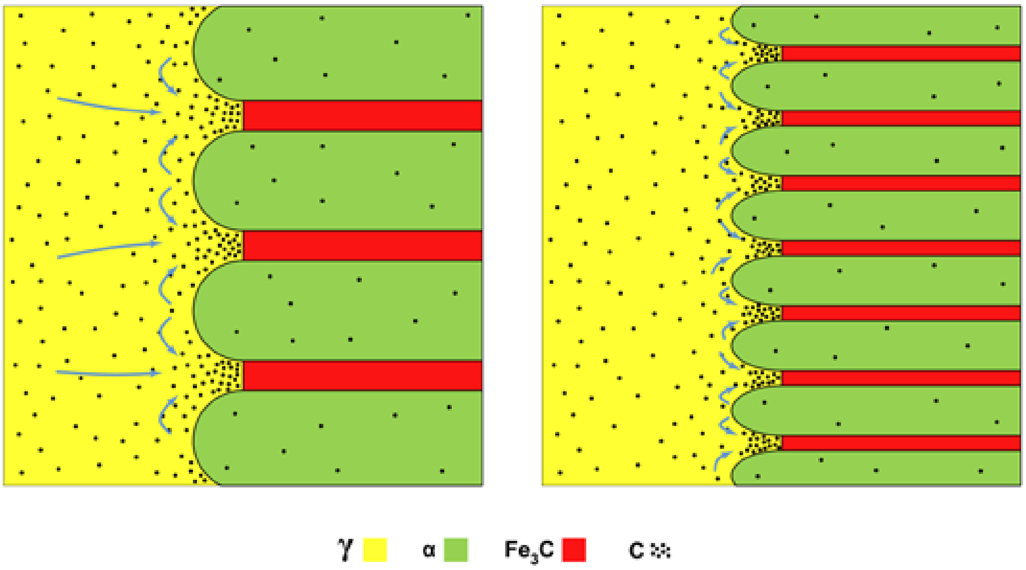

Figure 8.4 - Graphic representation of the nucleation and growth mechanisms of pearlite colonies: high-temperature transformation (to the left) and low-temperature transformation (to the right).

The pearlite colonies develop from the grain boundaries of the homogeneous crystals of γ-phase. The competitive growth of the various colonies leads to the formation of colonies of different sizes.

---

[5] *The transformation of austenite into pearlite occurs at eutectoid temperature for equilibrium cooling (Fe-C phase diagram) or during non-equilibrium cooling (T.T.T. or C.C.T. diagrams) when the cooling conditions are such to trigger it.*

Considering the transformation of a single grain of austenite, the greater the number of nucleation sites, the greater the number of pearlite colonies.
On the contrary, if the nucleation sites are few, the growth of pearlitic colonies is large (see Figure 8.5).

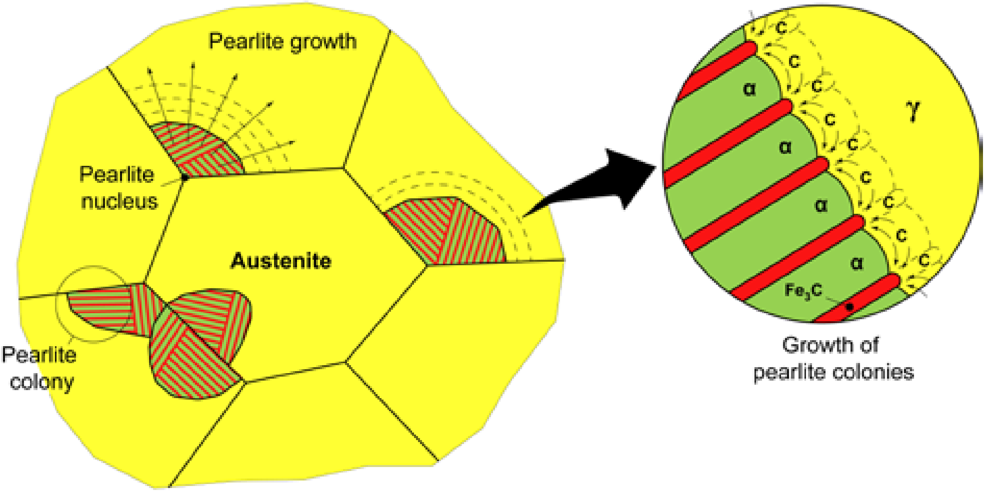

Figure 8.5 - Graphic representation of the nucleation and growth mechanisms of pearlite colonies [from Campbell 2008].

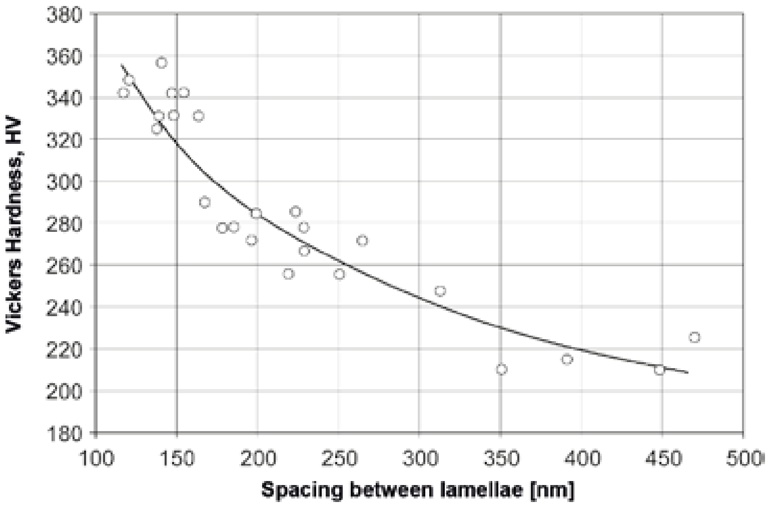

Figure 8.6 - Correlation between the spacing of pearlite lamellae and the Vickers hardness [from Clayton and Danks 1990].

In summary, if nucleation is favored, many small pearlite colonies (fine microstructure) are formed; if growth is favored, only a few pearlite colonies with large lamellae (coarse microstructure) are formed.

Typically, the hardness of pearlite in an annealed state is in the order of 200-350 HV, in relation to the spacing of the lamellae: the more the lamellar microstructure is fine, the greater is the hardness (see Figure 8.6).

At a metallographic level, pearlite, at least for magnifications up to 500x, has the shape of dark gray irregular grains. It is difficult to distinguish the lamellae of α-phase and the lamellae of Fe_3C phase[6] (Figure 8.7), and only with larger magnifications, for example, using scanning electron microscope, the pearlite microstructure can be easily resolved (Figure 8.8).

Except for steel with eutectoid composition, the pearlitic microstructure is usually fragmented with ferritic grains (hypoeutectoid steels) or cementite plates (hypereutectoid steel).

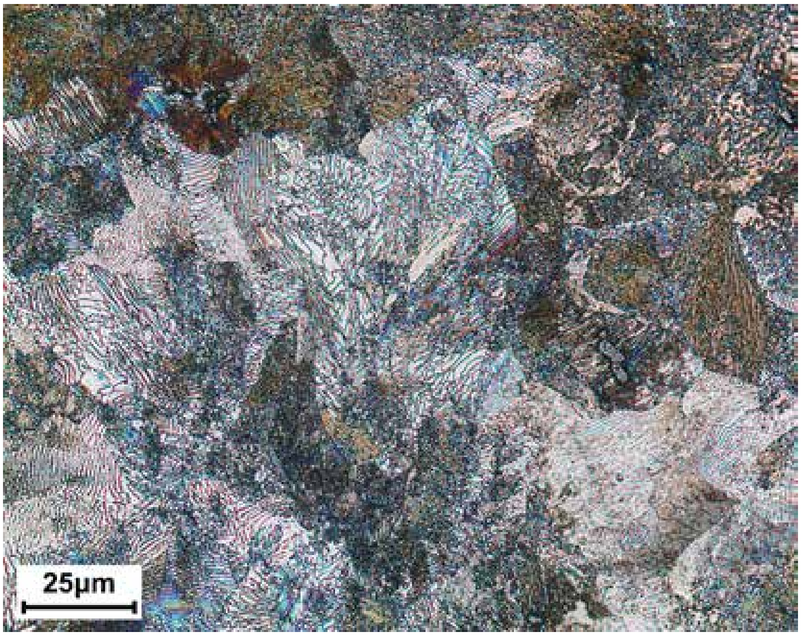

Figure 8.7 - Pearlitic microstructure of an EN R260Mn steel. Appearance under the metallographic microscope - Nital 2% etch. [Laboratori del Dipartimento di Meccanica del Politecnico di Milano - Milano].

---

[6] *The typical metallographic etchant used for carbon steel is Nital 2, which is a 2% solution of nitric acid in ethyl alcohol. Nital selectively "attacks" the grain boundaries and the interface between the lamellae, leaving the other areas of the crystallites unaltered. This is why pearlite is etched both internally and on the grain boundary assuming a typical dark gray color.*

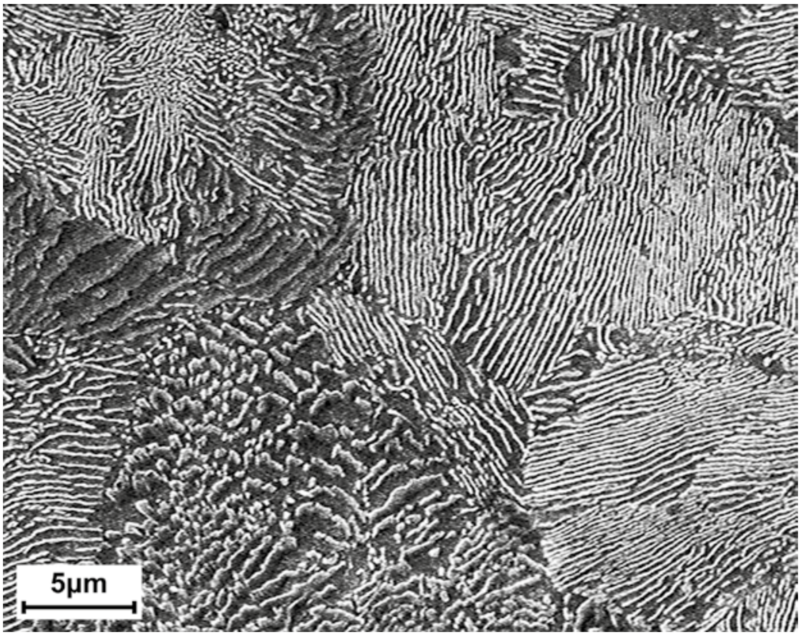

Figure 8.8 - Pearlitic microstructure of an EN R260M steel. Appearance under the scanning electron microscope - Nital 2% etch. [Laboratori del Dipartimento di Meccanica del Politecnico di Milano - Milano].

8.4 Ferrite

For a generic hypoeutectoid steel, before the pearlitic transformation occurs, γ-phase forms homogeneous grains of α-phase, i.e. ferrite: the new microstructure originates due to the variation of carbon solubility in γ-phase and it develops by nucleation and growth.

Ferrite nucleates on the grain boundary of the austenitic crystallites and it grows both along the grain boundaries and within the austenite grains (Figures 8.1 and 8.2).

In hypoeutectoid steel ferrite grows in combination with pearlite. The microstructure is almost all ferritic[7] only if the steel has a very low carbon content ($C < 0.02\%$).

The morphology of ferrite is a function of both the cooling method, as well as the manufacturing process: the grains - with an irregular shape - may be equiaxed (Figure 8.9) or arranged along the maximum deformation direction (Figure 8.10).

---

[7] *An exception are ferritic stainless steels that, due to their high chromium content, have a completely ferritic microstructure, from melting to room temperature. Stainless steels are not part of this volume, since they have already been treated in Boniardi M., Casaroli A., Stainless Steels, Lucefin, Esine, 2014 text.*

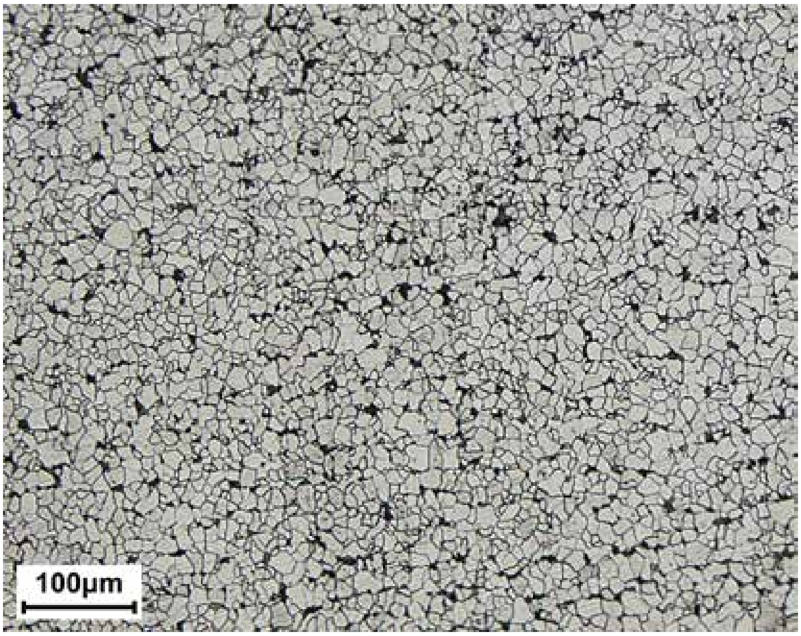

Figure 8.9 - Ferritic-pearlitic microstructure of an EN S235 steel. Appearance under the metallographic microscope - Nital 2% etch. [Laboratori Exova, Crema].

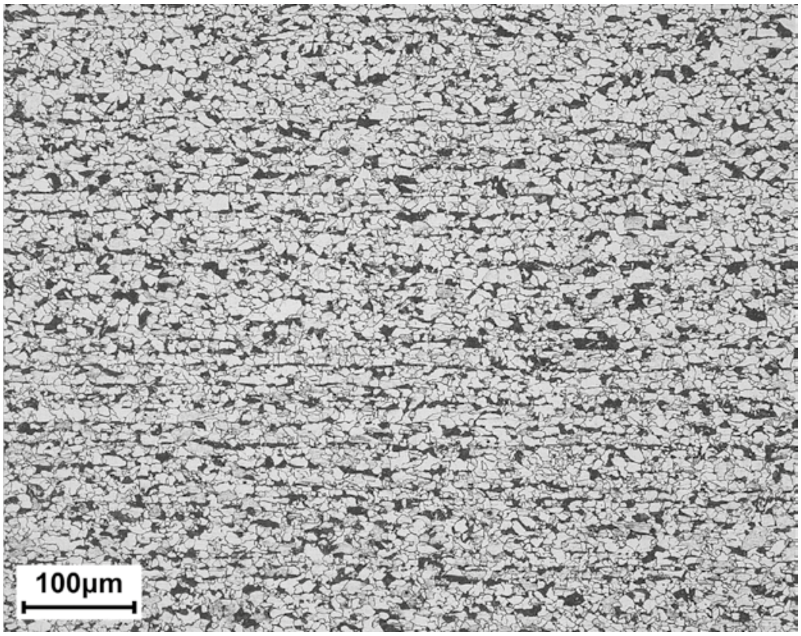

Figure 8.10 - Ferritic-pearlitic microstructure of an EN S355 steel. Appearance under the metallographic microscope - Nital 2% etch. [Laboratori Exova, Crema].

In medium-carbon steels, ferrite has slightly different characteristics. Both an homogeneously distributed microstructure of pearlite and ferrite (Figure 8.11) can be observed, as well as a microstructure where ferrite is predominantly along the grain boundary of pearlite (Figure 8.12).

In this second case, it is common to speak of proeutectoid ferrite.

Ferrite in annealed state has a very low hardness, in the order of 60-100HV, which can reach up to 250 HV, only due to a significant grain refining. Under a metallographic microscope, ferrite has a white or light gray color[8].

In hypoeutectoid steel, it is also possible to observe an acicular/needle-like ferrite, called Widmanstätten's ferrite[9]. This is obtained by the rapid cooling of austenite from high temperatures or through the transformation of an austenitic structure with a coarse grain[10] (see Figure 8.13).

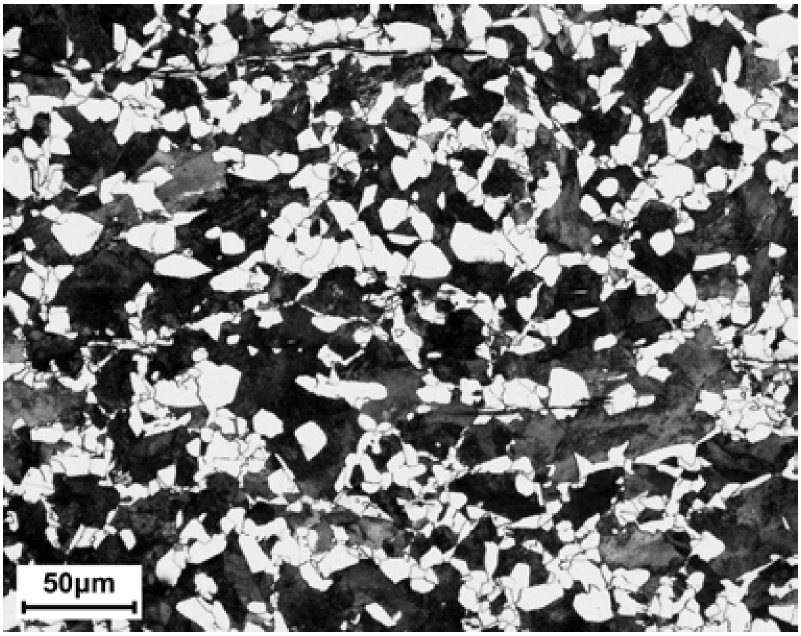

Figure 8.11 - Ferritic-pearlitic microstructure of an EN C40 steel. Appearance under the metallographic microscope - Nital 2% etch. [Laboratori Omeco, Monza].

---

[8] *Nital 2 selectively "attacks" only the boundaries of the crystallites. For this reason, the inner part of the ferrite grains is not attacked and the grains assume a typical white or light gray color.*

[9] *Alois von Beckh-Widmanstätten (1754-1849), Count of the Austro-Hungarian Empire, as well as typographer and scientist. He was director of the Vienna Imperial Porcelain Works. He has been attributed with the discovery of acicular microstructures that are observed after etching with nitric acid of the polished surfaces of iron-nickel meteorites.*

[10] *Typically, Widmanstätten's ferrite is observed on medium-carbon steel workpieces forged at 1,200°C -1,250°C and air-cooled or in the Heat Affected Zone (H.A.Z.) of the welded joints of low carbon steel.*

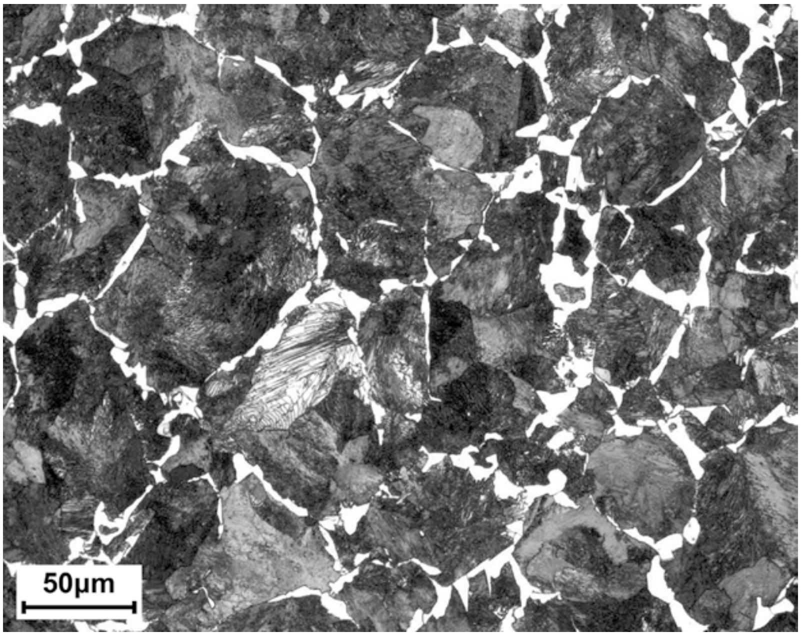

Figure 8.12 - Ferritic-pearlitic microstructure with proeutectoid ferrite of an EN C55 steel. Appearance under the metallographic microscope - Nital 2% etch. [Laboratori Omeco, Monza].

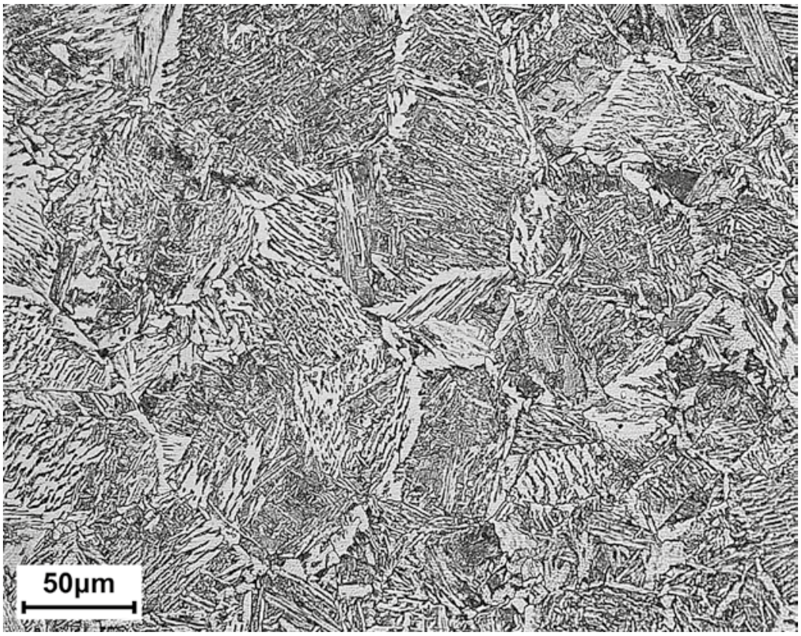

Figure 8.13 - Ferritic-pearlitic microstructure with Widmanstätten's ferrite of an ASTM F60 steel. Appearance under the metallographic microscope - Nital 2% etch. [Laboratori Hammer, Rho - Milano].

8.5 Cementite

Hypereutectoid steels form plates of Fe_3C phase on the grain boundary (cementite) befour γ-phase transforms into pearlite. As with ferrite, the new phase originates as a result of the variation of carbon solubility in γ-phase and proceeds through nucleation and growth.

Cementite nucleates and grows along the grain boundary of the austenitic grains. If steel contains alloying elements that reacts with carbon to form compound the term carbides is usually used instead of cementite[11].

In hypereutectoid steel, cementite is present in combination with pearlite. Its name derives from the analogy with cement that holds bricks together.

Under a metallographic microscope, cementite appears whitish, since it is not attacked by the etching typically used in metallography.

The typical morphology of cementite is showed in Figure 8.14.

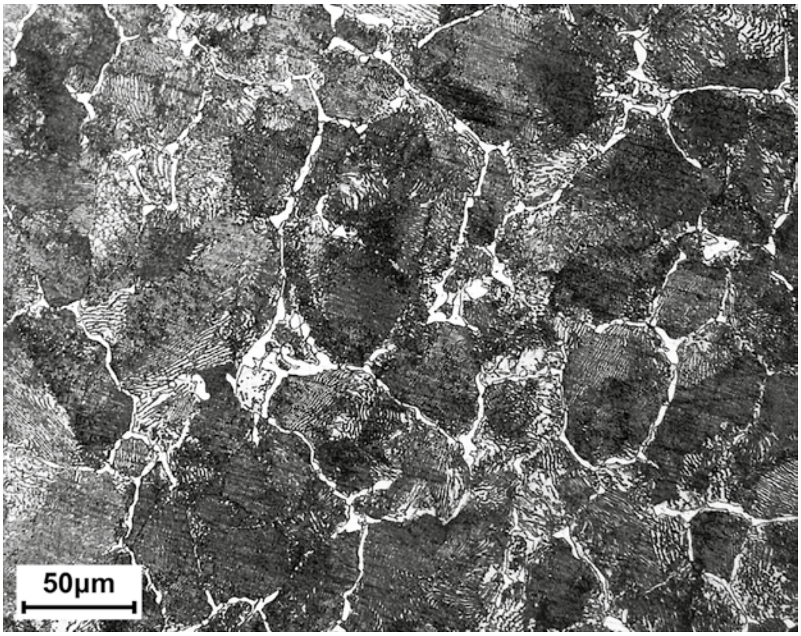

Figure 8.14 - Pearlite with cementite on the grain boundary of an EN C90 steel. Appearance under the metallographic microscope - Nital 2% etch. [Laboratori Exova, Crema].

---

[11] *This type of compound are very rich of the alloying elements (Cr, Mo, V, Ti, W, etc.). It would, therefore, be wrong to call them "cementite", a term that refers only to iron carbides (Fe_3C).*

8.6 Bainite

The T.T.T. and C.C.T. diagrams highlight the existence of two microstructures not present on the *Fe-C* phase diagram: bainite and martensite.

Bainite is a very fine aggregate of α-phase and Fe_3C phase, both with an acicular morphology formed at temperatures between 250°C and 550°C. Bainite is formed from austenite under non-equilibrium conditions, both for isothermal cooling (T.T.T. diagrams) and for continuous cooling (C.C.T. diagrams).

The transformation of austenite into bainite occurs through nucleation and growth and is governed by the diffusion of carbon. In relation to the transformation temperature, it is referred to as upper bainite and lower bainite (see Figure 8.15).

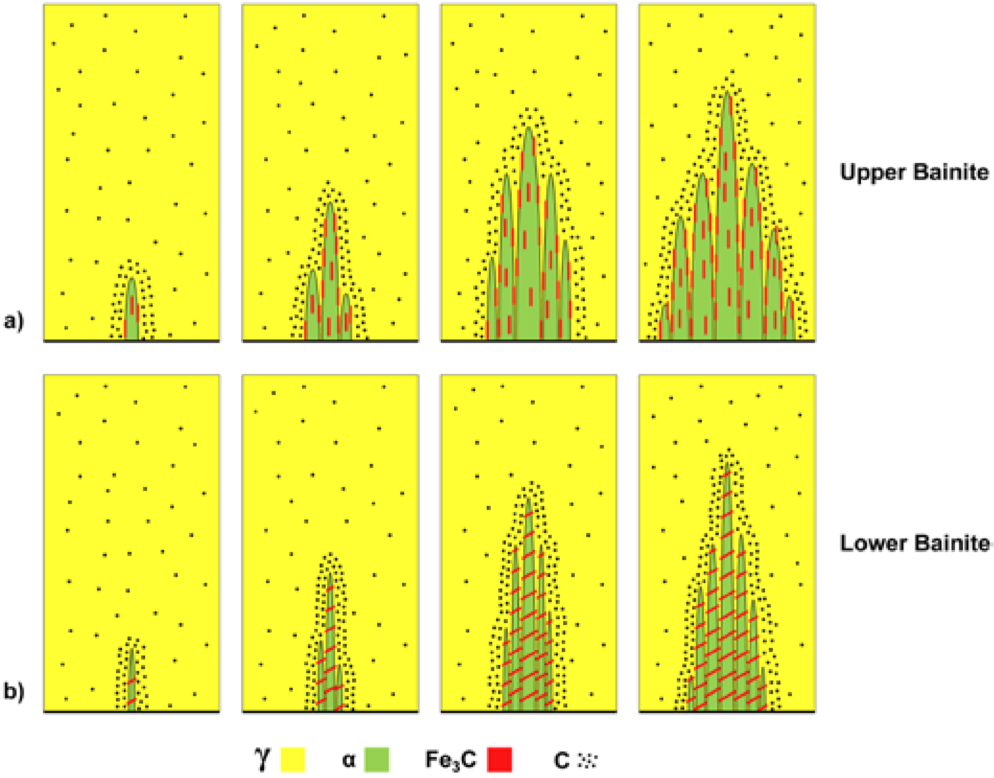

Figure 8.15 - Graphic representation of the nucleation and growth mechanisms of bainite: a) upper bainite; b) lower bainite.

Upper bainite transformation occurs between of 400°C and 550°C. At these temperatures the rate of carbon diffusion is less than what occurs during the pearlitic transformation and sharp laths of α-phase surrounded by acicular plates of Fe_3C phase form from austenite grain boundary. Both laths of α-phase and acicular plates of Fe_3C phase are oriented in the same direction (Figure 8.15a).

Upper bainite is a sort of degenerated pearlite in which the lower mobility of carbon prevents forming of lamellae (typical of pearlite) and allows the growth of lath of α-phases surrounded by acicular plate of Fe_3C phase (typical of bainite).

Lower bainite is similar to upper bainite. This is also obtained through nucleation and growth from austenite at temperatures between 250°C and 400°C. At these temperatures the mobility of carbon is further limited and the lath of α-phase are finer than the previous case, with plates of iron carbide (Fe_3C) tilted at approximately 60° with respect to the lat axis (Figure 8.15b).

The α-phase of bainite is harder than α-phase of pearlite, due to the high density of the dislocations. As a result, the hardness of bainite is greater than the hardness of pearlite and is between 300 and 650 HV (see Figure 8.16).

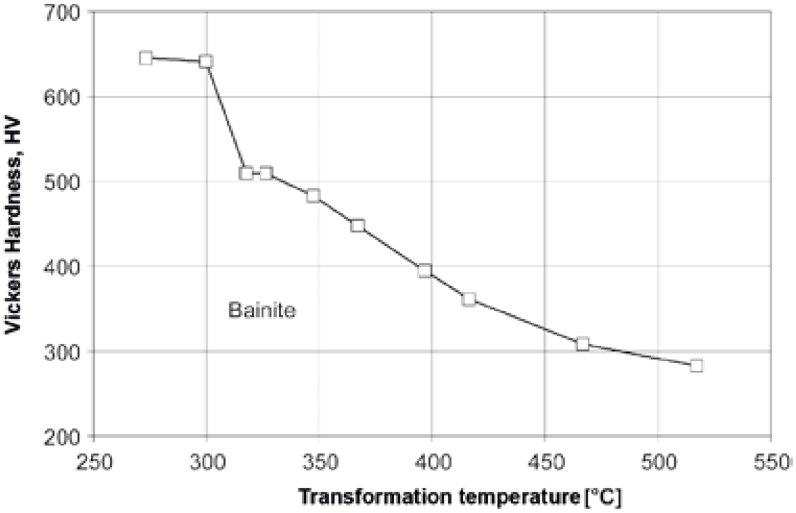

Figure 8.16 - Correlation between the isothermal transformation temperature of the bainitic microstructure and the Vickers Hardness for eutectoid steel [Ohmori and Honeycombe 1971].

Under a metallographic microscope, the acicular microstructure of bainite (Figures 8.17 and 8.18) cannot be distinguished, that is, it is not easy to observe the laths of α-phase and the acicular plates of Fe_3C phase.

Moreover, with classic metallographic techniques, lower bainite is very similar to martensite and is easily confused. The bainitic microstructure can be discriminated from the other microstructures (Figure 8.19) only through scanning electron microscope.

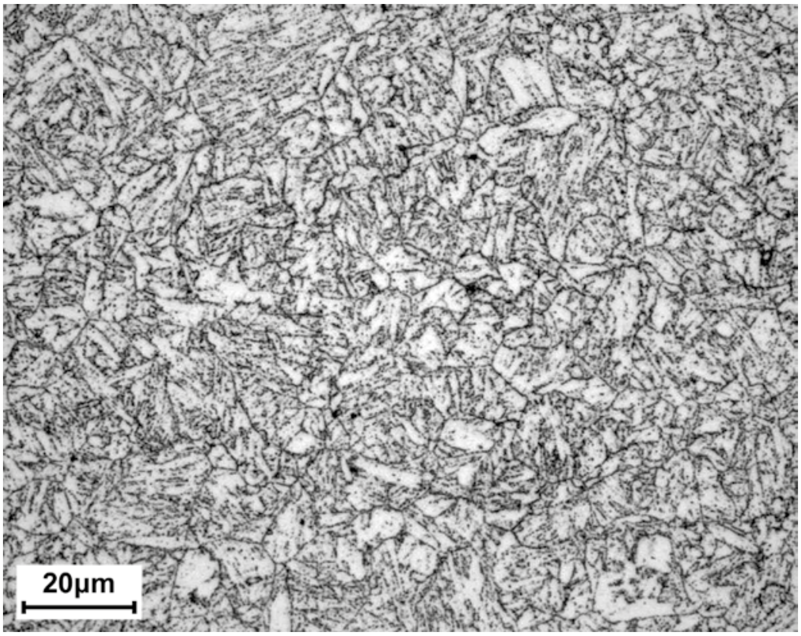

Figure 8.17 - Bainitic microstructure of an ASTM P91 / T91 (9Cr-1Mo) steel. Appearance under the metallographic microscope - Vilella etch. [Laboratori Omeco, Monza].

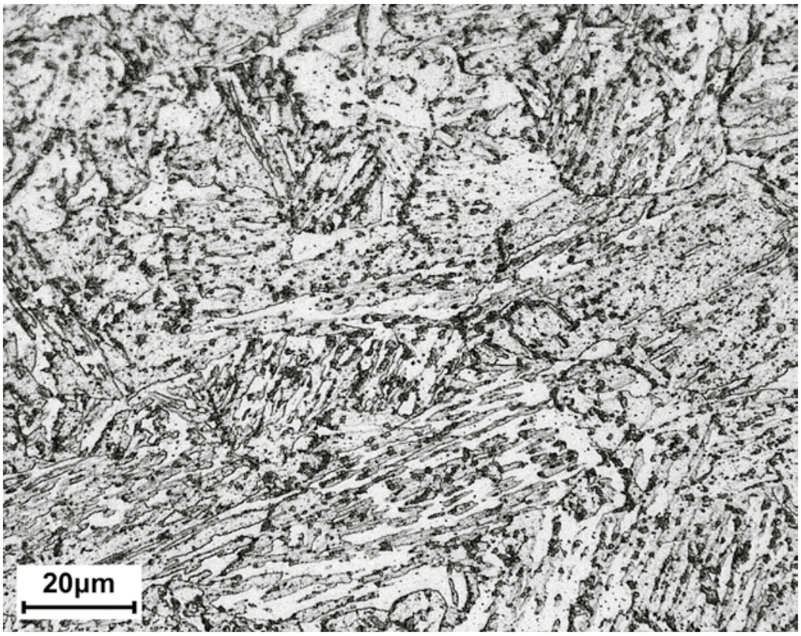

Figure 8.18 - Bainitic microstructure of an ASTM F22V steel (2.25Cr-1Mo-0.25V). Appearance under the metallographic microscope - Nital 2% etch. [Laboratori Hammer, Rho - Milano].

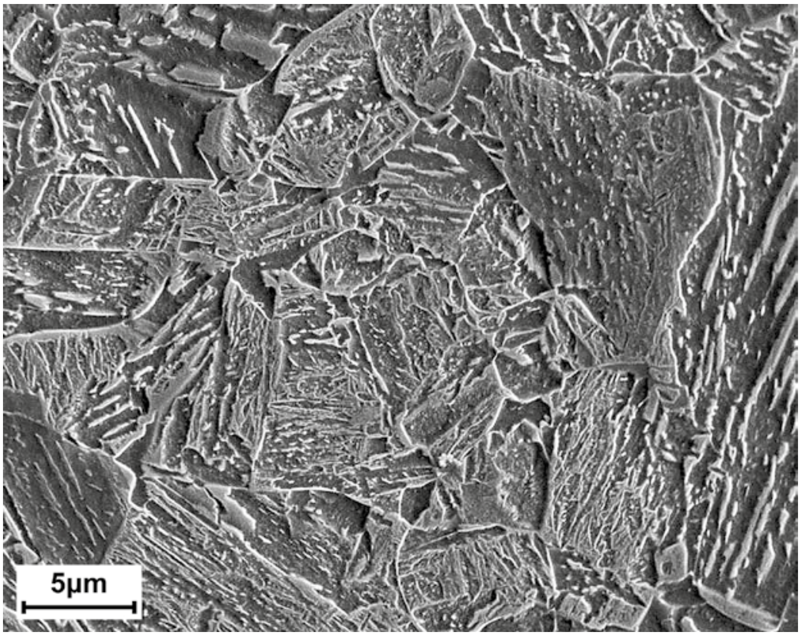

Figure 8.19 - Bainitic microstructure of an EN C70 steel. Appearance under the scanning electron microscope - Nital 2% etch. [Laboratori del Dipartimento di Meccanica del Politecnico di Milano - Milano].

8.7 Martensite and instantaneous transformations of steel

The austenite-martensite transformation is very different from all other observed previously. The martensite is obtained by instantaneous transformation of the austenite lattice[12], without diffusion phenomena.

The transformation from austenite to martensite is due to a rapid cooling when the cooling rate is higher than the cooling curve, v_s, on the C.C.T. diagrams.

The martensite is formed during the transformation of the F.C.C. lattice of γ-phase into the B.C.C. lattice of α-phase if carbon does not diffuse from the F.C.C. lattice, due to the rapid cooling. This microstructure has a body-centered tetragonal lattice (B.C.T.) and is called α'. Since carbon does not diffuse during transformation, the martensite has the same chemical composition of the austentite.

The austenite-martensite transformation is characterized by the rearrangement of the atoms of the lattice, that is, by their repositioning through a coordinated movement.

---

[12] *The rate of the austenite-martensite transformation is equal to the speed of sound in steel, i.e. about 5,500 m/s.*

The phenomena involved during martensitic transformation are listed below (Figure 8.20):

- at a high temperature, the austenite is stable and the dissolved carbon occupies the interstitial sites of the F.C.C. lattice of γ-phase;
- if the cooling curve were slow, the carbon would spread from the F.C.C. lattice of γ-phase, forming iron carbides (Fe_3C). If the carbon were no longer present, the F.C.C. lattice of γ-phase would transform into the B.C.C. of α-phase;
- Since, however, the cooling rate is very high, carbon remains trapped in the F.C.C. lattice of γ-phase, which turns into a distorted B.C.C. lattice, called α′-phase, with a body-centered tetragonal lattice (B.C.T.).

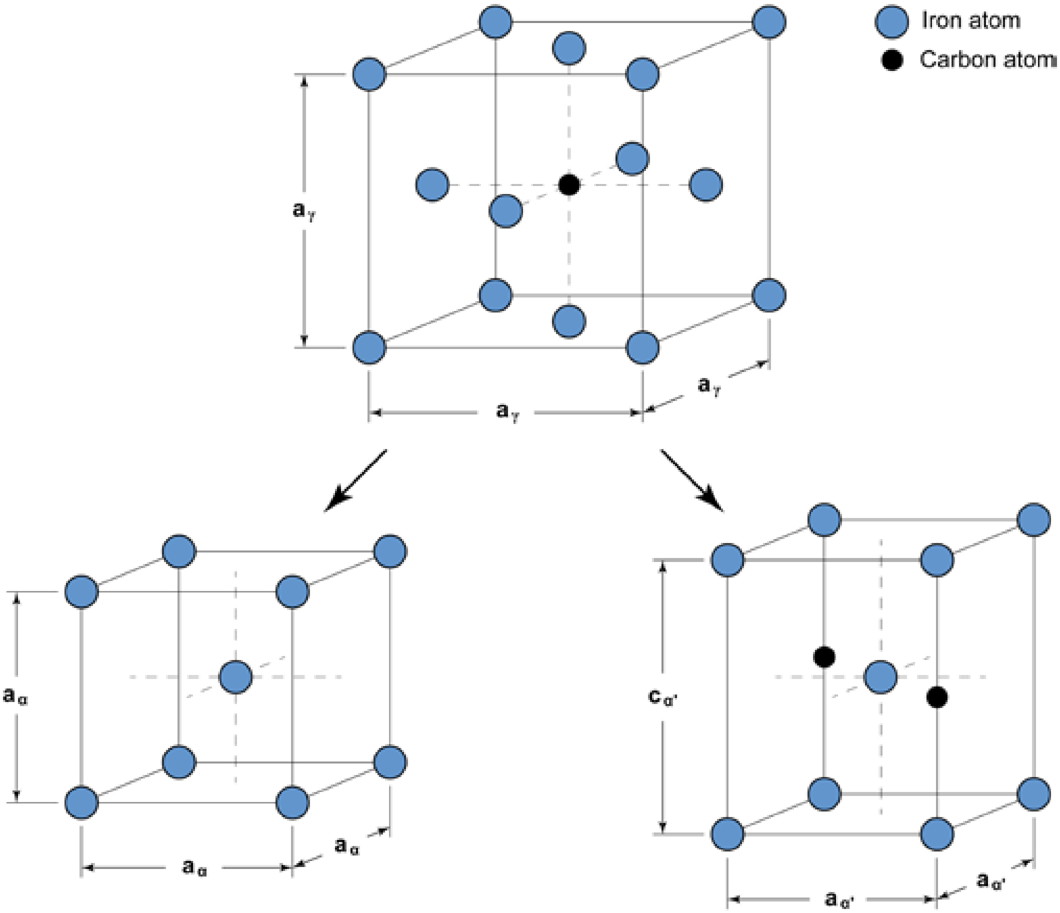

Figure 8.20 - Schematic representation of (i) the F.C.C. lattice of γ-phase of austenite, with a carbon atom in solution in the octahedral interstitial site, (ii) the B.C.C. lattice of α-phase of ferrite without carbon atoms in solution (carbon solubility is practically nil), (iii) the B.C.T. lattice of α′-phase of martensite, with carbon atoms in solution (in the original octahedral interstitial site of the F.C.C. lattice of austenite).

The B.C.T. lattice of martensite (α'-phase) is not very different from the B.C.C. lattice of ferrite (α-phase): this is a body-centered cubic lattice elongated along one of the three directions, that is, with one of the axes of the cube ($c_{\alpha'}$) larger than the other two axes ($a_{\alpha'}$).

The distortion of the martensite lattice derives from the carbon atoms trapped in the cell since diffusion phenomena are inhibited due to the high cooling rate[13]. For this reason, it can be said that martensite is a ferritic microstructure oversaturated with carbon.

To explain the martensitic transformation, one usually refers to the theory proposed by Bain. Consider two adjacent F.C.C. cells (γ-phase), having lattice constant a_γ: carbon atoms are dissolved within their lattice in correspondence of the octahedral interstitial site. Observing the two adjacent cells, it is easy to notice that the B.C.T. cell of martensite is already present within the original F.C.C. lattice. If the F.C.C. cell has lattice parameter a_γ, the B.C.T. has lattice parameters a_γ and $a_\gamma \frac{\sqrt{2}}{2}$ with carbon atoms arranged along the major edges (Figure 8.21).

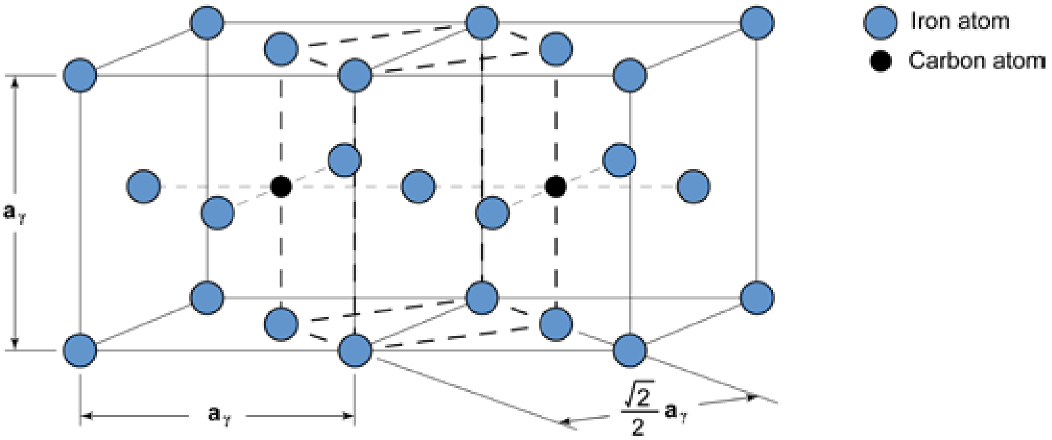

Figure 8.21 - Schematic representation of the austenite-martensite transformation. The B.C.T. cell (α'-phase) forms at cooling due to the coordinated movement of the iron atoms of the lattice.

When the F.C.C. cell of austenite cools down, it is transformed into the B.C.T. cell of martensite (α'-phase) as a result of the coordinated motion of the atoms of the lattice. At room temperature, the B.C.T. cell underwent a 20% contraction along the major edge (a_γ becomes $c_{\alpha'}$) and a 12% dilation of the two minor edges ($\frac{\sqrt{2}}{2} a_\gamma$ become $a_{\alpha'}$).

---

[13] *Note that carbon atoms do not occupy - statistically - all octahedral interstitial sites available in the F.C.C. cells of austenite. As a result, not all edges $c_{\alpha'}$ of the tetragonal cells of martensite are distorted in the same way.*

Simple geometric calculations highlight how the tetragonal cell of martensite at room temperature has a specific volume higher than the tetragonal cell, within the original γ-lattice; in fact, the martensitic transformation always produces an increase of volume of about 4.3 ÷ 4.5%.

The distortion of the martensite lattice at the end of the cooling is only a function of the carbon content trapped inside the cell (Figure 8.22): the greater the amount of carbon, the greater the lattice distortion.

The hardness of martensite is therefore only a function of the carbon content and is between 400 and 800 HV (see Figure 8.23).

The only way to change hardness of the martensitic microstructure is to change the carbon content[14], that is, to change the type of steel. The martensitic microstructure has always the same hardness for the same type of steel, and it makes no sense to speak of fine or coarse martensite since the austenite-martensite transformation is instantaneous and does not occur through nucleation and growth.

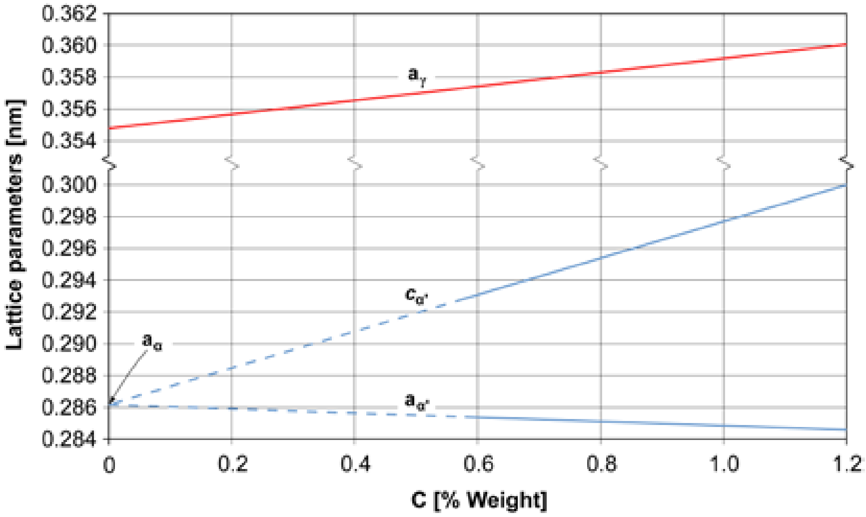

Figure 8.22 - Lattice parameters of the F.C.C. cell of γ-phase at 912°C, of the B.C.C. cell of α-phase at 20°C, and of the B.C.T. cell of martensite at 20°C [from Onink et al.1993 and Cheng et al.1991.

---

[14] *The correlation between the hardness of martensite and the content of carbon refers to as-quenched martensite. The correlation does not take into account the effect of other heat treatments (i.e. tempering).*

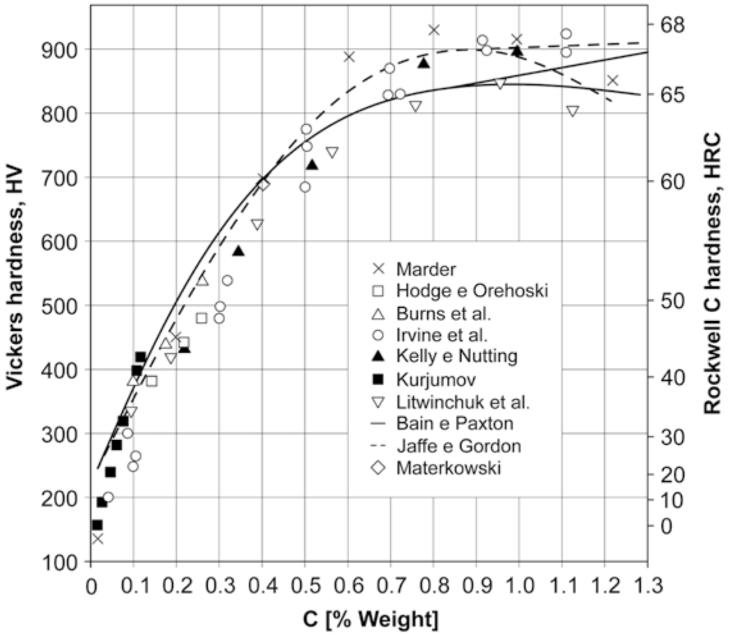

Figure 8.23 - The effect of carbon content on the hardness of as-quenched martensite [from Krauss 1980].

Under a metallographic microscope, martensite has an acicular morphology (Figure 8.24). For carbon contents lower than 0.6%, the microstructure is formed of lath *(lath martensite)*; instead, if the carbon content is greater than 1%, the microstructure is formed of plates *(plate martensite)*. Lastly, if the carbon content is between 0.6% and 1%, the microstructure is mixed. In both cases, the acicular microstructure of martensite consists of lath or plates arranged according to an equilateral triangle shape: this is the distinctive feature of the microstructure observed under a metallographic microscope (Figures 8.25 and 8.26) or under a scanning electron microscope (Figure 8.27).

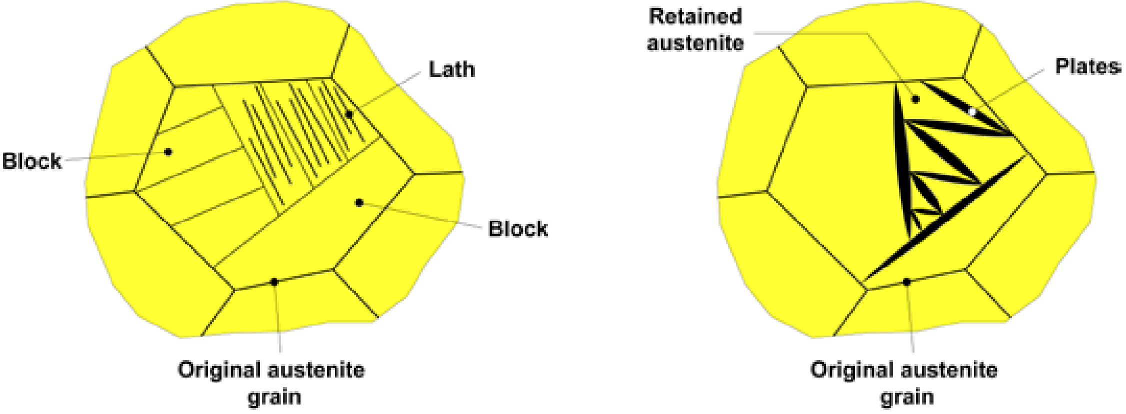

Figure 8.24 - Graphic representation of lath and plates of the martensitic microstructure [from Campbell 2008].

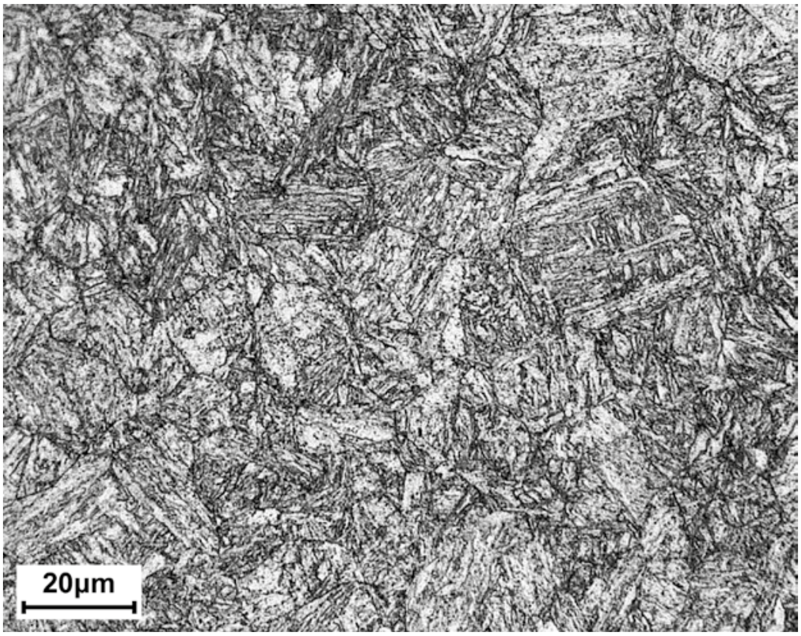

Figure 8.25 - Martensitic microstructure of an AISI 8630 steel. Appearance under the metallographic microscope - Nital 2% etch. [Laboratorio Hammer, Rho - Milano]

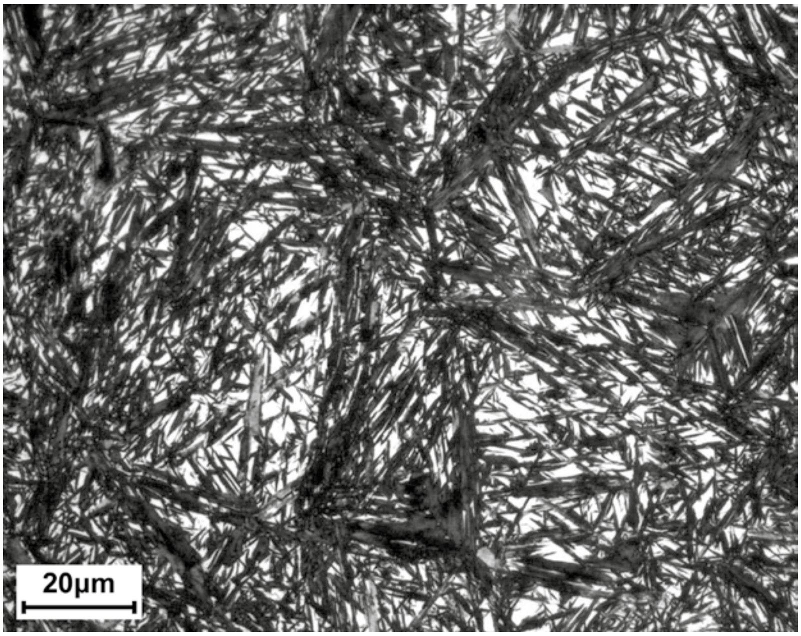

Figure 8.26 - Martensitic microstructure with retained austenite of an EN 100Cr6 steel. Appearance under the metallographic microscope - Nital 2% etch. [Laboratorio Omeco, Monza].

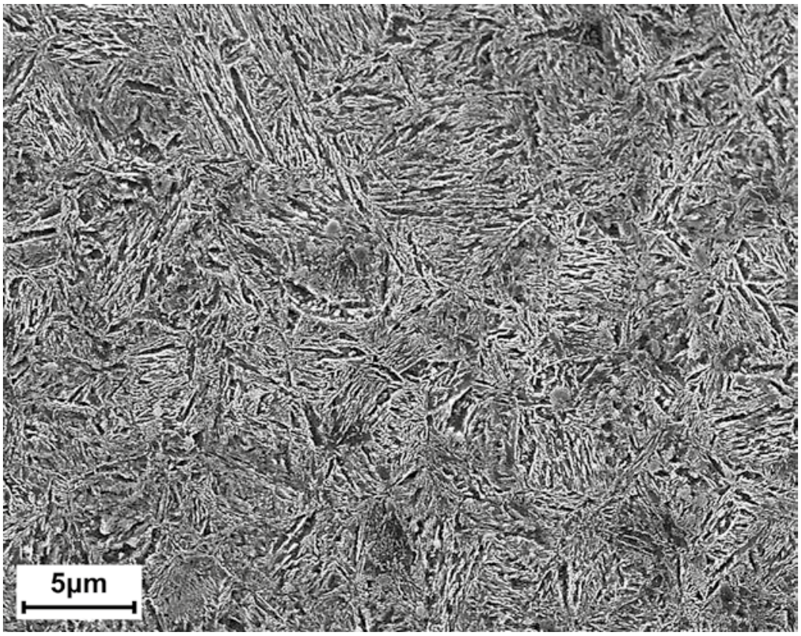

Figure 8.27 - Martensitic microstructure of an EN 42CrMo4 steel. Appearance under the scanning electron microscope - Nital 2% etch. [Laboratori del Dipartimento di Meccanica del Politecnico di Milano - Milano].

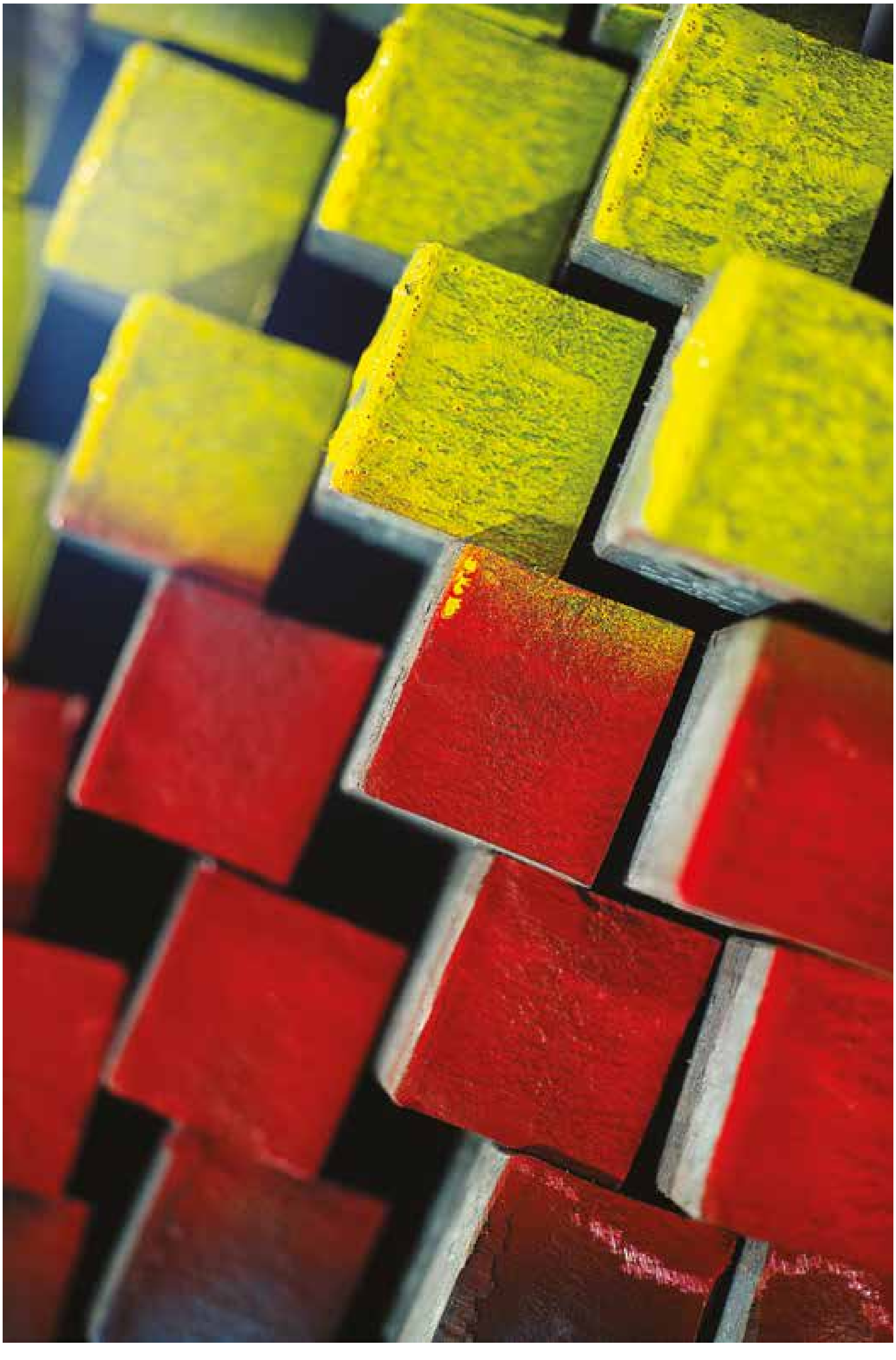

9. INDUSTRIAL HEAT TREATMENT FOR STEEL

9.1 What are industrial heat treatments?

Industrial heat treatments are thermal cycles that are performed on semi-finished products or mechanical components, in order to modify the mechanical properties of the steel. These consist in heating, holding, and cooling cycles, and are normally carried out using industrial furnaces.

There are several ways to classify industrial heat treatments. The most used is based on holding temperature. In summary, this refers to (Figure 9.1):

- heat treatments above critical points,
- heat treatments below critical points (sub-critical heat treatments).

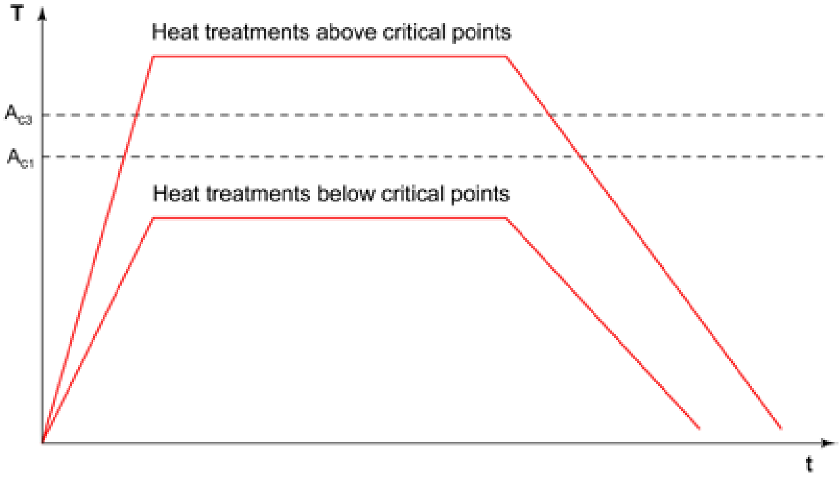

Figure 9.1 - Example of a heat treatment above or below critical points for a generic hypoeutectoid steel.

The main difference between the two types of heat treatment is related to the possibility of having or not having the transformation from γ-phase to α-phase during the heat treatment.

If the heat treatment exceeds critical points the final microstructure is different from the initial one. After heating and holding, the original microstructure transforms into austenite and, during cooling, the austenite forms new microstructures as a functin of the cooling rate. The morphological and mechanical properties of the microstructure are changed, such as the size of the crystallites, the level of strain hardening, the level of recovery or recrystallisation, the level of micro-hardness or residual stresses, etc.

If the heat treatment is sub-critical, the microstructure remains substantially unchanged; in fact, if the heating cycle is below critical points, no austenitic transformation occurs, and there is no microstructural transformation at the end of the cooling phase. The only alterations may be the morphological and mechanical characteristics of the microstructure, but not the type.

9.2 Main types of heat treatments

Heat treatments above critical points are called:

- annealing,
- normalising,
- hardening.

Annealing and normalising produce a microstructure of ferrite and pearlite (hypoeutectoid steels) or of pearlite and cementite (hypereutectoid steels) characterized by a medium/low hardness, good cold deformability and good machinability.

Instead, in the case of hardening, the objective is the opposite: to have a martensitic or bainitic/martensitic microstructure and give steel elevated hardness and mechanical strength.

Heat treatments below critical points are called:

- sub-critical annealing,
- tempering.

Sub-critical annealing includes various types of heat treatments, such as machinability, recrystallisation and stress-relief annealing. These heat treatments are performed when the microstructure is ferritic-pearlitic (or of pearlite and cementite) and are designed to further improve machinability and reduce residual stresses caused by previous machining.

Tempering, on the other hand, is carried out on martensitic or bainitic/martensitic microstructures, to improve the impact strength and lowering residual stresses caused by the hardening process[1].

There are also two important heat treatments combination: normalizing plus annealing for machinability and hardening plus tempering.

There is another group of heat treatments in addition to those above or below critical points: surface heat treatments. These are thermal or thermo-chemical treatments that affecting only the surface and they include surface hardening, carburising, carbonitriding, nitriding, nitrocarburising.

A summary of the main types of steel heat treatments is shown in Figure 9.2.

---

[1] *Another important function of tempering is to induce the transformation of retained austenite into bainite/martensite.*

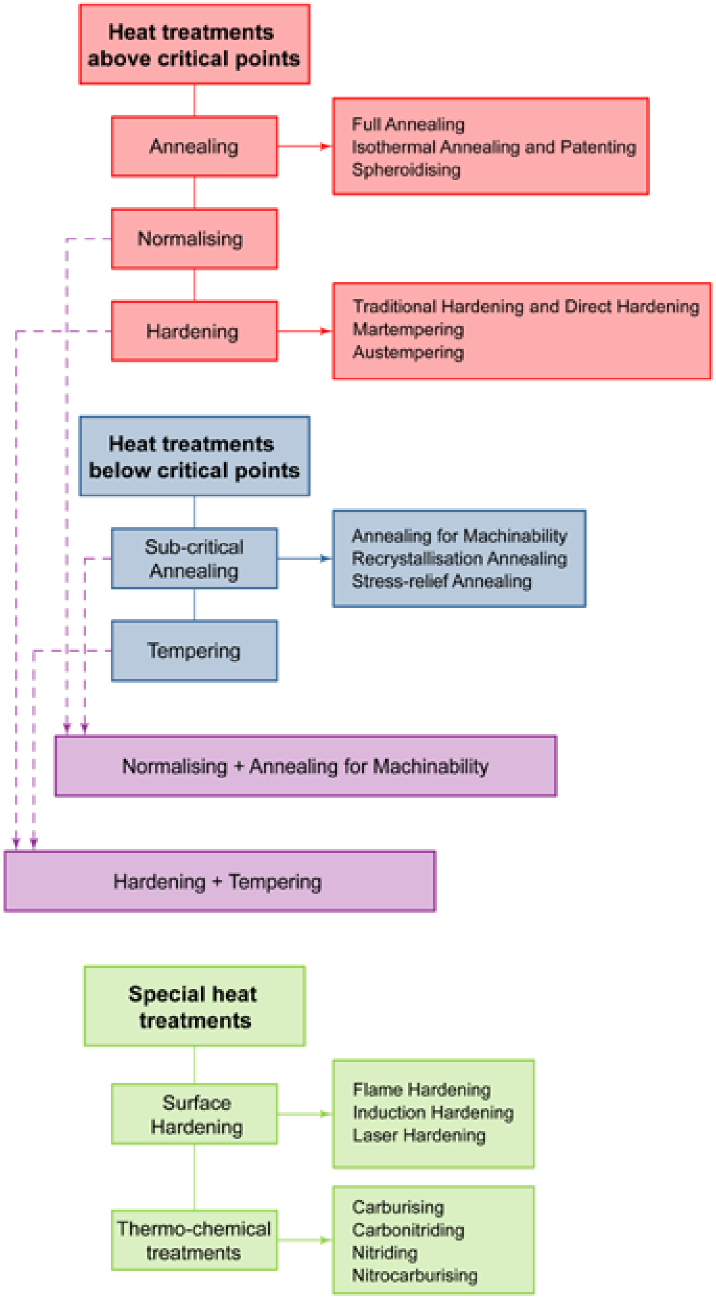

Figure 9.2 - Schematic representation of the main types of steel heat treatments.

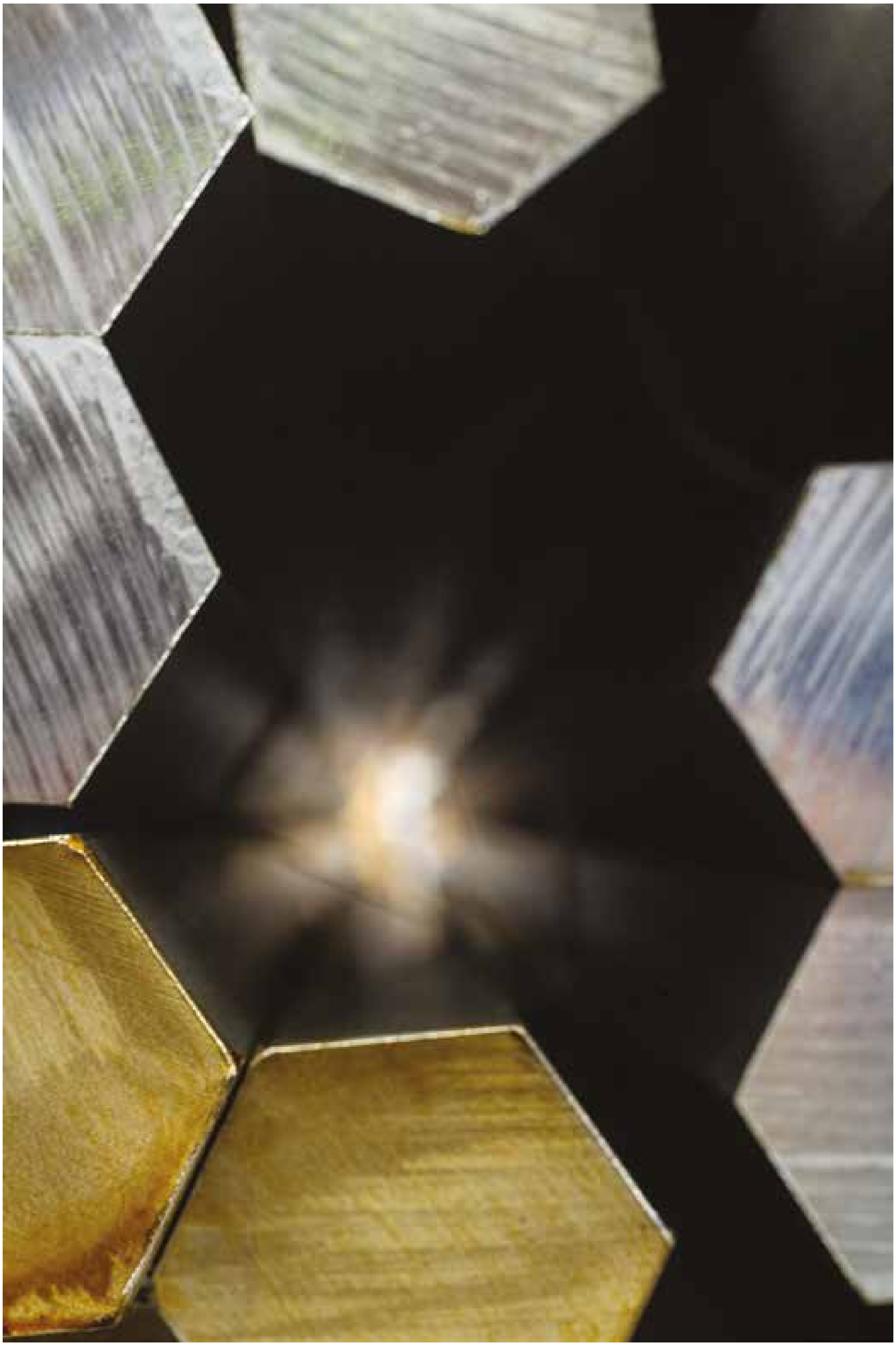

10. HEAT TREATMENTS ABOVE CRITICAL POINTS

10.1 Common aspects of heat treatments above critical points

As seen in Chapter 9 heat treatments above critical points are annealing, normalising, and hardening. Each of these provides three different phases: heating, soaking and cooling.

Before addressing their study in detail, some common aspects should be considered: for such treatments, heating and soaking are practically identical and have similar problems.

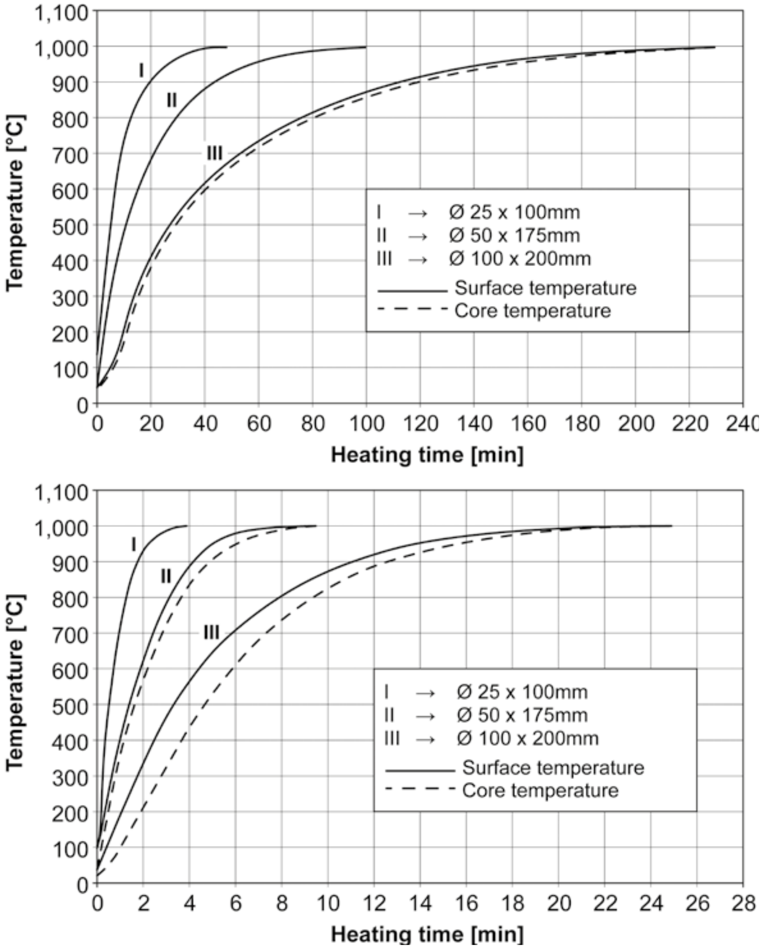

Figure 10.1 - Correlation between temperature and heating time for steel bars of different diameter and length, heated to 1,000°C in a muffle furnace (top) and in a salt bath furnace (bottom) [from Thelning 1975].

Heating

Heating can be carried out in different ways, as a function of the types of industrial furnaces, the size of the workpieces, and the thermal properties of the steels.

First of all, keep in mind that the heating rate is greatly influenced by both the thermal capacity of the furnace and the geometrical characteristics of the component. The heating phase must ensure that the heat generated by the furnace heating elements equally affects all the parts of the workpieces to be heat treated (Figures 10.1 and 10.2).

Another important aspect is the furnace temperature when the workpieces are inserted inside it; in fact, the furnace can be already hot or steel cold (Figure 10.3).

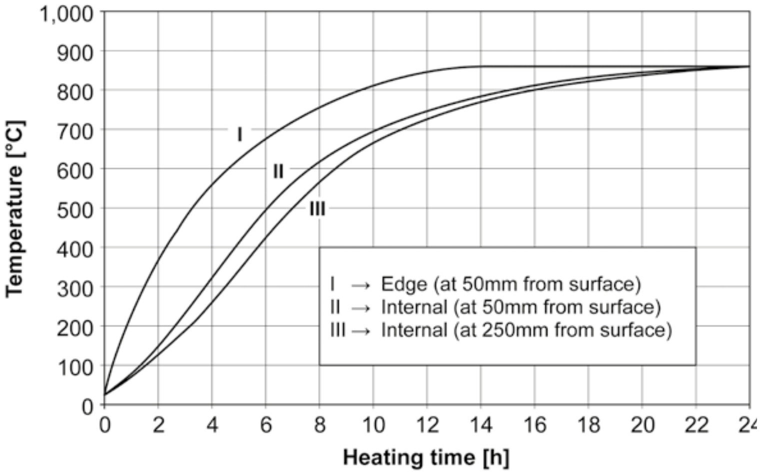

Figure 10.2 - Correlation between temperature and heating time for a 2,300 x 950 x 500 mm steel plate, heated at 850°C in a muffle furnace [from Thelning 1975].

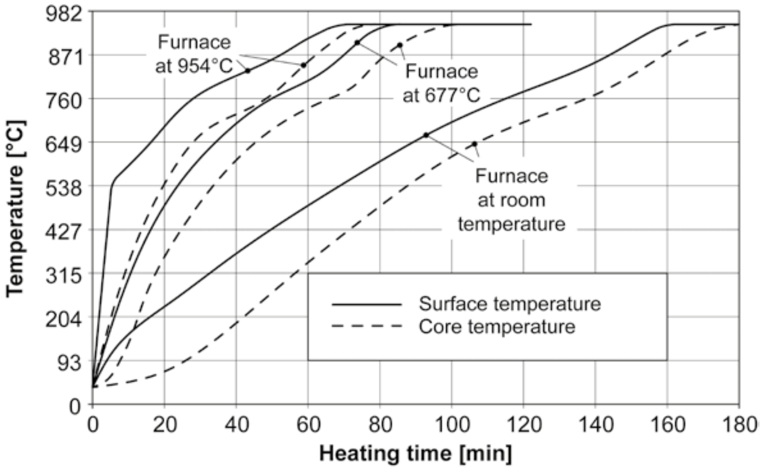

Figure 10.3 - Correlation between temperature and heating time for a 75mm thick steel plate, heated at 954°C and inserted into a cold or pre-heated muffle furnace [from Briggs 1958].

Other elements to consider are the geometry of the workpiece and the thermal conductivity of the steel[1]. In general, the time required to equalize temperature between the core and the surface increases as the size of the component increases and the thermal conductivity of the steel decreases.

If the steel conductivity is low or the component is large, the surface warms rapidly and dilates, while the core remains cold and does not deform. This temperature gradient generates stresses and/or irreversible deformations that can lead to scrapping the component[2]. Consequently, a great deal of attention should be paid to the heating rate of the componemt to be heat treated. To this regard, Figure 10.4 shows how heating carried out with a controlled method, reduces the temperature difference between the surface and the core of the component without increasing the heating time.

Other problems are related to the oxidation and decarburization of steel, resulting in carbon depletion on the surface. This aspect is of great importance when the workpieces are not further finished on machine tools. In some cases, it is convenient to perform the heat treatment in a non-oxidizing atmosphere. Nitrogen atmosphere or mixtres of inert and reducing gases (mixtures of N_2 with CO and/or H_2) are usually used to protect components from oxidizing, during heat treatment.

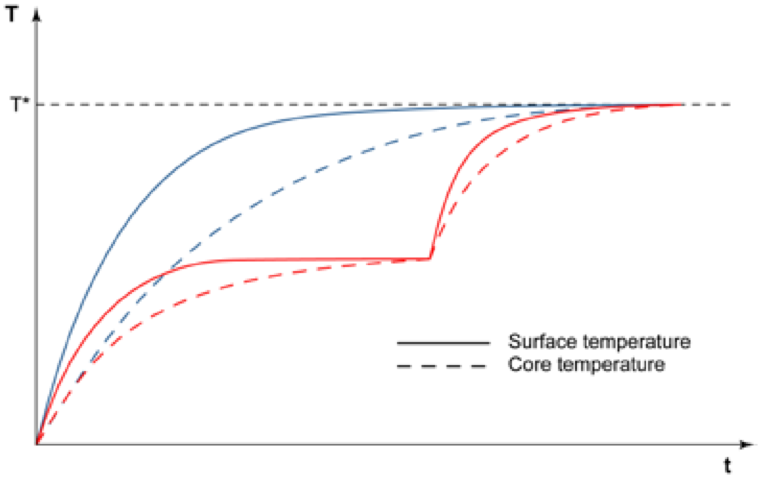

Figure 10.4 - Schematic representation of a continuous heating cycle (blue) and a step heating cycle (red): T^* is the heating temperature .

---

[1] *The thermal conductivity of steel, at least in first approximation, is inversely proportional to the amount of alloying elements. Materials with low thermal conductivity, therefore, belong to families of steels with high content of alloying elements, i.e. tool steels and stainless steels. These steels, especially on large-sized workpieces and/or with complex geometries, may have problems during heat treatment, both during heating and cooling.*

[2] *In addition to the dimension, even the shape of the component should not be underestimated. Very thick sections near very thin sections generate significant thermal gradient which can lead to a permanent deformation of the component during heating or cooling.*

Soaking

The soaking phase it is defined by two parameters: the heat treatment temperature and the holding time. While the holding temperature is defined by the type of heat treatment to be carried out, its duration is a function of the workpiece size: this represents the time that passes from when the furnace has reached the heating temperature until the beginning of cooling. There are two requirements to be met during soaking.

First, the workpieces must reach thermal equilibrium, that is, the core temperature is the same as that of the surface. Secondly, soaking should allow for the development of structural transformations requested by the heat treatment, such as the transformation of the original microstructure into austenite, the dissolution of carbides, the recrystallisation, the diffusion of the alloying elements, etc.

Empirical formulas can be used to estimate the holding time. They provide an estimate of the penetration rate of heat energy in the workpiece and are based on the principles of heat transmission in solids. If the heat treatment is carried out in air, the minimum holding time can be estimated in the range of one minute per millimeter or half an hour per inch, where the dimensional indication (millimeters or inches) refers to:

- the thickness of the section, in the case of plates with small thickness as compared to the other two sizes;
- the radius of the section, in the case of round pieces of infinite length.

For example, the soaking time of a cylindrical bar of 100 mm in diameter, or of a plate of 50 mm in thickness, made of carbon steel and heat treated in air, is equal to one hour.

For heat treatments performed in fused salt baths, holding times are cut in half (one minute every two millimeters or fifteen minutes per inch). For high-alloy steel, such as tool steel or stainless steel, the holding times must be increased by 20%.

Please note that this rule gives good results for sections of a thickness (or radius) between 10 mm and 100 mm. A thickness (or radius) of less than 10 mm has an holding time longer than what was calculated; on the contrary a thickness (or radius) greater than 100 mm, has a shorter holding time. These empirical formulas does not take into account the thermal characteristics of the furnaces used and how the components are loaded into the furnace.

If a greater level of detail is needed, the thermal behavior of the components to be treated and the furnaces to be used can be investigated through suitable thermocouples applied to specific samples. An example is shown in Figure 10.5.

10.2 Full annealing

Full annealing involves the progressive heating until a temperature of 20°C-50°C above critical point A_{c3} if the steel is hypoeutectoid, or between critical point A_{c1} and critical point A_{cm} if steel is hypereutectoid (see Figure 10.6).

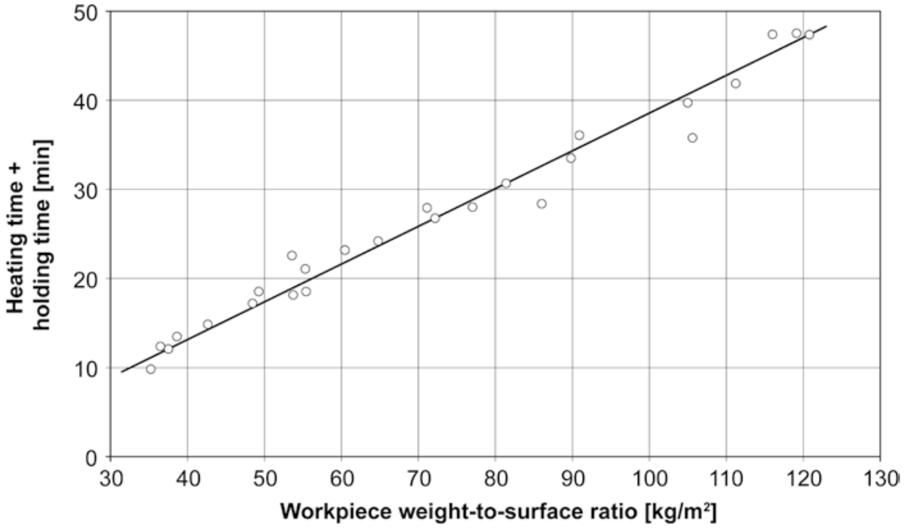

Figure 10.5 - The effect of workpiece weight/surface ratio on the heating plus holding time. This diagram is valid only for a resistance heating muffle furnace having a power of 8 kW and dimensions of 240mm x 240mm x 400mm [from Jost et al.1976].

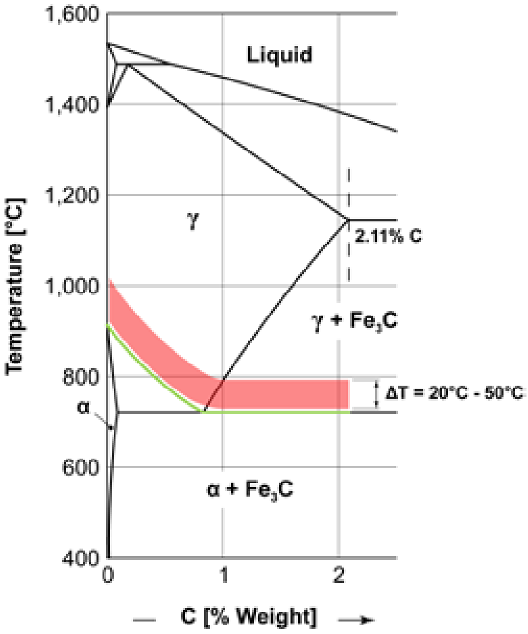

Figure 10.6 - The effect of steel carbon content on the holding temperature for full annealing (red band). The green line highlights critical points.

Soaking time should be long enough to equalize the temperature within the semi-finished product/component to be treated (see Paragraph 10.1), and to form austenite (if the steel is hypoeutectoid) or austenite and cementite (if the steel is hypereutectoid) in the whole component. The holding temperature varies between 760°C and 900°C, depending on steel chemical composition. Generally, it is never advisable to exceed these values because of the risk of grain growth and worsening of mechanical properties.

It is also worth mentioning a distinction between hypoeutectoid and hypereutectoid steels after the heating and soaking phase: while the first are completely austenitized, the latter, have a microstructure consisting of austenite plus carbides[3] due to the holding temerature between A_{c1} and A_{cm}. In fact, an holding temperature between A_{c1} and A_{cm} prevent the risk of grain growth or, worse, steel burning[4].

The cooling phase is very slow, in the order of 5°C-30°C/hour, and is carried out in the furnace. Usually, after reaching 300°C, the workpiece is extracted from the furnace and cooled in air.

With reference to the C.C.T. diagram of a generic hypoeutectoid steel, the cooling phase can be compared to what is shown in Figure 10.7.

At the and of the annealing, a coarse microstructure of ferrite and pearlite (if the steel is hypoeutectoid), or pearlite and cementite (if the steel is hypereutectoid), is formed.

The microstructure is very homogeneous both from a chemical and morphological point-of-view, with equally-sized coarse grains. Hardness is very low and, consequently, cold deformability is high. Machinability may not be optimal due to the high level of grain growth[5].

Typically, full annealing is performed on semi-finished products obtained by forging, stamping or hot rolling, or on workpieces that require very slow cooling to form a microstructure with a good machinability[6].

---

[3] *Due to the holding temperatures between A_{c1} and A_{cm}, the hypereutectoid steel has not a completely austenitic microstructure before cooling.*

[4] *Burning is a phenomenon that occurs when the heating temperature is to high and cause the formation of liquid metal along the grain boundaries (i.e. areas with a lower melting temperature). If burning occurs, the components permanently lose their mechanical properties and they must be scrapped.*

[5] *Extremely coarse crystallites facilitate the formation of build up edge on the tool face, causing premature wear.*

[6] *Steel used for tools or bearings, martensitic stainless steel and air hardening steel.*

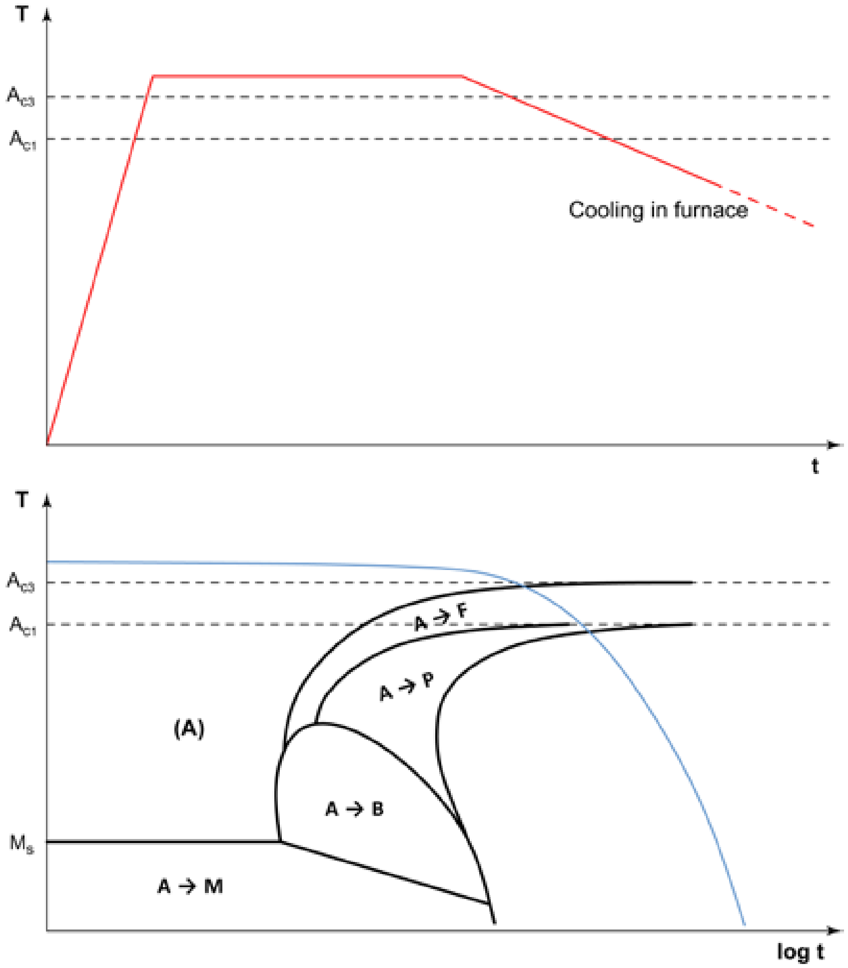

Figure 10.7 - Schematic representation of full annealing for a generic hypoeutectoid steel (on the top). The cooling curve is superimposed on the C.C.T. diagram (on the bottom).

10.3 Isothermal annealing and patenting

Full annealing is rarely performed, because of the high costs due to the extended use of the heat treatment furnace. An economical alternative is the isothermal annealing that produces results similar to full annealing. To understand what occurs during this heat treatment, see Figure 10.8.

Steel is initially heated and holded at the austenitization temperature (temperatures are the same as full annealing), therefore, a rapid cooling is carried out, in order to prevent the austenite transformation.

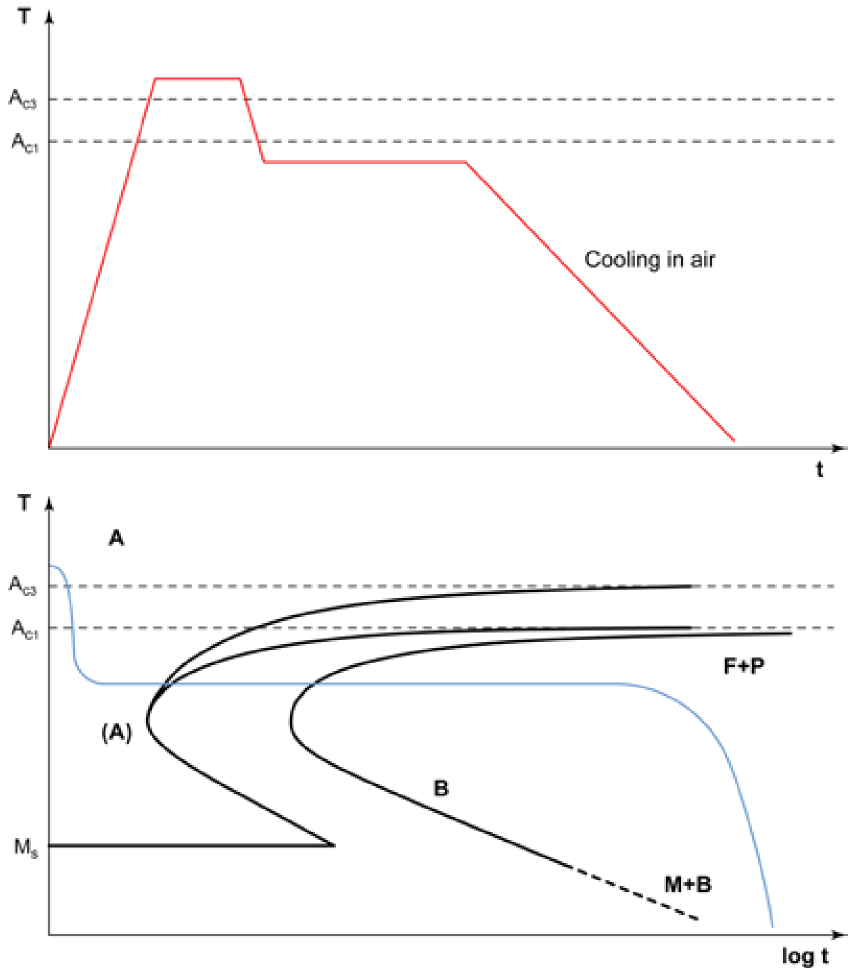

Figure 10.8 - Schematic representation of the isothermal annealing for a generic hypoeutectoid steel (on the top). The cooling curve is superimposed on the T.T.T. diagram (on the bottom).

The rapid cooling phase ends at a temperature between critical point A_{c1} and the nose of the T.T.T. diagram (indicatively at temperatures ranging between 600°C and 700°C). The system remains at this temperature, called isothermal holding temperature, until the austenite transformation is completed.

The new microstructure is formed of ferrite and pearlite (hypoeutectoid steel). Instead, if the steel is hypereutectoid, the microstructure is formed of cementite and pearlite.

Another alternative to full annealing is spheroidising. This heat treatment can be carried out according to different methods (Figures 10.9 and 10.10).

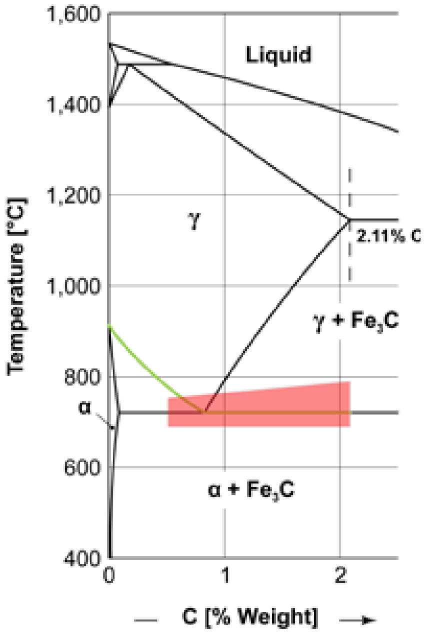

Figure 10.9 - The effect of steel carbon content on the holding temperature for spheroidising (red band). The green line highlights the critical points.

In the case of hypoeutectoid steel with a medium carbon content, the holding temperature is slightly lower than critical point A_{c1} (Figure 10.10a) and the cooling phase is carried out it in the furnace (very slow cooling). Alternatively, the component may be warmed slightly above critical point A_{c1} and than gradually cooled the temperature below the same critical point. Also in this case, the final cooling is carried out in the furnace (Figure 10.10b).

In the case of hypereutectoid or hypoeutectoid steels with a high carbon content steel is heated just above critical point A_{c1}, it is holded at that temperature for one to two hours, and then it is cooled just below the same critical point A_{c1}, for one or two hours. This sequence is then repeated two or three times.The final cooling is carried out in the furnace (Figure 10.10 c).

Spheroidising promotes carbon diffusion: at the end of the heat treatment the microstructure is globular with α-phase matrix scattered with globular shaped iron carbides. In all these cases, we speak of a globular pearlitic microstructure (Figure 10.11).

Spheroidising is the typical heat treatment carried out on tool or bearing steels and, in general, on all steels with a medium-high carbon content, in order to form a microstructure with low hardness, good cold deformability, and high machinability.

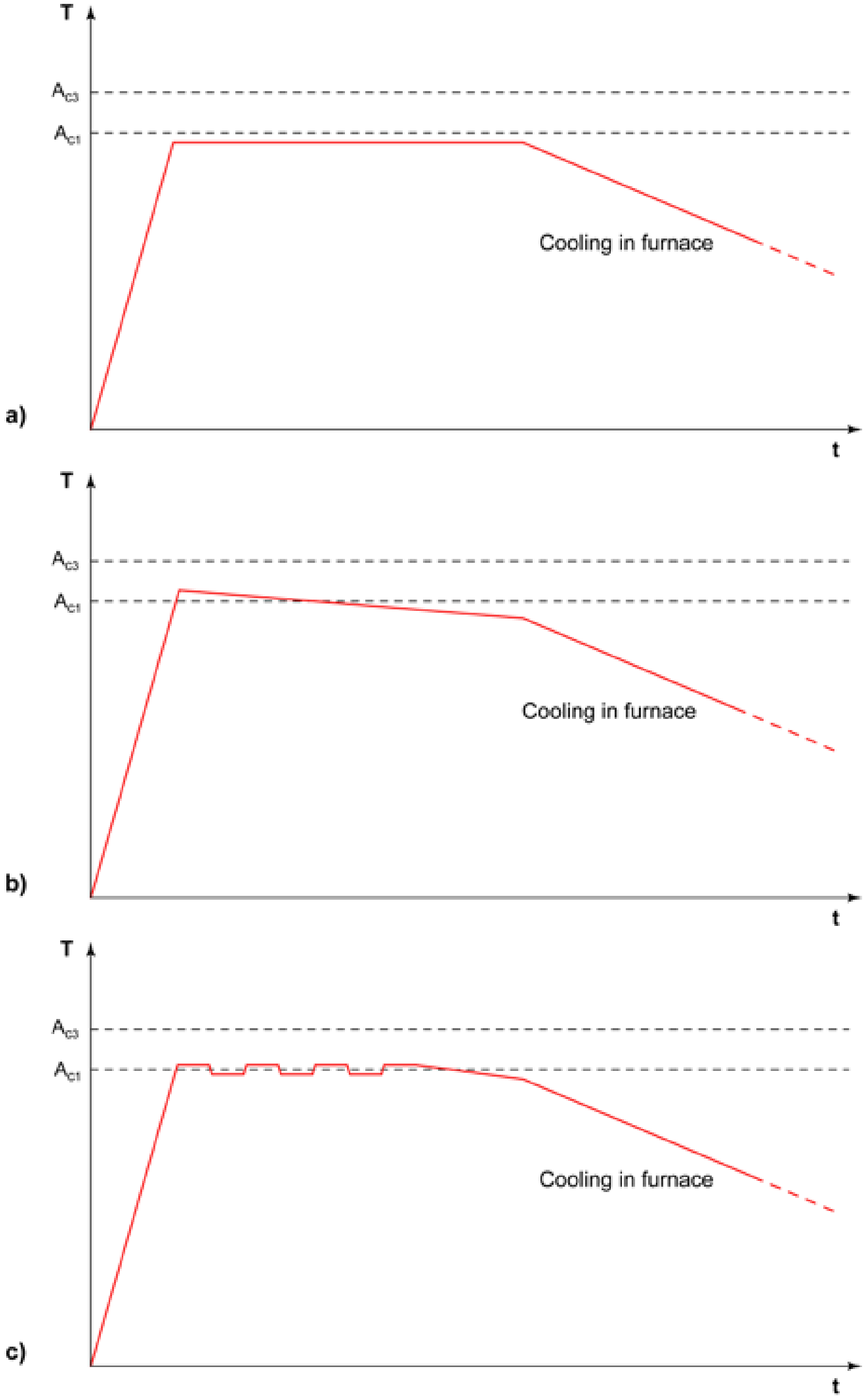

Figure 10.10 - Schematic representation of spheroidising; a) constant holding ~20°C below A_{c1}, b) heating ~10°C above A_{c1}, and very slow cooling at ~30°C under A_{c1}, c) oscillations ± 5°C around A_{c1} [from Spur and Stöferle 1980-1994].

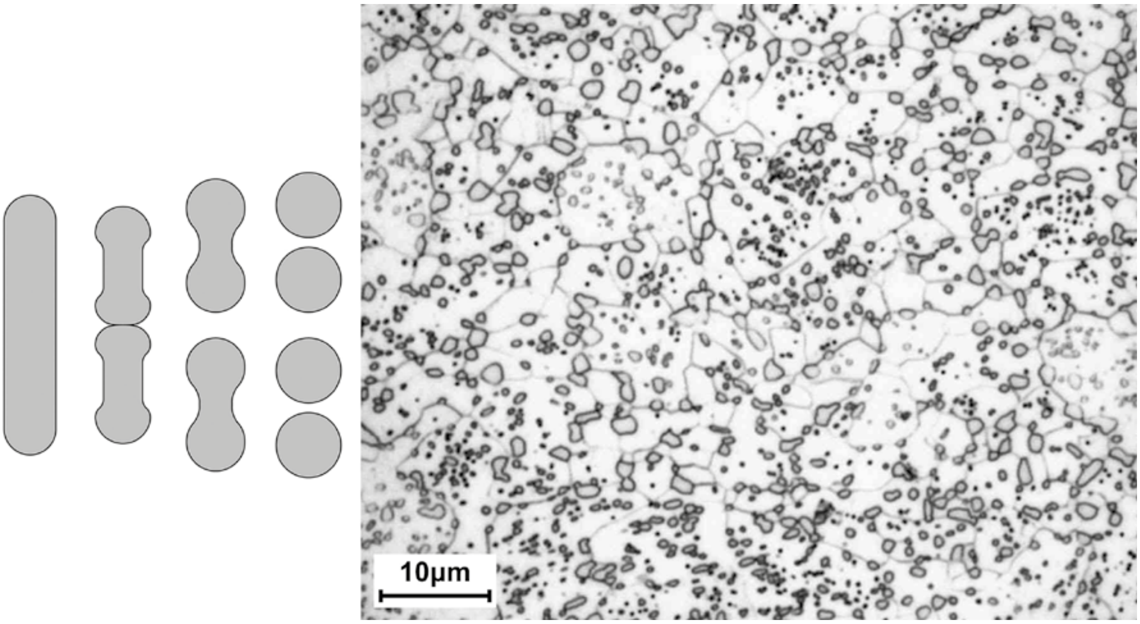

Figure 10.11 - Schematic representation of the transformation of Fe_3C phase from lamellar to globular shape during spheroidising (to the left). Globular pearlitic microstructure of an EN C67 steel (to the right). Appearance under the metallographic microscope - Nital 2% etch. [Laboratori Omeco, Monza].

10.4 Normalising

Normalising involves the progressive heating until a temperature of 40°C-80°C above critical point A_{c3} if the steel is hypoeutectoid, or between critical point A_{c1} and critical point A_{cm} if the steel is hypereutectoid (see Figure 10.12). The heating temperature is therefore between 780°C and 930°C, that is, temperatures very similar to those of full annealing.

Also the soaking phase is similar to the case of full annealing. At the end of the holding phase the microstructure consists of austenite (If the steel is hypoeutectoid) or austenite and cementite (if the steel is hypereutectoid).

Cooling is carried out by extracting the workpiece from the furnace and leaving it to air cool. The cooling rate is in the order of 10°C-50°C/ min, depending both on the size of the component and the characteristics of the air flux (temperature, turbulence, etc.).

The C.C.T. diagram of Figure 10.13 shows the cooling curve during the normalising of a generic hypoeutectoid steel. The microstructure downstream of normalising is made up of ferrite and pearlite, if the steel is hypoeutectoid, or cementite and pearlite, if the steel is hypereutectoid. In both cases, the microstructure is homogeneous and the grains have small dimensions, smaller than those generated by full annealing.

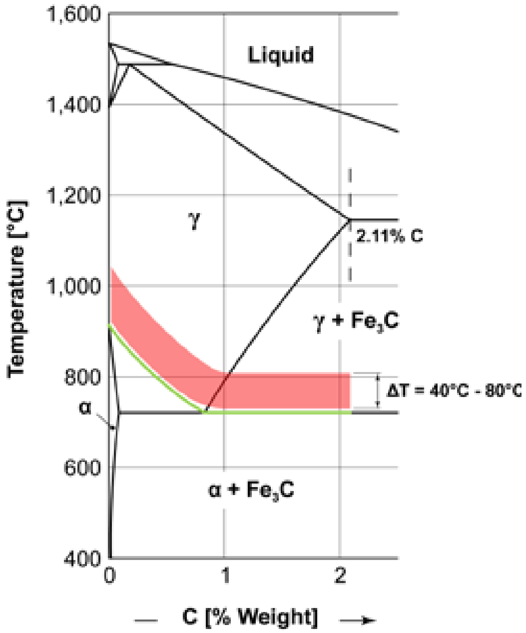

Figure 10.12 - The effect of steel carbon content on the holding temperature for normalising (red band). The green line highlights the critical points.

Usually, normalising produces a refining of the grain dimension[7], due to the structural transformation $\gamma \longrightarrow \alpha$, and the cooling in the air. Normalising removes unwanted acicular microstructures (Widmannstätten microstructures), which are typical of forging, and it reduce the amount of segregation bands, which are quite common in semi-finished products after hot working.

10.5 Hardening

The last heat treatment above critical points is hardening. Heating and soaking are identical to those already described for normalising. The material is brought to a temperature of 40°C-80°C above critical point A_{c3} if the steel is hypoeutectoid, or between the critical points A_{c1} and A_{cm} if the steel is hypereutectoid. The holding temperature is between 780°C and 930°C and the microstructure at the end of the holding phase is austenite (hypoeutectoid steels) or austenite plus carbides (hypereutectoid steels). The difference with annealing or normalising lies in the cooling phase, which must be sufficiently rapid to form martensite. In particular, the cooling rate must be greater than the cooling curve, v_s, shown in the C.C.T. diagram[8]. At the end of the heat treatment, the microstructure is martensitic in the case of hypoeutectoid steel or martensitic plus carbides in the case of hypereutectoid steel.

---

[7] *Semi-finished products subjected to normalising are tipically forged or hot-rolled workpieces.*

[8] *See Paragraphs 7.3 and 7.4 of Chapter 7.*

Cooling after hardening is normally carried out by immersing the workpiece in fluids such as water, caustic aqueous solutions, aqueous solutions of organic polymers, mineral oils. The average cooling rate on the surface of the workpieces is in the order of 200-600°C/min and depends on the quenching medium and the size of the semi-finished product. As an alternative a salt bath or a high pressure gas stream can be used. For specific types of steels, such as air hardening steels, martensitic stainless steels and tool steels, even the air cooling can guarantee the formation of martensite. The cooling phase for a generic hypoeutectoid steel is similar to what is shown in Figure 10.14.

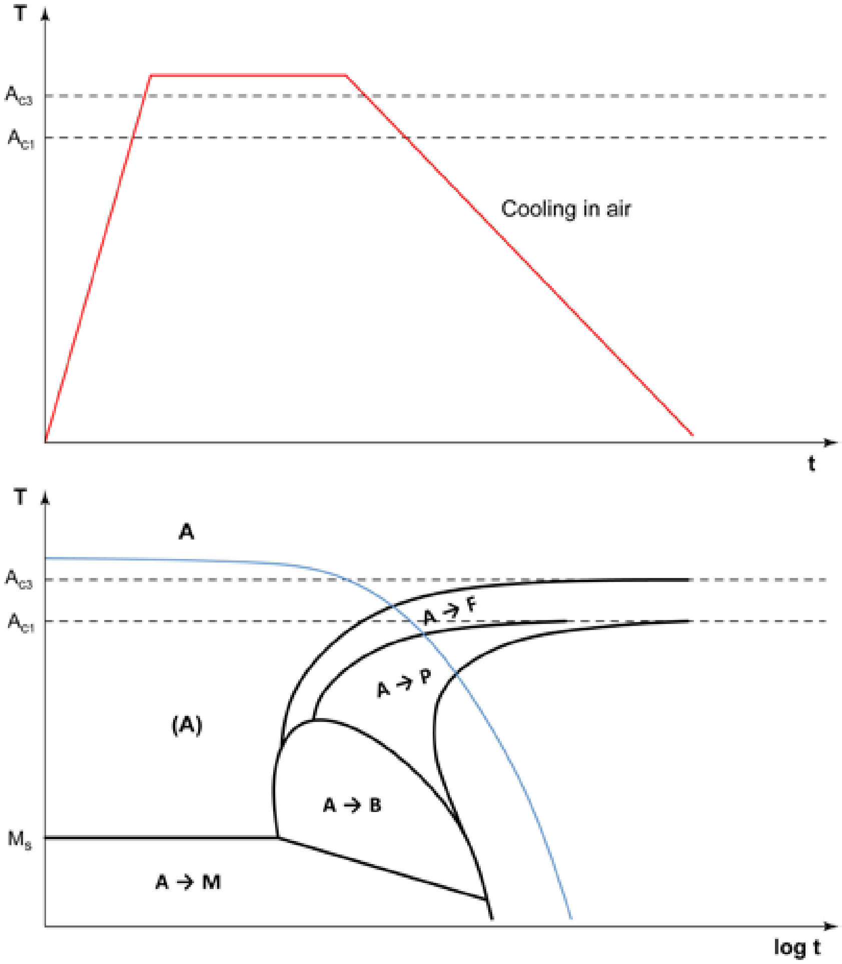

Figure 10.13- Schematic representation of normalising for a generic hypoeutectoid steel (on the top). The cooling curve is superimposed on the C.C.T. diagram (on the bottom).

---

[8] *See paragraphs 7.3 and 7.4 of chapter 7.*

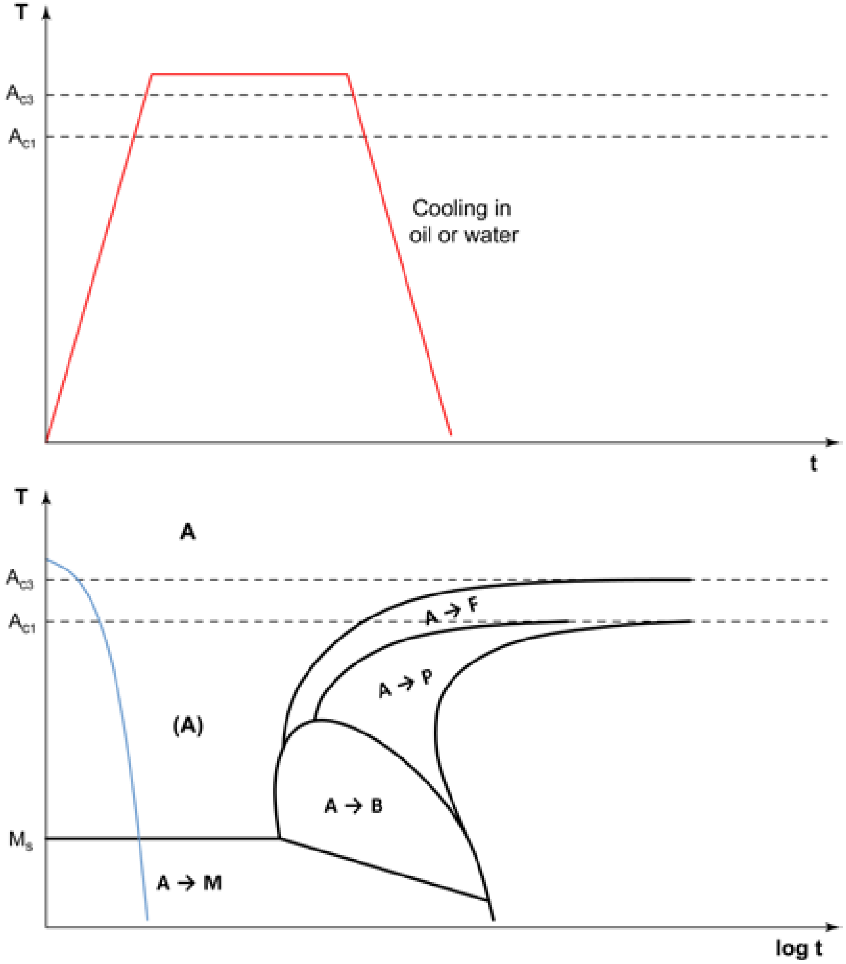

Figure 10.14 - Schematic representation of hardening for a generic hypoeutectoid steel (on the top). The cooling curve is superimposed on the C.C.T. diagram (on the bottom).

The cooling curve for hardening is not described by a specific cooling method (in furnace or in air, as in the case of full annealing or normalising), but it is defined by the microstructure.

The purpose of hardening is to form martensite in order to increase as much as possible the mechanical properties of the steel, i.e. hardness, yield strength and ultimate tensile strength.

Hardening must be followed immediately by tempering, in order to mitigate the excessive hardness and brittleness of the martensite (see Chapter 11).

10.6 Hardening and quenching media

If the quanching media has a boiling point much lower than that of the workpiece, the cooling phase always follows three steps. Initially, the liquid evaporates instantly and forms a stable vapor layer around the component: this first stage is called the Leidenfrost phenomenon[9]. The vapor layer causes a very low cooling rate, since the heat exchange is mediated by a gaseous phase. When the temperature of the workpiece drops below a given limit threshold (called Leidenfrost temperature), the vapor layer becomes unstable. Steam bubbles begin to form on the surface of the component, and new liquid comes into contact with the hot workpiece, vaporizing immediately. This phenomenon allows for extremely high cooling rates.

The third phase occurs when the temperature of the component equals the boiling point of the liquid: the component will be in constant contact with the fluid that will no longer evaporate. In this phase, the heat exchange proceeds by convection between a liquid and a solid and the cooling rate becomes low, again. The description is shown in Figure 10.15.

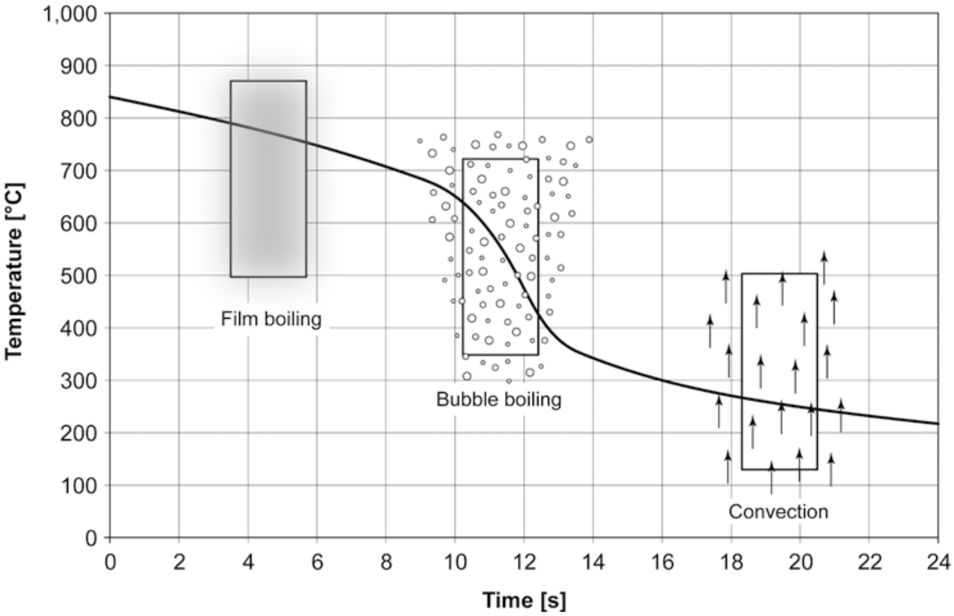

Figure 10.15 - Schematic representation of the cooling rate of a hot component immersed in a quenching medium [from ASM-H.4 1991].

---

[9] *The phenomenon was first described by German physician, Johann Gottlob Leidenfrost, in the book: De Aquae Communis Nonnullis Qualitatibus Tractatus, published in 1746.*

Ideally, a quenching medium should allow for a very rapid cooling rate in the initial stages, when the temperature is high, and then becomes lower when approaching the austenite-martensite transformation[10]. This means that real fluids must raise the Leidenfrost temperature and must reduce the time when the vapor forms a stable film around the workpiece.

The Figure 10.16 shows several examples of cooling curves produced by the most common quenching media.

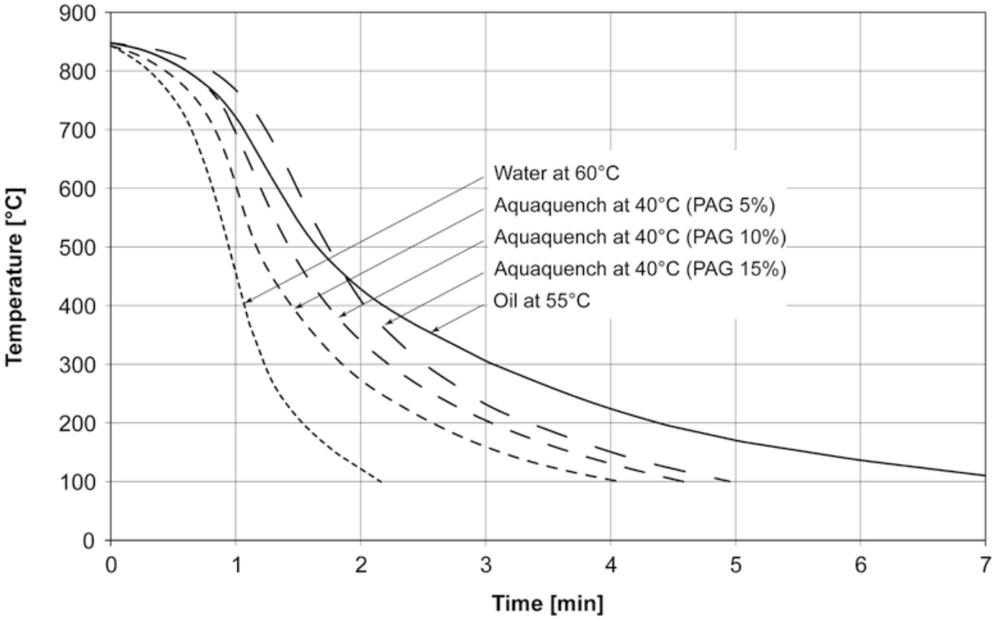

Figure 10.16 - Cooling curves produced by different quenching media as measured in the center of stainless steel bars (length:150mm, diameter:75mm) [from Thelning 1975].

A parameter used to simplify the behavior of the hardening fluids is the so-called "quenching intensity factor", indicated by the letter *H*: this represents the greater or lesser aptitude of a quenching medium to cool a steel component.

In general, the quenching intensity factor depends on the nature of the fluid: water has a *H* higher than oil which, in turn, has a *H* higher than a molten salt bath. The quenching intensity factor is also a function of the fluid temperature and its level of agitation.

To exemplify all these concepts, consider that agitated water at 20°C has a *H* higher than agitated water at 60°C or agitated oil at 20°C has a *H* higher than the still oil at 20°C.

---

[10] *The high cooling rate at the initial stage allows to cool the metallic mass to the martensite start temperature without intersecting the transformation area of the austentite into ferrite and pearlite (hypoeutectoid steel) or into cementite and pearlite (hypereutectoid steel). Below* M_s *, instead, the cooling rate must become lower in order to reduce the residual stress caused by the martensitic transformation.*

A quantitative definition of the quenching intensity factor H of a quenching medium was given by Grossman[11], and results in:

$$H = \frac{h}{2k} \qquad [10.1]$$

where h is the heat transfer coefficient of the interface between the workpiece and fluid[12] and k is the thermal conductivity of the metal mass. The experimental evaluation of H, allows to categorise the quenching media in terms of quenching intensity factor.

A fluid is considered ideal when there is no resistance to thermal exchange between the component and the quenching medium ($h \to \infty$), that is, the surface of the workpiece is instantly brought to the temperature of the fluid that sorrounds it: in this case the value of H is conventionally set to ∞.

In real fluids, the value of H is always lower than the ideal one and it is affected by the nature of the fluid, its temperature, and its agitation level. At room temperature and without agitation, water has a quenching intensity factor equal to 1, oil equal to 0.3, and air equal to 0.05[13]. Some examples of the quenching intensity factor is shown in Table 10.1.

Quenching medium	Temperature [°C]	Agitation [m/s]	Index of drasticity H [in^{-1}]
Water	32°	0 0.25 0.51 0.76	1.1 2.1 2.7 2.8
Water	55°	0 0.25 0.51 0.76	0.2 0.6 1.5 2.4
Oil for hardening	65°	0.51	0.7
Oil for rapid hardening	60°	0 0.25 0.51 0.76	0.5 1 1.1 1.5
Air	27°	0 2.54 5.08	0.05 0.06 0.08

Table 10.1: Quenching intensity factor for various quenching media.

---

[11] *Grossman M.A., Elements of Hardenability, American Society for Metals, Metals Park, Ohio, USA, 1952.*

[12] *The heat transfer coefficient, h, is the inverse of the resistance that the component opposes to the heat exchange with the fluid. h is defined as $h = q/A\ ({}_1 - T_2)$ where q is the heat that comes out of the workpiece towards the fluid, A is the surface of the workpiece, T_1 the temperature of the component and T_2 the fluid temperature. h is expressed in W/m^2K.*

[13] *The unit of measure of H expressed in the International System of Units (S.I.) is [m^{-1}]. However, the values of H are normally indicated in [in^{-1}], following the Anglo-Saxon unit of measure used by Grossmann.*

10.7 Steel hardenability

The hardening heat treatment described in paragraphs 10.5 and 10.6 is valid for small-sized components, i.e, when the cooling rate can be considered almost identical in every point of the component.

If you consider a medium or a large sized components, instead, the surface tends to cool quite quickly due to direct contact with the quenching medium, while the core follows a lower cooling rate.

Let us, therefore try to understand the effects produced by this phenomenon on the microstructure. Suppose you want to harden a medium-sized component in oil, made with a low carbon steel (steel *A*).

We use a series of numbers, from 1 to 7, to indicate some points along the section of the component (from 1 - the surface up to 7 - the core): therefore, we overlap the cooling curves of each point with the C.C.T. diagram and evaluate the microstructures (see Figure 10.17).

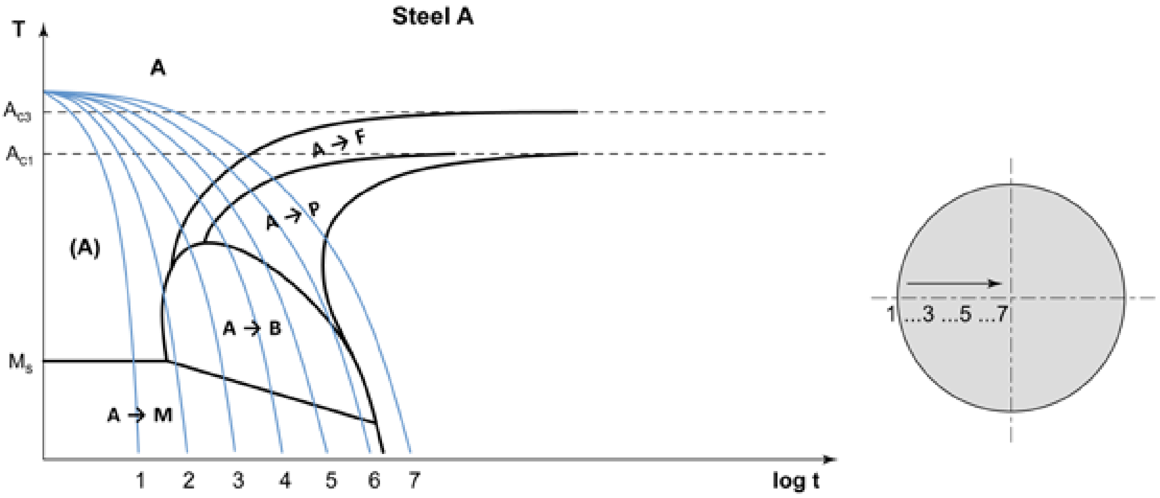

Figure 10.17 - Cooling curves for hardening in oil superimposed on the C.C.T. diagram of a steel with low hardenability (low carbon steel).

The Figure 10.17 shows how only with cooling curve 1 the microstructure is completely martensitic. With cooling curves from 2 to 6, the microstructure is a mixture of bainite, ferrite, pearlite, and martensite; with curve 7 the microstructure is only ferritic-pearlitic.

Let us now evaluate what happens if we decide to harden in oil the same workpiece but made with a low alloy steel (steel *B*).

Since the component and the quenching medium have not changed, the cooling curves are virtually identical[14].

The C.C.T. diagram is instead moved more downward and to the right with respect to the temperature-time axes (the steel *B* contains more alloying elements with respect to the steel *A*).

---

[14] In addition to the quenching medium and the component size, the cooling rate is also influenced by the chemical composition of the steel. However, this parameter has a very limited effect and it can be ignored.

In this second case, cooling curves 1, 2, and 3, form only martensite, while curves from 4 to 7, form also other microstructures (Figure 10.18).

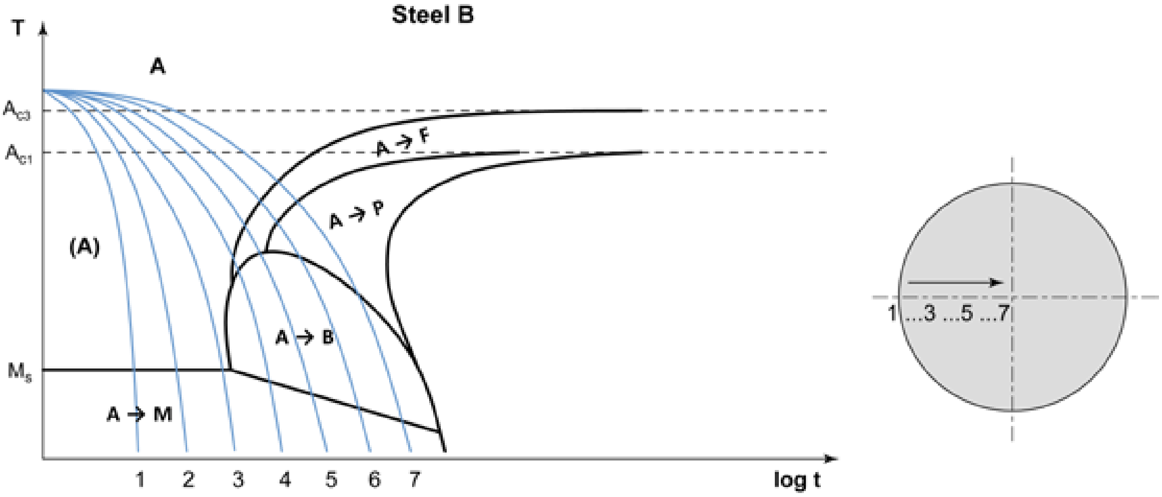

Figure 10.18 - Cooling curves for hardening in oil superimposed on the C.C.T. diagram of a steel with medium hardenability (low alloy steel).

Since a given hardness is associated to each cooling curve, it is possible to trace the hardness profile along the section of the component at the end of the hardening. The result shown in Figure 10.19 highlights the importance of the chemical composition of steel: the amount of martensite and therefore the hardness profile, is different even if the two components has the same size and they are heat treated with the same quenching medium.

A typical example is shown in Figure 10.20, which shows the hardness profile along the section of round bars made of carbon steel (EN C50) or low alloy steel (EN 42CrMo4).

The ability of steel to form martensite is called hardenability. Consequently, it is common to speak of more or less hardenable steels in relation to their ability to form martensite.

Hardenability is a property that is strictly dependent on the chemical composition of the steel. Hardenability increases:

- as the amount of alloying elements, including carbon, increases,
- as the average size of the crystallite increases.

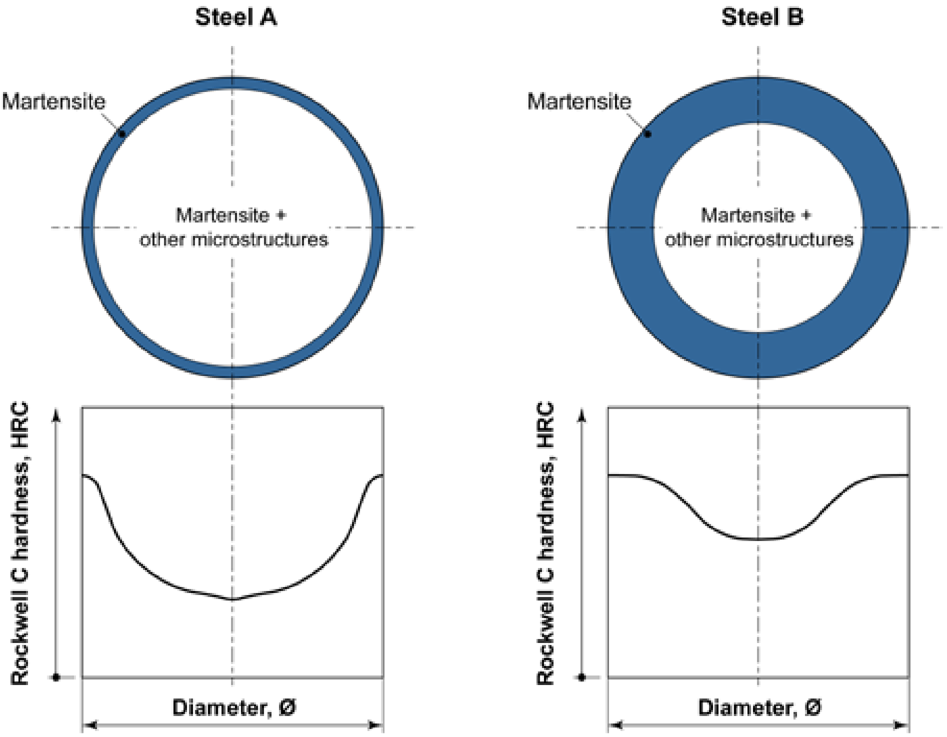

Figure 10.19 - Radial hardness profile along the section of two cylindrical bars with the same size but made of low carbon steel (steel *A*) or low alloy steel (steel *B*) and hardened in oil.

The hardenability is independent of the workpiece shape and of the quenching medium. Hardenability is also an important parameter used to define the behavior of mechanical components.

A mechanical component with ideal features should have the same impact strength, hardness, and tensile strength throughout its section and length.

Since the homogeneity of mechanical properties is a function of the steel microstructure after hardening, it is always advisable to have martensite throughout the component. In fact, martensite has to great advantages: (i) it is the microstructure with the highest mechanical strength and (ii) it has always the same hardnes for a given chemical composition[15]. This means that, where there is martensite, there is also homogeneity in mechanical behavior.

---

[15] *The hardness of martensite after hardening depends only on the steel carbon content.*

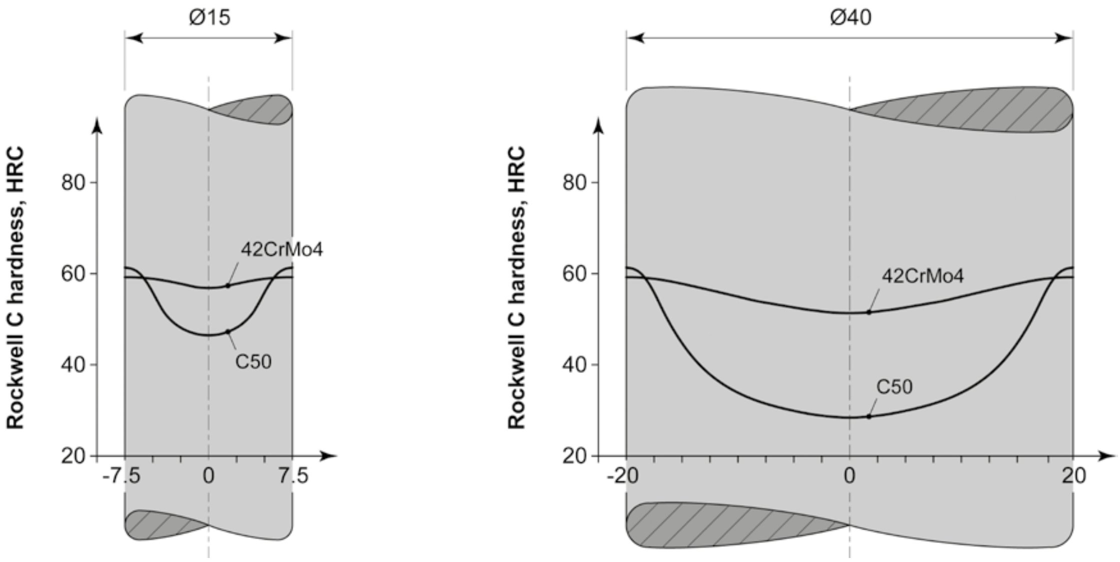

Figure 10.20 - Radial hardness profile along the section of two cylindrical bars (Ø15mm and Ø40mm) made of EN C50 or EN 42CrMo4 steel, and hardened in water at 30°C with an agitation level of 0.3 m/s [from Totten 2006].

A workpiece is completely hardened when it has the 100% of martensite in the core and, therefore, at all other points in the section. As a result, the workpiece has a uniform hardness and a uniform mechanical strength everywhere.

Practically, only workpieces of small size and made of steels having a medium-high hardenability show uniform hardness everywhere. Nevertheless, a component is considered satisfactory if, after hardening, has an amount of martensite in the core of 50% for hardened and tempered steels, of 70% for case hardening steels, and of 80% for spring steels. As a rule of thumb, steel hardenability must increase, as the component size increase.

10.8 Evaluation of steel hardenability and the Jominy test

There are many methods to quantify the hardenability of a steel: the most important is the "Jominy test". This is described by the EN-ISO 642 standard in Europe and the ASTM A 255 standard in the United States. The samples for the Jominy test must be taking from the component to be tested. The samples must have a diameter of 25 mm, a length of 100 mm and an abutting surface at one of the two ends.

The sample is first introduced into a special ceramic jacket (in order to reduce the oxidizing effect of the atmosphere), and than is placed in a muffle furnace where it is austenitized at the desired temperature[16] for 30 minutes. Immediately after the extraction from the furnace, the sample is inserted into a perforated support and its free end, called the "quenched end", is quenched with a jet of water at a temperature of 20°C ± 5°C (Figure 10.21).

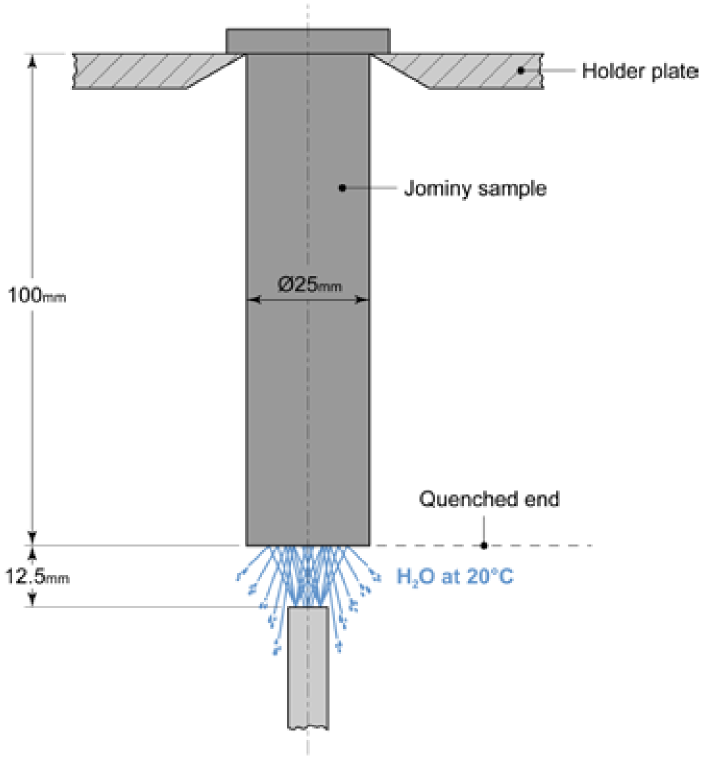

Figure 10.21 - Execution method of the Jominy test.

As a result sample undergo a cooling rate that is more rapid the closer the sample sections are to the quenched end. At the end of the test, sample is grinded along a line on the cylinder surface: the grinding depth is in the order of 0.4÷0.5mm. The hardness measurements are performed on the grinded surface using a Rockwell C hardness tester, progressively moving away from the quenched end.

The so-called Jominy hardenability curve is obtained by representing the hardness values on a graph, as a function of the distance from the quenched end. A typical example is shown in Figure 10.22.

---

[16] *Since the austenitization phase affects the mean grain size and the steel hardenability, it is important to select the correct heating temperature for the Jominy test.*

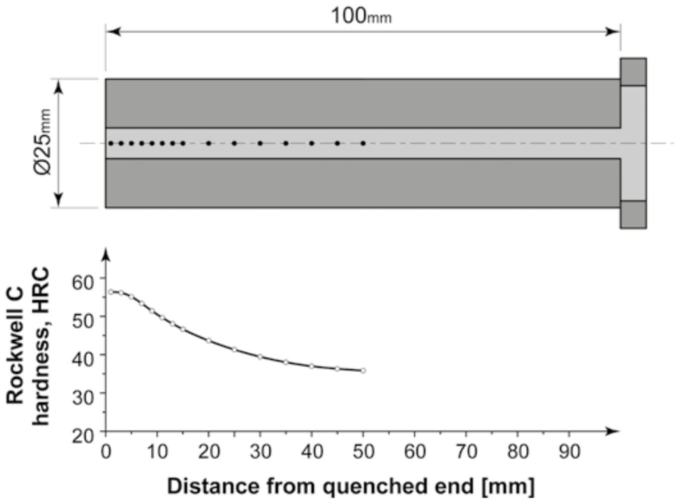

Figure 10.22 - Schematic representation of a typical Jominy hardenability curve.

For example, Figure 10.23 shows the comparison between EN 42CrMo4 steel and EN C50 steel.
the 42CrMo4 steel has a higher hardenability than C50 steel, even if the latter shows a higher hardness on the surface, since it has a higher carbon content. A component in 42CrMo4 steel has therefore more homogeneous hardness along the section compared to the same component in C50 steel.

The hardness profile along the Jominy sample is similar to that of a real cylindrical component cooled in a quenching medium. The surface of the workpiece is similar to the quenched end of the Jominy sample while the core has a cooling rate that is more similar to section far from the quenched end[17].
Consequently, if the Jominy hardenability curve is flat, the microstructure along the entire section of the cylindrical component is homogeneous and there are no major variations in hardness and mechanical properties. On the contrary, if the Jominy sample shows a sharp change in hardness, the mechanical strength of the cylindrical component is higher on the surface than in the core.
Therefore large-sized components must be made of steel with a high hardenability while components with a small or medium size can also be produced using steel with a more limited hardenability.

---

[17] *Never the less the two hardness profile can not be overlapped. Even if the Jominy hardenability curve is similar to the hardness profile along the section of a hardened cylindrical component, the hardness of the real workpieces must be evaluated experimentally.*

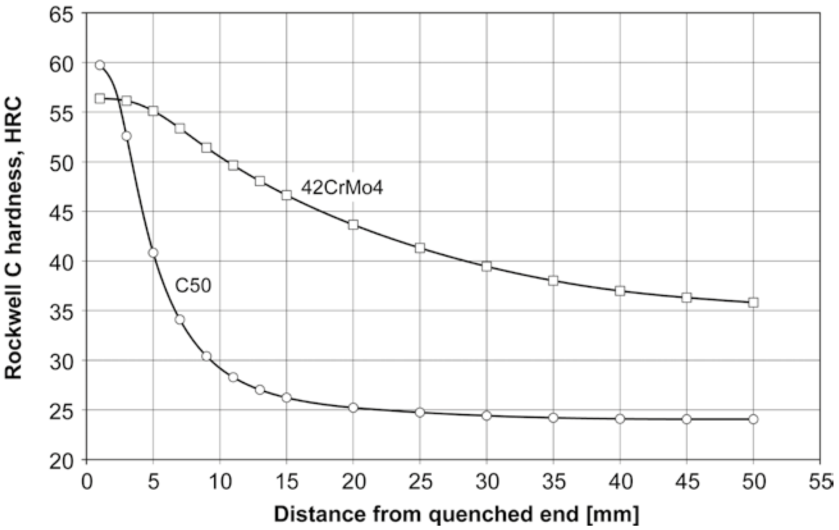

Figure 10.23 - Comparison between the Jominy hardenability curves of an EN C50 steel and an EN 42CrMo4 steel.

10.9 Hardenability and the chemical composition of steel

The hardenability is closelly related to the chemical composition of the steel. In general, the greater the amount of alloying elements, including carbon, the greater the steel hardenability.

The increase in hardenability caused by the alloying elements depends directly on the movement of the T.T.T. and C.C.T. diagrams. Since the addition of alloying elements moves the T.T.T. and C.C.T. diagrams down and to the right, it is easier to form martensite even if the cooling rate is low.

Not all alloying elements, however, have the same effect: chromium, manganese, molybdenum, and vanadium, has a major effect on hardenability while other elements such as nickel, for example, have little effect. Carbon has a mild effect on the steel hardenability, even though it is the alloying element that makes the martensite hard.

Also the mean size of the austenitic grains affects the hardenability: a coarse grain increase the hardenability while a very fine grain reduces it.

Several researchers have worked on numerical correlations between the hardenability of steel and its chemical composition. This work gave rise to several formulas to estimate the Jominy hardenability curve.

A simple example are the formulas proposed by Just[18]. This formulas allow to calculate the hardness along the Jominy sample at distance E (in mm) from the quenched end as a function of the chemical composition of the steel and the mean size of the austenitic grain G[19].

At the quenched end (J_0 , $E = 0$ mm) hardness is only a function of the carbon content[20]. The correlation proposed by Just is [$C < 0.6\%$]:

$$J_0 = 60\sqrt{C} + 20\ HRC \qquad [10.2]$$

At distance $E = 1$ mm from the quenched end (J_1) the result is:

$$J_1 = 60\sqrt{C} + 1.6Cr + 1.5Mn + 16\ HRC \qquad [10.3]$$

At distances between $E = 6$ mm and $E = 80$ mm from the quenched end ($J_{6\text{-}80}$), the result for many of steels (hardened and tempered steel, case hardening steel, spring steel, etc.) is[21]:

$$J_{6-80} = 95\sqrt{C} - 0.0028E^2\sqrt{C} + 20Cr + 14Mn + 6Ni + 38Mo + 6Si + 39V + 96P + \\ - 0.8G - 12\sqrt{E} + 0.9E - 13\ HRC \qquad [10.4]$$

If the values of $J_{6\text{-}80}$ are higher than J_0 or than J_1, $J_{6\text{-}80}$ must be placed equal to the lowest among the values of J_0 o J_1.

A simplified version of [10.4], valid between 6mm and 40mm for hardened and tempered steels, is:

$$J_{6-40} = 102\sqrt{C} + 22Cr + 21Mn + 7Ni + 33Mo - 15.47\sqrt{E} + 1.102E - 16\ HRC \qquad [10.5]$$

while for case hardening steels, it is:

$$J_{6-40} = 74\sqrt{C} + 14Cr + 5.4Ni + 29Mo + 16Mn - 16.8\sqrt{E} + 1.386E + 7\ HRC \qquad [10.6]$$

10.10 Hardenability problems for large-sized workpieces

In case of large-sized workpieces to be heat treated it may be useful to estimate the hardness profile produced by hardening. In these cases, the hardness profile can be estimated using the so-called "Lamont diagrams"[22] (Figures 10.24-10.29).

---

[18] *Just E., Formul der Härtbarkeit, Härterei Technische Mitteilungen, Vol.23 (2), pp. 85-100, 1968 and Just E., New Formulas for Calculating Hardenability Curves, Metal Progress, n. 11, pp. 87-88, 1969.*

[19] *The mean size of the austenitic grain according to the ASTM E112 standard is determined by optical microscopy (the sample is grinded and etched according to specific procedures, for example with the McQuaid-Ehn method). The mean grain size G is the number of grains n that can be observed on a surface of 25.4x25.4mm (inch^2) at 100 magnifications according to the formula $n = 2^{G-1}$. G is an increasing number as the mean grain size decreases. A microstructure with a mean grain size crystallites of an average size equal to 5.6μm corresponds with $G = 12$, 11μm to $G = 10$, 22μm to $G = 8$, 45μm to $G = 6$, 90μm to $G = 4$, 180μm to $G = 2$. Typically, a good quality steel has a mean grain size ranging from $G = 6$ to $G = 10$.*

[20] *The hardness of martensite is only a function of the steel carbon content (Paragraph 8.7 - Figure 8.23). Therefore, if the microstructure is completely martensitic, as in the case of the quenched end of the Jominy sample, the hardness is proportional to the carbon content. In this section the alloying elements have no effect.*

[21] *Just formulas are valid within very vast compositional limits ($C < 0.6\%$, $Cr < 2\%$, $Mn < 2\%$, $Ni < 4\%$, $Mo < 0.5\%$, $V < 0.2\%$).*

[22] *Lamont J.L., How to Estimate Hardening Depth in Bars, Iron Age, vol. 152, pp. 64-70, 1943.*

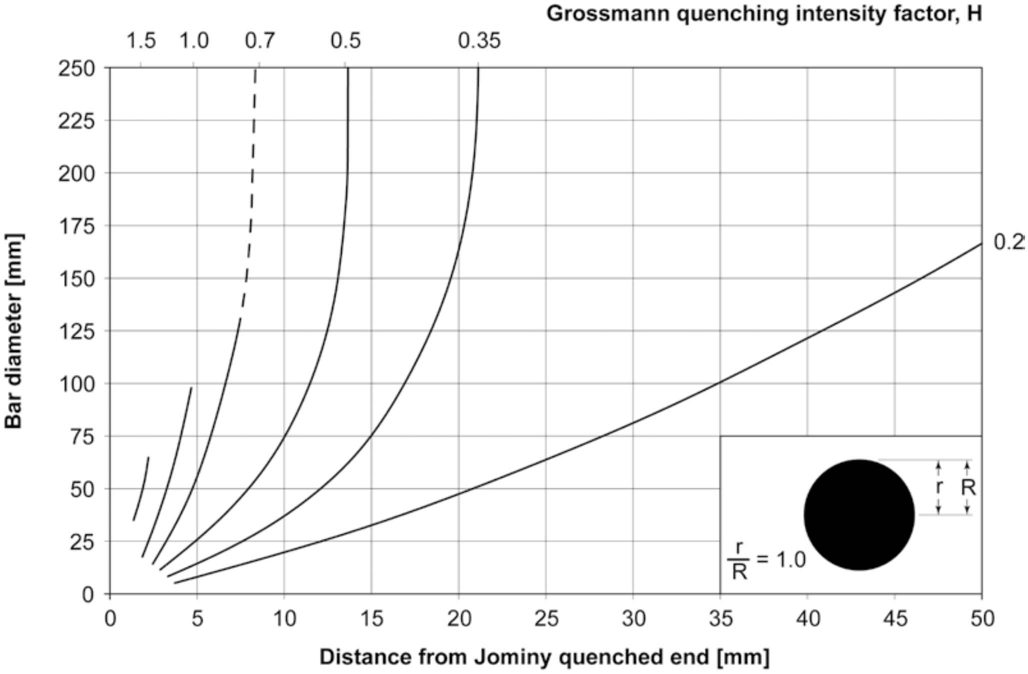

Figure 10.24 - Lamont diagram for points located at distance $r = R$ from the center of the bar of radius R [from Lamont 1943].

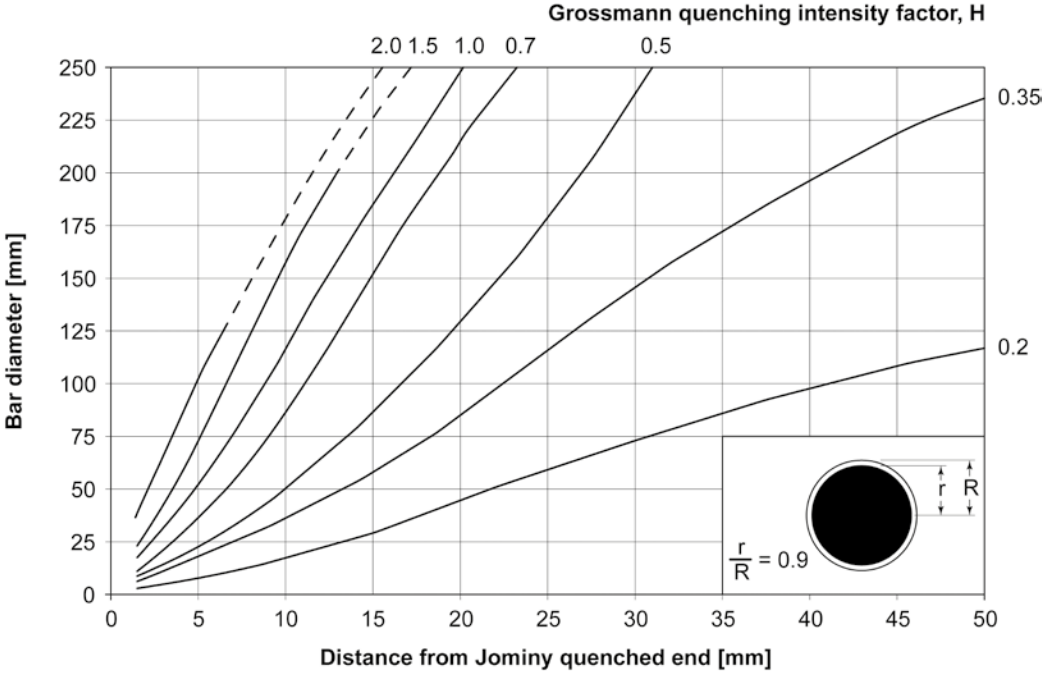

Figure 10.25 - Lamont diagram for points located at distance $r = 0.9 \cdot R$ from the center of the bar of radius R [from Lamont 1943].

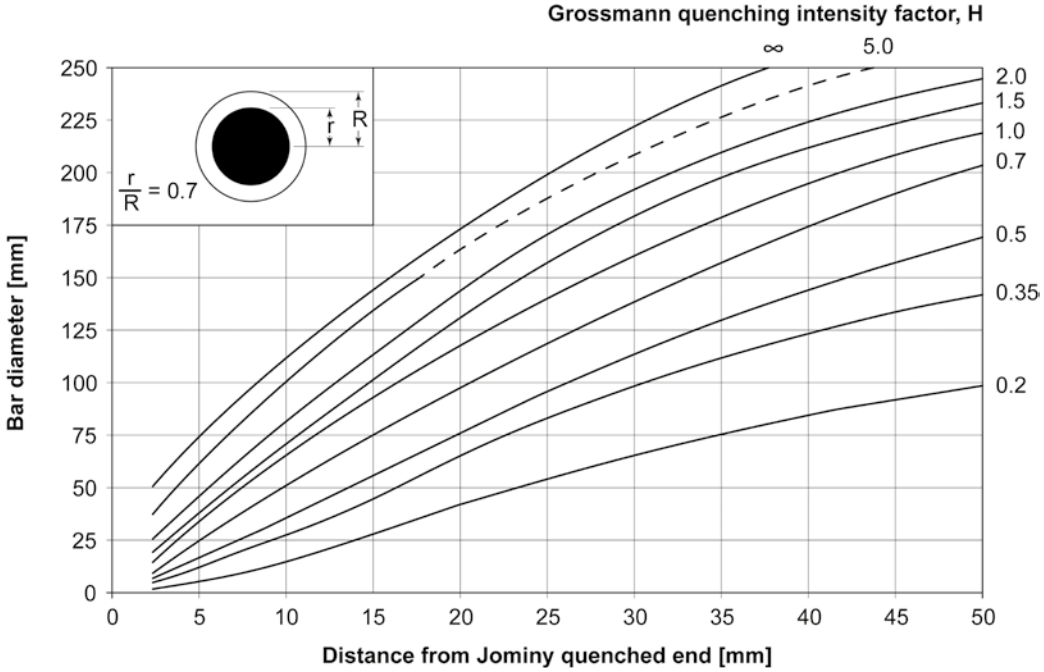

Figure 10.26 - Lamont diagram for points located at distance $r = 0.7 \cdot R$ from the center of the bar of radius R [from Lamont 1943].

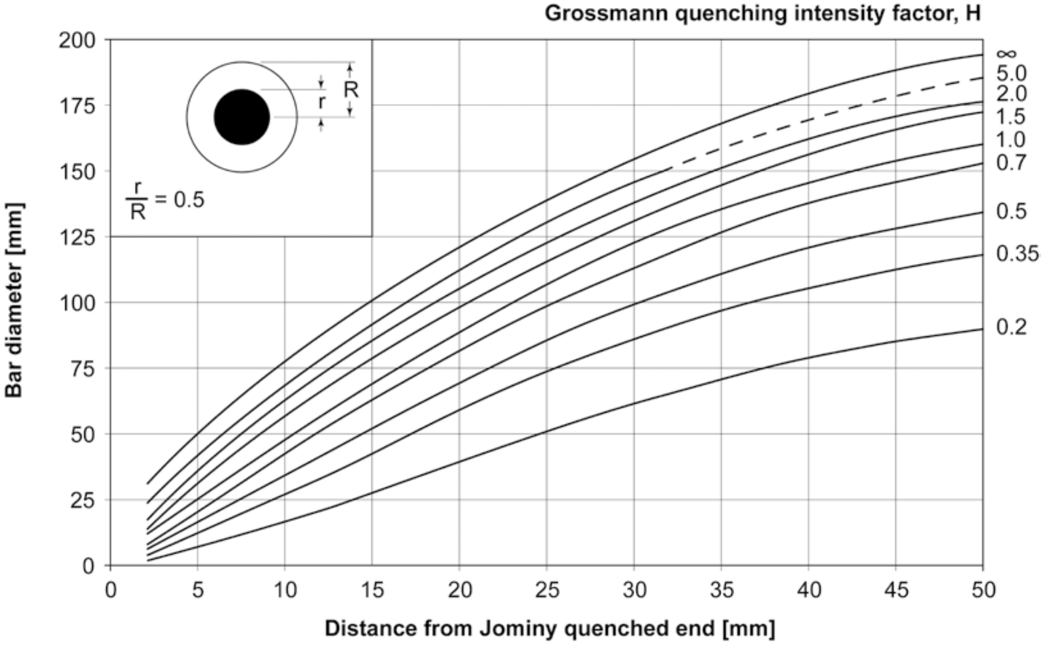

Figure 10.27 - Lamont diagram for points located at distance $r = 0.5 \cdot R$ from the center of the bar of radius R [from Lamont 1943].

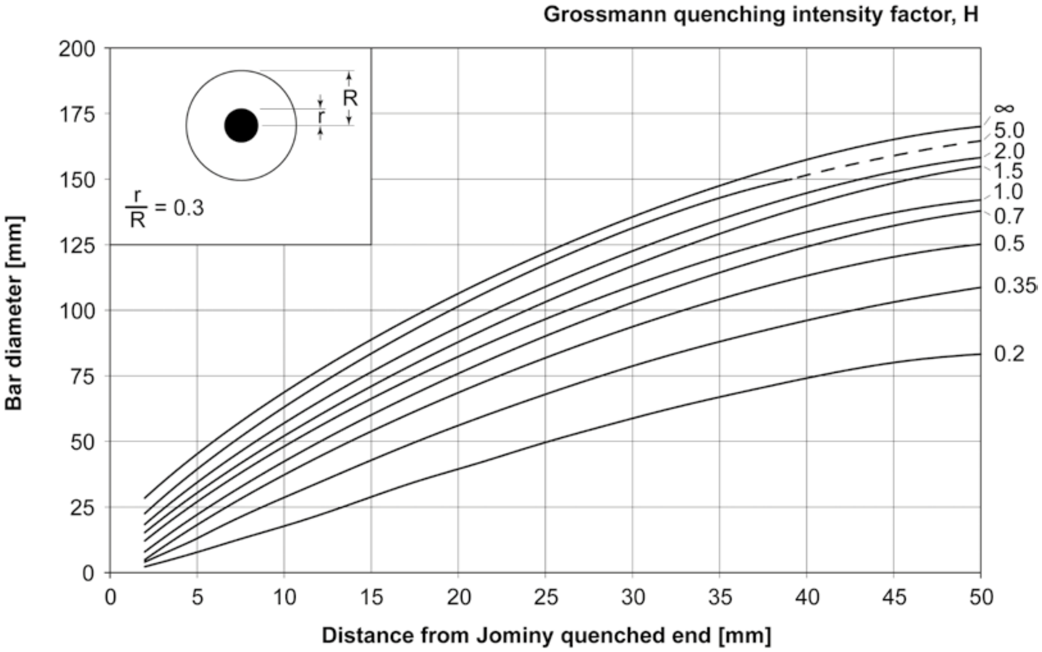

Figure 10.28 - Lamont diagram for points located at distance $r = 0.3 \cdot R$ from the center of the bar of radius R [from Lamont 1943].

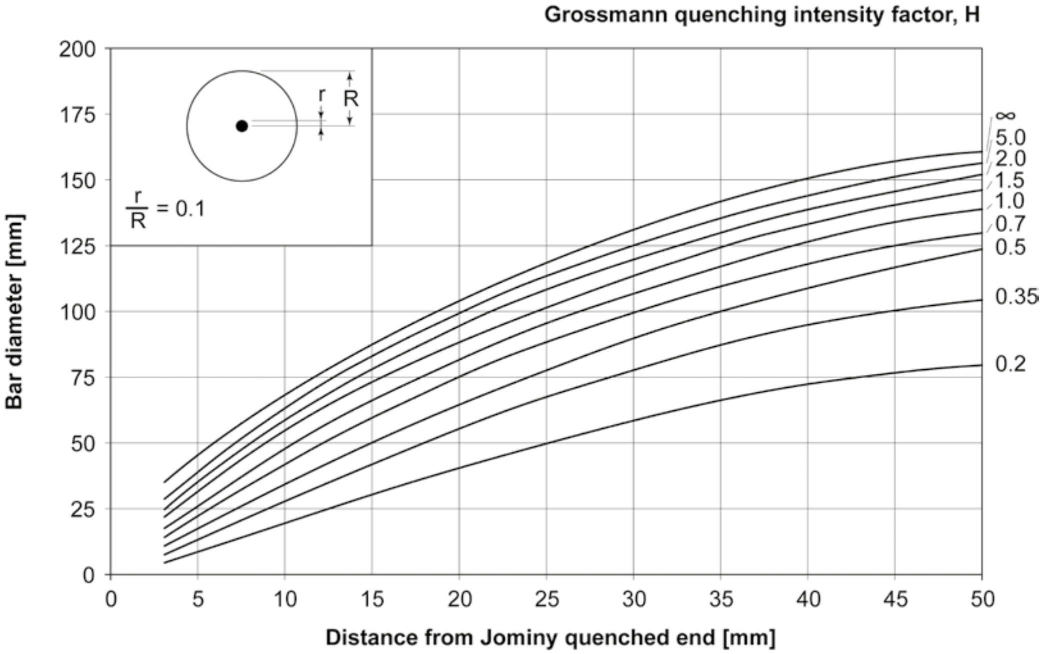

Figure 10.29 - Lamont diagram for points located at distance $r = 0.1 \cdot R$ from the center of the bar of radius R [from Lamont 1943].

The Lamont diagram are very useful because they correlate the hardness along the Jominy hardenability curve (in absicssa) with the hardness along the section of a cylindrical bar of radius R made with the same material of the Jominy sample (in ordinate), when H of the quenching medium varies.

To understand the use the Lamont diagrams let's take an example using Figure 10.25, that represents the generic radial position $\frac{r}{R} = 0.9$.

Let us suppose we want to quench a steel bar of 100 mm in diameter in non-agitated oil ($H = 0.5$): the hardness at 45 mm from the center of the bar (if $Ø = 100mm \rightarrow R = 50mm$ then $r = 0.9 \cdot R = 45mm$) is equal to the hardness that can be read on the Jominy hardeanbility curve at a distance of 17 mm from the quenched end.

10.11 Practical applications of steels hardenability

Some practical application may be helpful in clarifying the use of the Just formulas and the Lamont diagrams.

Case 1

The first problem is to estimate the Jominy hardenability curve of four hardened and tempered steel: EN C40, EN 25CrMo4, EN 39NiCrMo3, and EN 34CrNiMo6.

The nominal composition of the four types of steel is shown in Table 10.2. The Just formulas [equations 10.2, 10.3, and 10.5] can be used to estimate the Jominy hardenability curve starting from the nominal composition (see Figure 10.30).

	C40	25CrMo4	39NiCrMo3	34CrNiMo6
C	0.40	0.25	0.39	0.34
Mn	0.75	0.75	0.80	0.70
Si	0.20	0.20	0.20	0.20
Cr	---	1.00	0.65	1.50
Ni	---	---	0.75	1.30
Mo	---	0.20	0.20	0.20

Table 10.2 - Nominal composition of four hardened and tempered steels EN C40, EN 25CrMo4, EN 39NiCrMo3, and EN 34CrNiMo6.

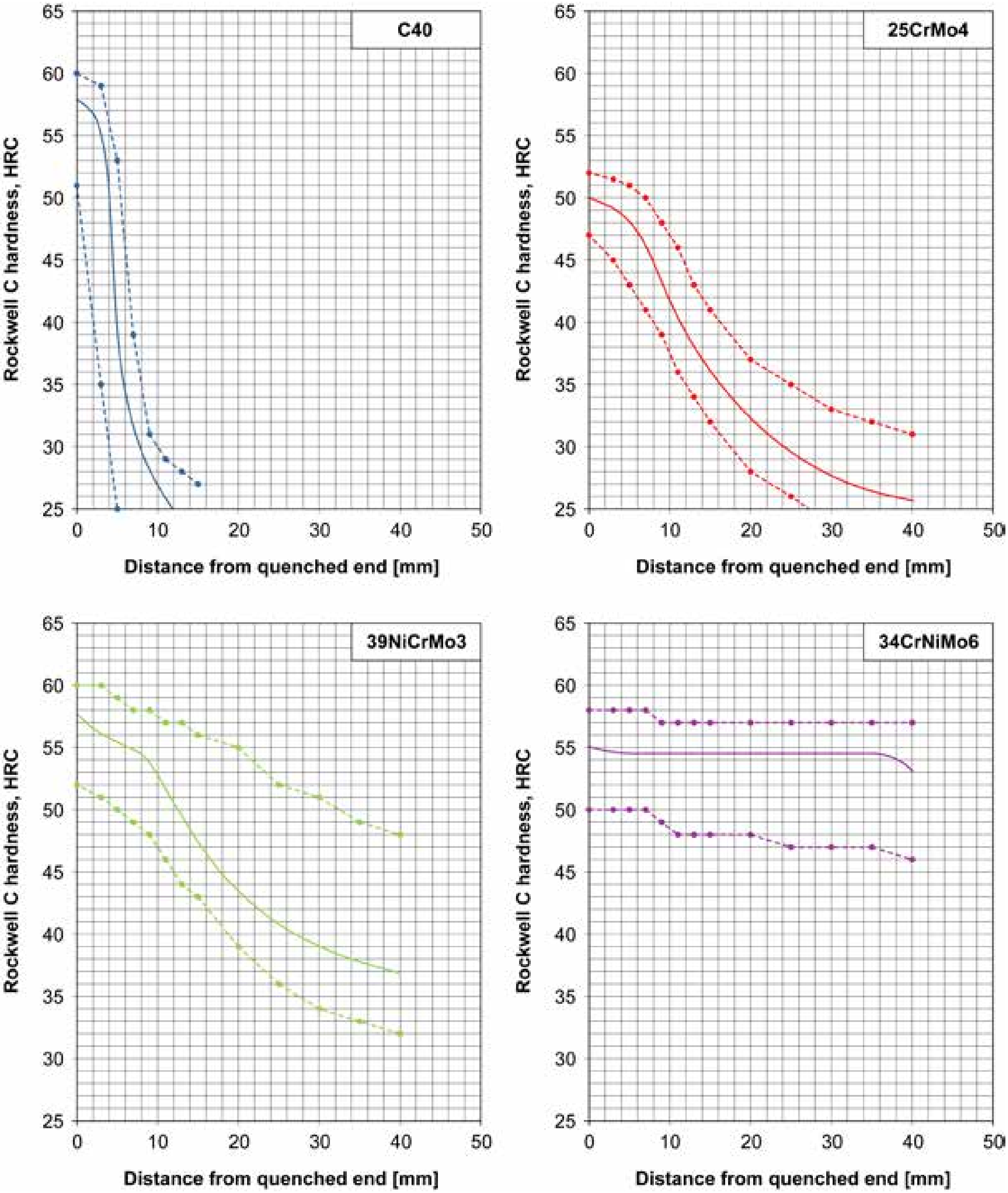

Figure 10.30 - Jominy hardenability curves for EN C40, EN 25CrMo4, EN 39NiCrMo3, and EN 34CrNiMo6 steel: estimate according to the Just formulas (continuous lines), maximum and minimum hardenability limits according to EN 10083 standard (dotted lines).

Case 2

Suppose you have to harden in non-agitated oil ($H = 0.5$, see Table 10.1) two cylindrical bars of 100 mm in diameter, one made of EN 39NiCrMo3 steel and the other made of EN 34CrNiMo6 steel: what you want to know is the radial hardness profile at the end of the hardening.

The problem can be solved by using the Lamont diagrams (Figures 10.24 to 10.29) starting from the result of Case 1 (Figure 10.30[23]).

At first, we consider the EN 39NiCrMo3 steel and refer to the surface of the bar (Figure 10.24). If we use the curve defined by $H = 0.5$ and we enter the value of 100 mm in ordinate, the value of 12 mm is found in abscissa. This means that on the surface of the bar ($r = R$) the hardness is equal to that on the Jominy hardenability curve for EN 39NiCrMo3 steel at 12mm from the quenched end. In this case: 50.5HRC. Similarly, for the other radial positions:

- $r = 0.9 \cdot R$ (r = 45mm) → 17mm → 45.5HRC (Figure 10.25)
- $r = 0.7 \cdot R$ (r = 35mm) → 26mm → 40.5HRC (Figure 10.26)
- $r = 0.5 \cdot R$ (r = 25mm) → 30mm → 39HRC (Figure 10.27)
- $r = 0.3 \cdot R$ (r = 15mm) → 33mm → 38.5HRC (Figure 10.28)
- $r = 0.1 \cdot R$ (r = 5mm) → 35mm → 37.5HRC (Figure 10.29)

On the other hand, if EN 34CrNiMo6 steel is considered:

- $r = R$ (r = 50mm) → 12mm → 54.5HRC (Figure 10.24)
- $r = 0.9 \cdot R$ (r = 45mm) → 17mm → 54.5HRC (Figure 10.25)
- $r = 0.7 \cdot R$ (r = 35mm)→ 26mm → 54.5HRC (Figure 10.26)
- $r = 0.5 \cdot R$ (r = 25mm) → 30mm → 54.5HRC (Figure 10.27)
- $r = 0.3 \cdot R$ (r = 15mm) → 33mm → 54.5HRC (Figure 10.28)
- $r = 0.1 \cdot R$ (r = 5mm) → 35mm → 54.5HRC (Figure 10.29)

The radial hardness profiles of the EN 39NiCrMo3 and EN 34CrNiMo6 steel bars are shown in Figure 10.31. This example highlights that:

- the hardness of EN 39NiCrMo3 steel decreases quickly to a few millimeters from the surface;
- the hardness of steel EN 34CrNiMo6 is substantially constant up to the center of the bar.

These two results are in perfect agreement with the Jominy hardenability curves of the two steel (Figures 10.30): the EN 39NiCrMo3 steel has a decreasing Jominy curve, while the Jominy curve of EN 34CrNiMo6 steel is almost flat, at least for the first 30mm from the quenched end. As already noted the radial hardness profile of a cylindrical steel bar is closely related to the Jominy hardenability curve of the same steel[24].

---

[23] *If available, the actual Jominy hardenability curves of the steel should be used.*

[24] *Be careful not to confuse the hardness profile (along the section of a component or along the Jominy sample) with the absolute value of this mechanical property.*

Figure 10.31 also shows a significant difference between the surface hardness values of the two cylindrical bar.

The surface hardness value of the cylindrical bar made of EN 39NiCrMo3 is much lower than that of the quenched end of the Jominy sample (50.5 HRC has compared to 57.5 HRC).

On the contrary the surface hardness value of the cylindrical bar made of EN 34NiCrMo6 is similar to that of the quenched end (54.5 HRC as compared to 55 HRC).

This difference depends on the different level of hardenability of the two steels.

The EN 34CrNiMo6 steel is much more hardenable than the EN 39NiCrMo3 steel. The higher hardenability favors therefore the formation of martensite also on the surface of the bar even if it is larger than the Jominy sample and the oil's quenching intensity factor is lower than that of water.

This result should not be surprising, the hardness values on the surface of a cylindrical bar is strongly influenced by the hardenability of the steel, as well as by the workpiece size and by the quenching intensity factor of the quenched medium.

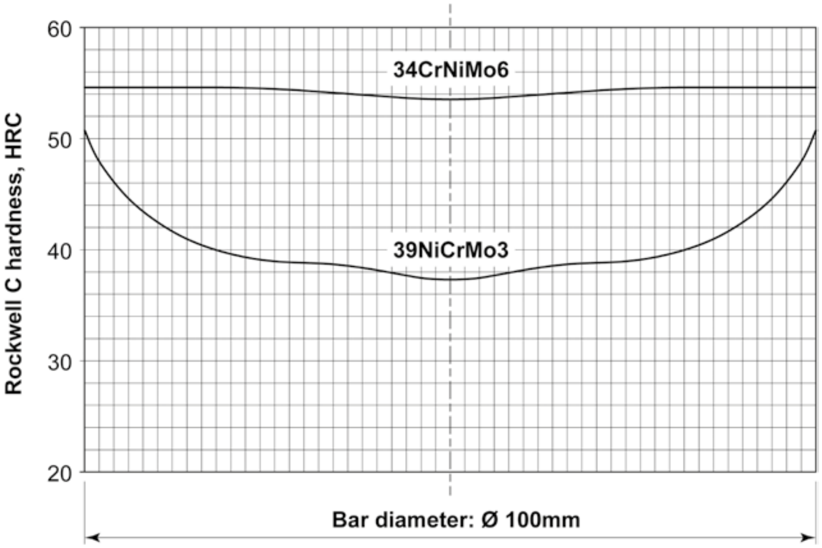

Figure 10.31 - Radial hardness profiles of two bars of 100mm in diameter and made of EN 39NiCrMo3 steel and EN 34CrNiMo6 steel after quenching in non-agitated oil. The radial hardness profiles have been estimated with the Lamont diagrams

.

10.12 Hardening and residual stresses

The austenite-martensite transformation occurs gradually along the section of the component: the transformation begins on the surface and ends in the core of the component.

A direct consequence is the creation of residual stresses at the end of the hardening. In fact, martensite has a specific volume greater than austenite[25] and, if the transformation takes place at distinct times between the core and the surface, residual stresses are invariably created. Apart from special cases, such as large-sized workpieces, the residual stresses are always of tension on the surface and of compression in the core[26]. The phenomenon can be explained in a simplified way by observing Figure 10.32, that shows what occurs in a cylindrical bar during hardening; *S* and *C* represent the cooling curves of the surfaces and of the core of the workpiece.

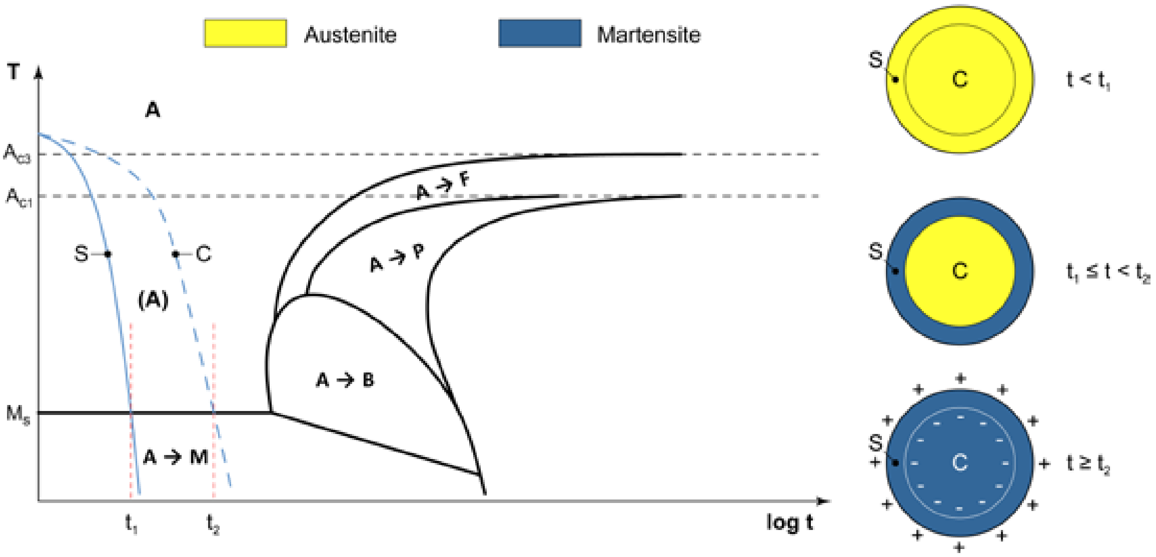

Figure 10.32 - Schematic representation of hardening for a medium/small-sized cylindrical bar made of a generic hypoeutectoid steel. The cooling curve of the surfaces *S* and the core *C* are superimposed on the C.C.T. diagram.

When time t is less than t_1, both the surface and the core are at a high temperature and have an austenitic microstructure: internal stresses are practically nil. Beyond t_1 and up to t_2 only the surface forms martensite, while the core still has an austenitic microstructure.

---

[25] *The transformation of austenite into bainite, pearlite, ferrite, or cementite always produces an increase of the specific volume of the steel. However, the austenite-martensite transformation causes the greatest volumetric variations.*

[26] *See Note 4 of Chapter 4.*

At this stage any increase in volume are easily compensated by the austenite. Also in this second case, the residual stresses are practically nil.

Beyon the time t_2, the surface has a martensitic microstructure, while the core is still transforming. In this condition, the increase in volume of the core is obstructed by the martensite at the surface. The result is a thrust towards the surface, and the subsequent formation of tensile stresses that are compensated by the formation of compressive stresses in the core.

The level of residual stresses increases with the increase of the cooling rate, that depends on:

- the quenching procedures (the higher the quenching intesity factor of the quenching medium, the higher the residual stresses);
- the size and the shape of the semi-finished products (the larger the component and/or the more complex the shape, the higher the residual stresses).

If the stress level is too high, permanent distortions and/or cracks may occur, which can make the workpieces useless (Figure 10.33). This is one of the reasons why it is necessary to temper the as-quenched martensite, as described in Chapter 11.

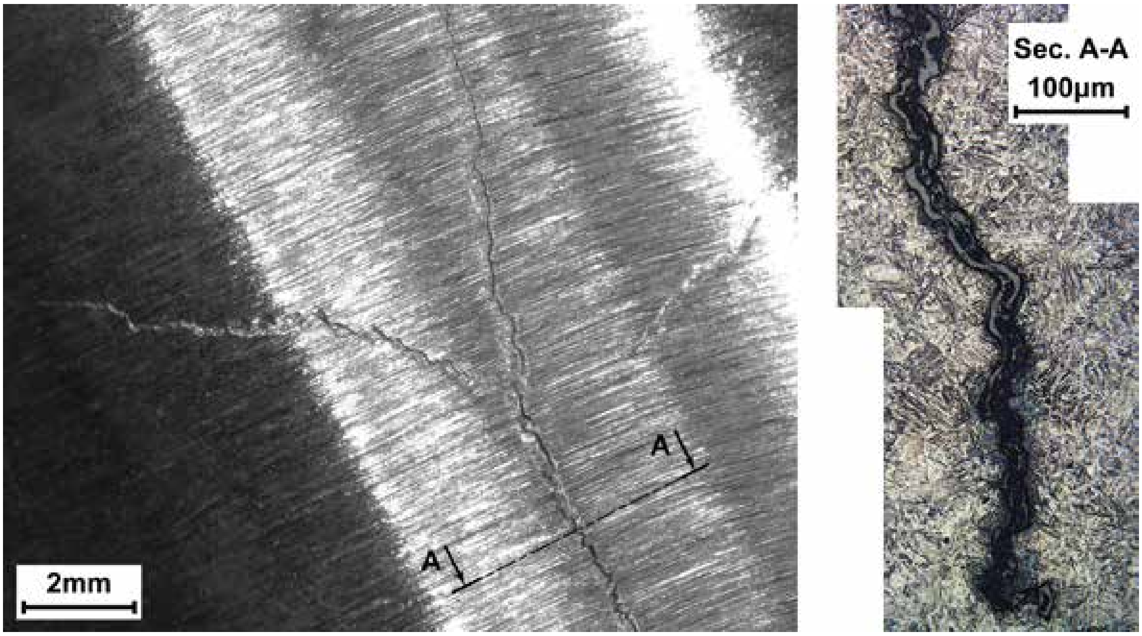

Figure 10.33 - Cracks in an EN 42CrMo4 steel bar after hardening: to the left, the outer surface, to the right, the microstructure along section A-A [Laboratori del Dipartimento di Meccanica del Politecnico di Milano - Milano].

To limit residual stresses, steel should be chosen following the same rules used for hardenability. Large-sized components must be produced with very hardenable steel so that they can be cooled by using quenching media with a low quenching intensity factor; medium or small-sized components, on the other hand, can be produced with steel that is not very hardenable and cooled by using quenching media with a high quenching intensity factor.

10.13 Martempering and Austempering

The level of residual stresses produced by hardening can be drastically reduced by using to alternative heat treatments: martempering and austempering. Martempering is similar to classic hardening. The difference lies in the cooling phase, which is carried out using a thermal bath of molten salts at a temperature higher than M_s[27].

The holding time in the salt bath is long enough to equalize the temperature within the component, without intercept the bainitic transformation area on the T.T.T. diagrams.

Finally, when the temperature is uniform the component is cooled in oil or in air up to room temperature. The austenite-martensite transformation occurs only during the final part of the cooling phase. (Figure 10.34).

The goal of martempering is to slow down cooling before austenite-martensite transformation, in order to equalize the temperature within the workpiece. In this way the austenite-martensite transformation occurs almost simultaneously along the whole section of the component. Martempering limits therefore the residual stresses and the permanent deformations of the component, reducing the risk of cracks during the heat treatment.

After martempering, the microstructure is made of martensite, in the case of hypoeutectoid steels, or martensitic plus carbides in the case of hypereutectic steels. The microstructure has a high toughness with a low level of internal stresses and tempering can be carried out at a low temperature (See Chapter 11).

Martempering is a heat treatment that requires specific plants for its execution and, therefore, it has higher costs than traditional hardening and tempering. Martempering is carried out on semi-finished products of small or medium size or on components with. Martempering is also used for the heat treatment of tool steel, in order to prevent deformation or distortion.

---

[27] *The temperature of M_s is between 200°C-350°C in relation to the type of steel, as calculated with the formulas proposed in Paragraph 7.5 of Chapter 7.*

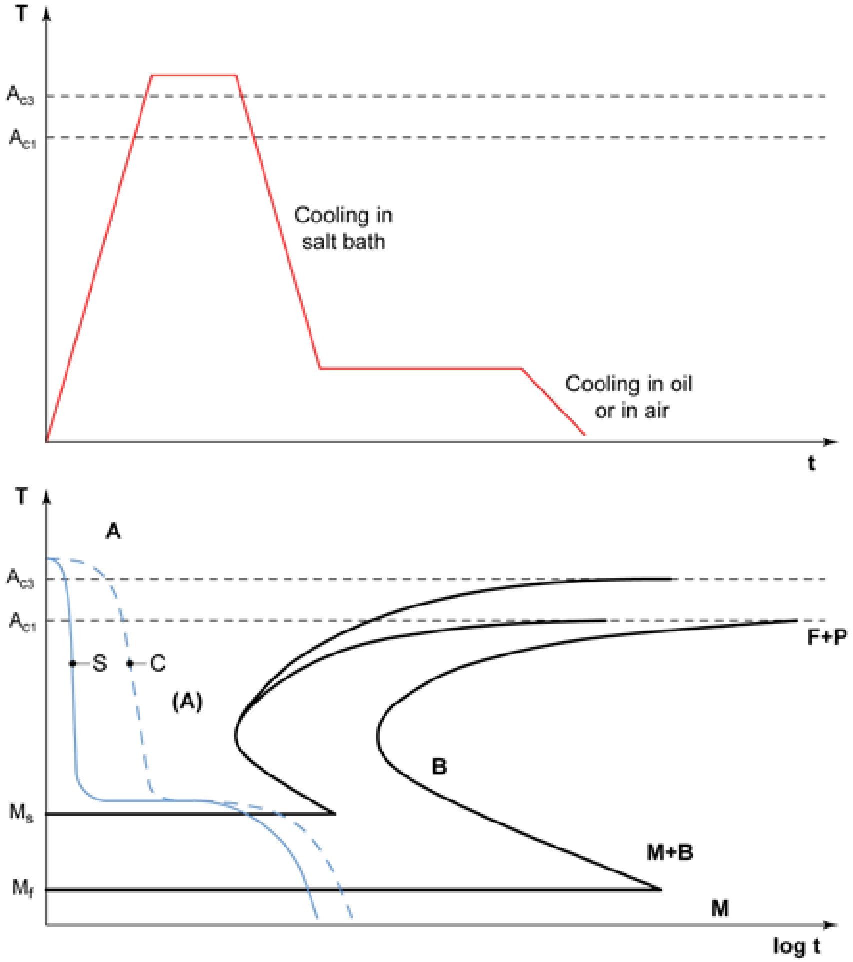

Figure 10.34 - Schematic representation of martempering for a generic hypoeutectoid steel (on the top). The cooling curve of surfaces *S* and core *C* are superimposed on the T.T.T. diagram (on the bottom).

Austempering is similar to martempering: steel is heated above the critical points and then cooled in a molten salt bath at a temperature slightly above M_s. In the case of austempering, however, the workpiece is holded in the salt bath until the isothermal transformation of the austenite into bainite is completed (Figure 10.35). After austempering, tempering is not required.

The goal of austempering is both to limit the permanent deformations and the risk of cracks of the component, as well as to improve its mechanical properties. After the heat treatment the microstructure is made of very fine bainite characterized by higher mechanical properties, as compared to martensite after hardening and tempering.

Austempering is used for the same types of steel and components that are heat treated with martempering. Also the costs are similar and are higher than those of a traditional hardening and tempering.

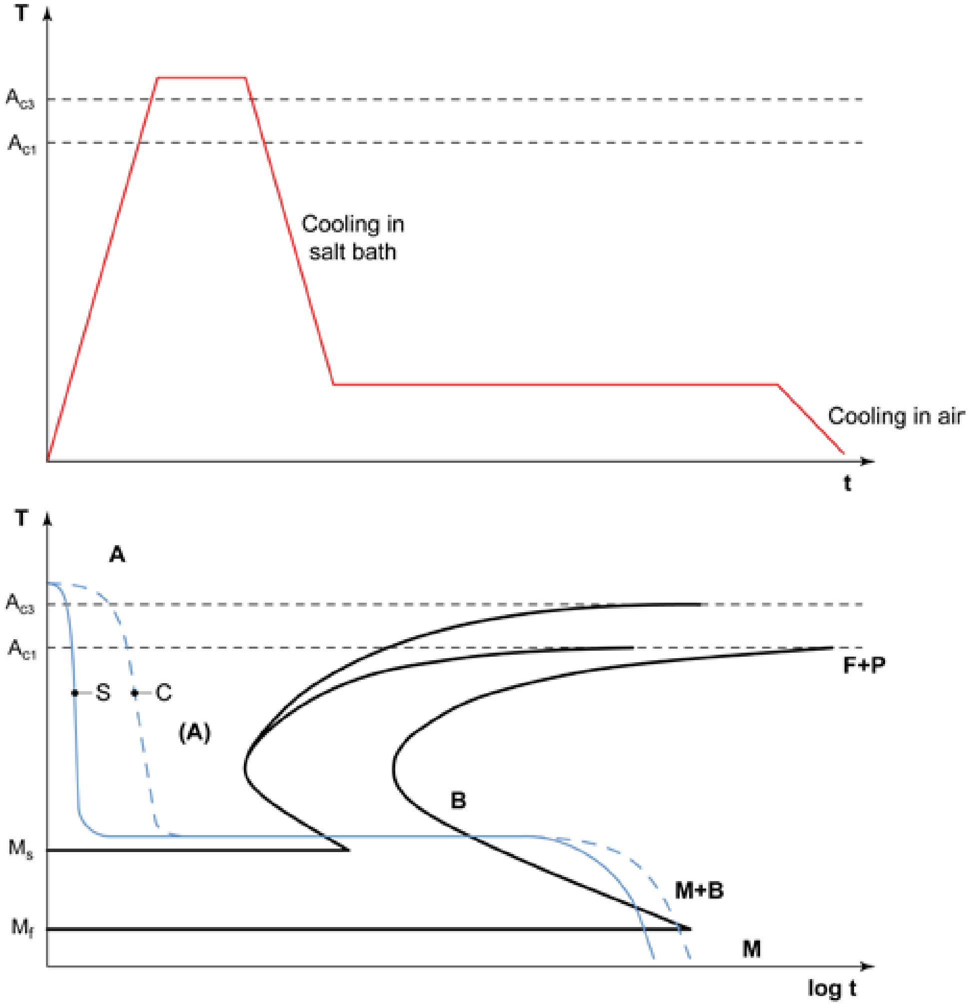

Figure 10.35 - Schematic representation of austempering for a generic hypoeutectoid steel (on the top). The cooling curve of surfaces *S* and core *C* are superimposed on the T.T.T. diagram (on the bottom).

11. HEAT TREATMENTS BELOW CRITICAL POINTS

11.1 Classification of subcritical treatments

Subcritical heat treatments have always the holding temperature below critical points and, therefore, they do not have the γ-phase $\rightarrow$ α-phase transformation. Consequently, at the end of the heat treatment the steel microstructure is almost unchanged. The subcritical heat treatments are divided into two categories:

- heat treatments that work on pearlitic-ferritic microstructure;
- heat treatments that work on martensitic microstructure.

At the first group was given the name of subcritical annealing, while at the second one was given the name of tempering. In both cases the soaking temperatures are similar, what makes the difference are the microstructural changes that occur during the heat treatment.

11.2 Subcritical annealing

The name subcritical annealing is used for various heat treatments. These heat treatments are quite similar (Figure 11.1) and their results are mainly a function of the type of component to be treated and the microstructural changes that occur. The subcritical annealing are commonly divided into three categories:

- annealing for machinability: this heat treatment is performed to reduce the hardness in order to increase the machinability of the steel;
- stress-relief annealing: this heat treatment is performed to reduce residual stresses caused by previous manufacturing processes (i.e. welding, machining, etc.);
- recrystallisation annealing: this heat treatment is performed to reduce the level of cold work caused by previous manufacturing processes (i.e. drawing, cold rolling, etc.).

There are also heat treatments similar to subcritical annealing, but with a very specific goal: a typical example is hydrogen annealing[1], which is performed to reduce the hydrogen content in casted or forged semi-finished products.

Annealing for machinability

The annealing for machinability has a holding temperature of 30°C-50°C below critical point A_{c1}. The holding time is instead a function of the microstructural changes that you want to create in the steel.

---

[1] *The hydrogen annealing has very long holding time (a several dozen hours) at temperatures between 600°C and 650°C, in order to favour the diffusion of hydrogen out from the semi-finished products (typically casted or forged workpieces).*

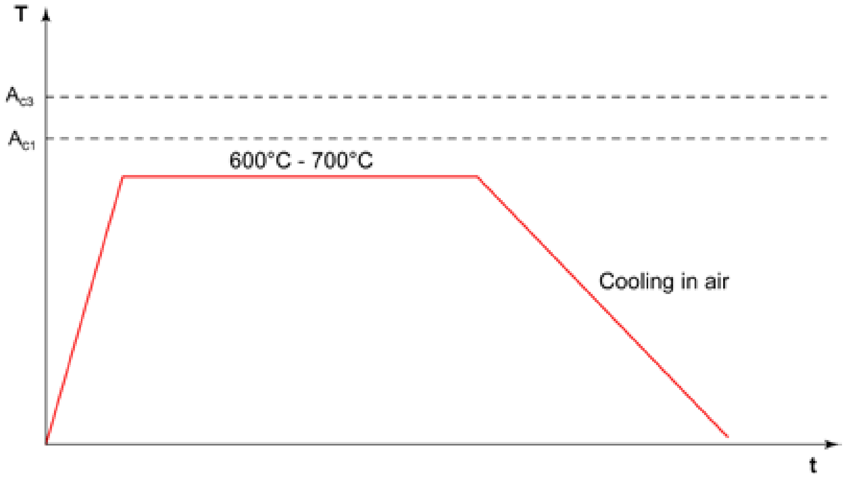

Figure 11.1 - Schematic representation of subcritical annealing.

Typically, the annealing for machinability has a holding temperature between 600°C and 700°C and a holding time of 2-4 hours. At the end of soaking, slow cooling is carried out in furnace or in air.

The main goal of annealing for machinability is to modify the shape of the Fe_3C phase from lamellar to globular, in order to reduce the hardness and increase the machinability of the ferritic-pearlitic microstructure (Figure 11.2). However, if compared to spheroidising[2], the coalescence level of the Fe_3C phase is lower and is never complete.

Generally annealing for machinability is carried out after normalising; often, however, this heat treatment is carried out on forged or laminated semi-finished products, immediately after hot working. In these cases, the non-homogeneities of the steel (segregation bands, chemical composition non-homogeneities, etc.) remain unaltered. Consequently, after annealing for machinability, the new microstructure is affected by original non-homogeneities.

Stress-relief annealing

Stress-relief annealing is similar to annealing for machinability. The main goal of this heat treatment is to remove the residual stresses induced by previous manufacturing processes.

---

[2] *See paragraph 10.3 of Chapter 10.*

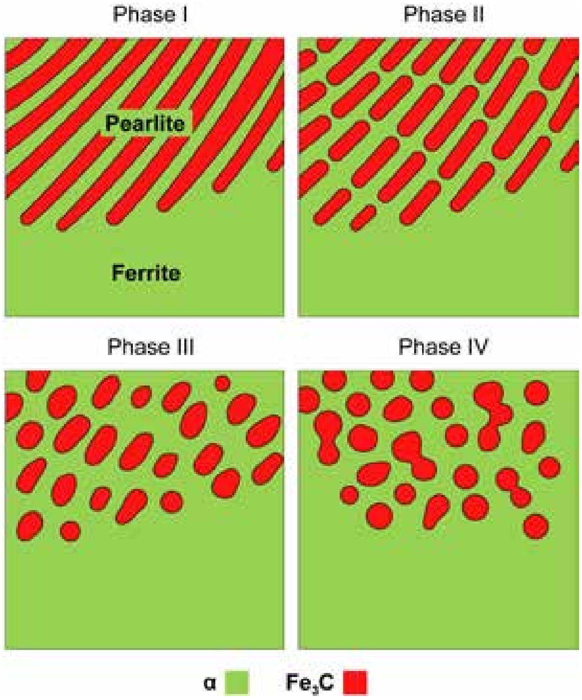

Figure 11.2 - Decomposition process of the *Fe_3C* phase from lamellar to globular. Phases II and III show the typical result of annealing for machinability, instead Phase IV shows the typical result of spheroidising [from Higgins 1993].

In the case of steel castings or after heavy mechanical machining, it is useful to carry out stress-relief annealing at temperatures between 600°C and 700°C for a few hours. Subsequently, the component is cooled in furnace up to 400°C and then in air. These subcritical treatments are performed to avoid brittle fracture or to limit the degradation phenomena caused by residual stresses[3].

Post weld heat treatments (P.W.H.T.) are also a type of subcritical annealing and are carried out to remove residual stresses and to improve the resistance to brittle fractures of welding structures (Figure 11.3).

---

[3] *Stress Corrosion Cracking is a degradation phenomenon that affect components with residual tensile stresses, made of a specific material and in contact with a specific aggressive environment. The elimination of one of these three factors makes the corrosive phenomenon impossible to happen (for a closer look, see Boniardi M., Casaroli A., Stainless Steels, ed.Lucefin, Esine, 2014).*

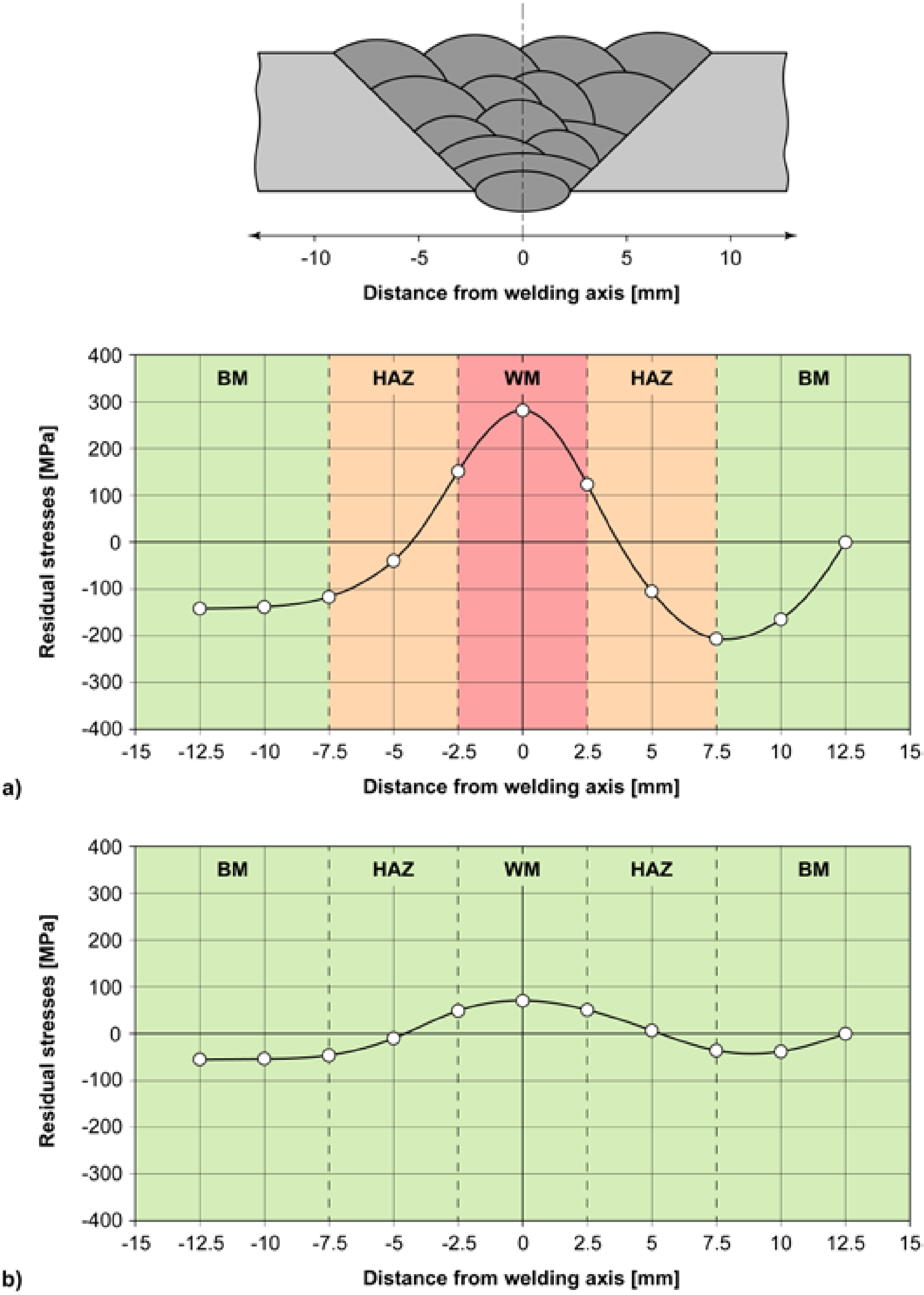

Figure 11.3 - Residual stresses field along the longitudinal direction of a welded joint made of low carbon steel: (a) before and (b) after stress-relief annealing at 650°C for 2 hours. The steel has been preheated at 250°C-300°C and the welding has been made with automatic submerged arc welding.

Recrystallisation annealing

If the steel is cold work, subcritical annealing always triggers recovery, recrystallisation, and grain growth phenomena described in Chapter 4. In these cases, the heat treatment is called recrystallisation annealing. Recrystallisation annealing can be carried out at different temperatures and holding times, as a function of the desired level of recovery, recrystallisation, and grain growth. The initial level of strain hardening has a great influence on the final result (Figure 11.4). In general, the mean grain size increases (Figure 11.5):

- as the annealing temperature increases,
- as the holding time increases,
- as the strain hardening level of the steel decreases[4].

Recrystallisation annealing is very important in cold deformation processes because it restore the original deformability level of the steel. For example, during drawing or cold rolling, the strain hardening levels can exceed the permissible limit of the material, causing the component to break. In these cases, recrystallisation annealing is required to continue to reduce the section.

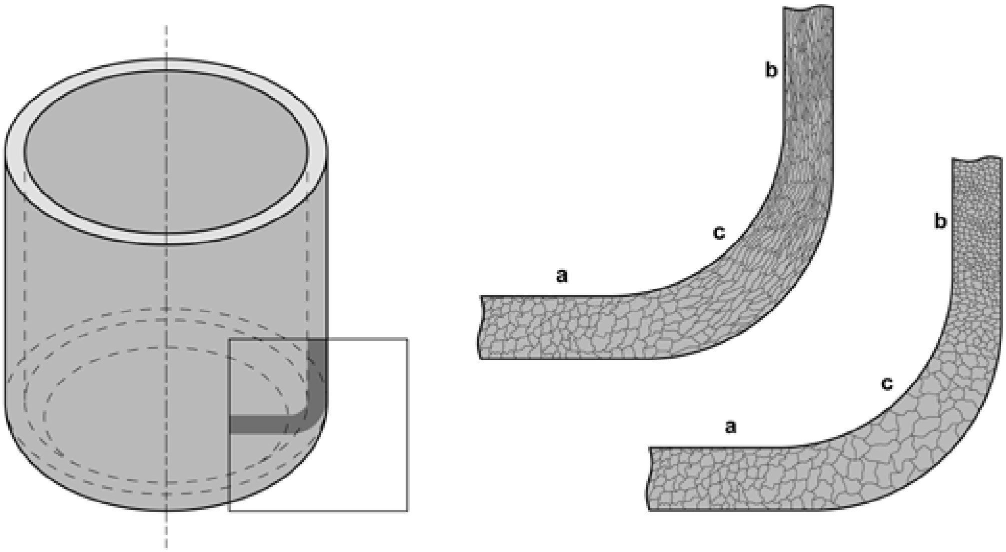

Figure 11.4 - Schematic representation of the mean grain size in a deep-drawn component before and after recrystallisation annealing: (a) in the bottom area the strain hardening is nil and therefore the recrystallisation is also nil; (b) in the side area the strain hardening is high and therefore the recrystallisation produces a very fine grain; (c) in the middle area the strain hardening level is lower than the side area but higher than the bottom one. In this area recrystallisation produces grains larger than the original ones [from Higgins 1993].

---

[4] Recrystallisation does not occur at any strain hardening level. In fact, recrystallisation starts only if a critical cold deformation threshold (called χ_{min} in Figure 11.5) is exceeded.

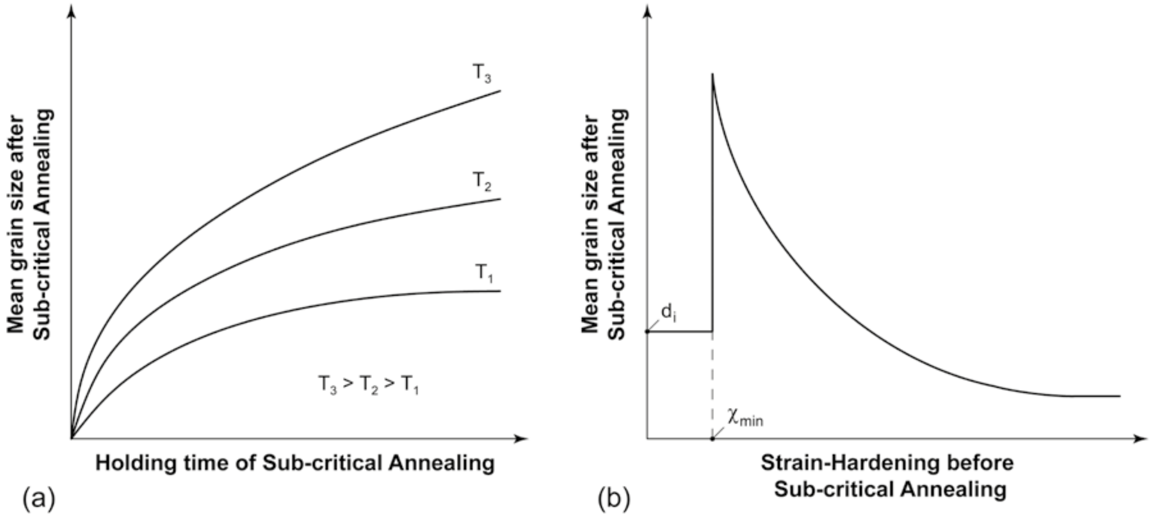

Figure 11.5 - The effect of holding temperature/time (a) and strain hadrening level on mean grain size after recrystallisation (d_i is the mean grain size before strain hardening; χ_{min} is the minimum level of strain hardening that activates recrystallisation).

11.3 Tempering

The as-quenched martensite[5] is very hard and, above all, very brittle and characterized by high level of residual stresses. Therefore, the workpieces cannot be immediately used after hardening, since they would risk sudden breakage. To overcome these problems, it is important to carry out another heat treatment after hardening, the so called "tempering".

Tempering should be started immediately after hardening, in order to limit the risk of cracks caused by residual stresses. Ideally, components should be tempered when they are not completely cool (50°C-70°C). Tempering has a slow heating up to a temperature below the critical points. Generally a preheated furnace is used[6]. The heating time is a function of the workpiece size and the type of the furnace.

---

[5] *Generally, during hardening, austenite does not transform completely into martensite. The amount of martensite is a function of the hardenability of the steel and the cooling rate of the workpiece. Therefore, the considerations in Paragraph 11.3 relate only to portions of material where martensite is formed.*

[6] *If, for example, the heating temperature is equal to 600°C, it may be useful to preheat the furnace at temperatures of 250°C to 300°C. However, if the steel has high conductivity (i.e. carbon steel) and the components have not complex shape, it is also possible to set the furnace at maximum temperature without preheating.*

The typical soaking temperature is between 600°C and 650°C, even if soaking temperatures between 150°C and 200°C or 400°C and 460°C[7] are also used. In fact, the holding temperature and the holding time are a function of the required mechanical strength at the end of the sub-critical annealing. Tempering ends with cooling in air, or sometimes in oil (Figure 11.6).

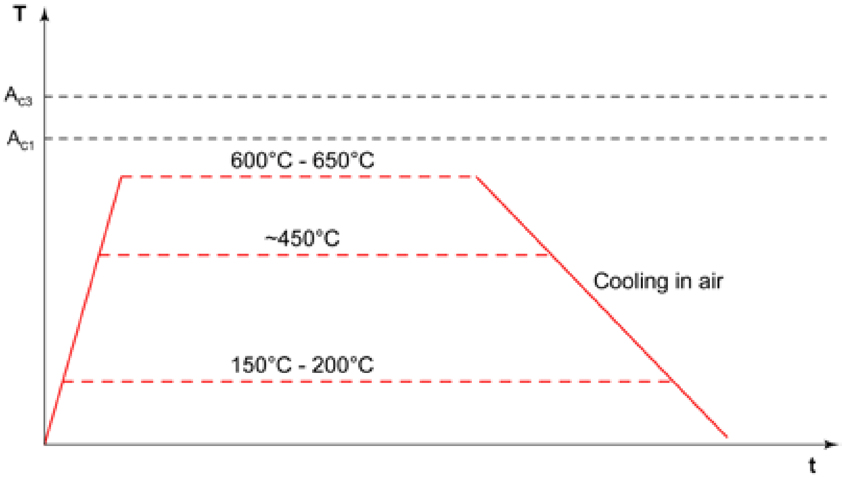

Figure 11.6 - Schematic representation of tempering.

Tempering has two important goals:

- remove the typical brittleness of the as-quenched martensite;
- reduce the residual stresses caused by hardening.

These results are due to the microstructural changes that occur during tempering. Starting at 80°C, carbon diffuses out from the tetragonal lattice of the as-quenched martensite.

As a result, the as-quenched martensite transforms into "tempered martensite". This microstructure has a body-centered cubic lattice and is characterized by a toughness level higher than as quenched martensite; in fact, when the temperature increases, the lattice parameter c_α decreases until it becomes equal to the parameter a_α (Figures 8.20 and 8.22).

The diffusion of carbon out from the tetragonal lattice of the as-quenched martensite causes the formation of carbides. If temperature is between 100°C and 200°C carbides are made of $Fe_{2\div3}C$ phase (ε carbides) while if temperature is between 200°C and 400°C carbides are made of Fe_3C phase and their shape is acicular.

---

[7] Tempering between 250°C and 380°C or between 480°C and 570°C causes the embrittlement of the tempered martensite. In both cases, after tempering, steel is very brittle and shows low impact strength. Therefore, tempering should never be performed at these temperatures.

At temperature between 450°C and 650°C carbides are still made of Fe_3C phase but their shape becomes globular. Finally, at temperature over 600°C carbides coalesce together, increasing in size. Tempering also causes the transformation of retained austenite, which turns to bainite for temperatures between 200°C and 400°C, or to martensite for temperature between 450°C and 650°C. The Figure 11.7 shows both a schematic representation of what previously described, as well as, the effect of tempering temperature on hardness of different iron-carbon alloys.

Alloying elements can influence the end result of tempering. Silicon and manganese counteracts the softening effect[8] since they delay the formation of carbides of Fe_3C phase. Chromium, molybdenum, vanadium, tungsten, and titanium form carbides harder than martensite, which preserve their hardness at high temperature and reduce the softening effect. Other chemical elements, such as nickel, have instead very limited effect on softening.

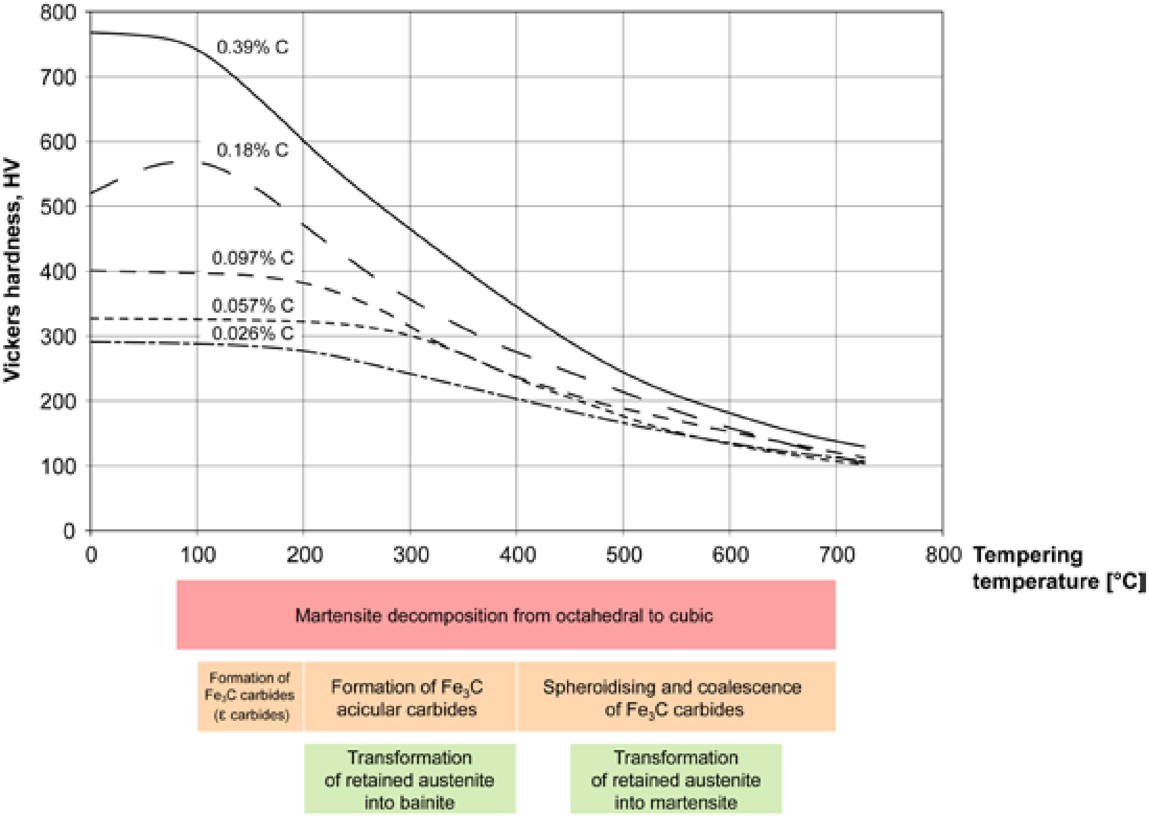

Figure 11.7 - The effect of tempering temperature (holding time:1 hour) on the hardness of different iron carbon alloys [from Speich 1969].

---

[8] *The term "softening" refers to the decay of hardness of steel components exposed to high temperature (up to ~500°C), such as tool steels.*

The tempering temperature has an important effect on all the engineering properties of steel. Figures 11.8 and 11.9 show the effect of tempering temperature on tensile strength, yield strength, elongation at fracture and impact strength of two commonly used hardened and tempered steels (EN C40 and EN 39NiCrMo3). As is typical of all hardened and tempered steels, when the tempering temperature increases, hardness and tensile strength decrease (R_m and $R_{p0.2}$) while elongation at fracture and impact strength increase.

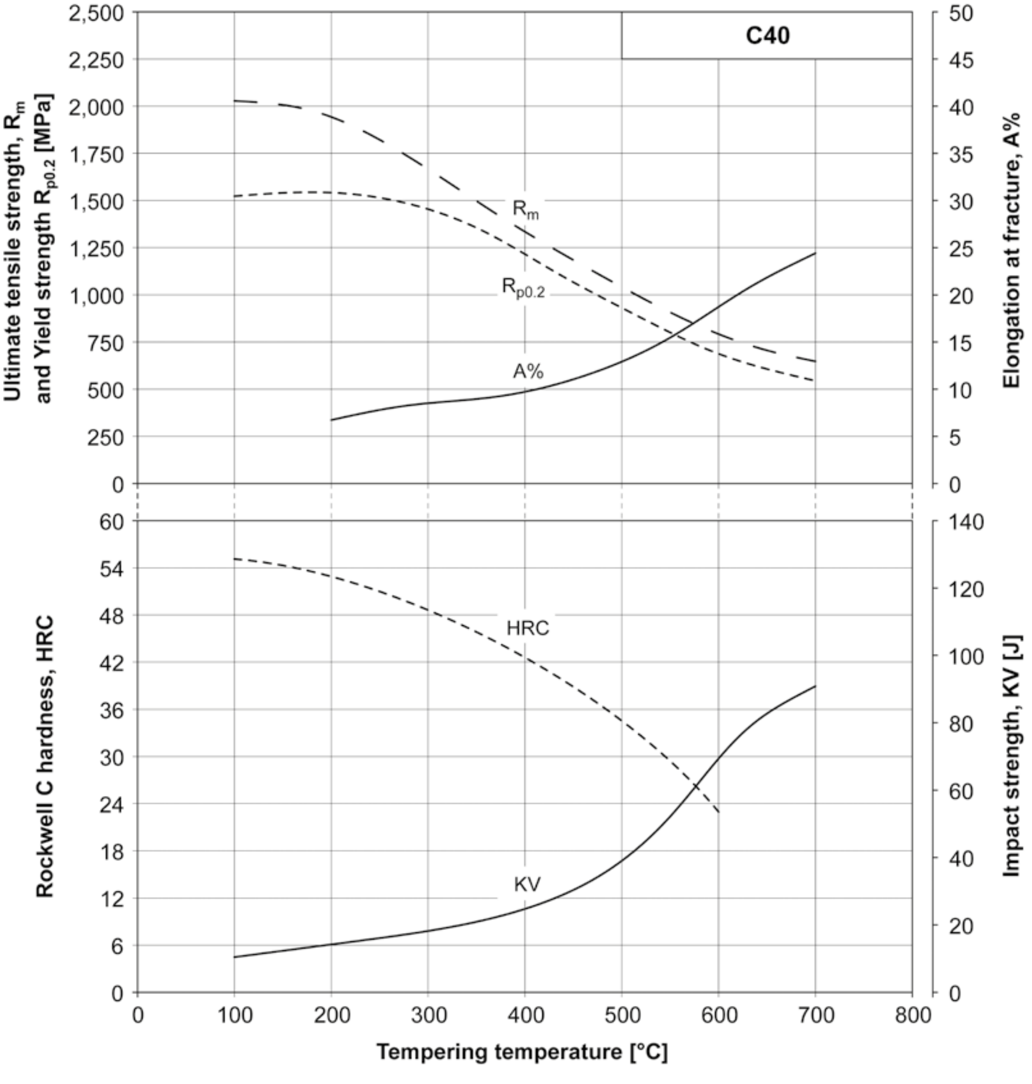

Figure 11.8 - The effect of tempering temperature on tensile strength (R_m and $R_{p0.2}$), elongation at fracture (A%), Rockwell C hardness (HRC), and impact strength (KV) of an EN C40 steel (cylindrical bars of 10mm in diameter austenitized at 840°C for 1 hour and hardened in water). [Laboratori del Dipartimento di Meccanica del Politecnico di Milano - Milano].

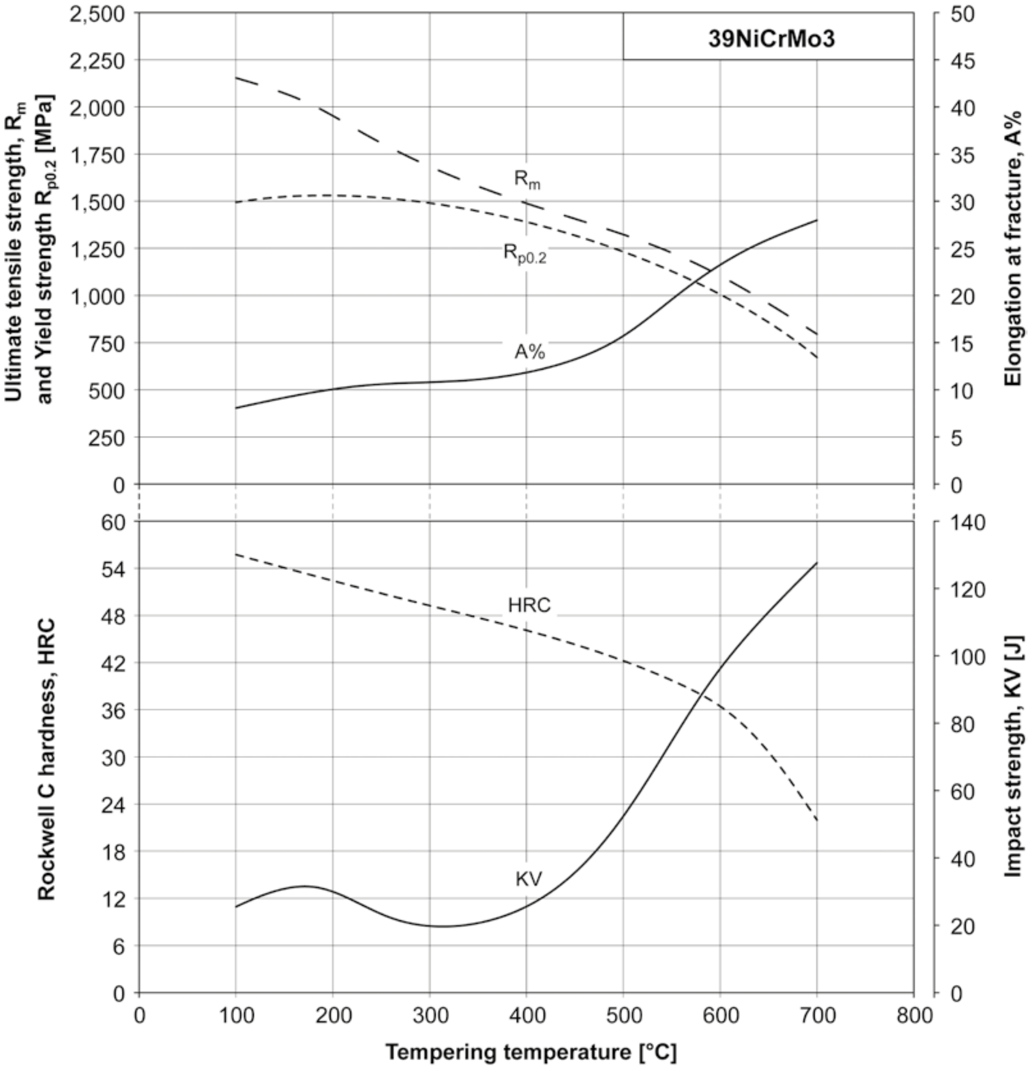

Figure 11.9 - The effect of tempering temperature on tensile strength (R_m and $R_{p0.2}$), elongation at fracture (A%), Rockwell C hardness (HRC), and impact strength (KV) of an EN 39NiCrMo3 steel (cylindrical bars of 10mm in diameter austenitized at 850°C for 1 hour and hardened in oil). [Laboratori del Dipartimento di Meccanica del Politecnico di Milano - Milano].

Tempering has another important effect: the progressive decrease of residual stresses. Figures 11.10 and 11.11, show the effect of tempering temperature on the level of residual stresses, which is practically nil for tempering temperatures between 550°C and 600°C.

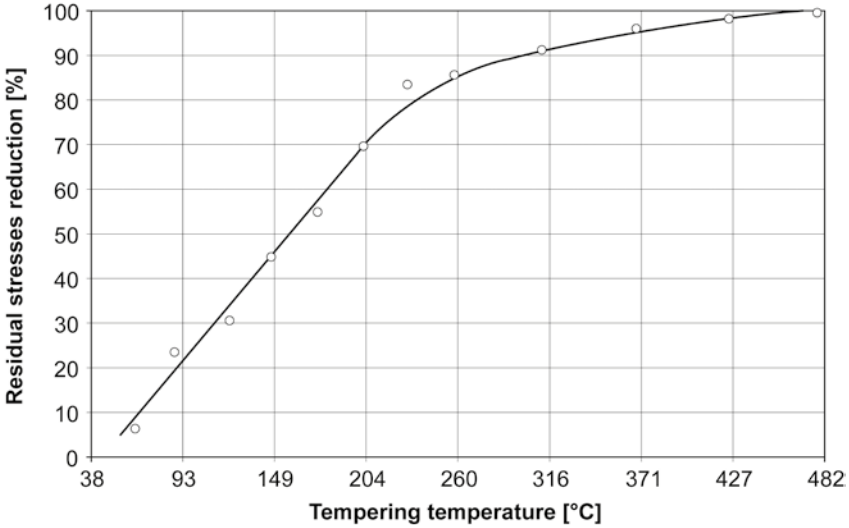

Figure 11.10 - The effect of tempering temperature on the level of residual stresses for a bearing steel (EN 100Cr6). The holding time is equal to 1 hour. [from Brown and Cohen 1962].

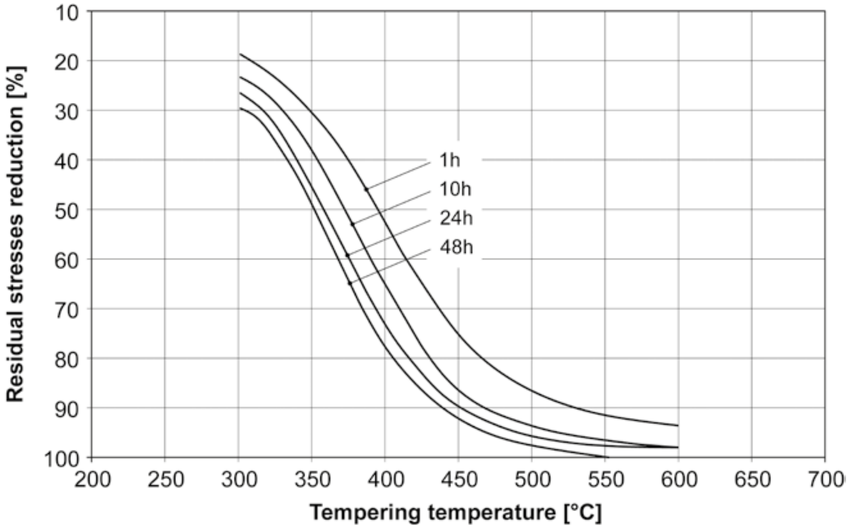

Figure 11.11 - The effect of tempering temperature and holding time on the level of residual stresses for an hardened and tempered steel [Spur and Stöferle 1980-1994].

11.4 Estimation of hardness after tempering

The hardness of tempered martensite can be estimated by various calculation methods. Here the formulas proposed by Hollomon and Jaffe[9] is presented. These formulas are valid for carbon steel but, thanks to the studies carried out by Grange and Baughman[10], their use has also been extended to low alloy steels. The calculation method proposed by Hollomon and Jaffe is based on the experimental evidence that the hardness of tempered martensite is a function of a parameter called the Hollomon-Jaffe Parameter and indicated with the letter P. The P parameter depends in turn on temperature and holding time of tempering, according to the equation:

$$P = 1.8 \cdot T \cdot (C + log_{10}t) \cdot 10^{-3} \qquad [11.1]$$

where T is the tempering temperature in Kelvin, t is the soaking time in hours, and C is a constant (for many steels C = 18). Figure 11.12 shows the effect of P parameter and carbon content on hardness of tempered martensite. If the steel has other alloying elements, other than carbon, the previously estimated hardness value must be increased by the ΔH quantity, which is defined by the equation 11.2:

$$\Delta H = f_{Mn} \cdot Mn + f_{Si} \cdot Si + f_{Ni} \cdot Ni + f_{Cr} \cdot Cr + f_{Mo} \cdot Mo + f_V \cdot V \qquad [11.2]$$

The concentration of each alloying element must be multiplied by its f_{El} coefficients taken from Table 11.1. However, this calculation method does not apply to steel showing the secondary hardness phenomenon (see Paragraph 11.5).

Case 1

We would like to know the hardness after hardening and tempering at 600°C for 2 hours on an EN C40 and EN 39NiCrMo3 steels; their nominal composition is shown by Table 11.2.

First of all, you have to evaluate the P parameter. From equation 11.1, we have:

$$P = 1.8 \cdot (600 + 273) \cdot (18 + log_{10}2) \cdot 10^{-3} \cong 28.76$$

The Figure 11.12 shows that, for C = 0.39% and P = 28.76, the Vickers Hardness of C40 steel after tempering is equal to[11]:

$$H_{C40} \cong 245\ HV$$

---

[9] *Hollomon J.H., Jaffe L.D., Time-temperature relations in hardened and tempered steel, Transactions of AIME, vol. 162, pp. 223- 249, 1945.*

[10] *Grange R.A., Baughman R.W., Hardness of tempered martensite in carbon and low alloy steels, ASM Transactions, vol. 48, pp.165- 197, 1956.*

[11] *The manganese and the silicon contents are not to be considered because they are lower than those given in Table 11.1. For these quantities the effect of the two alloying elements is already considered in the carbon effect shown by Figure 11.12.*

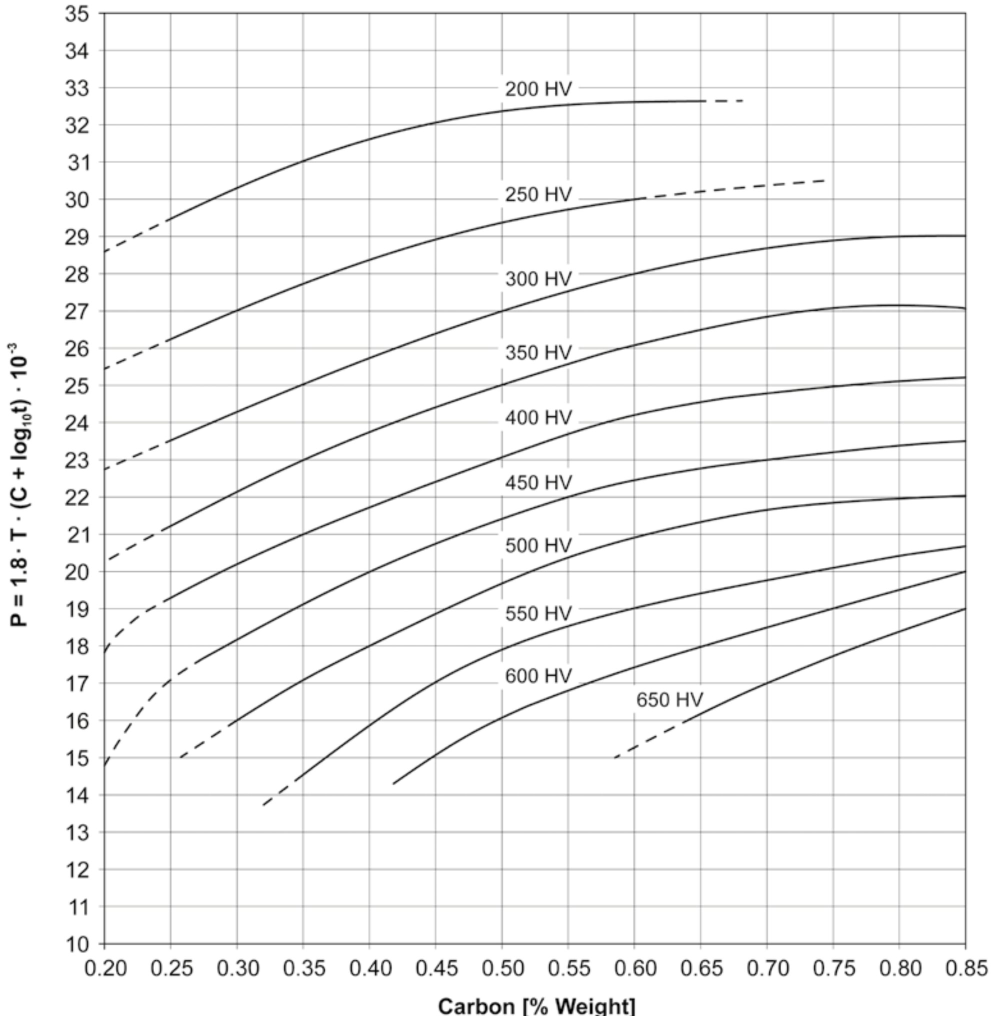

Figure 11.12 - The effect of *P* paramiter and carbon content on hardness of tempered martensite [from Hollomon and Jaffe 1945].

In case of 39NiCrMo3 steel, the effect of alloying elements must be evaluated (the effect of carbon is the same because the content of carbon is the same for both types of steel).
The coefficients to be used in formula 11.2 are taken from table 11.1. Since $P = 28.76$ the effect of alloying element (ΔH) is between:

$$\text{for} \quad P = 28 \;\rightarrow\; \Delta H = 8 \cdot 0.75 + 55 \cdot 0.65 + 120 \cdot 0.2 = 65.75$$
$$\text{for} \quad P = 30 \;\rightarrow\; \Delta H = 6 \cdot 0.75 + 55 \cdot 0.65 + 105 \cdot 0.2 = 61.25$$

The linear interpolation between the two values is equal to:

$$\Delta H = 64$$

Therefore, the hardness after tempering of an EN 39NiCrMo3 steel is equal to:

$$H_{39NiCrMo3} = 245 + 64 \cong 310 \; HV$$

		Value of parameter *P*					
Element	**level %**	**20**	**22**	**24**	**26**	**28**	**30**
Manganese (*Mn*)	0.85-2.1	35	25	30	30	30	25
Silicon (*Si*)	0.3-2.2	65	60	30	30	30	30
Nickel (*Ni*)	0-4	5	3	6	8	8	6
Chromium (*Cr*)	0-1.2	50	55	55	55	55	55
Molybdenum (*Mo*)	0-0.35	40 20*	90 45*	160 80*	220 110*	240 120*	210 105*
Vanadium (*V*)**	0-0.2	0	30	85	150	210	150

Notes
** Use these factors if the chromium content is between 0.5% and 1.2%*
*** Use these factors for low alloy steels with chromium or chromium-vanadium; not valid for steels where vanadium is the only carbide forming element.*

Table 11.1 - The f_{El} coefficients for various alloying elements in relation to parameter *P* [from Grange and Baughman 1956].

	C40	**39NiCrMo3**
C	0.39	0.39
Mn	0.75	0.80
Si	0.20	0.20
Cr	---	0.65
Ni	---	0.75
Mo	---	0.20

Table 11.2 - Nominal composition of EN C40 steel and EN39NiCrMo3 steel.

Case 2

In this second example we would like to know the holding time t_x of a tempering carried out at 550°C on an EN 39NiCrMo3 steel, so that the hardness is the same as in previous Case 1, i.e. $H_{39NiCrMo3} \cong$ 310 HV (tempering at 600°C for two hours). Since we want the same hardness values, the *P* parameter must remain constant:

$$P_{550°C,\,t_x} = P_{600°C,\,2h} = 28.76$$

$$1.8 \cdot (550 + 273) \cdot (18 + log_{10}t_x) \cdot 10^{-3} = 28.76$$

Developing the calculations, the following occurs:

$$1{,}481.4 \cdot (18 + log_{10}t_x) = 28{,}760$$

$$log_{10}t_x \cong 1.41407$$

$$t_x \cong 25h\ and\ 56min$$

These result allow to estimate the effect of temperature and holding time on the effectiveness of tempering. In fact, case 2 shows an increase in soaking time of almost 13 times (from 2 hours to about 26 hours) if the temperature is reduced by 50°C (from 600°C to 550°C). Note that the hardness of tempered martensite is the same in both cases 1 and 2.

11.5 Tempering of high alloy steel and secondary hardness

Tempering produces always a progressive decrease in hardness of carbon or low alloy steel. However, if the steel has alloying elements such as chromium, molybdenum, tungsten, vanadium, and titanium, the metal mass forms very hard and very small carbides, during tempering. These carbides are uniformly dispersed in martensitic microstructure and act as obstacles to the dislocation motion, increasing the hardness of steel. This phenomenon is called secondary hardness to distinguish it from primary hardness of martensite.

This phenomenon is due to the greater affinity for carbon that the above mentioned alloying elements have as compared to iron. In fact, at high temperature the carbide forming elements favour the decomposition of Fe_3C carbides, forming at the same time stable carbides of MC type (i.e. VC, TiC and WC), M_2C type (i.e. Mo_2C and W_2C), M_6C type (i.e. Fe_3W_3C and Fe_3Mo_3C), and $M_{23}C_6$ type (i.e. $Cr_{23}C_6$), much harder than Fe_3C carbides (Figure 11.14).

The secondary hardness phenomenon generally occurs at temperatures between 400°C and 600°C, with a peak value of the hardness around 550°C. To this regard, Figure 11.15 shows the secondary hardness effect for several types of tool steels after hardening and three tempering[12].

The secondary hardness phenomenon is extremely important to reduce the softening effect that occurs in steels exposed to high temperature (up to ~500°C), such as tool steels. In fact, without the secondary hardness phenomenon, there would be a progressive decrease in hardness and a consequent loss of wear resistance.

---

[12] *Steel with significant quantities of alloying elements has a rather large amount of retained austenite, due to the downward shift of the horizontal line of martensite finish, Mf (see Paragraph 7.5 of Chapter 7). It is, therefore, necessary to perform repeated tempering, in order to transform the retained austenite into martensite.*

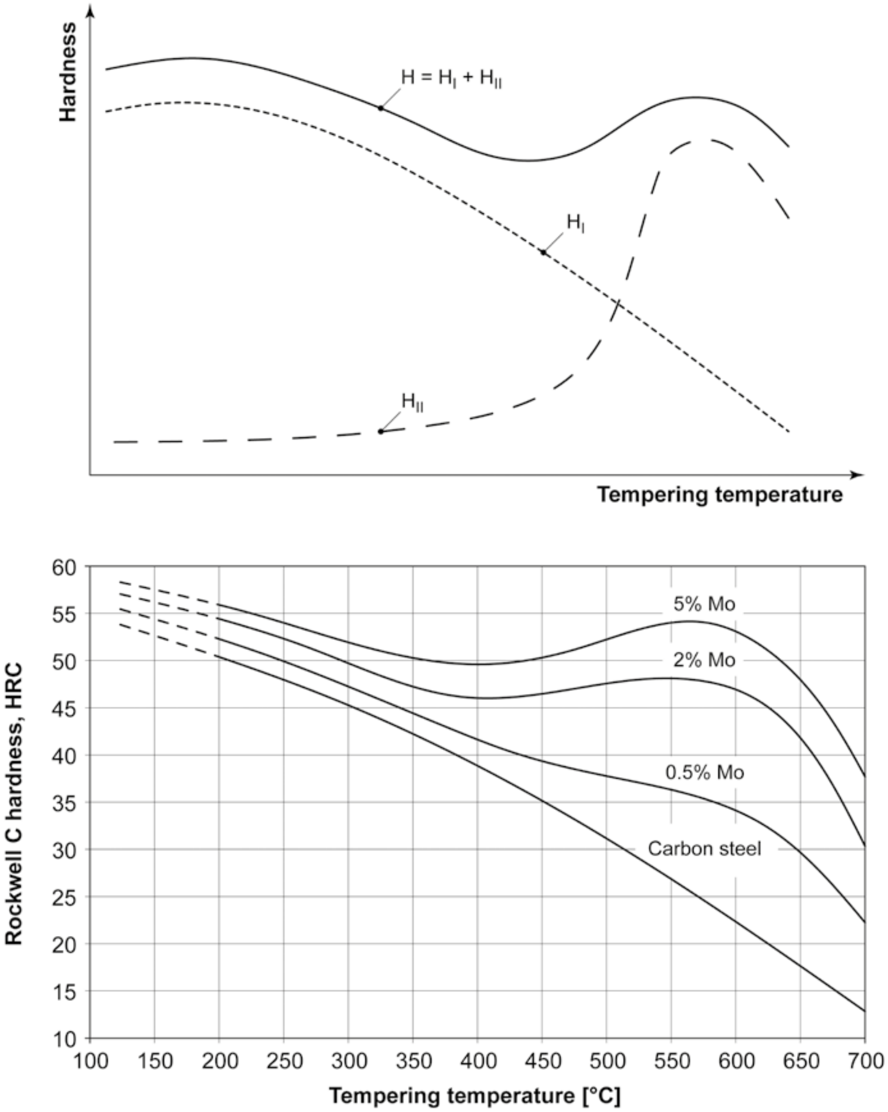

Figure 11.13 - (top) Schematic representation of the primary and secondary hardening effects (H_I: primary hardness due to solid solution of carbon in martensite; H_{II}: secondary hardness due to carbide precipitation; $H = H_I + H_{II}$: final steel hardness after tempering); (bottom) Example of the phenomenon for steels containing increasingly amount of molybdenum [from ASM-H4 1991].

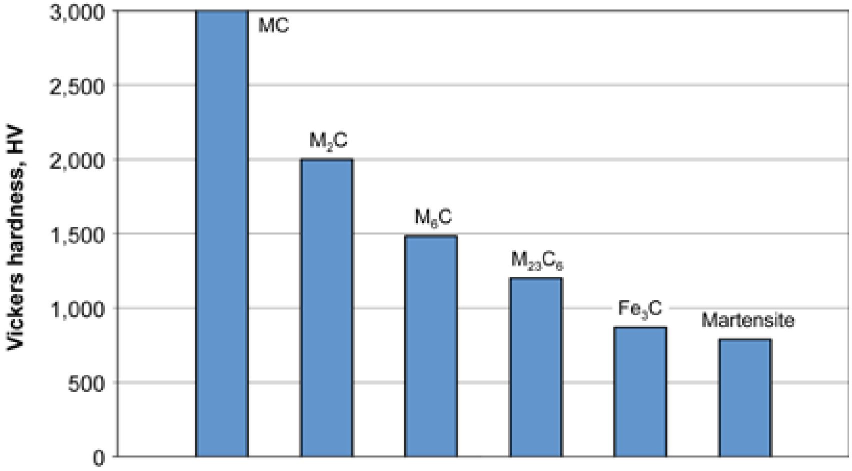

Figure 11.14 - Hardness of different types of carbides compared to martensite [from Wells and Lherbier 1980].

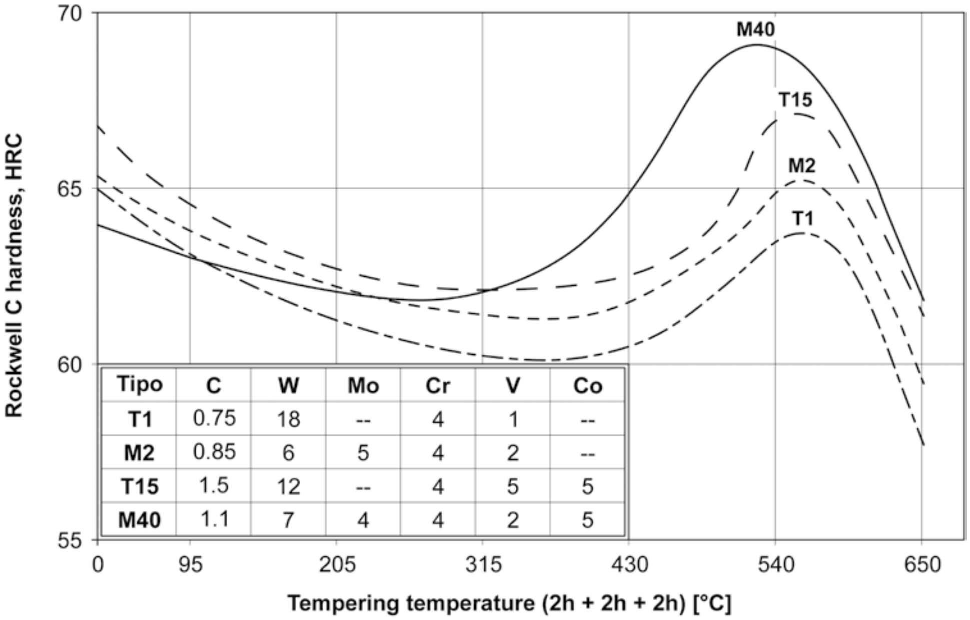

Tipo	C	W	Mo	Cr	V	Co
T1	0.75	18	--	4	1	--
M2	0.85	6	5	4	2	--
T15	1.5	12	--	4	5	5
M40	1.1	7	4	4	2	5

Figure 11.15 - Hardness for several types of tool steels after hardening and three tempering [from Hoyle 1988].

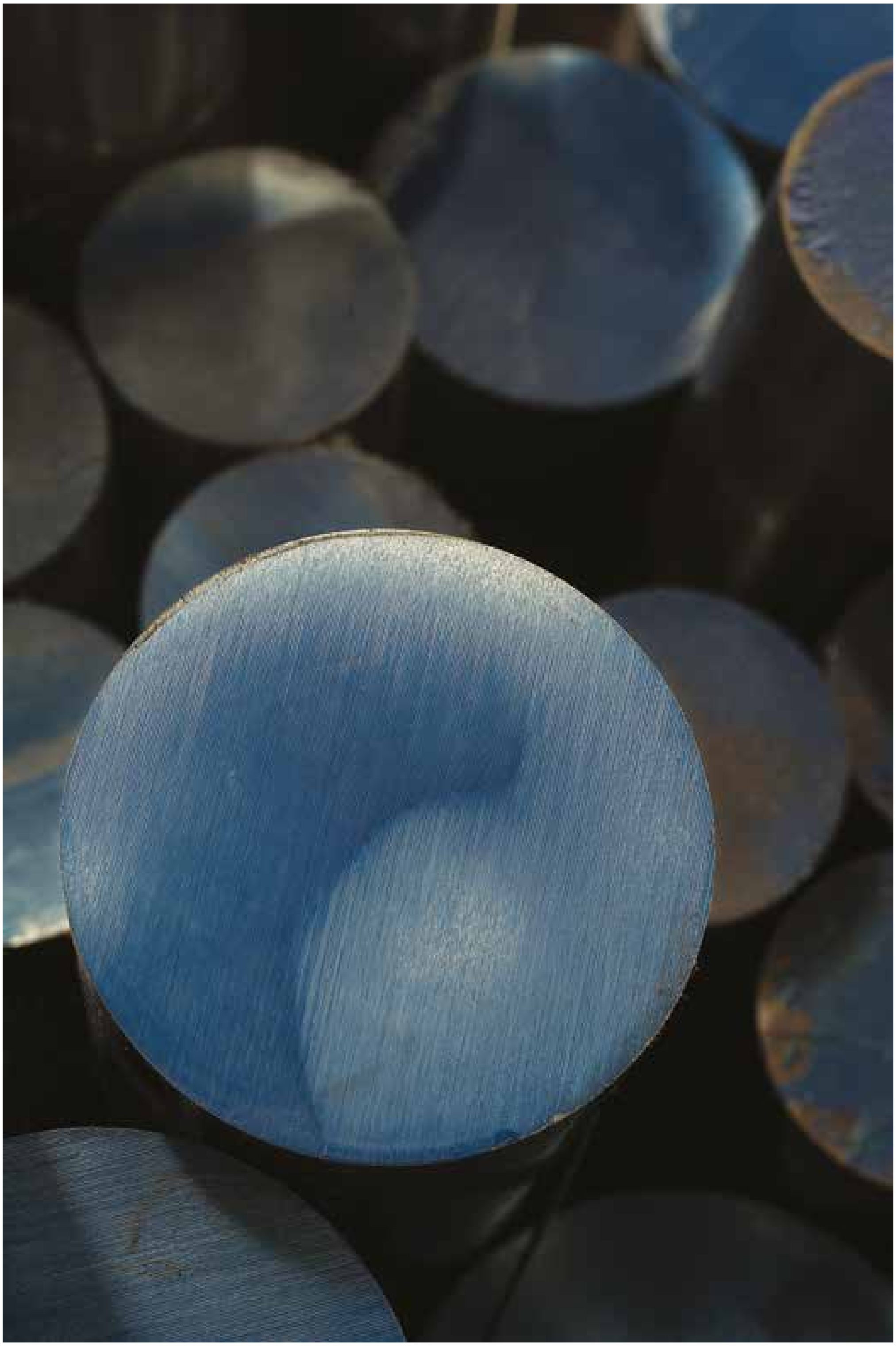

BIBLIOGRAPHIC RECOMMENDATIONS

It is not easy to give detailed advice regarding the topic of this book. In fact, a bibliography that deals with Steel Metallurgy is vast.

Two useful texts to begin with are those of Prof. Walter Nicodemi entitled: "Metallurgia" (volume 1) and "Acciai e leghe non ferrose" (volume 2) both published by Zanichelli in Bologna, in 2007 and 2008. These books not only concern steels (carbon, special, stainless, etc.), but also non-ferrous alloys (aluminum, copper, titanium, etc.).

Certainly useful for those who prefer to read in Italian are the book by Prof. Aurelio Burdese, "Metallurgia e tecnologia dei materiali metallici", UTET, Torino, Italia, 1992, and Claudio Cibaldi's volumes, "I criteri di scelta e di trattamento degli acciai da costruzione e da utensili", 5 voll., AQM, Provaglio d'Iseo (BS), Italia, 2006-2010.

Numerous important bibliographic references exist in English.

Very interesting is the almost rare volume by Karl Erich Thelning, Steel and its Heat Treatment, Bofors Handbook, Butterworth, London, UK, 1975. Originally written in German and then translated into English, it contains all that can be useful with regard to steels and their heat treatment: not by chance this bibliographic reference is cited by all authors who, from that moment on, have been dealing with the metallurgy of steels.

The most recent American source is the collective volume edited by Flake C. Campbell, Elements of Metallurgy and Engineering Alloys, ASM International, Metals Park Ohio, USA, 2008. The author, a Boeing Engineer for 38 years, was awarded the Honorary Professorship of the University of Missouri (USA) in 2005.

Specifically on steels are also two books by George Krauss, Principles of Heat Treatment of Steels, ASM International, Metals Park, Ohio, USA, 1980 and Steels: Processing, Structure, and Performance, ASM International, Metals Park, Ohio, USA, 2005.

A great book, perhaps more for scientists than for technicians, is by the Persian author, Reza Abbaschian, Physical Metallurgy Principles, Cengage Learning, Stamford, USA, 2009, head of the Engineering Department of the University of California Riverside and emeritus professor of Mechanical Engineering.

BIBLIOGRAPHY

[Abbaschian et al. 2009] Abbaschian R., Abbaschian L., Reed-Hill R. E., Physical Metallurgy Principles, 4th ed., Cengage Learning, Stamford, USA, 2009.

[Andrews 1965] Andrews K.W., Empirical formulae for the calculation of some transformation temperatures, Journal of the Iron and Steel Institute, n.7, pp.721-727, 1965.

[ASM-H.3 1992] ASM Handbook Committee, ASM Handbook, Vol. 3 – Alloy Phase Diagrams, 10th ed., ASM International, Metals Park, Ohio, USA, 1992.

[ASM-H.4 1991] ASM Handbook Committee, ASM Handbook, Vol. 4 – Heat Treating, 10th ed., ASM International, Metals Park, Ohio, USA, 1991.

[Bain e Paxton 1966] Bain E. C., Paxton H. P., Alloying Elements in Steel, 2nd ed., American Society for Metals, Metals Park, Ohio, USA, 1966.

[Briggs 1958] Briggs C. W., The Effect of Heat Treatment Variables on the Toughness of Cast Steel and Cast Armor, Steel Founders' Society of America, Cleveland, Ohio, USA, 1958.

[Brown e Cohen 1962] Brown R. L., Cohen M., Stress Relaxation of Hardened Steel, Metal Progress, n.2, pp. 66-71, 1962.

[Callister 2007] Callister W. D., Material Science and Engineering: An Introduction, 7th ed., John Wiley & Sons, New York, USA, 2007 (trad. it., Caneva C. (a cura di), Scienza e ingeneria dei materiali – un'introduzione, 2a ed., Edises, Roma, Italia, 2007).

[Campbell 2008] Campbell F. C. (ed.), Elements of Metallurgy and Engineering Alloys, ASM International, Metals Park Ohio, USA, 2008.

[Campbell 2003] Campbell J., Castings, 2nd ed., Butterworth-Heinemann, Oxford, UK, 2003.

[Cheng et al. 1991] Cheng L., Van der Pers N.M., Böttger A.,De Keuser Th.H., Mittemeijer E.J., Lattice Changes of Iron Carbon MartensiteAging at Room Temperature, Metallurgical Transaction A, Vol. 22, pp. 1957-1967, 1991.

[Chipman 1972] Chipman J., Thermodynamics and Phase Diagram of the Fe-C System, Metallurgical Transaction B, Vol. 3, pp. 55-64, 1972.

[Clayton e Danks 1990] Clayton P., Danks D., Effect of Interlamellar Spacing on the Wear Resistance of Eutectoid Steels under Rolling/Sliding Conditions, Wear, Vol. 135, p.369-387, 1990.

[Dieter 1988] Dieter G. E., Mechanical Metallurgy, McGraw Hill, London, UK, 1988.

[Gerold 1979] Gerold V., Precipitation Hardening; Dislocations in Solids, Vol. 4 – Dislocations in Metallurgy, North-Holland Publishing Company, Amsterdam, Holland, 1979.

[Ginzburg 2005] Ginzburg V.B., Metallurgical Design of Flat Rolled Steels, Marcel Dekker, New York, USA, 2005.

[Gladman 2004] Gladman T., Grain Size Control, Maney Pubblishing, London, UK, 2004.

[Grange e Baughman 1956] Grange R.A., Baughman R.W., Hardness of tempered martensite in carbon and low alloy steels, ASM Transactions, Vol. 48, pp.165-197, 1956.

[Higgins 1993] Higgins R.A., Engineering Metallurgy – Part I: Applied Physical Metallurgy, 6th ed., Arnold, London, UK, 1993.

[Hollomon e Jaffe 1945] Hollomon J.H., Jaffe L.D., Time-temperature relations in tempering steel, Transactions of AIME, Vol. 162, pp. 223-249 , 1945.

[Hosford 2005] Hosford W. F., Physical Metallurgy, Taylor & Francis Group, Boca Raton, Florida, USA, 2005.

[Hoyle 1988] Hoyle G., High Speed Steels, Butterworths, London, 1988.

[Krauss 1980] Krauss G., Principles of Heat Treatment of Steels, ASM International, Metals Park, Ohio, USA, 1980.

[Krauss 2005] Krauss G., Steels: Processing, Structure, and Performance, ASM International, Metals Park, Ohio, USA, 2005.

[Kurz e Fisher 1992] Kurz W., Fisher D.J., Fundamentals of Solidification, Trans Tech Publications, Switzerland, 1992.

[Jost et al. 1976] Jost S., Langer H., Pietsch D., Uligh P., Rechnerische Ermittlung der Erwärmdauer bei der Wärmebehandlung von Stahl, Fertigungstechnik und Betrieb, Vol. 26, pp.298-301, 1976.

[Lamont 1943] Lamont J.L., How to Estimate Hardening Depth in Bars, Iron Age, Vol. 152, pp. 64-70, 1943.

[Nicodemi 2007] Nicodemi W., Metallurgia, 2a ed., Zanichelli, Bologna, Italia, 2007.

[Nicodemi 2008] Nicodemi W., Acciai e leghe non ferrose, 2a ed., Zanichelli, Bologna, Italia, 2008.

[Ohmori e Honeycombe 1971] Ohmori, Y. and Honeycombe, R. W. K., Ohmori, Y. and Honeycombe, R. W. K. Proceedings ICSTIS, The Isothermal Transformation of Plain Carbon Austenite, Proceedings ICSTIS, Transactions of the Iron and Steel Institute of Japan, Vol. 11, pp. 1160-1164, 1971.

[Onink et al. 1993] Onink M., Brakman C. M., Tichelaar F. D., Mittemeijer E. J., van der Zwaag S., Root J. H., Konyer N. B., The Lattice Parameters of Austenite and Ferrite in Fe-C Alloys as functions of Carbon Concentration and Temperature, Scripta Metallurgica et Materialia, Vol. 29, pp. 1011-1016, 1993.

[Rocha et al. 2012] Rocha A.S., Nunes R.M., Hirsch T., Analysis by Design of Experiments of Distortion Potentials in Drawn and Induction Hardened Wire, Materials Research, Vol. 15(2), pp. 266-276, 2012.

[Singh 1999] Singh V., Physical Metallurgy, Standard Publishers Distributors, New Delhi, India, 1999.

[Smith e Hashemi 2006] Smith W.F., Hashemi J., Foundations of Materials Science and Engineering, 4th ed., McGraw-Hill, New York, 2006.

[Speich 1969] Speich G. R., Tempering of Low-Carbon Martensite, Transactions of TMS-AIME, Vol. 245, pp. 2552-2564, 1969.

[Spur e Stöferle 1980-1994] Spur G., Stöferle T. H. (ed.), Handbuch der Fertigungstechnik, 6 Vol., Carl Hanser Verlag, Munich, West Germany, 1980-1994.

[Steven e Haynes 1956] Steven W., Haynes A.G., The Temperature Formation of Martensite and Bainite in Low Alloy Steels, Journal of the Iron and Steel Institute, Vol. 183, pp. 349-359, 1956.

[Thelning 1975] Thelning K.-E., Steel and its Heat Treatment, Bofors Handbook, Butterworth, London, UK, 1975.

[Thompson 1985] Thompson C.V., Secondary grain growth in thin films of semiconductors: Theoretical aspects, Journal of Applied Physics, Vol.58, pp.763-772, 1985.

[Totten 2006] Totten G. (ed.), Steel Heat Treatment: Metallurgy and Technologies, CRCnet base, Taylor & Francis Group, Boca Raton, Florida, USA, 2006.

[Wells e Lherbier 1980] Wells M.G.H. e Lherbier L.W., Processing and Properties of High Speed Tool Steels, TMS-AIME, New York, 1980.

[Wever et al. 1954/56/58] Wever F. et al., Atlas zur Warmebehandlung der Stahle, Verlag Stahleisen mbH, Dusseldorf, West Germany, 1954/56/58, Wever F., Rose A., Vol. 1; Rose A., Peter W., Strassburg W., Rademacher L., Vol. 2

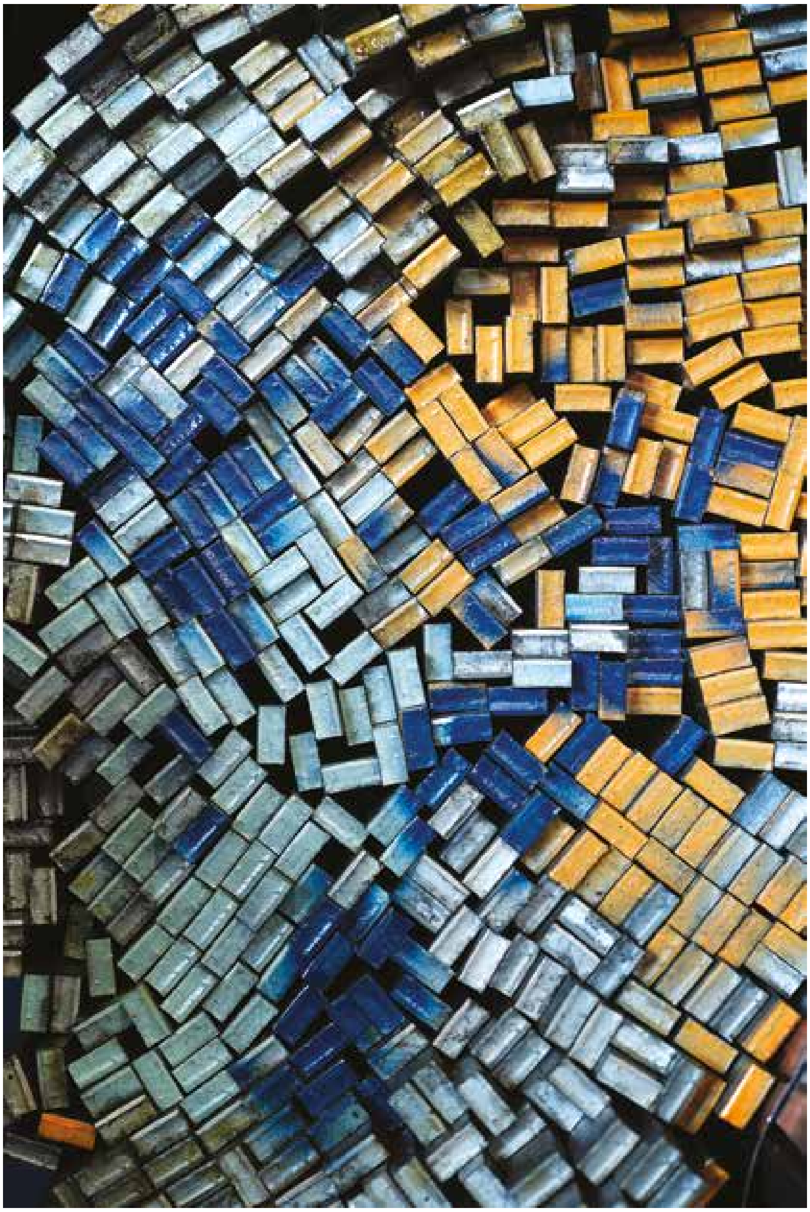

Lucefin SpA
I-25040 Esine (Brescia) Italy
www.lucefin.com

Graphic design: Lucefin SpA Parlatotriplo divsion
Print: Graphicscalve - Vilminore di Scalve (BG)

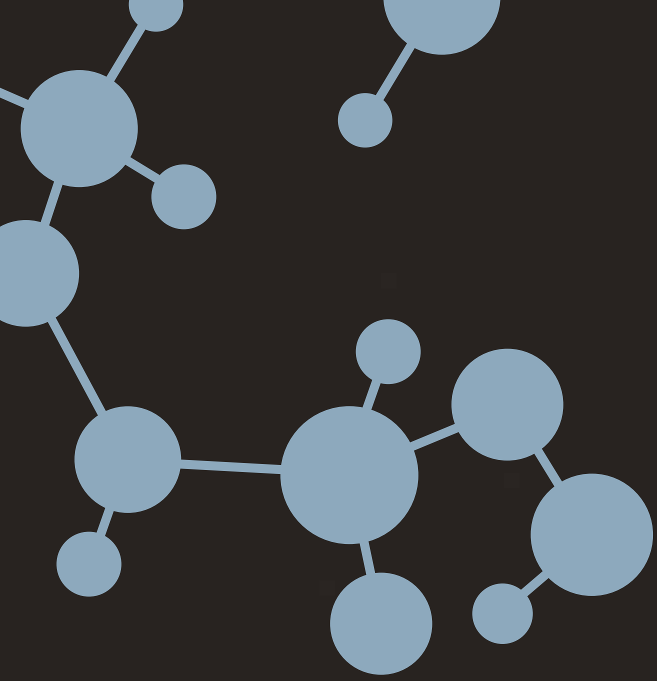

GRUPPO
LUCEFIN

Lucefin S.p.A.
I-25040 Esine (Brescia) Italy
www.lucefin.com

ISBN 978-88-909837-1-9